REPUBLIQUE ALGERIENNE DEMOCRATIQUE ET POPULAIRE
MINISTERE DE L'ENSEIGNEMENT SUPERIEUR ET DE LA RECHERCHE SCIENTIFIQUE
UNIVERSITE FERHAT ABBAS - SETIF 1
UFAS (ALGERIE)

THESE

Présentée à La Faculté de Technologie

Département de Génie des Procédés

Pour l'Obtention du Diplôme de

DOCTORAT EN SCIENCES

Option : Génie des Polymères

Par

Mr. BAOUZ TOUFFIK

THEME

MODIFICATION DE RESINES POLYESTERS PAR DES ADDITIFS NATURELS ET/OU SYNTHETIQUES

Soutenue le: 25 / 06 / 2015 devant un Jury composé de

Président :	**Prof. DJAFER BENACHOUR**	**Université Ferhat Abbas, Sétif 1**
Rapporteur :	**Prof. FAROUK REZGUI**	**Université Abderrahmane Mira, Bejaia**
Examinateurs :	**Prof. HOCINE DJIDJELLI**	**Université Abderrahmane Mira, Bejaia**
	Prof. AMAR BOUKERROU	**Université Abderrahmane Mira, Bejaia**
	Prof. MOHAMED TAHAR BENANIBA	**Université Ferhat Abbas, Sétif 1**

ABSTRACT

The main objective of the present research study was to toughen poly(lactic acid) (PLA) using rubber-toughening technique without adversely affecting its stiffness and strength. PLA was melt blended in a twin screw extruder with an ethylene-methyl acrylate-glycidyl methacrylate (E-MA-GMA) impact modifier in the range 5-30 wt% in the presence of 2 wt% of an organomodified montmorillonite (OMMT) to minimize the loss of stiffness and strength of PLA. The first part of this work reports on the study and comparaison of PLA/E-MA-GMA blends and PLA/E-MA-GMA/OMMT ternary nanocomposites prepared by mixing all ingredients simultaneously in the hopper of the extruder. Scanning electron microscopy (SEM) revealed that PLA and E-MA-GMA form an immiscible blend in which the rubber formed sub-micron particles the size of which increased with increasing rubber content. Impact strength and ductility of the blends increased with increasing rubber content but at the expense of stiffness and strength. Ternary nanocomposites exhibited intercalated/partially exfoliated structure, whereas the ternary nanocomposites at 10 wt% rubber ratio showed complete exfoliation of OMMT as detected by x-ray diffraction (XRD) and confirmed by transmission electron microscopy (TEM) which thus resulted in balanced properties. The viscosity of the mixtures as measured by melt flow index was found to be highly influenced by the addition of the rubber and the OMMT. In the second part of this work and with the same aim of increasing further PLA toughness, the effects of four addition protocols of the components of the ternary nanocomposites were investigated. It was found that both clay dispersion and morphology were influenced by the blending method as detected by XRD and observed by TEM and SEM. The XRD results, which were also confirmed by TEM observations, demonstrated that the OMMT dispersed better in PLA than in E-MA-GMA. All formulations exhibited intercalated/partially exfoliated structure with the best clay dispersion achieved when the clay was first mixed with PLA before the rubber was added. According to SEM, the blends exhibited fine dispersion of the rubber in the PLA with differences in the mean particle sizes that depended on the addition order. Balanced stiffness-toughness was noticed at 10 wt% rubber content in the compounds without significant sacrifice of the strength. High impact toughness

was attained when PLA was first mixed with the clay before the rubber was added, and the highest tensile toughness was obtained when PLA was first compounded with the rubber, and then clay was incorporated into the mixture. Thermal characterization by DSC carried out in both parts of this research work confirmed the immiscibility of the blends, but in general, it was revealed that the thermal parameters and the degree of crystallinity of the PLA were not affected by the preparation procedure. Furthermore, both the clay and the rubber were found to decrease the crystallization temperature of the PLA by acting as nucleating agents.

ORIGINAL CONTRIBUTION TO SCIENTIFIC KNOWLEDGE

Peer-Reviewed Journal Publications:

1- **Touffik Baouz**, Farouk Rezgui, Ulku Yilmazer, **Ethylene-Methyl Acrylate-Glycidyl Methacrylate Toughened Poly(lactic acid) Nanocomposites**, Journal of Applied Polymer Science, Volume 128, pages 3193-3204, **2013**.

2- **Touffik Baouz**, Eda Açik, Farouk Rezgui, Ulku Yilmazer, **Effects of Mixing Protocols on Impact Modified Poly(lactic acid) Layered Silicate Nanocomposites**, Journal of Applied Polymer Science, Volume 132, **2015**.

Conference Publications:

Touffik Baouz, Farouk Rezgui, Ulku Yilmazer, "Impact Modified Poly(lactic acid)-Organoclay Nanocomposites Prepared by Twin Screw Extruder", 3rd International Polymeric Composites Symposium, Exhibition and Workshop, 9-12 November 2012, Izmir-Turkey.

ACKNOWLEDGEMENTS

In the name of God, most Gracious, most Compassionate, and peace be upon his messenger Mouhamed who exhorted his followers to seek for knowledge from cradle to grave. It is of my duty to express, in this small allowed space, all my heartfelt gratitude to all who have contributed to the completion of the present modest work.

I would like to express my sincere and deepest gratitude to my supervisor, Pr. Dr. Farouk Rezgui for his continuous technical guidance, constructive criticism, patience and insight throughout elaboration of this research work. I am also highly indebted to Pr. Dr. Ülkü Yılmazer from Chemical Engineering department of Middle East Technical University (METU-Ankara-Turkey) who trusted me and accepted me in his laboratory. I am forever grateful to him for his inspiring, guidance, valuable scientific contribution and critics and also for his endless support and warm care during my stay in Ankara. I am also grateful to Pr. Dr. Göknur Bayram from Department of Chemical Engineering (METU) for allowing me to use some of the instruments in her laboratory.

Special thanks are also addressed to the committee members Pr. Dr. Djafer Benachour, Pr. Dr. M. Tahar Benaniba, Pr. Dr. Amar Boukerrou and Pr. Dr. Hocine Djidjelli who have accepted to review my thesis, to evaluate my research work and to attend the defense of the thesis.

My beloved wife deserves special thanks for the unconditional sacrifices she made, her understanding and encouragement, and also for her moral support for which I was in great need all along the completion of this modest research work.

Thanks are also due to my dear friend B. Elbirly and his wife Nimet for their encouragement, moral support and advices during may stay in Turkey.

I also extend my heartfelt gratitude and thanks to all my lab fellows and friends in METU, especially Eda Açik, Ali Sinan Dike, Sengor Irem, Yuksel Sayin, Miray Yasar and Sertan Yeşil for their great help either scientific or social and also for their understanding and moral support which have made my stay in Ankara memorable. Also, I am very grateful to all the technicians of the Chemical Engineering Department of METU especially Mihrican Açıkgöz for her assistance with all thermal analysis.

Last but not least, I wish to express my sincere thanks to all who have contributed either directly or indirectly to the fulfillment of this project.

TABLE OF CONTENT

TABLE OF CONTENT

Chapter III - PLA Modifications : Litterature Survey and Previous Research Studies

Chapter IV - Materials and Experimental Procedures

Chapter V - Ethylene-Methyl Acrylate-Glycidyl Methacrylate Toughened Poly(lactic acid) Nanocomposites

Chapter VI - Effects of Mixing Protocols on Impact Modified Poly(lacticacid) Layered Silicate Nanocomposites

Chapter VII - General Conclusions and Recommendations

LIST OF FIGURES

LIST OF TABLES

LISTE OF ABREVIATIONS

ABS acrylonitrile-butadiene-styrene copolymers
ABS-g-GMA ethylene glycidyl methacrylate grafted acrylonitrile-butadiene-styrene

ATEC acetyltriethyl citrate
ATBC acetyltributyl citrate
ATH aluminum hydroxide

CNT carbon nanotubes
CEC cation exchange capacity

DSC differential scanning calorimetry
DMA dynamic mechanical analysis
DMTA dynamic mechanical thermal analysis
DCP dicumyl peroxide

E-MA-GMA ethylene-methyl acrylate and glycidyl methacrylate
ESO soybean oil
EG expanded graphite
EPR-MAH ethylene propylene rubber
EVA ethylene-co-vinyl acetate
FDA Food and drug Administration
FTIR Fourier Transform Infrared
ETPB ethyltriphenyl phosphonium bromide
EGMA poly(ethylene-co-glycidyl methacrylate)
E-BA-GMA ethylene-butyl acrylate glycidyl methacrylate
ENR epoxidized natural rubber
EAA Ethylene-acrylic acid
EPDM ethylene-propylene-diene monomer

GPa giga Pascal
GRAS generally recognized as safe
GMO genetically modified organisms
GMA glycidyl methacrylate

HDT heat distortion temperature
HNT holloysite nanotubes
HIPS high impact polystyrene

IR isoprene rubber

LDPE low density poly(ethylene)
LLDPE linear low density polyethylene
LDPE-g-MAH Low Density Polyethylene grafted maleic anhydride
LDH layered double hydroxide
LTI Lysine triisocyanate
lbs/ft pound/foot

MPa mega Pascal
MKT metric kilo tone
MT metric tone
Mw molecular weight
meq milli-equivalent
MT2EtOH methyl, tallow, bis-2-hydroxyethyl, quaternary ammonium
MMT montmorillonite
MFI melt flow index
MBS methyl methacrylate-butadiene-styrene

NR natural rubber
NPCC nanoprecipitated calcium carbonate
NBR acrylonitrile-butadiene rubber
NR-g-PMMA natural rubber grafted with poly(methyl methacrylate)

NR-g-PVAc natural rubber grafted poly(vinyl acetate)
NR-g-GMA natural rubber grafted glycidyl methacrylate

OMLS Organically Modified Layered Silicates
OMMT organomodified Montmorillonite

PBSGAT poly(butylene succinate-co-glutarate-co-adipate-co-terephtalate)
PAE polyamide elastomer
PEU poly(ester-urethane)
PEO-g-PLA poly(ethylene octane) grafted PLA
PC polycarbonate
PLA-g-MAH PLA grafted Maleic anhydride
PTAT poly(tetramethylene-co-adipateterephthalate)
PPC poly(propylene carbonate)
PP polypropylene
PP-g-MAH polypropylene grafted maleic anhydrid
POSS polyhedral silesquioxane
PNC polymer nanocomposite
PHA polyhydroxyalkanoates
PHO Poly(hydroxyoctanoate)
PHB polyhydroxybutyrate
PHH polyhydroxyhexanoates
PEA polyethylene adipate
PHV hydroxyl-valerate
PHBV polyhydroxybutyrate-valerate
PBS poly(butylene succinate)
PBSA poly(butylene succinate adipate)
PCL poly(capro lactone)
PBAT poly(butylene adipate terephthalate)
PBA poly(butylene adipate)
PVA poly(vinyl alcohol)
PEO poly(ethylene octane)

PAA polyacrylic acid
PA Polyamide
PTT poly(trimethylene terephthalate)
PET poly(ethylene terephthalate)
PVC poly(vinyl chloride)
PE poly(ethylene)
PP poly(propylene)
PEA poly(esteramide)
PLS Polymer Layered Silicate
PLA poly(lactic acid)
PDLLA poly-D,L-lactic acid
PDLA poly-D-lactic acid
PES poly(ethylene succinate)
PBST poly(butylene succinate terephthalate)
PGA polyglycolic acid
PLGA poly(lactic-co-glycolic acid)
PEG polyethylene glycole
PS polystyrene
PVC polyvinyl chloride
PPG poly(propylene glycol)
PLA-EG polylactic acid grafted expanded graphite
PBSL poly(butylene succinate-co-L-lactate)
PIP-g-PVAc polyisoprene grafted poly(vinyl acetate)
PU polyurethanes
PVAc poly(vinyl acetate)
PIP polyisoprene
PE-g-GMA polyethylene-g-glycidyl methacrylate
PEO-g-GMA poly(ethylene octane) grafted glycidyl methacrylate

ROP ring opening polymerization
RuO4 ruthenium tetraxide

SEM scanning electron microscopy
SEBS hydrogenated styrene-butadiene-styrene block copolymer

SEBS-g-MAH maleic anhydride grafted SEBS

SnO tin oxide

$SnCl_2$ Tin chloride

SAN-g-GMA styrene-acrylonitrile grafted glycidyl methacrylate copolymer

SAN styrene-acrylonitrile copolymers

SAXS small angle x-ray scattering

TPU thermoplastic polyurethane

TPUE thermoplastic polyurethane elastomer

TPS thermoplastic starch

TEM transmition electron microscopy

TEC triethyl citrate

TBC tributyl citrate

TGA thermogravimetric analysis

TPP triphenyl phosphite

TPEE thermoplastic polyester elastomer

T_g glass transition temperature

T_c crystallization temperature

T_m melting temperature

UV ultra-violet

WAXD wide angle x-ray diffraction

WVP water vapor permeation

XRD x-ray diffraction

ε_b elongation at break

σ tensile strength

ΔH_c crystallization enthalpy

ΔH_m melting enthalpy

ΔH_f enthalpy of fusion

OsO_4 Osmium tetroxide

Chapter I

INTRODUCTION

Chapter I - INTRODUCTION

I-1 General Background

Over the last century, conventional materials (wood, metals, paper and glass etc.) have been continuously substituted by plastics in diverse applications including but not limited to packaging, construction, agriculture, aerospace, automotive and sports. The ubiquitous presence of plastics in all aspects of modern society is due to their high performance, versatility, light weight and low cost.**[1]**

The increasing requirements and demands for plastics of higher performance to endure increasingly stringent conditions have been fulfilled by blending of existing polymers or by composites production.**[1,2]** A polymer based composite is a structural multiphase material made up of a polymeric matrix in which a filler is dispersed. The matrix can be thermoplastic, thermoset or rubber, and the filler can be organic or inorganic, synthetic or natural with specific geometries and shapes such as fibers, flakes, spheres, whiskers, platelets, or particles.**[2]** In conventional polymer composites the content of macro and/or microscale filler may reach 40% and more. At this level of reinforcement the design limits of optimizing composites performance is reached due to property trade-off such as for instance stiffness is traded-off for toughness, and toughness is obtained at the cost of strength.**[3-5]** This limitation has been overcome by scaling the particle size of the filler down to the nanometer scale in the composite. Recently, these new hybrid materials known as nanocomposites have captured the interest of both academia and industry because not only they show dramatic improvements of performance at very low filler content (1-5%), but also exhibit new functional properties that are not observed in their parent polymers or their conventional composites counterparts.**[3,6,7]**

The plastics industry has been essentially supplied by synthetic hydrocarbon polymers derived from fossil resources. It is forecasted that the global production of plastics is estimated to surpass 300 million tons by 2015 with an annual growth of approximately 5% (14 million tons per annum).**[8-10]** The ever expanding use of long-lasting plastics at this high rate in their diverse forms (resins, composites, nanocomposites and blends) has raised environmental concerns owing to accumulation

of their persistent wastes in the environment.**[1,3,6,8]** Recycling, incineration and landfilling have been and are the three alternative ways for plastics waste management. However, recycling is not economically viable because it requires large expenditure of labor and energy, and incineration contributes to pollution and global warming through the emission of toxic gases while landfilling suffers from shortage of satisfactory landfills.**[1,6]** In addition, the high dependency of plastics industry on oil and gas resources has also triggered sustainability issues associated with depletion of the nonrenewable finite/limited natural fossil reserves that compromises the future of coming generations.**[8]** For these reasons, and with increasing environmental awareness and more stringent legislation regarding recyclability and restrictions on waste disposal, biodegradable polymers that satisfy to the requirements of sustainability and low toxicity of their monomers and their degradation by-products are envisioned to play a major role in solving environmental issues bring about by the plastics wastes accumulation and to alleviate the over-dependence on oil of plastics industry which has led to increasing oil prices.**[1,3,6,8]**

Biodegradable polymers (BPs) are materials that can undergo microbially induced chain scission leading to mineralization, that is conversion to water, carbon dioxide, methane and a new cell biomass.**[1,3]** BPs have promising properties and are competing well with most commodity petrochemical-based polymers.**[7,8]** The best known BPs are polyesters that can be derived either from non-renewable and renewable sources, but the last group is of much interest from sustainability and environmental concerns.**[3,7,8]** Among a number of thermoplastic polyesters, poly(lactic acid) (PLA) is a commercially available linear aliphatic polyester produced by ring opening polymerization of lactic acid monomer. In addition, PLA is a bio-based and sustainable biopolymer since its monomer is produced by microbial fermentation of 100% annually renewable agro-resources mainly carbohydrate rich substances such as sugar, corn, beet, and potatoes.**[3,7,10]** Currently, PLA is at the forefront of biopolyesters that competes well with many available synthetic polymers owing to its good mechanical and physical properties, biocompatibility, ease of processability and much more importantly its renewability. All of these attributes make it an outstanding candidate with high potential to substitute for petroleum-

derived polymers in various applications such as biomedical, packaging, automotive and others.**[11]** In addition, the latest breakthrough in PLA production has motivated many companies to express their interest in producing PLA on commercial scale which has contributed to bring down its price to come close to that of commodity plastics such as PE and PP.**[10]**

I-2 Problematic Associated with PLA

Despite all the progress achieved to increase PLA market share, this biodegradable polymer still faces some limitations and challenges in terms of performance.**[10]** Its inherent brittleness and low glass temperature hinder its use in a wide range of applications where toughness is of paramount importance. To address these shortcomings considerable scientific and engineering efforts have been devoted to broaden PLA applications window. In this direction, various modification strategies have been investigated including copolymerization, plasticization, addition of organic/inorganic fillers, and melt-blending with either biodegradable or nonbiodegradable polymers.**[12,13]**

Copolymerization is proposed as a versatile way to adjust PLA physical and mechanical properties, but it generally requires the use of complex multi-step synthesis and of highly toxic organometallic catalysts.**[14]** Therefore, up to now, none of the PLA copolymers are reported to be economically feasible or commercially available.**[15,16]** Blending PLA with plasticizers (Plasticization) has also been known as an effective way to impart PLA with flexibility, to increase its extensibility and to improve its toughness and processability. However, researchers are facing two major issues with this technique: evaporation of small-sized plasticizers during processing at elevated temperatures and embrittlement of the matrix during aging owing to migration of the plasticizers to the surface of the polymer matrix.**[17,18]** As for rigid fillers, metal oxides,**[19]** calcium carbonate,**[20]** hydroxyapetite**[21]** and organically modified clays were investigated.**[22,23]** Organically modified layered silicates are favored since their high aspect ratio was shown to bring superior mechanical, rheological, fire retardancy and gas barrier properties.**[24-26]**

Melt blending with various flexible polymers has proven to be a viable and preferred strategy in toughening PLA. In the aim of preserving PLA biodegradation, numerous biodegradable polymers were reported to have been melt blended with PLA to enhance toughness.**[27,28]** PLA was also toughened with miscellaneous non-biodegradable polymers such as linear low density polyethylene**[29]** polycarbonate,**[30]** and poly(ethylene oxide).**[31]**

Similar brittleness problems have been solved before by using rubber toughening methodology such as in the case of the brittle polystyrene (PS) which was toughened by chemical mixing with polybutadiene rubber to form high impact polystyrene (HIPS).**[32]** Inspired from this first rubber-toughened polymer, addition of suitable rubbery polymer was also investigated as an effective way to enhance PLA toughness. However, Addition of a flexible polymer or rubber to a rigid one is always accompanied by a concomitant loss of stiffness and strength.**[27-29]** This has been addressed by applying nanocomposites technology mainly through addition of nanolayered silicates, combining thus the advantages of the layered silicates and rubbers is another alternative to improve the properties of PLA.**[4,5]**

In rubber-toughened systems, the rubber is intended to dissipate the stress so that the blend shows ductility and plastic deformation. Numerous factors govern the performance of rubber-toughened polymers among which the most important are components ratios and their properties, interfacial tension and viscosity ratio between the components, rubber particle size and shape, processing conditions and preparation methods.**[33,34]** Considering the number of factors, much work remains to be carried out in this area of research to understand the effects of these factors on property-structure relationships of flexible polymers toughened PLA systems.

I-3 Motivations and Research Project Objectives

Our literature survey revealed that while investigations on PLA modification by melt blending with flexible and rubber compounds are rather largely well documented, their ternary nanocomposites studies are very scarce. In addition, little information is available on either toughening PLA using impact modifiers or on their ternary nanocomposites. Considering the number of parameters influencing ternary

nanocomposites performance, up to now none of them has been deeply investigated and more specifically that related to the effects of addition procedures of the components of the PLA ternary nanocomposite. Consequently, these above main points are behind our motivations to undertake the present research project.

The purpose of the present research study is to develop a toughened PLA nanocomposite suitable for packaging applications using an ethylene-methyl acrylate-glycidyl methacrylate copolymer (E-MA-GMA) impact modifier as a toughner and an organo-modified montmorillonite (OMMT) as nanofiller. To achieve this aim, the thorough literature survey allowed us to fix three following specific objectives to conduct the project:

1- Investigation of possible enhancement of PLA extensibility and toughness with incorporation of the E-MA-GMA, with the aim to determine the effects of composition of the PLA/E-MA-GMA blends on structure-property relationships.

2- Counteract the softening effects of the E-MA-GMA on PLA via addition of an organo-montmorillonite, followed by a systematic comparaison of the binary and ternary nanocomposites.

3- With the aim to further increase the PLA extensibility and toughness, it was decided to investigate the effects of mixing protocols of the components of the ternary nanocomposites (PLA/E-MA-GMA/OMMT).

I-4 Thesis Overview and Organization

The thesis is divided into 6 chapters. **Chapter 1** introduces the main background details of the thesis topic and the problematic related to the research study. Motivations behind the present research work and the main objectives together with the organization of the thesis are also described in this chapter. Literature review relevant to the content and objectives of the present thesis is given in **Chapter 2**. It covers general current information on polymer nanocomposites, but mainly focuses on polymer layered silicates nanocomposites, their development and their preparation methods in relation with their structures. This chapter also includes general

background information on biodegradable polymers and those specific to PLA. **Chapter 3** presents the literature survey concerning the up-to-date research progress devoted to PLA modifications and more specifically that related to melt blending with flexible and rubber compounds together with their nanocomposites counterparts which represent the topic of our research project. **Chapter 4** is devoted to the description of the materials and the experimental methods used for the preparation of the studied formulations and their characterization. A brief and essential background of each experimental technique is also provided in this chapter. **Chapter 5** reports the results of PLA extensibility and toughness improvements through melt mixing with an ethylene-methyl acrylate-glycidyl methacrylate copolymer in presence of an organo-montmorillonite type layered silicate, which is then concluded with the main findings. **Chapter 6** focuses on the effects of mixing protocols on modified PLA ternary nanocomposites. The results are presented and discussed thoroughly and a conclusion relevant to the main findings is given at the end of the chapter. Finally, **Chapter 7** provides general conclusions of the present research work including some future perspectives.

REFERENCES

[1] Ali Shah, A.; Hasan, F.; Hameed, A.; Ahmed, S., Biotech. Adv., Vol. 26, pp 246 **(2008)**.

[2] Callister, Jr.W.D., "Materials Science and Engineering: An Introduction", 7th edition, John Wiley & Sons, Inc. USA **(2007)**.

[3] Sinha Ray, S.; Bousmina, M., Prog. Mat. Sci., Vol. 50, pp 962 **(2005)**.

[4] Leu, Y.Y.; Mohd Ishak, Z.A.; Chow, W.S., J. Appl. Polym. Sci., Vol. 124, pp 1200 **(2012)**.

[5] Bitinis, N.; Verdejo, R.; Maya, E.M.; Espuche, E.; Cassagnau, P.; Lopez-Manchado, M.A., Comp. Sci. Tech., Vol. 72, pp 305 **(2012)**.

[6] Masami Okamoto, "Biodegradable Polymer/Layered Silicate Nanocomposites: A Review; in: Mallapragada, S. and Narasimhan, B. "Handbook of Biodegradable Polymeric Materials and Their Applications", American Scientific Publishers, Vol.1, Chapter 8, pp 1-45 **(2005)**.

[7] Bordes, P.; Pollet, E.; Avérous, L., Prog. Polym. Sci., Vol. 34, pp 125 **(2009)**.

[8] Reddy, M.M.; Vivekanandhan, S.; Misraa, M.; Bhatia, S.K. ; Mohanty, A.K., Prog. Polym. Sci., Vol. 38, pp 1653 **(2013)**.

[9] Institute for Bioplastics and Bioplastics, http://en.european-bioplastics.org (Last accessed on March **2014**).

[10] Nampoothiri, K.M.; Nair, N.R.; John R.P., Biores. Techn., Vol. 101, pp 8493 **(2010)**.

[11] Yeh, J.; Tsou, C.; Li, Y.; Xiao, H.; Wu, C.; Chai, W.; Lai, Y.; Wang, C.J. Polym. Res., Vol. 19, pp 9766 **(2012)**.

[12] Zeng, J.; Li, Y.; He, Y.; Li, S.; Wang, Y., Ind. Eng. Chem. Res., Vol. 50, pp 6124 **(2011)**.

[13] Zhao, Q.; Ding, Y.; Yang, B.; Ning, N.; Fu, Q., Polym. Test., Vol. 32, pp 299 **(2013)**.

[14] Varmaa, I.K.; Albertssonb, A.C.; Rajkhowaa, R. Prog. Polym. Sci., Vol. 30, pp 949 **(2005)**.

[15] 5- Liu, H.; Zhang, Z.J., Polym. Sci. Part B: Polym. Phys., Vol. 49, pp 1051 **(2011)**.

[16] Meng, B.; Tao, J.; Deng, J.; Wu, Z.; Yang, M., Mater. Lett., Vol. 65, pp 729 **(2011)**.

[17] Ljungberg, N.; Andersson, T.; Wesslén, B., J. Appl. Polym. Sci., Vol. 88, pp 3239 **(2003)**.

[18] Martino, V. P.; Jiménez, A.; Ruseckaite, R.A., J. Appl. Polym. Sci., Vol. 112, pp 2010 **(2009)**.

[19] McManus, A.J.; Doremus, R.; Siegel, R.; Bizios, R., J. Biomed. Mater. Res. A, Vol. 72, pp 98 **(2005)**.

[20] Kasuga, T.; Maeda, H.; Kato, K.; Nogami, M.; Hata, I.; Ueda, M., Biomaterials, Vol. 24, pp 3247 **(2003)**.

[21] Kasuga, T.; Ota, Y.; Nogami, M.; Abe, Y., Biomaterials, Vol.22, pp 19 **(2001)**.

[22] Marras, S.I.; Zuburtikudis, I.; Panayiotou, C., Eur. Polym. J., Vol. 43, pp 2191 **(2007)**.

[23] Carrascoa, F.; Gamez-Perez, J.; Santanac, O.O.; Maspoch, M.L.L., Chem. Eng. J., Vol.178, pp451 **(2011)**.

[24] Chow, W.S.; Lok, S. K.; J. Thermo. Comp. Mater., Vol. 21, pp 265 **(2008)**.

[25] Kusmono; Ishak, Z.A.; Chow, W.S.; Takeichi, T.; Rochmadi, Euro. Polym. J., Vol. 44, pp 1023 **(2008)**.

[26] Chow, W.S.; Lok, S.K., J. Therm. Calorim., Vol. 95, pp 627 **(2009)**.

[27] Kumar, M.; Mohanty, S.; Nayak, S.K.; Parvaiz, M.R., Biores. Techn., Vol. 101, pp 8406 **(2010)**.

[28] Li, Y.; Shimizu, H. Macromol Biosci, Vol.7, pp 921 **(2007)**.

[29] Balakrishnan, H.; Hassan, A.; Wahit, M.U.; Yussuf, A.A.; Abdul Razak, S.B., Mat. Des., Vol. 31, pp 3289 **(2010)**.

[30] Lee, J.B.; Lee, Y.K.; Choi, G.D.; Na, S.W.; Park, T.S.; Kim, W.N., Polym. Degrad. Stab., Vol. 96, pp 553 **(2011)**.

[31] Nijenhuis, A.J.; Colstee, E.; Grijpma, D.W.; Pennings, A.J., Polymer, Vol. 37, pp 5849 **(1996)**.

[32] Theryo, G.; Jing, F.; Pitet, L.M.; Hillmyer, M.A., Macromolecules, Vol. 43, pp 7394 **(2010)**.

[33] Ishida, S.; Nagasaki, R.; Chino, K.; Dong, T.; Inoue, T., J. Appl. Polym. Sci., Vol. 113, pp 558 **(2009)**.

[34] Petchwattana, N.; Covavisaruch, S.; Euapanthasate, N., Mat. Sci. Eng. A, Vol. 532, pp 64 **(2012)**.

Chapter II

General Background and Litterature Review

Chapter II - General Background and Literature Review

II-1 Composites

Polymers are versatile materials with good properties and low price that have been widely used in many applications as substitutes for metals, ceramics, glass, wood etc. However, polymers exhibit low mechanical, physical, thermal properties that are inadequate for some application domains, therefore they are generally modified to meet desired characteristics and comply with performance requirements. The most common method of polymer modification is mixing polymers with fillers to form polymer composites of tailored specific properties.**[1-8]**

The concept of combining materials to form composite materials is not new, but has been a common practice since the antiquity. The ancients Israelites used mud and chopped straw to produce bricks, the Egyptian sarcophagi were made from glued wood laminates,**[9]** Romans used ground marble as reinforcement in their mortar,**[10]** and Mangol warriors' bows were fabricated from cattle tendons, wood and silk bonded together.**[11]** A composite is a structural multiphase material made up of two or more distinct components mixed together at a macroscopic scale to form a synergistic assembly that exhibits the characteristics of both components. Even though the components of the composite are physically and chemically identifiable in the composite, the composite behaves as a single product with highly improved performance far superior to its original individual constituents acting independently.**[3,5,6]**

The high content component in a composite forms the continuous phase known as the matrix and the low content constituent that is embedded in the matrix makes the dispersed reinforcing phase. The region of contact of these two phases is called the interface/interphase that is also considered as a separate third phase that controls adhesion between the components of the composite and through which the properties change from one side to another.**[5-8,12]** Depending on the type of the matrix, composites can be categorized as ceramic, carbon, metallic and polymer matrix composites. The continuous matrix constitutes the binder that holds the components of

the composite together; it protects the reinforcement and acts as the main load-bearing phase, thus governing the properties of the composite. The second phase, which is dispersed into the continuous phase, is stiffer, harder and stronger than the matrix that imparts structural properties like strength, stiffness and thermal/dimensional stability to the final composite.**[1,2,5-8]**

Polymer-matrix composites are the most developed composites since they offer interesting advantages over other type of composites such as light weight, low cost, ease of processing and fabrication at low temperatures and pressures. The matrix can be thermoplastic, thermoset or rubber, and the filler/reinforcing agent can be organic or inorganic, synthetic or natural with certain geometries and shapes such as fibers, flakes, spheres, whiskers, platelets, or particles.**[4,6-8]** Both natural and synthetic fillers have been traditionally used in polymers as extending additives to lower cost, or as functional fillers to impart changes in various behaviors such as electrical conductivity/insulation, thermal and magnetic properties, thermal stability, density, optical and acoustical properties effects etc.. Composites can be classified according to the type of the matrix (metallic, ceramic, carbon and polymeric), to the shape of the reinforcement (particulate, fibrous, laminar) or to the size of the reinforcement (macrocomposites, microcomposites and nanocomposites).**[2-8]**

The performance of a composite is dictated not only by the properties of its constituent phases and their relative amounts, but also by the shape, size, distribution and orientation of the reinforcing component as well as on adhesion between the reinforcement and the matrix at the interface.**[1-5,8,9]** The extent of adhesion between the phases is a critical factor for effective transmission of load from the matrix to the reinforcement. The strength of the interface is significantly affected by several interrelated parameters such as surface tension between the constituents, interfacial bonding, molecular orientation/conformation at the interphase, chain entanglement and polymer mobility.**[13]**

Polymer composites have been developed since the Second World War as a consequence of increasing demand of materials that are stiffer and stronger, but yet lighter. Since then, the development of new and improved composites manufacturing

processes and design flexibility offered by these materials provided unlimited selection of properties and product opportunities with low cost making thus composites the common engineering materials that are designed and manufactured for diverse application domains. Modern composites have found widespread end uses in miscellaneous fields such as sports, aeronautic, automotive, marine, construction, civil engineering and other structural applications.**[1-5,14]**

In conventional polymer composites the content of macro and/or microscale fillers may reach up to 40% and more. At this level of reinforcement the design limits of optimizing composites is reached due to property trade-off such as for instance stiffness is traded-off for toughness, and toughness is obtained at the cost of optical clarity.**[1-3,5,7,8]** It has been demonstrated that such compromises can be overcome if the size of the filler is scaled down to the nanoscale size dimensions.**[14,15]**

Recently, nanotechnology has been successfully used to develop nanoscale particles and fillers that are used to develop and to produce new generation of composites known as nanocomposites to solve and overcome limitations observed with traditional composites. Nanocomposites are particulate filled composites containing fillers with at least one dimension at the nanoscale level and exhibiting unlimited combinations of composites properties at filler level as low as 5-10% that are impossible with conventional composites at this filler content.**[14-20]**

II-2 General Aspects of Polymer Nanocomposites

Nature, which is the source of inspiration for human beings, contains exceptional nanocomposites such as spider silk, mother of pearl (nacre) and wood. Other nanocomposites examples can also be found in living organisms such as muscles, bones, enamel and dentine in teeth (**Figure II.1)**.**[19,21]** Recently the rapid progress in nanotechnology has been playing important role in numerous engineering fields to mimic these amazing materials.**[16,17,20]** In plastics area, nanotechnology allowed the synthesis and production of nanofillers that when incorporated into polymers resulted in the production polymer nanocomposites (PNCs) that are a new

and emerging class of composites exhibiting unexpected and unique properties as compared to traditional polymer composites.**[15,18]**

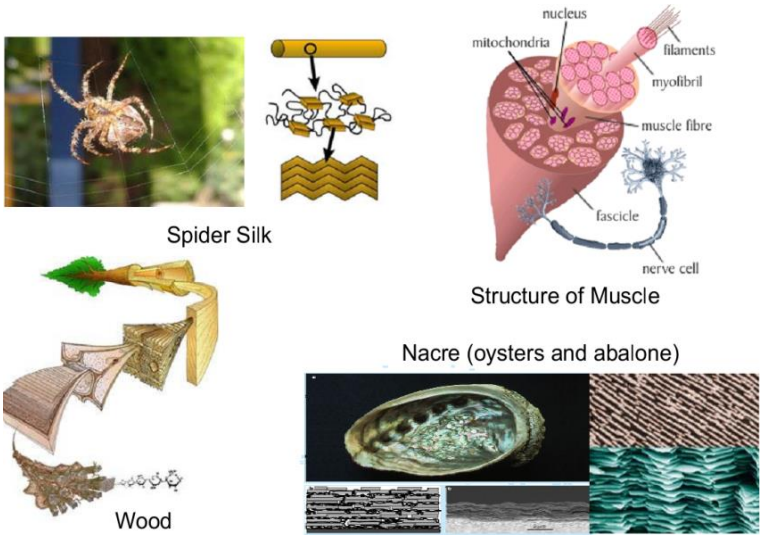

Figure II.1 Some Natural Polymer Nanocomposites: Spider silk, Muscle, Wood, and Mother of Pearl.**[21]**

The first breakthrough in the field of polymer nanocomposites was that reported on polyamide with montmorillonite developed by the Toyota research group,**[22,23]** followed by that of Vaia et al.**[24]** who have achieved the first melt intercalation of layered silicates using conventional plastics equipments. These two major findings have fuelled the interest in these new hybrid materials because of their performance and high potential for a variety of applications such as automotive, food packaging, electronics and many others.**[12,20,25-28]**

PNCs can be defined as particle-filled composites wherein at least one dimension of the dispersed filler is at the nanometer scale (1-100nm).**[29]**The synthesis of polymer nanocomposites is an integral aspect of polymer nanotechnology that has provided polymer industry with a new important class of structural materials that are suitable alternatives to conventionally filled polymers, because not only they exhibit outstanding enhancements in performance and properties at low filler concentration but most importantly they also show new value-added functional properties that are not observed in the unfilled polymers or in their conventional composites counterparts such as barrier properties, flame retardancy and others.**[12,14-**

29] These improvements include but not limited to enhanced modulus,**[30]** toughness,**[31]** thermal stability,**[32,33]** optical properties,**[33,34]** and reduced flammability,**[33,35]** permeability to gases,**[35,36]** and barrier properties.**[37]** These improvements are sensitive to the dispersion degree of the nanofiller within the polymer matrix that is in turn governed by components properties, composition, structure, the extent of polymer-filler interactions and preparation method as it is the case of any heterogeneous system including traditional polymer composites. **[15,38,39]**

Fillers used to prepare nanocomposites can range from isotropic (sphere) to anisotopic ones (sheet-like, nanotube etc.).**[28]** As illustrated in **Figure II.2**, nanofillers used to prepare nanocomposites can be distinguished in three main types of nanoreinforcements depending on the number of dimensions that are at the nanoscale range among the three spatial dimensions of the nanoparticle: **(i) nanoparticles (0D),** also known as iso- or zero-dimentional nanoadditives that have all three dimensions at nanometer scale like spherical silica nanoparticles and polyhedral silesquioxane (POSS), **(ii) fibrous** nanoadditives **(1D)** are distinguished by an elongated structure of two dimensions at the nanometer range such as carbon nanotubes (CNT), Halloysite nanotubes (HNT), and sepiolite and **(iii) nanolayers (2D)** characterized by one nanometric dimension that include for example montmorillonite (MMT), layered double hydroxide(LDH) and graphite.**[16,18,20,28,40-42]**

Example of the various types of inorganic nanofillers that have been used to prepare nanocomposites encompass layered particles like montmorillonite,**[43]** expanded graphite (EG),**[44]** mica,**[45]** layered double hydroxide (LDH),**[46,47]** nanoparticles such as SiO_2,**[48,49]** TiO_2,**[50]** Fe_3O_4,**[51]** $CaCO_3$,**[52,53]** polyhedral silesquioxane (POSS)**[54,55]** and also nanotubes including carbon nanotubes (CNT),**[56,57]** , holloysite nanotubes (HNT)**[58]** etc.. But, up to now, among all of these nanofillers, layered silicates have attracted the greatest interest, not only because of their availability and low cost but also because of their ease of processability and known chemistry. Carbon nanotubes are the second most reported fillers used to prepare special nanocomposites because of their high price.**[59]**

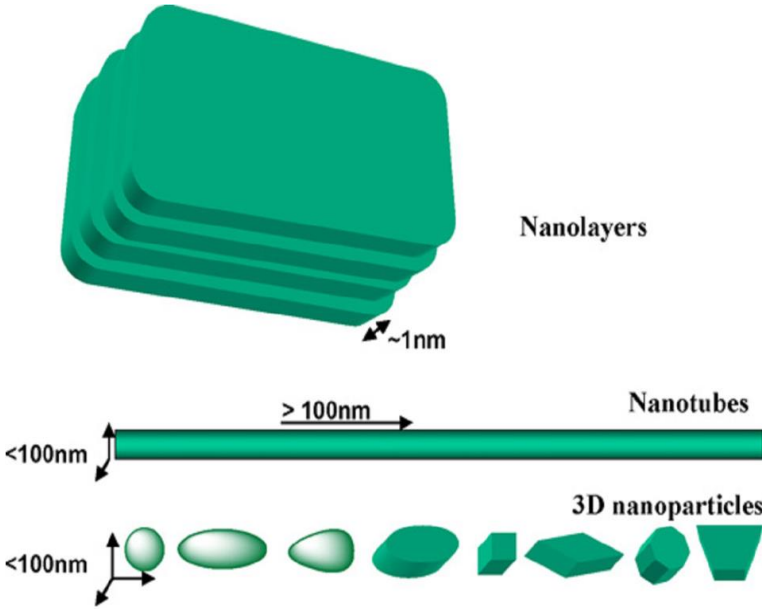

Figure II.2 Various Geometries of Nanoscale Fillers.**[20]**

When properly dispersed and individualized in a polymer, nanoadditives are effective at very low loading levels (2-5%) as compared to micro- and macro-sized particles (30-50%) owing to their ultra-large surface area to volume ratio (high aspect ratio) in which the distance between the nanoelements begins to approach molecular dimensions creating thus higher polymer-filler specific interfacial interactions than in conventional composites.**[15,16,28,40,60]** Consequently, these are the two main key factors behind the unusual and spectacular improvements observed for polymer nanocomposites since most of the chemical, physical and mechanical properties are governed by surfaces and surface properties.**[15,18,28]** In addition the low filler loadings provide ease of nanocomposites processing and additional advantages of light weight and low cost without, in general, compromising transparency.**[41,61]**

Despite the tremendous progress accomplished in the field on nanocomposites, both in theoretical fundamentals and experimental, there are yet some challenges to overcome such as finding out an effective synthesis method, issues related to dispersion and orientation of nanofillers and the cost effectiveness of these nanocomposites that is related to that of the nanofillers prices and to the volume rate of production.**[27,28]**

II-3 Polymer Layered Silicate (PLS) Nanocomposites

Polymer layered silicate nanocomposites are hybrid two-dimensional materials synthesized by the intercalation of a polymer or a mononomer (that is subsequently polymerized) inside the interlayer of layered filler.**[14-18,25-28]** During the last decades these new materials have received a great deal of attention from both academia and industry because they exhibit outstanding enhancements in a number of physical and mechanical properties including, stiffness, strength, thermal flammability resistance and gas barrier properties etc., compared to their parent polymers and to their conventional composites counterparts.**[25-28]**

There is a wide variety of both natural and synthetic-layered fillers that are able, under specific conditions, to intercalate a polymer.**[20,38-41,60],** Layered silicates, layered double hydroxide, natural flack graphite, metal phosphates and others represent typical examples of known layered nanoreinforcements (**Table II.1**).**[20,62]** Among the large variety of inorganic layered nanofillers that offer the possibility of intercalation by organic polymers, layered silicates are the most known and important nanofillers that have been and are still extensively studied and used in the preparation and design of PLS nanocomposites.

The exfoliating capability of layered silicates within the polymer matrix results in unique nanometer-size dispersion of layered silicate particles with high strength, huge aspect ratio and large specific surface area. **[12, 14-18, 38-41, 60-62]**This is very important in improving properties at very low reinforcement loadings (1-5%) of layered silicates in contrast to the high fraction loadings (~50%) used in their traditional composites counterparts. **[42,62]** Consequently, and in addition to their lightweight, this type of polymer materials are promising organic-inorganic composites both from economical and performance standpoints. **[12,14-18, 38-41]**

The unprecedented PLS nanocomposite dates back to the pioneering work achieved and reported by researchers at the Toyota Central Research and Development Laboratories in Japan.**[22,23]** This group of researchers developed Nylon6/clay hybrid nanocomposite by in situ polymerization of ε-caprolactam in the presence of 4 wt%

organically modified layered silicate (montmorillonite). The product that was intended for use in a timing belt cover for Toyota Camry exhibited a significant property improvement with 40% increase in tensile strength, 68% increase in tensile modulus, and an increase of 87°C in the heat distortion temperature (HDT) compared with pure nylon-6. The second breakthrough in the field of PLS nanocomposites was the work of Vaia et al.,**[24]** who have demonstrated that layered silicates can be admixed to polymers in molten state using existing plastics processing facilities, avoiding thus the use of solvents that are expensive and noxious for the environment. Since these two innovative findings, the concept of PLNCs has been expanded to all types of polymer matrices that resulted in new materials with broad range of improved properties. A great deal of research and developments have been accomplished in this field and some of PLNCs materials have already found some commercial applications.**[12,25-27]**

Table II.1 Potential Candidates of Layered Nanoparticles for Preparing Polymer Nanocomposites.**[20]**

S.No.	Group (type)	Examples
1.	Element	Graphite
2.	Oxides	Graphite oxide, V_6O_{13}, $HTiNbO_5$, $W_{0.2}V_{2.8}O_7$
3.	Phyllosilicates (pyrophyllite–talc, smectite, vermiculite, illite, mica, palygorskite–sepiolite, chlorite)	Kaolinite, dickite, nacrite, halloysite, chrysotile, antigorite, lizardite, montmorillonite, bentonite, nontronite, beidellite, colknskonite, hectorite, pyrophyllite, talc, vermiculite, illite, glauconite, muscovite, celadonite, phlogopite, taenolite, margarite (brittle mica), palygorskite, sepiolite, clinochlore
4.	Layered silicic acids	Kanemite, makamite, octosilicate, magadite, kenyaite, layered organo-silicates
5.	Mineral-layered hydroxides	Brucite ($Mg(OH)_2$), gibbsite ($Al(OH)_3$)
6.	Layered double hydroxides (LDHs)	$M_6A_{l2}(OH)_{16}CO_3 \cdot nH_2O$ (M: Al, Zn)
7.	Layered alumino-phosphates	Berlinite, vantasselite ($Al_4(PO_4)_3(OH)_3 \cdot 9H_2O$)
8.	Metal (M^{4+}) phosphates	M^{4+}: Zr, Ti or Sn; $Zr(HPO_4)$
9.	Chloides	$FeCl_3$, FeOCl, CdI_2, $CdCl_2$
10.	Metal chalcogenides	$(PbS)_{1.18}(TiS_2)_2$, TiS_2, MoS_2, MoS_3
11.	Cyanides	$Ni(CN)_2$

II-3-1 Layered Silicates

Among the wide variety of both synthetic and natural (organic or inorganic) layered fillers that are able of undergoing intercalation and/or exfoliation by host polymers, layered silicates materials have attracted great interest and special attention in numerous industrial fields. Layered silicates are natural or synthetic minerals consisting of ultrafine crystalline layers. Natural silicates are extensively used in

polymer nanocomposites owing to their versatility, natural abundance, low cost, ease of processing and environmentally friendliness.**[29,39,63,64] Figure II.3** illustrates a general classification of the most known natural silicates.

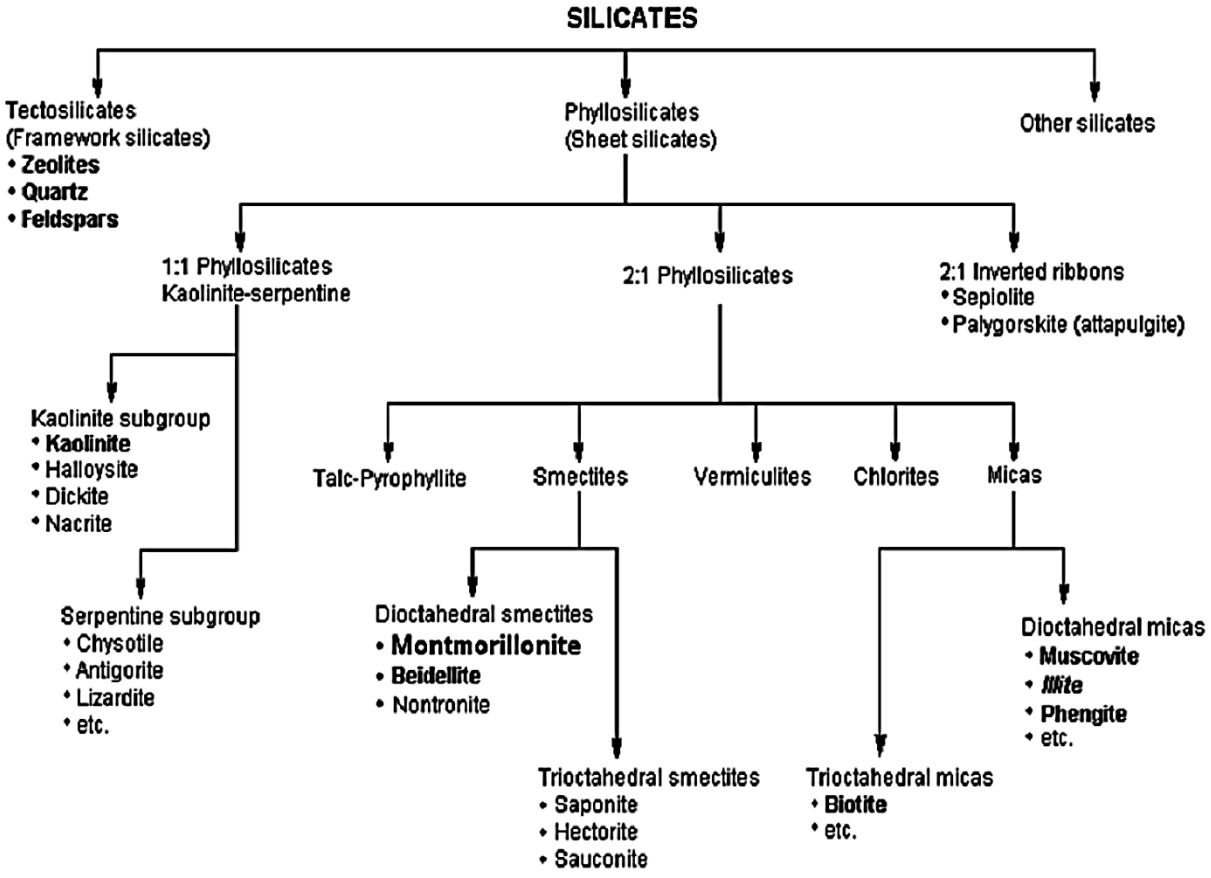

Figure II.3 Classifications of Silicates.**[65]**

Other particular interrelated features of layered silicates that are exploited in preparing nanocomposites are their moderate negative surface charge (cation exchange capacity "CEC"), their ability to disperse as high strength-high stiffness and high aspect ratio individual layers with significantly large specific surface area in excess of 750 m^2/g (700-800m^2/g in the case of montmorillonite),**[28,62,64,66-68]** and also their mastered surface chemistry that can be readily fine-tuned through ion exchange reactions with organic and inorganic cations.**[69-73]** All of these attributes make layered silicates the nanofillers of choice for the production of PLS nanocomposites, justifying thus why most of the studied nanocomposites evolved clay as inorganic reinforcing materials.

II-3-2 Phyllosilicates: Types, Structure and Properties

The most important layered silicates, commonly known as clay minerals or as nanoclays, belong to the phyllosilicates group; the structural unit of which is made up of tetrahedral (T) and octahedral (O) sheets. Depending on the stacking of these sheets within the crystal, three different types of phyllosilicates can be distinguished (**Table II.2**). The 1:1 or (T:O) are the non-swelling clays that have a crystal lattice consisting of one tetrahedral and one octahedral sheets, while that of the 2:1 (T:O:T) swelling clays is formed with the stacking of an octahedral sheet sandwiched between two tetrahedral sheets. The 2:1:1 or (T:O:T:O) type is made up of a 2:1 layer configuration with an additional octahedral sheet between the 2:1 layers.

Table II.2 Classification and Examples of Clay Minerals.**[28]**

Structure type	Group	Mineral examples	Ideal composition	Basal spacing (Å)
2 : 1(TOT)	Smectite	Montmorillonite	$[(Al_{3.5-2.8}Mg_{0.5-0.2})(Si_8)O_{20}(OH)_4]\ Ex_{0.5-1.2}$	12.4–17
		Hectorite	$[(Mg_{5.5-4.8}Li_{0.5-1.2})(Si_8)O_{20}(OH)_4]\ Ex_{0.5-1.2}$	
		Saponite	$[(Mg_6)(Si_{7.5-6.8}Al_{0.5-1.2})O_{20}(OH)_4]\ Ex_{0.5-1.2}$	
2 : 1(TOT)	Illite	Illite	$[(Al_4)(Si_{7.5-6.5}Al_{0.5-1.5})O_{20}(OH)_4]K_{0.5-1.5}$	10
2 : 1(TOT)	Vermiculite	Vermiculite	$[(Al_4)(Si_{6.8-6.2}Al_{.1.2-1.8})O_{20}(OH)_4]Ex_{1.2-1.8}$	9.3–14
1 : 1(TO)	Kaolin-serpentine	Kaolinite, dickite, nacrite	$Al_4Si_4O_{10}(OH)_8$	7.14

II-3-3 Structure of Phyllosilicates

The structural unit of phyllosilicates is made up of two tetrahedrally coordin ated silicon atoms fused to an edge-shared octahedral sheet of either aluminum or magnesium hydroxide as illustrated in **Figure II.4**. In the tetrahedral layer (silicate sheet SiO_4) silicone is the main component surrounded by 4 oxygen atoms, and the octahedral layer (gibbsite sheet) comprises divers metal types such as aluminum, magnesium, iron or lithium surrounded by 6 oxygen atoms or hydroxyls.**[39]**

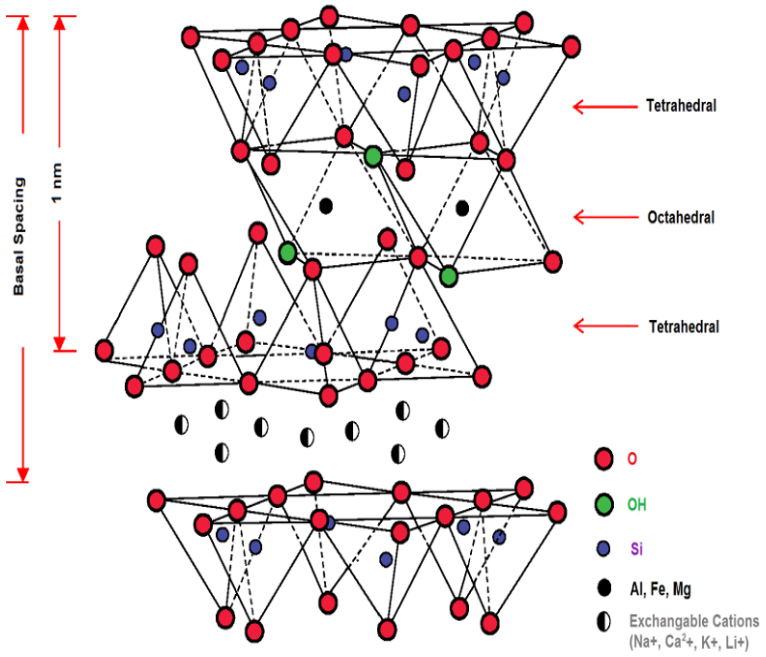

Figure II.4 Schematic Representation of the Crystal Structure of 2:1 Layered Phyllosilicate.**[74]**

The three layers constituting the lattice structure of the phyllosilicate form one clay sheet having a thickness around 1 nm and lateral dimensions ranging from 30 nm to several microns or even larger depending on the type of the clay.**[20,27-29,62-64,66,70-73,75-77]**Therefore, if properly dispersed and delaminated to individual sheets of the layered silicates lead to a reinforcement of very high aspect ratio (10-1000).**[28,29,66,67,72] Figure II.5** compares the dimensions of a glass fiber and a clay layer, and shows that the glass fiber is 3×10^9 times the size of a typical silicate layer. In other words, if the same volumes of glass fiber and silicate were evenly dispersed in a polymer, there would be roughly 10^9 fold excess of silicate layers, with an exponentially higher specific surface available.**[78]** This huge large interfacial area and the nanoscopic dimensions between constituents differentiate polymer layered nanocomposites from traditional composites and filled plastics.**[27-29,62-64]**

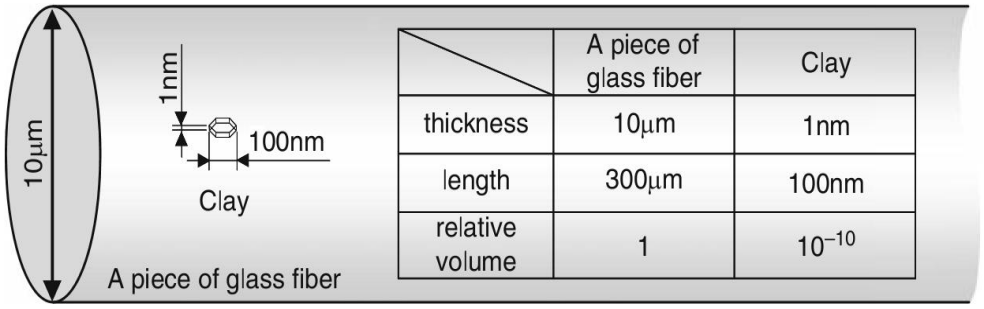

	A piece of glass fiber	Clay
thickness	10μm	1nm
length	300μm	100nm
relative volume	1	10^{-10}

Figure II.5 Comparaison of a Piece of Glass Fiber and a Clay.**[78,79]**

II-3-4 Cation Exchange Capacity (CEC) of Phyllosilicates

Isomorphic substitution of cations within the layers by others of low valence, for example Al^{+3} replaced by Mg^{+2} or Fe^{+2}, or Mg^{+2} replaced by Li^{+} in the octahedral layer, and Si^{+4} replaced by Al^{+3} or Fe^{+3} in the tetrahedral layer generates excess of negative electrostatic charges at the layers surfaces (charge deficiency), the quantity of which is a specific characteristic of each layered silicate. The negative charges are generally counterbalanced by hydrated alkali and alkaline earth cations (Na^{+}, Li^{+}, K^{+}, Ca^{+2} or Mg^{2+}) located inside the galleries.**[64,66,70,71,76]** The CEC is a mesure of the maximum capacity of the clay mineral to exchange its compensating cations. It measures the number of moles of monovalent cations that is possible to substitute to the exchangeable cations (Na^{+}, Li^{+}, K^{+}, Ca^{+2} or Mg^{2+}) to compensate the electric charge of 100g of calcinated clay at pH7.**[72]** CEC is generally expressed in meq(moles)/100g and is in the range 80-150 meq/100g for smectites **(Table II.2)**.**[39,42,63,64,70,75]**

II-3-5 Hierarchical Organization of Phyllosilicates Structure

Layered silicates possesses hierarchical organization defined by three levels of structures (**Figure II.6**).**[62,64]** The layer having a width varying from 10 nm to 1mm and a thickness of 1 nm, the primary particle composed of 5-10 stacked platelets that may contain hundreds to thousands of individual layers staking and held together by Van der Waals and electrostatic attraction forces between the cations and the platelets and the aggregate (agglomerate) is the association of primary particles orientated in all

the directions the size of which varies from 0.1 to 10mm.**[64,80]** Crystallite or tactoid is not a part of the layered silicate organization, but is a term widely used in literature that describes an assembly of layers made of compact face-to-face stacking of as many as 100 individual layers. Intercalated clay sheets consist of bundles of layers the galleries of which have been expanded by an intercalating agent.**[64]**

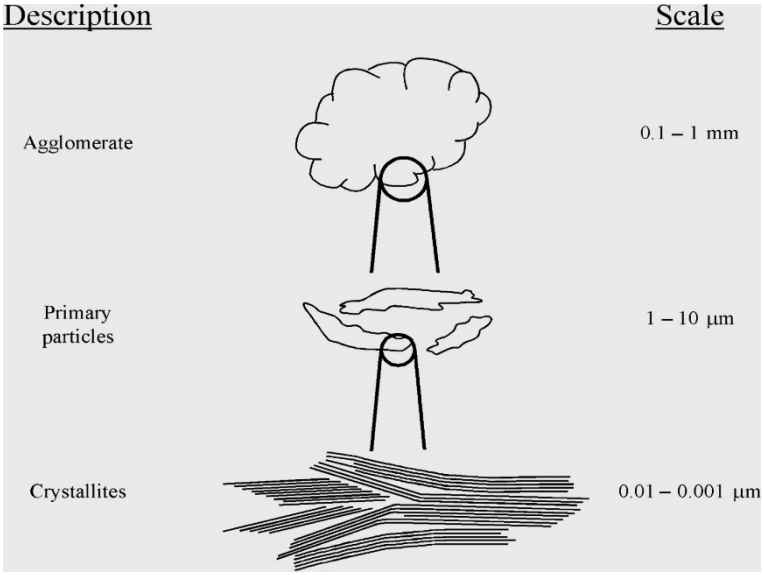

Figure II.6 A Schematic Overview of the Different Silicate Layer Organization Modes.**[62,80]**

II-3-6 Organically Modified Layered Silicates (OMLS)

As for MMT, all phyllosilicates are hydrophilic thereby require an organic treatment prior to be used as nanofillers for nanocomposites. Usually, the organomodification is carried out by replacing the compensating cations of the clay with long chain organophilic cations that are commonly organic cationic surfactants (onium ions) through cation-exchange reactions. The modified layered silicate is known as organically modified layered silicate and abbreviated "OMLS" which is also referred to as "organoclay".**[39,41]**

The cation-exchange process schematically represented in **Figure II.7,** not only improves the wetting characteristics of the inorganic host clay, but also swells the galleries spacings between the silicate layers owing to its bulky structure that are favorable changes for effective diffusion of monomer or polymer chains within the

intergalleries of the layered nanofiller during the PLS nanocomposite production. The extent of organic modification and initial layers expansion depend on the CEC of the clay and type of the surfactant.

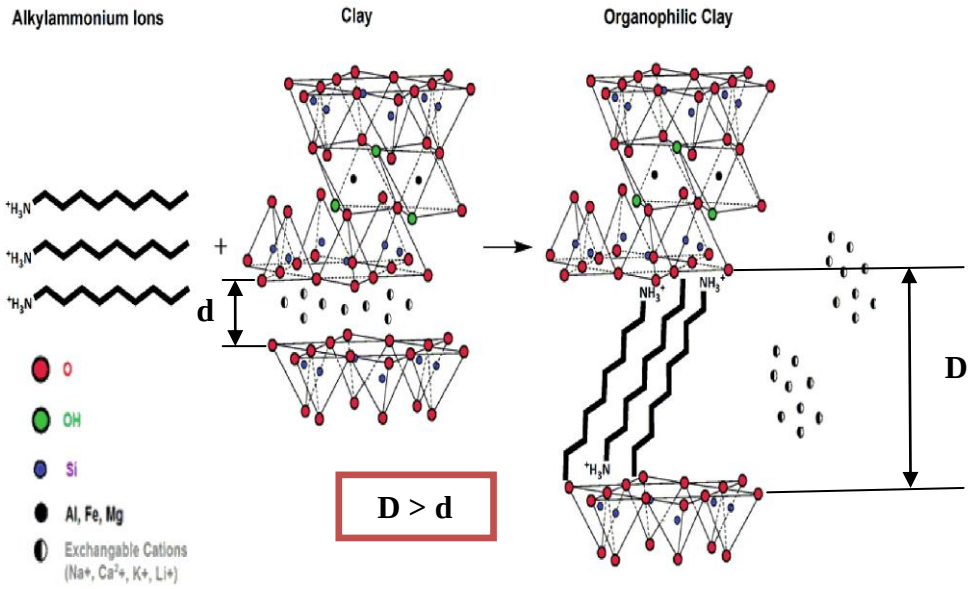

Figure II.7 The Cation-Exchange Process Between The Alkylammonium Ions and The Exchangeable Cations of Layered Silicate.**[74]**

The most common exchangeable surfactants bearing at least one long alkyl chain (C_{12}-C_{18} carbon atoms) include primary, secondary, tertiary or quaternary bulky organoalkylammonium salts.**[15,18,20,25-29,38,39,40,42,62-64,66,68-71,75-77,78]** However, other surfactants withstanding higher processing temperatures than alkylammoniums are also used such as, alkylphosphonium,**[81]** alkylimidazolium,**[82,83]** alkylstibonium compounds.**[84] Table II.3** lists some of the commercially available surfactants suitable for clays modification. Functional surfactants are generally preferred because they can provide opportunities for additional reactivity and interactions between the clay and the polymer that are favorable for better adhesion and strong interface between the components of the nanocomposites.**[39,40,42]**

Table II.3 Chemical Structure of the Most Commonly Used Surfactants for the Modification of Clays.**[85]**

Preparation method	Chemical formula	Abbreviations
Methyl tallow bis-2-hydroxyethyl quaternary ammonium	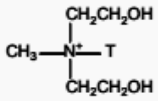	MT2EtOH
Dimethyl benzyl hydrogenated tallow quaternary ammonium	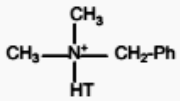	2MBHT
Octadecyl amine	CH3(CH2)16CH2NH2	ODA
Dimethyl octadecyl amine	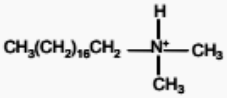	2MODA
Hexadecyltrimethyl ammonium	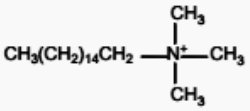	3MODA
Dodecyl trimethylphosphonium	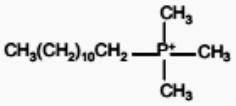	BtC10P

The surfactant chains inside the interlayers of the clay arrange themselves into monolayer, bilayer, pseudo-trimolecular layer, or inclined paraffin structure (**Figure II.8**). These possible chain aggregations determine the initial increase of the clay interlayer spacing and are function of layer charge density of the clay, temperature and the surfactant chain length.**[39,73,80,86]**

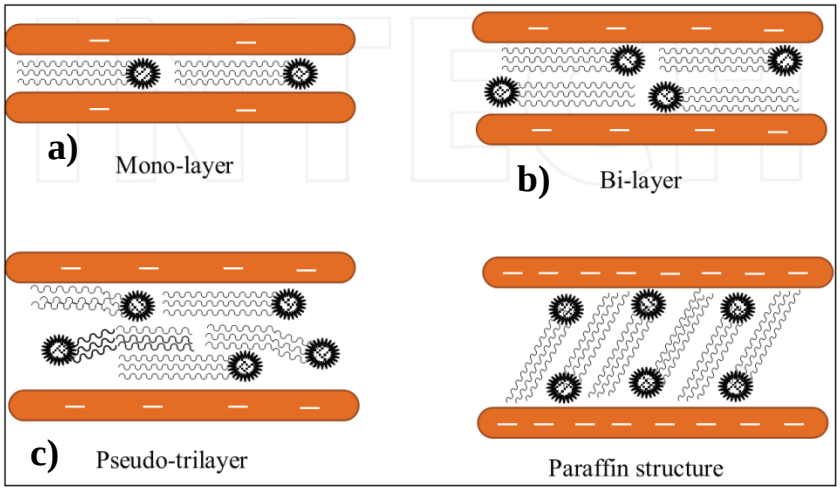

Figure II.8 Alkyl Chain Aggregation in Layered Silicates: **(a)** monolayer, **(b)** bilayer, **(c)** pseudo-trilayer and **(d)** paraffin-type monolayer.**[87]**

Beside the commonly known cation-exchange method used for clay modification, other original modification techniques that are of practice include organosilanes grafting,**[88-90]** ionomers**[91]**or block copolymers adsorption.**[92]** In complement to clay organic modification, a polymeric compatibilizer can also be used to further enhance clay dispersion.**[93-95]**

II-3-7 Montmorillonite (Smectite clay)

The most widely investigated layered silicates for preparing nanocomposites are the 2:1 (T:O:T) phyllosilicates especially the smectite group that encompasses montmorillonite, hectorite, saponite and beidellite (**Figure II.4**). Typical synthetic 2:1 phyllosilicates are fluorohectorite, Fluoromica, laponite and magadiite,**[29]** while natural ones include mica, pyrophyllite-talc, brittle mica, smectite, vermiculite, and illite.**[20,25,86]** **Table II.4** lists some of the most important properties of these valuable phyllosilicates.

Table II.4 Structure, Chemistry and Some Properties of Commonly Used 2:1 Phyllosilicates.**[70]**

2:1 phyllosilicates	Chemical formula	CEC (mequiv/100 g)	Particle length (nm)
Montmorillonite	$Mx(Al_{4-x}Mg_x)Si_8O_{20}(OH)_4$	110	100–150
Hectorite	$Mx(Mg_{6-x}Li_x)Si_8O_{20}(OH)_4$	120	200–300
Saponite	$MxMg_6(Si_{8-x}Al_x)Si_8O_{20}(OH)_4$	86.6	50–60

M, monovalent cation; *x*, degree of isomorphous substitution (between 0.5 and 1.3).

Among these smectite layered silicates, montmorillonite has evoked the greatest interest for nanocomposites because of its natural abundance, wide commercial availability and its unique features such as high swellable (expandable) layered structure, moderate surface charge (CEC of 70 to 120 meq/100 g, and more importantly its huge surface area of 750 m^2/g, and its high aspect ratio in the range 100-1000 if it is completely exfoliated. Also of central interest is the existence of readily exchangeable cations that allow for organic substitution (modifications).**[28,39,62,64,68,70-72]** **Table II.5** summarizes some of the most important characteristics of MMT.

Table II.5 General Properties of Montmorillonite.**[78]**

Properties			
Swelling		ml/2 g	65
pH (2% aqueous dispersion)		–	10.2
Electric conductivity		μS/cm	675
Viscosity (4% aqueous dispersion)		mPa s	280
Visible light transmittance (1% aqueous dispersion)		%	1
Particle diameter		nm	100–2,000
Specific surface (N_2, BET)		m^2/g	20
MB (methylene blue) absorbed amount		mmol/100 g	130
Cation exchange ability		meq/100 g	108.6
Precipitation cation amount	Na^+	meq/100 g	114.1
	K^+	meq/100 g	2.8
	Mg^{2+}	meq/100 g	3.4
	Ca^{2+}	meq/100 g	18.2
Chemical composition	SiO_2	%	64.4
	Al_2O_3	%	25.9
	Fe_2O_3	%	3.5
	MgO	%	2.4
	CaO	%	0.7
	Na_2O	%	2.3
	K_2O	%	0.1

Montmorillonite is a naturally-occurring hydrous aluminosilicate clay mineral mined for the first time in Montmorillon (France) from which its name is derived.**[28,72]** Chemically it is hydrated sodium calcium aluminum magnesium silicate hydroxide $M_x(Al_{4-x}Mg_x)Si_8O_{20}(OH)_4$ nH_2O where x and n vary depending on the type of clay and degree of hydration.**[39,63,66,70]** In its native state, the crystal structure of MMT is similar to that of talc and mica, but with different layer charge density which makes it more attractive for nanocomposites.**[25,96]** The structure of MMT is composed of layers made up of octahedral sheet of either aluminum or magnesium hydroxide sandwiched between two tetrahedral silica layers.**[70]** The presence of hydrated cations (Na^+, K^+ etc.) in the galleries confers to the pristine MMT hydrophilic character that hampers its homogeneous dispersion in the majority of polymers that are mostly hydrophobic, and as such it can only be miscible with hydrophilic polymers.**[72]** To address this issue, and to make MMT clay compatible with a wide range of polymers, organic modification of the clay is required to match its polarity with that of the hydrophobic polymers. The treated MMT is converted from hydrophilic to organophilic or hydrophobic generally known as an organically modified montmorillonite (OMMT).**[78]** **Table II.6** gives a non-exhaustive list of some commercially available organically modified montmorillonites (OMMT).

Table II.6 Commercial (O)MMT and their Characteristics.**[66]**

Commercial clays Supplier/trade name/designation		Clay type	Organomodifier type	Modifier concentration (meq/100 g)	Δw[a] (%)	*d*-spacing (Å
Southern Clay Products (USA)						
Cloisite®Na	CNa	MMT	–	–	7	11.7
Cloisite®15A	C15A	MMT	$N^+(Me)_2(tallow)_2$	125	43	31.5
Cloisite®20A	C20A	MMT	$N^+(Me)_2(tallow)_2$	95	38	24.2
Cloisite®25A	C25A	MMT	$N^+(Me)_2(C_8)(tallow)$	95	34	18.6
Cloisite®93A	C93A	MMT	$NH^+(Me)(tallow)_2$	90	37.5	23.6
Cloisite®30B	C30B	MMT	$N^+(Me)(EtOH)_2(tallow)$	90	30	18.5
Süd-Chemie (Germany)						
Nanofil®804	N804	MMT	$N^+(Me)(EtOH)_2(tallow)$		21	18
Laviosa Chimica Mineraria (Italy)						
Dellite® LVF	LVF	MMT	–	105	4–6	9.8
Dellite® 43B	D43B	MMT	$N^+(Me)_2(CH_2\text{-}\phi)(tallow)$	95	32–35	18.6
CBC Co. (Japan)						
Somasif	MEE	SFM	$N^+(Me)(EtOH)_2$(coco alkyl)	120	28	
	MAE	SFM	$N^+(Me)_2(tallow)_2$	120	41	

Tallow: ~65% C_{18}; ~30% C_{16}; ~5% C_{14}.
[a] %Weight loss on ignition.

II-4 Structures of Polymer Layered Silicate Nanocomposite

The key to the high performance of a PLS nanocomposite is related to how well the nanoclay is dispersed into the polymer matrix.**[26]** On mixing a layered silicate with a polymer, the main target is to achieve a true nanocomposite characterized by homogeneous clay dispersion throughout the matrix phase at nanometer scale wherein the platelets are individually separated in order to take the maximum advantage from its incorporation.**[38]**

It is not always possible to end up with a nanocomposite when clay is admixed to a polymer. Individualization (exfoliation) of nanoclay layers is generally not an easy task, and it still remains a major central scientific issue and technical challenge for materials scientists due to the large lateral dimensions of the layers (1 mm or larger), high intrinsic viscosity of the polymer resins, and strong tendency of clay platelets to agglomerate.**[78] Figure II.9** exhibits the possible structures that can be obtained when mixing layered silicates with polymers, and **Figure II.10** shows these structures along with examples of their transmission electron microscopy (TEM) images and their related XRD patterns.**[26]** Depending on the polymer/clay interactions, the nature of the components, the clay loading, and the method and conditions of the nanocomposite preparation, three main morphologies governed by interplay of

entropic and enthalpic factors are thermodynamically possible viz., phase-separated/immiscible, intercalated and exfoliated structures.**[69,70, 80]**

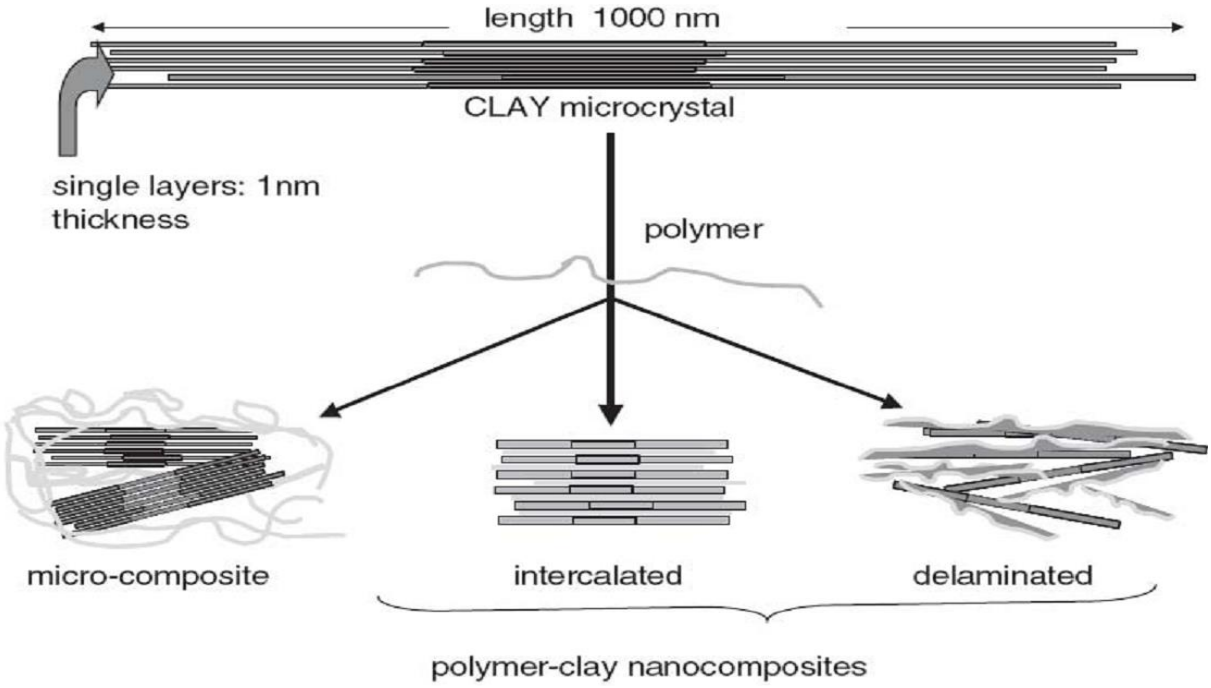

Figure II.9 Schematic Representation of Possible Composite Formation with Layered Silicates.**[97]**

II-4-1 Phase-Separated Composites (microcomposites)

A phase separated composite is obtained when there is immiscibility between the polymer and the clay owing to a mismatch of surface energy between the components. In such case the polymer is unable to penetrate into the interlayer spaces between the sheets of the layered silicate, consequently the clay conserves its original structural state made up of large stacks of layers (tactoids) and/or agglomerates (**Figure II.10(a)**). Therefore, the clay acts as traditional microscale filler and the formed composite behaves in terms of performance much like a conventional micrococomposite the properties of which are only slightly improved, if not decreased. X-ray scan (XRD) of phase separated composites exhibit the same characteristic peak or peaks of the sole clay at the same position and with the same intensity (**Figure II.10(a)**).

II-4-2 Intercalated Nanocomposites

This common type of nanocomposites results when polymer chains partially enter into the clay galleries without being able to break up totally the attractive forces that hold clay sheets face to face and regularly spaced. As a result, a well-ordered multilayer morphology builds up with alternating polymeric and inorganic layers in which the distance between the layers is moderately expanded (few nanometers), while the clay layers still retain its periodic stacking order with galleries (d spacings) in the range 20-80Å.**[80]** This intercalated structure is an intermediate morphology between phase separated and exfoliated structures and consequently it is suggested as the precursor structure for complete exfoliation of the clay. The XRD of an intercalated nanocomposite shows a shift to lower angle of the characteristic peak or peaks of the pristine clay (**Figure II.10(b)**), and in general the enhancement in properties is moderate. Under some conditions, and because of the hydroxylated edge to edge interactions between silicate layers of the clay, an intercalated/flocculated structure can also form which is conceptually similar to that of an intercalated nanocomposite.**[70]**

II-4-3 Exfoliated Nanocomposites

In exfoliated or delaminated nanocomposites the ordered layered structure of the clay is broken down owing to the extensive polymer chains insertion into clay basal spacing that totally separates the clay sheets and distorts the clay crystal morphology in such a way that the clay sheets exhibit no long-range order or parallel multilayer stacking and no apparent inter-particle interactions, exhibiting thus higher phase homogeneity than intercalated counterparts (**Figure II.10(c)**).**[29]** Such structure consists of silicate particles that are completely delaminated to single individually separated sheets at nanoscale dimension (~1nm thick) that are uniformly and randomly distributed throughout the continuous polymer matrix. The exfoliation of clay sheets increase the aspect ratio of the nonofiller and makes the whole surface of the clay available for increased interfacial contact with the polymer matrix. Consequently polymer-clay interactions are maximized which enables to capitalize the benefits from layered silicates and should lead to better clay dispersion and ultimate improvements in nanocomposite properties and performance.**[38,68,78]**

This structure is characterized by the absence of any peak on the XRD pattern of the nanocomposites due to loss of the structural registry of the nanoclay layers. Note that, when mixing nanoclays with polymers, in general a mixture of these above discussed structures can be obtained resulting thus in a range of nanocomposites with structures from intercalated to exfoliated depending on the degree of penetration of the polymer chains into the silicate galleries.**[80]**

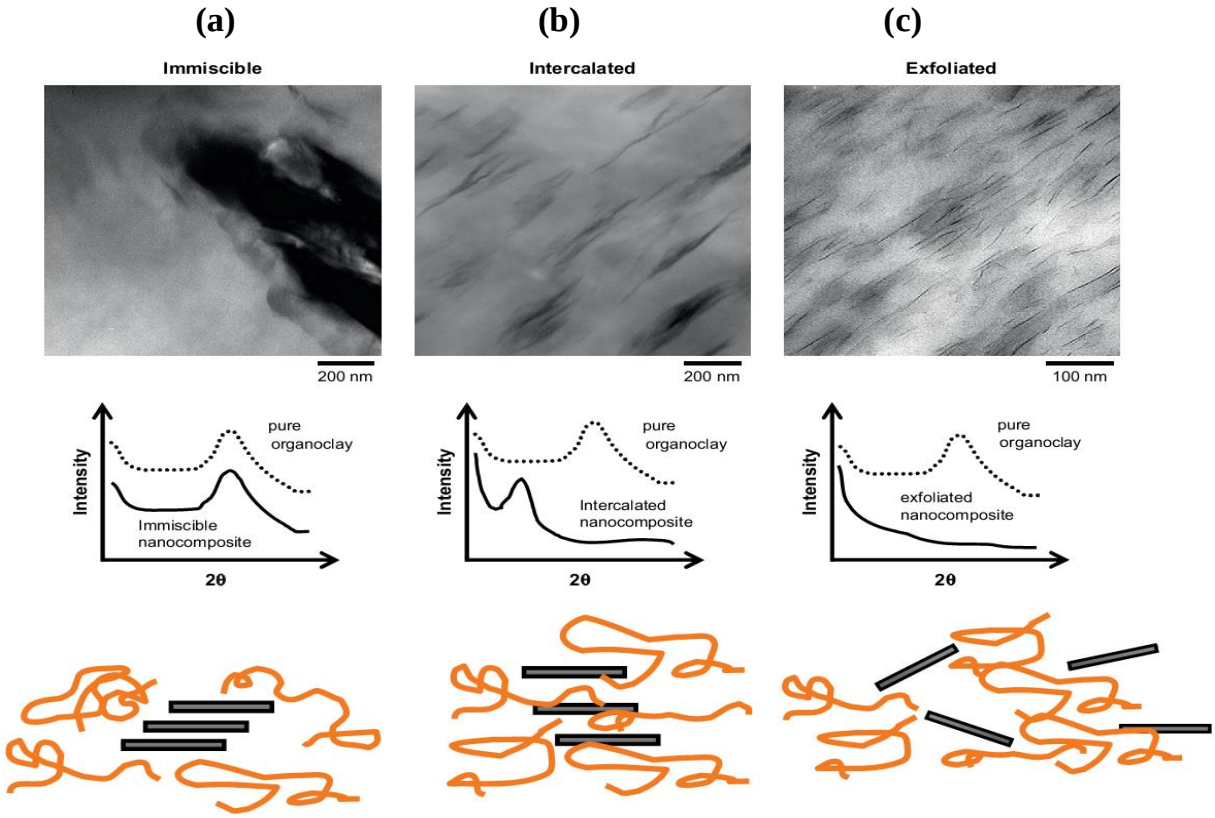

Figure II.10 Illustration of Different States of Dispersion of Organoclays in Polymers with Corresponding XRD Scans and TEM Micrographs.**[26]**

II-5 Preparation Methods of PLS Nanocomposites

Intercalation of polymer chains into the galleries of inorganic layered nanofillers, such as layered silicates/clays, has proven to be a successful approach to synthesize PLS nanocomposites.**[70]** Typically, three different techniques have been adopted to synthesize this type of polymer nanocomposites: solution intercalation method, in situ intercalative polymerization and melt intercalation processing.**[41]** The

selection of the appropriate fabrication method depends greatly on the type of polymer involved and to a large extent, on the nanofiller in question.**[85]**

II-5-1 Intercalation of Polymers or Prepolymers from Solution

This simple technique is illustrated in **Figure II.11**. It is based on a common solvent or a solvent system in which polymers or pre-polymers (in case of insoluble polymer) are soluble and the silicate layers are swellable.**[63,70]** In this procedure, selection of a proper solvent is therefore the primary criterion to achieve the desired level of silicate dispersion into the polymer.**[39]** Practically, the layered silicate is completely dispersed in an adequate organic solvent due to the weak van der Waals force that stacks the layers together, and the polymer is dissolved separately in the same solvent. When the polymer solution and the layered silicate dispersion are mixed, the polymer chains intercalate within the interlayer of the silicate and adsorb onto the expanded silicate sheets while the solvent is displaced out of the silicate galleries.**[63]** The resulting structure depends on the interaction between polymer and clay surface. One disadvantage of this method is that few exfoliated nanocomposites are prepared via this method, because in general, after solvent removal or polymer precipitation, the nanoparticles reassemble, sandwiching the polymer to form intercalated structure. **[39,76]** Among other shortcomes, is the large amount of solvent required by this methodology, which makes it costly, environmentally unfriendly with associated health and safety concerns. Furthermore, a compatible polymer-clay solvent system is not always available, limiting thus the applicability of this method.**[39,41]** Because of all these reasons, this technique is not effective and viable for industrial application.**[39]** Consequently it is limited to laboratory scale and research purposes.**[64,85]** Nevertheless, this method is suitable to prepare nanocomposites based on water soluble polymers (PEO, PAA, PVA) and layered silicates because both ingredients are hydrophilic permitting favorable interactions in the aqueous solutions eliminating thus clay and/or polymer modification step.**[41]**

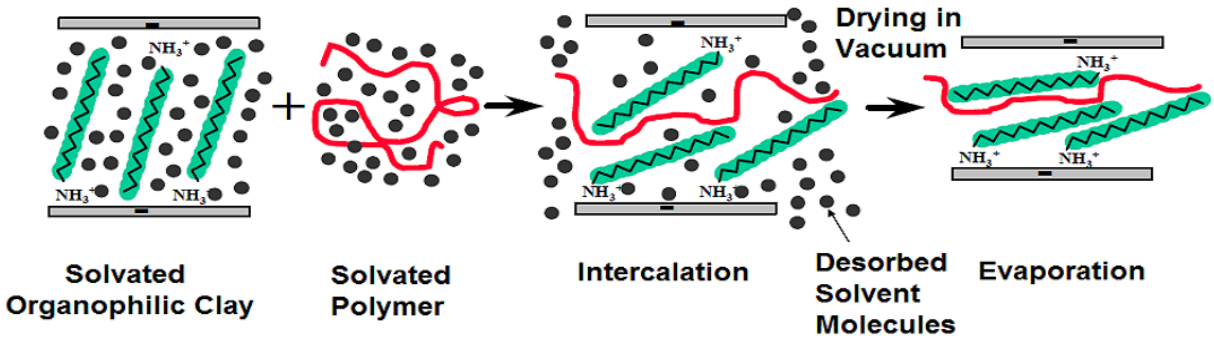

Figure II.11 Schematic Representation of the Solution Intercalation Method.**[98]**

II-5-2 In Situ Intercalative Polymerization Method

This technique was first used by the Toyota research group in their pioneering work to produce polyamide-6/clay nanocomposites.**[22,23]** This method is a two-step process as schematically described in **Figure II.12**.

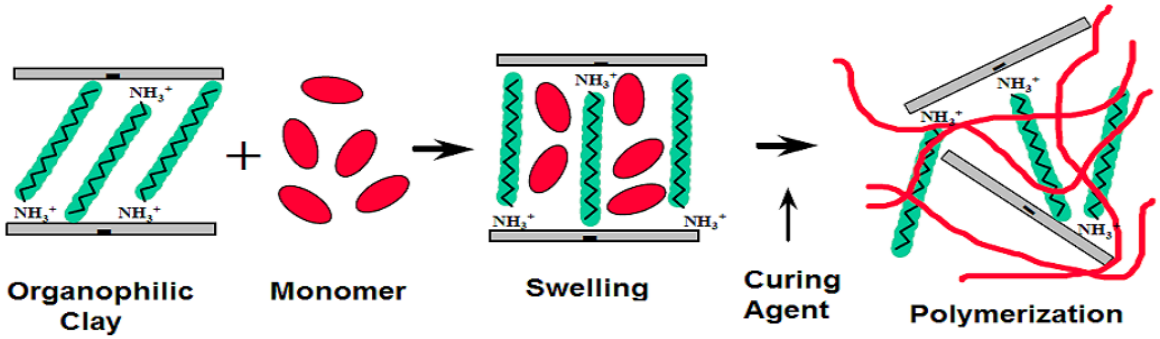

Figure II.12 Schematic Representation of the in situ Polymerization Method.**[98]**

For most thermoset polymers, in situ polymerization is the only viable method to prepare nanocomposites.**[41]** The layered silicate, either natural or modified, is firstly swollen with a liquid monomer or a monomer solution assisted by mechanical mixing. The swelling step requires high shear mixing for high diffusivity rate of the monomer into the clay galleries and also a certain period of time depending on the polarity of the monomer, the surface modification of the clay and the swelling temperature.**[38]** Therefore by tailoring the interactions between the monomer, the surfactant, and the clay surface, exfoliated nanocomposites are readily achievable.**[41]** Polymer formation takes place in the second step through polymerization reaction (emulsion, solution, bulk, or suspension) in the confined spaces between the silicate layers. As the reaction proceeds, expansion and dispersion of the nanoclay enhance

and the obtained nanocomposite exhibits in most of the cases a fully exfoliated structure.**[63]** Tough this technology results in the highest clay dispersion level among the other preparative methods, the presence of additives in the system that complicate the reaction conditions, and the high capital investment of this procedure make the production of nanocomposites by this method unlikely in industry.

II-5-3 Melt Intercalation Method

The process of the melt intercalation technique, which was first reported by Vaia and coworkers,**[24]** is schematically represented in **Figure II.13**. In this technique, the polymer is mechanically melt-mixed with an appropriately modified layered silicate above the softening point of the polymer.[**70**]

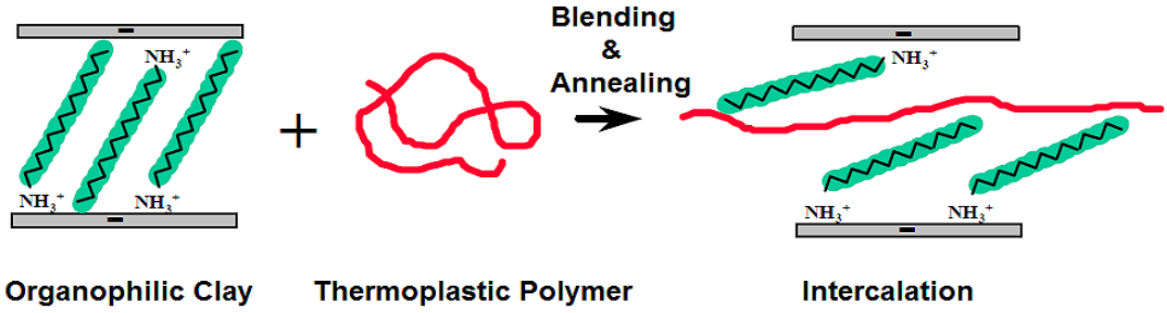

Figure II.13 Schematic Representation of the Melt Intercalation Process.**[98]**

If the clay is sufficiently compatible with the polymer, the high shear imposed on the melt is transmitted to the clay particles which peels off the clay platelets when the hydrodynamic separating forces exerted by the molten matrix exceed the cohesive forces between clay platelets. This high shear also permits the polymer chains to diffuse from the bulk polymer melt into the galleries between the silicate layers (**Figure II.14**).**[64]** This mechanism allows production of a wide range of nanocomposites with structures from intercalated to exfoliate depending on the degree of penetration of the polymer chains into the silicate galleries.**[20,63]** In addition to the polymer/clay compatibility, degree of clay dispersion by this technique is dependent on various key parameters that have to be optimized including: residence time, level of shear, operating conditions of the processing equipment, polymer/clay composition and preparation.**[26,80]**

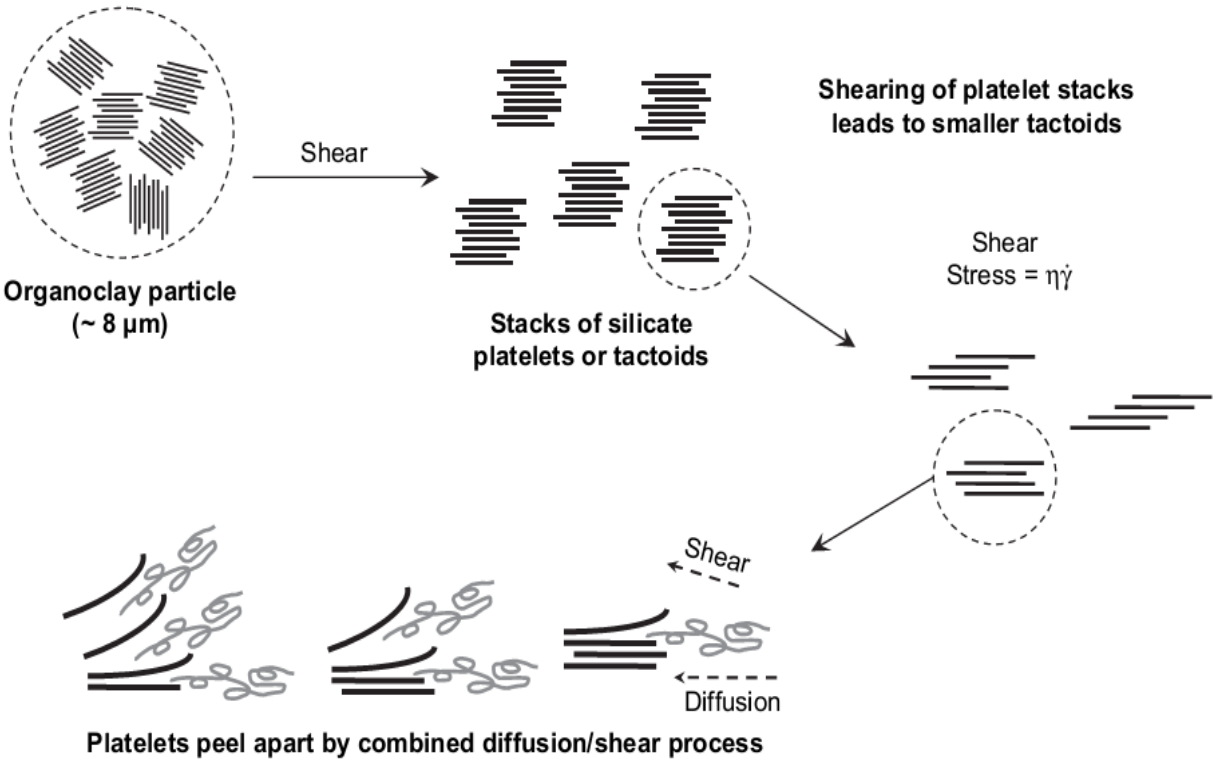

Figure II.14 Mechanism of Organoclay Dispersion and Exfoliation During Melt Processing of Nanocomposites**.[99]**

Nowadays, this solvent free technique is the most attractive and has become standard for the production on large volume scales of various PLS nanocomposites because it offers many advantages over either in situ intercalative polymerization or polymer solution intercalation.**[63,77]** For example, it is environmentally benign because it does not require any solvent which helps avoiding environmental hazards, and is also economically viable because it uses available processing equipments such as extruders, injection molding machines etc., reducing thus the capital investments.**[63,70,73]** Furthermore direct melt intercalation allows the preparation of nanocomposites from polymers which were not possible to process using in situ polymerization or solution intercalation methods.**[63,70]** The main disadvantages of the melt intercalation is related to a low thermal stability of the onium modifiers,**[39]** and 100% exfoliated structures at clay concentrations greater than about 4 wt% have not been possible yet.**[72]**

In conclusion, melt intercalation is the most attractive because it is versatile and aligns well with the currently established industrial equipments. The other two methods are limited owing to environmental concerns triggered by their use of solvents and monomers which are also costly and not readily available.[**41] Table II.7**, depicts a comparative summary of these preparative techniques together with their advantages**,** limits, and some examples.**[100]**

Table II.7 General Features of Processing Techniques of PLS Nanocomposites.**[100]**

Processing	Drive Force	Advantages	Disadvantages	Examples
In-situ polymerization	Interaction strength between monomer and silicate surface: enthalpy evolvement during the interlayer polymerization.	Suitable for low or non-soluble polymers: a conventional process for thermoset nanocomposites.	Silicate exfoliation depends on the extent of silicate swelling and diffusion rate of monomers in the gallery: oligomer may be formed upon incompletely polymerization.	Nylon 6, epoxy, polyurethan, polystyrene, polyethylene oxide, unsaturated polyesters, polyethylene terephthalate.
Solution approach	Entropy gained by desorption of solvent, which compensates for the decrease in conformational entropy of intercalated polymers.	Prefer to water-soluble polymers.	Compatible polymer-silicate solvent system is not always available; use of large quantities of solvent; co-intercalation may occur for solvent and polymer	Epoxy, polyimide, polyethylene, polymethylmethacrylate
Melt Intercalation	Enthalpic contribution of the polymer-organosilicate interactions.	Environmental benign approach: no solvent is required.	Slow penetration of polymer within the confined gallery.	Nylon 6, polystyrene, polyethylene terephthalate.

II-6 Biodegradable polymers

II-6-1 Introduction

During the past century, plastics markets have been essentially supplied by petrochemical-based polymers. These have been extensively used in various applications areas to meet our daily needs including packaging, construction, aerospace, automotive, sports, agriculture and medical. Undoubtedly, this is due to their low cost, high speed production, ease of fabrication, light weight and high mechanical performance over traditional materials such as metals, glass and others.**[19,29]** Being derived from nonrenewable fossil fuel and gas resources these plastics are persistent to chemical, physical, and biological degradation. Therefore once discarded in nature after their service life, their wastes, are not biodegraded but accumulated in landfills owing to increasing difficulties of these wastes disposal.**[42,72]** This plastic pollution brings about severe environmental and ecological concerns that have to be solved in the near future. Recycling, incineration and burial of these wastes in landfill sites are the popular approaches for plastics waste management to keep the environment free from these plastics wastes. However these methods are not 100% efficient and not often feasible to solve totally the problem because each has its own advantages and disadvantages regarding economical, processing, and technological aspects.**[72,75]** Disposal of these persistent plastics wastes by incineration and/or pyrolysis suffers considerable public opposition because it always releases large amount of carbon dioxide, noxious and toxic gases which contribute to global warming and pollution. On the other hand, wastes burial faces decreasing availability of satisfactory landfills and will remain buried for thousands of years without rotting constituting a time bomb for the next generations.**[42]** Recycling is another viable and favorable method for plastics waste management, however it is most of the time not feasible and economically not convenient because it requires considerable expenditure of labor and energy: removal of plastics wastes, separation according to the types of plastics, washing, drying, grinding and, only then, reprocessing to final product.**[29]** Besides these above critical issues, the high dependence of the plastics industry on oil is contributing to the depletion of the nonrenewable fossil resources and to the increased price of crude oil due to shortage

and to intensifying expenses of petroleum production resulting from the diminution of the most easily reachable reserves.**[101]**

Considering the above mentioned concerns, and owing to the stringent sustainable development policies, there is an urgent need to find alternative "environmentally-friendly" substitutes to the conventional plastics which satisfy the requirement of sustainability and degradability to low-toxic degradation products.**[102]** In this regard biodegradable polymers produced from low cost renewable resources and with lower energy consumption that are biodegradable and non-toxic to the environment have gained wide spread interest over the recent past decades.**[75]** Being produced from renewable resources and also because of their desirable properties, recyclability, compostability and natural abundance the use of biodegradable polymers is viewed as an ultimate solution for reducing the over dependency of plastic industry on fossil fuels.**[19,29]** Furthermore, these also help in reducing environmental pollution since these are recycled by biological processes, i.e once disposed in bioactive environments they are degraded and converted by the enzymatic action of microorganisms such as bacteria, fungi, and algae or by nonenzymatic processes such as chemical hydrolysis to water, CO_2, CH_4, biomass humic matter, and other natural substances.**[103]**

II-6-2 Definition and Types of Biodegradable Polymers

The terminology used in the field of biopolymers is sometimes misleading. Bioplastic materials are those produced from a biological source (short carbon cycle) i.e. either renewable-based, biodegradable or both. While according to ASTM D6400-04, a biodegradable plastic is defined as ‘‘a plastic that degrades because of the action of naturally occurring microorganisms such as bacteria, fungi, and algae,’’ and a compostable plastic is ‘‘a plastic that undergoes degradation by biological processes during composting to yield carbon dioxide, water, inorganic compounds, and biomass at a rate consistent with other known compostable materials and leaves no visually distinguishable or toxic residues.**[102,104]**

During the last few decades, a wide variety of different types of biodegradable plastics have been introduced into the plastics markets to compete with petrochemical

plastics in different sectors such as packaging, automotive, biomedical and textile.**[105,106]** Their importance and use are prone to gain momentum in the coming future owing to improvements in their production technology and the continuous increase of oil price. The production of bio-based nonbiodegradable polymers such as PE and PET that exhibit similar performance as their fossil-based counterparts also gained more and more importance in the field of biopolymers and might present a viable alternative, if they become cost competitive in the future.**[107]** Biodegradable plastics have dominated the bioplastics market with a roughly 90% share. However, durable plastics based on renewable resources are also forecasted to increase their market share from 10% in 2010 to about 50% by 2018.**[108]**

II-6-3 Classification of Biodegradable Polymers

As shown in **Figure II.15**, biodegradable polymers can be classified into two main families according to their origin (natural or synthetic) and into four categories, depending on their synthesis.**[66,104,109]**

(a) polymers from biomass such as the agro-polymers from agro-resources which are also known as natural polymers, e.g., starch, cellulose, proteins like gelatin, casein, and silk, and marine prokaryotes chitin chitosan, etc.

(b) polymers obtained by microbial production, e.g., the polyhydroxyalkanoates (PHA), polyhydroxybutyrate (PHB), hydroxyl-valerate (PHV), bacterial cellulose, xanthan, and pullan etc.

(c) polymers chemically synthesized using monomers obtained from agro-resources, e.g., poly(lactic acid).

(d) polymers whose monomers and polymers are both obtained by chemical synthesis from fossil resources, like aliphatic polyesters (e.g poly(butylene succinate) PBS and copolyesters (poly(butylene succinate adipate) PBSA, poly(capro lactone) PCL aromatic copolyester (poly(butylene adipate terephthalate) PBAT, aromatic polyesters (PCL), poly(vinyl alcohol) PVA).

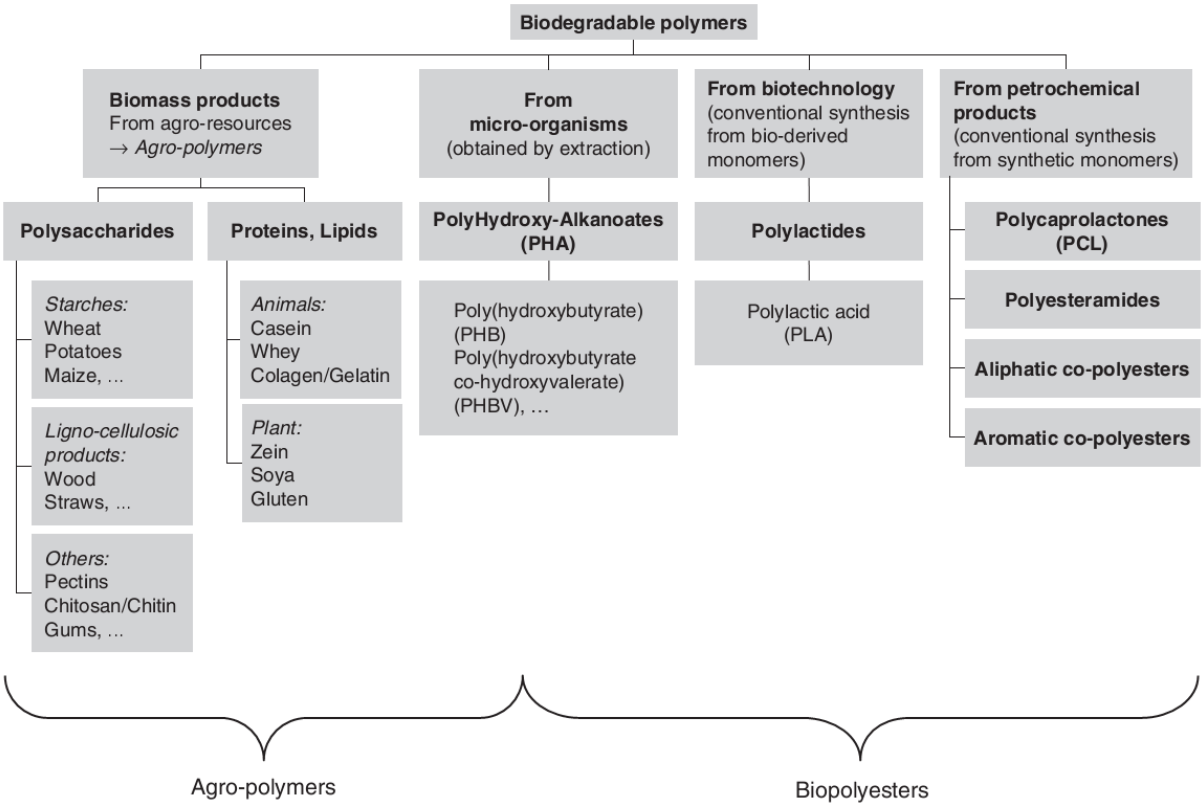

Figure II.15 Classification of the Biodegradable Polymers.**[110]**

Extensive research work undertaken by different plastics companies dedicated to the synthesis of raw materials from biomass led to few bio-monomers such as 1,3-propanediol, 1,4-butane diol, c-butyrolactone, adipic acid, n-methyl-pyrrolidone, succinic acid and lactic acid produced by fermentation from renewable resources which are potential candidates for production of biodegradable polymers.**[101]** Consequently, various synthetic biopolymers such as polyamides, polyesters and polyolefins are produced from renewable resources or from mixed sources of biomass and petroleum.

- **Polyamides,** such as PA11 is produced from castor oil therefore it is 100% bio-based material, while PA6,10 is 60% bio-based material synthesized from sebacic acid and castor oil.
- **Polyesters:** These are made from combinations of bio-based and petroleum monomers. They include polymers like poly(trimethylene terephthalate) (PTT) and poly(ethylene terephthalate) (PET). PTT from DuPont is produced from polycondensation of bio-based 1,3-propandiol and the terephtalic acid or the

dimethyl terephtalate that are both from petrochemical industry. Bio-based PET and other polyesters are under research and development.

- **Polyolefins** : Biobased polyethylene and polypropylene are obtained from bio-ethanol that is synthesized from sugar fermentation. Note that the bio-ethylene from bio-ethanol is also used to prepare bio-poly(vinyl chloride) (PVC).

A number of other synthetic polymers that have also been found to be biodegradable and evoked interest are polyurethanes, polyureas, polyanhydrides, poly(vinyl alcohol)s, polyacrylates etc.. These have interesting properties but their high cost production prohibited their large scale utilization.**[66,102]**

All of these above discussed bio-based polymers are chemically identical to their petrochemical counterparts with similar properties and currently have a greater potential for substituting fossil derived polymers.**[111]** Eventhough these materials are biobased, they are not biodegradable indicating that 'biodegradability' of plastics is dependent on the molecular structure of the material and not on the origin of its constituents used for its production.**[75,101]** For example, 100% bio-based PE from bioethanol, and PTT manufactured using petroleum derived terephtalic acid and biologically derived 1,3-propandiol (mixed source) are not degradable, whereas 100% petro-derived PBAT is biodegradable.**[75]**

Figure II.16 shows the chemical structures and the different synthesis routes of the most important bioplastics (biodegradable and durable) that are available in the market, and **Table II.8** shows the important bio-based durable polymers, their synthetic routes together with their leading manufacturers.

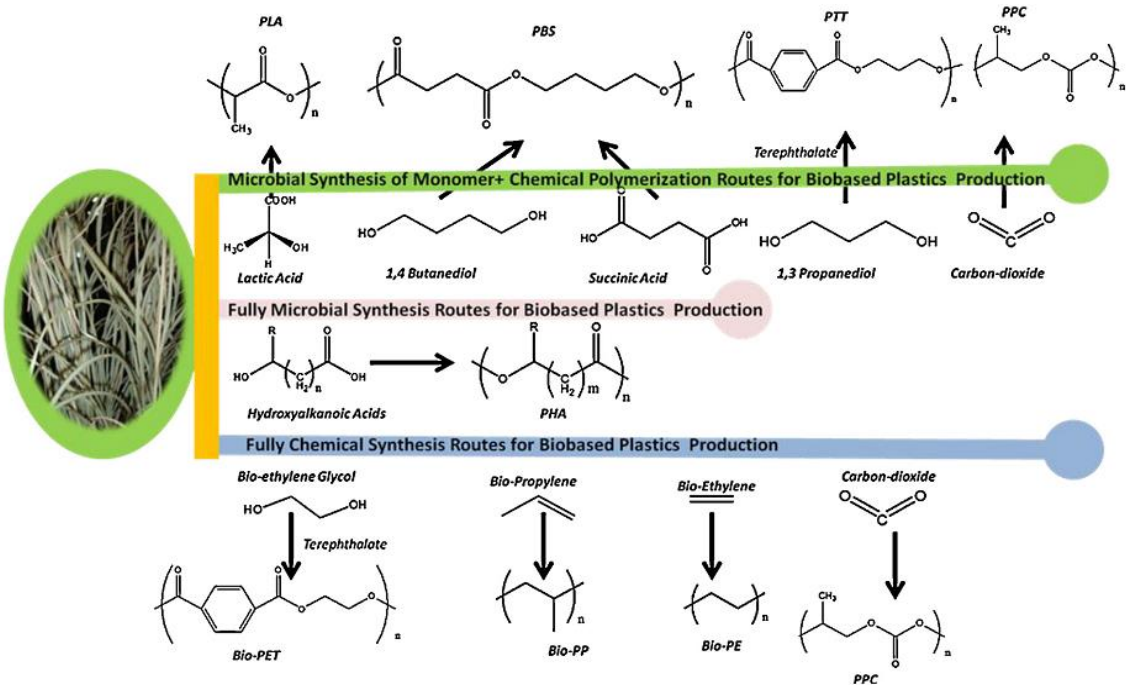

Figure II.16 Biobased Polymers and their Monomers Produced by Microbial Fermentations Combined with Chemical Synthesis.**[112]**

Table II.8 New Biobased Polymers and the Leading Manufacturers.**[75]**

Biobased polymer	Synthesis route	Manufacturer
Bio-Poly (butylene succinate) (PBS)	$Glucose \xrightarrow{Fermentation} Succinic\ acid$ $Succinic\ acid \xrightarrow{Hydrogenation} 1,4\ Butanediol$ $Succinic\ acid + 1,4\ Butanediol \xrightarrow{Melt\ Polymerization} Poly\ butylene\ succinate$ [9]	1. Bio-Amber 2. Mitsubishi Chemicals 3. DSM- Roquette 4. Showa Denko K.K (SDK) 5. Myriant Technologies
Bio-Poly(trimethylene terephthalate) (PTT)	$Corn\ Syrup \xrightarrow{Fermentation\ (E.coli)} 1,3-Propanediol$ $Terephthalic\ acid + 1,3-Propanediol \xrightarrow{Condensation\ Polymerization} Poly(trimethylene\ terephthalate)$	1. DuPont
Bio-Polyethylene (PE)	$Glucose \xrightarrow{Fermentation\ (Yeast)} Etholol \xrightarrow{Dehydration} Ethylene \xrightarrow{Polymerization} Polyethylene$	1. Braskem 2. Dow Chemical – Mitsui JV
Bio-Polypropylene (PP)	$Glucose \xrightarrow{Fermentation\ (E.Coli)} isobutanol \xrightarrow{Dehydration} Butylenes \xrightarrow{Intermediate\ Steps} Propylene \xrightarrow{Polymerization} Polypropylene$	1. Braskem
Bio-Polyethylene Terephthalate (PET)	*(Partial biobased-PET)* $Glucose \xrightarrow{Fermentation\ (Yeast)} Etholol \xrightarrow{Dehydration} Ethylene \xrightarrow{Oxidation} Ethylene\ glycol$ $Terephthalic\ acid + Ethylene\ glycol \xrightarrow{Polymerizatoin} Polyethylene\ Terephthalate$ *(100% Biobased -PET)* $Glucose \xrightarrow{Fermentation\ (Yeast)} Etholol \xrightarrow{Dehydration} Ethylene \xrightarrow{Oxidation} Ethylene\ glycol Sugar \xrightarrow{Catalytic\ Conversion} Bio\ paraxylene \xrightarrow{Catalytic\ Conversion} Bio-Terephthalic\ acid$ $Bio-Terephthalic\ acid + Bio-Ethylene\ glycol \xrightarrow{Polymerization} Bio-Polyethylene\ Terephthalate$	1. Toyota Tsusho Corporation 2. Futura Polyesters 1. Coca-Cola – Gevo Venture 2. PepsiCo- Virent Venture (Not in Commercial scale yet)

II-6-4 Biodegradable Polymers Production, Market and Applications

II-6-4-1 Biodegradable Polymers Production

According to "European Bioplastics", production of bioplastics reached nearly 1.4 metric kilo tones (MKT) in 2012 most of which is made up of bio-based non-biodegradable biopolymers such as PET (38.8%) and PE (14.3%) (**Figure II.17**).**[113]** Even though it sounds like lot, it only accounts for less than 0.5% of the ≈300 MKT of the synthetic plastics the world produced in 2012. The world production capacity of bioplastics is estimated to reach 6.185 MT by the year 2017 which represents six fold increase compared to that of 2012, with predominance of bio-based/non-biodgradable bioplastics over biodegradable ones with a production capacity of 84% of the total market. One of the reasons leading to this trend might be the better performance of the bio-based/non-biodgradable bioplastics compared to the biodegradable ones and to considerable changes in legislation related to compostable products in recent years.**[107]**

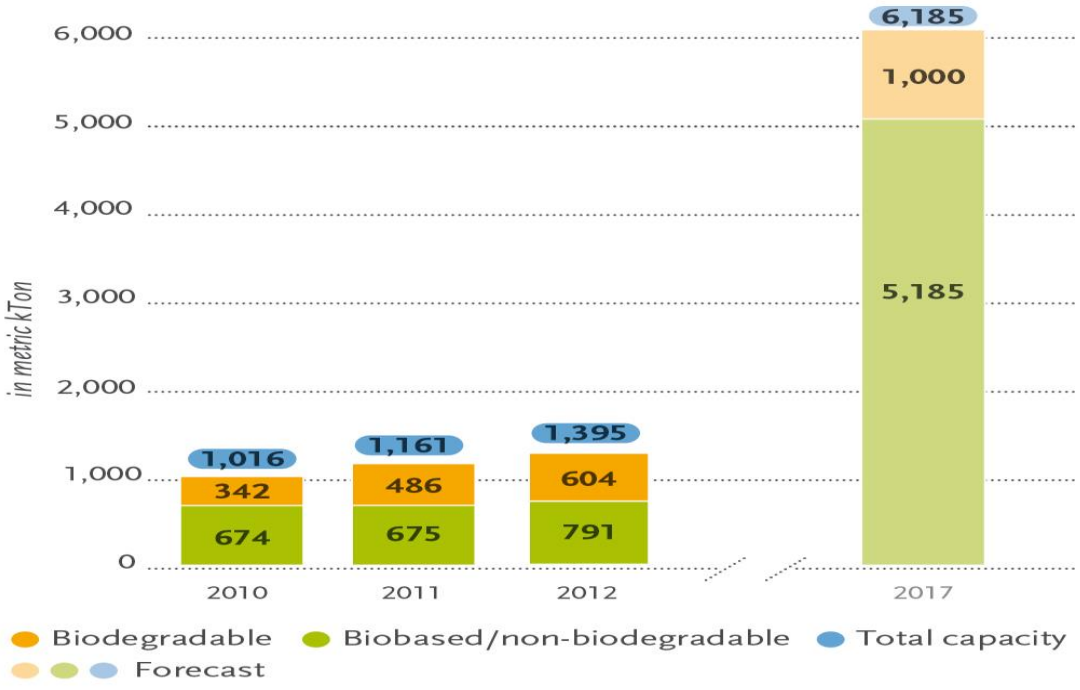

Figure II.17 Global Production Capacities of Biopolastics.**[113]**

Currently, several different types of biodegradable polymers have been developed and entered the marketplace with a prediction of an increasing share in the

next years.**[105]** Among the most important biodegradable that have attracted interest are Polylactides (PLA), PCL, PHA, PBAT, TPS etc.. **Table II.9** summarizes the main commercially available biodegradable polymers together with some of the most important worldwide leading companies evolved in their production.**[114]**

Table II.9 Commercially Available Biodegradable Polymers and their Leading Manufacturers.**[114]**

Trade Name	**Supplier**	**Origin**	**Website**
NatureWorks (PLA)	Cargill Dow	USA	www.natureworksllc.com
CAPA (PCL)	Perstorp	UK	www.perstorp.com
Biopol (PHA)	Metabolix	USA	www.metabolix.com
Bioplast (TPS)	Biotem	Germany	www.biotec.de
Tenite (Cellulose esters)	Eatsman	USA	www.eastman.com
Binolle 1000 (PBS)	Showa high polymer	Japan	www.showa-denko.com
SkyGreen SG 200 (PBSA)	SK Polymers	Japan	www.skchemical.com
Binolle 6000 (PES)	Showa high polymer	Japan	www.showa-denko.com
Biomax (PBST)	DuPont	USA	www.dupont.com
Ecoflex (PBAT)	BASF	Germany	www.basf.com
Sorona (PTT)	DuPont	USA	www.dupont.com
Polyvinol (PVA)	Vinavil Spa	Italy	www.vinavil.com

TPS: thermoplastic starch

PLA is one of the most produced biodegradable polyester in 2012 with a total world production capacity of 13.4% which nearly equals that of all other biopolyesters together. PHA ranked fourth with a production capacity of only 2.4% (**Figure II.18**). Long-term predictions indicate that by 2020 the most important bio-based polymers will be starch (1.3 MT), PLA (0.8 MT), PHAs (0.4 MT) and bio-based PE (0.6 MT).**[115]**

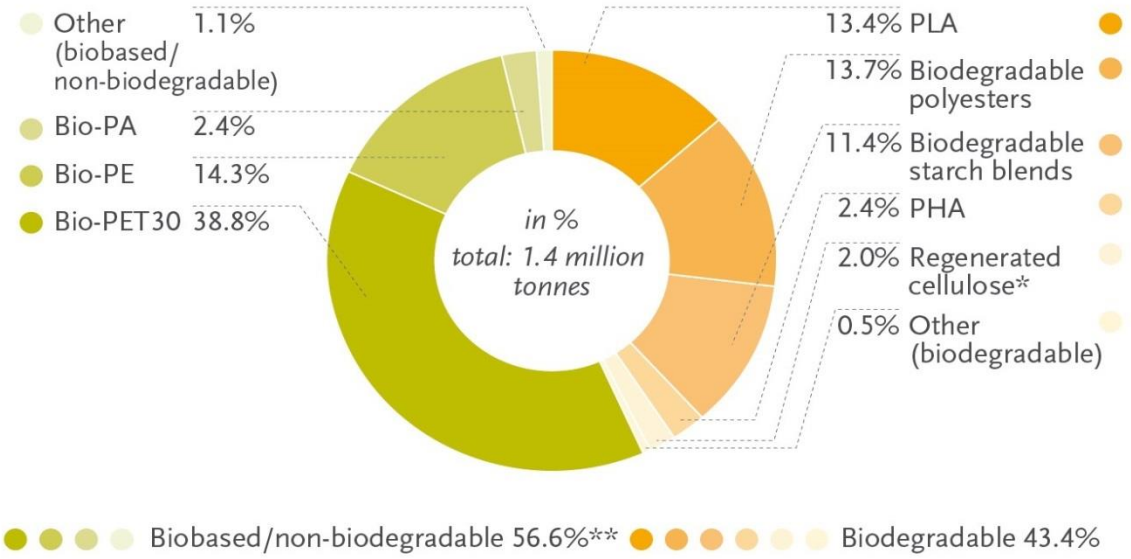

Figure II.18 Bioplastics Production Capacities on 2012 (By Material Type).**[113]**

II-6-4-2 Biodegradable polymers: Applications and Market

Bio-based and biodegradable polymers present a wide range of promising properties in a number of applications (**Figure II.19**). Because of their biodegradability, bioresorbability and compatibility and also due to their initial high price, biopolymers such as PLA, PGA, PLGA and PHA first found use exclusively in the biomedical and pharmaceutical domains. In these high added value fields, biodegradable polymers were involved as implants (vascular and orthopedic), bone fixation devices, various pins and screws, absorbable surgical sutures and drug delivery systems.**[102]** During the last decades of the last century, breakthrough and technical innovations in the synthesis of biopolymers led to their mass production which helped decreasing their price. This coupled with advanced knowledge of how biopolymers properties can be modified and tuned to meet market and end-use requirements has fueled interest in these materials to be used in other fields. Because of their good competitiveness they are establishing themselves as alternatives to petrochemical polymers in a number of different markets such as biomedical, agriculture and packaging applications. In the packaging industry, biopolymers

continue to attract more and more attention.**[102]** They are used as food and nonfood packagings, composting and carrier bags and food-service applications.**[63,102]** In the agricultural application, biodegradable polymers are used as agricultural mulch film, planting containers and controlled release of agricultural chemicals, and in the textile sector they are used as woven and nonwoven fabrics, and in some personal hygienic products such as disposable diapers.**[102]**

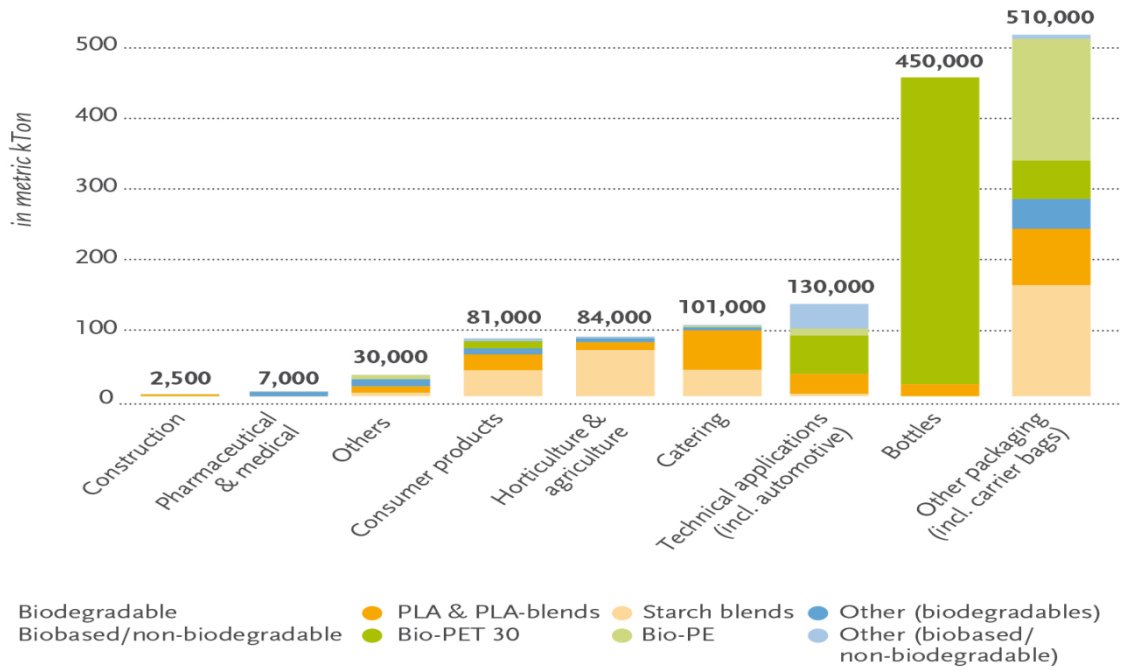

Figure II.19 Global Production Capacities of Biopolastics on 2012 (By Market Segment).**[113]**

Figure II.19 depicts the world production capacities of biodegradable polymers for different applications. As can be noticed the most important quantity was consumed by the packaging industry for which biobased nonbiodegradable biopolymers were predominantly used. PLA constituted a tiny share in the production of bottles, but holds half of the production capacity destined to other packaging applications.**[113]**

In the last decades, the attention and worldwide consumption of biodegradable polymers have increased even though competition with commodity fossil based

plastics, which are cheaper and well-known to customers, slows down their commercialization, but this is not for long because of the expected continuation of high crude oil and natural gas prices, which will allow biodegradable polymers to become more cost-competitive with petroleum-based resins. But despite their increasing market share in different fields and flourishing situation in the plastics markets, biodegradable polymers are now under intensive research studies to tailor and improve their properties through functionalization and modification technologies to broaden their applications.**[105,108]**

II-7 Biodegradable Polyesters

Synthetic polymers from nonrenewable sources, in general, are nonbiodegradable. However, polymers with hydrolysable backbone such as polyesters are susceptible to hydrolysis and enzymatic biodegradation; consequently these are the best known nonrenewable biodegradable polymers that have been widely used since long time.**[102]** As can be noticed from **Figure II.15**, most of the biodegradable polymers belong to the polyesters family (biopolyesters) that is made of two major groups: aliphatic (linear) and aromatic (aromatic ring) polyesters both of which can be bio-sourced or petroleum derived (**Figure II.20**). These polyesters play a predominant role in the field of bioplastics owing to their known biodegradability and susceptibility to hydrolytic degradation via the ester bond.**[102]**

Commercially available polyesters derived from petroleum are polycaprolactone (PCL), polybutylene succinate (PBS), poly(butylene succinate-co-butylene adipate) (PBSA), poly(butylene adipate-co-terephthalate) (PBAT), poly(trimethylene terephthalate) (PTT) etc. From the perspective of sustainability and environmental concerns, polyesters from renewable resources that can completely degrade at the end of their service life to nontoxic substances satisfying thus the environmental requirements have gained increasing attention during these last decades. **[85,102]** Typical examples of these polyesters that are now commercially available are polylactides (PLA) and polyhydroxyalcanoates (PHA), polyhydroxyhexanoates (PHH), polyhydroxybutyrates (PHB) and polyhydroxyvalerates (PHV).**[85]**

Figure II.21 and **Table II.10** show the chemical structures, trade names and the main properties of commercially available biopolyesters.

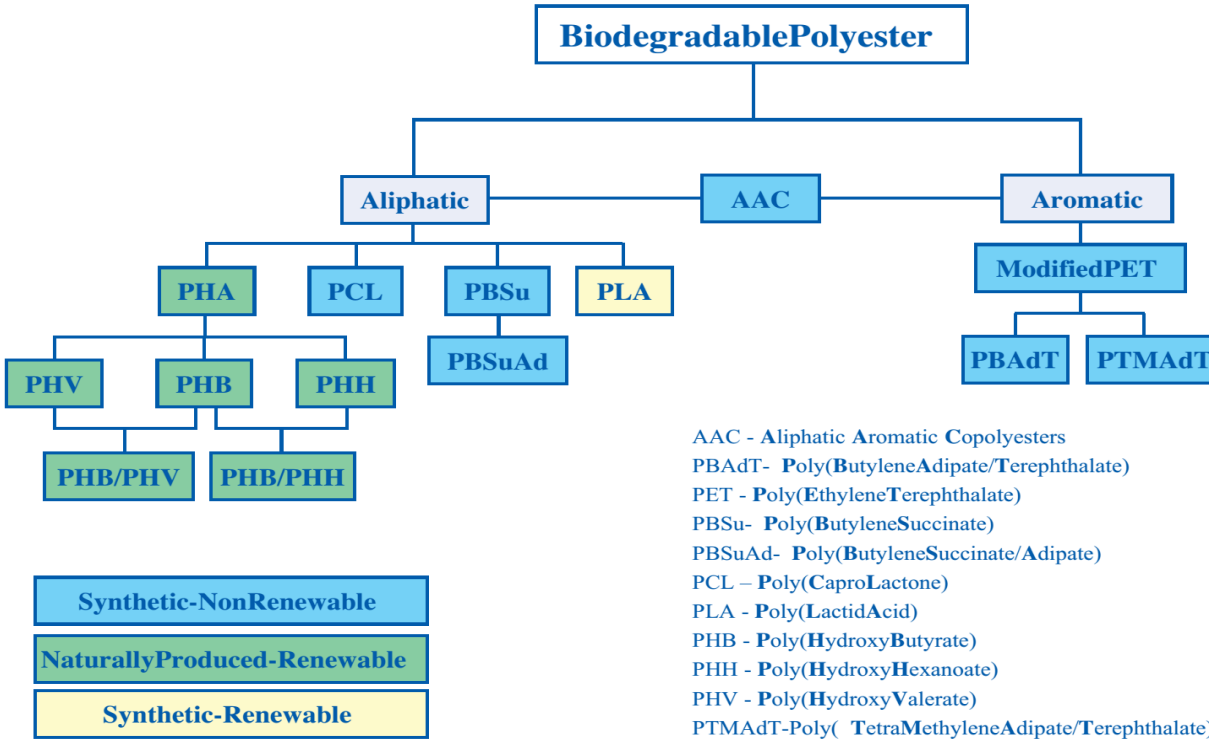

Figure II.20 Familly of Biodegradable Polyesters.**[105]**

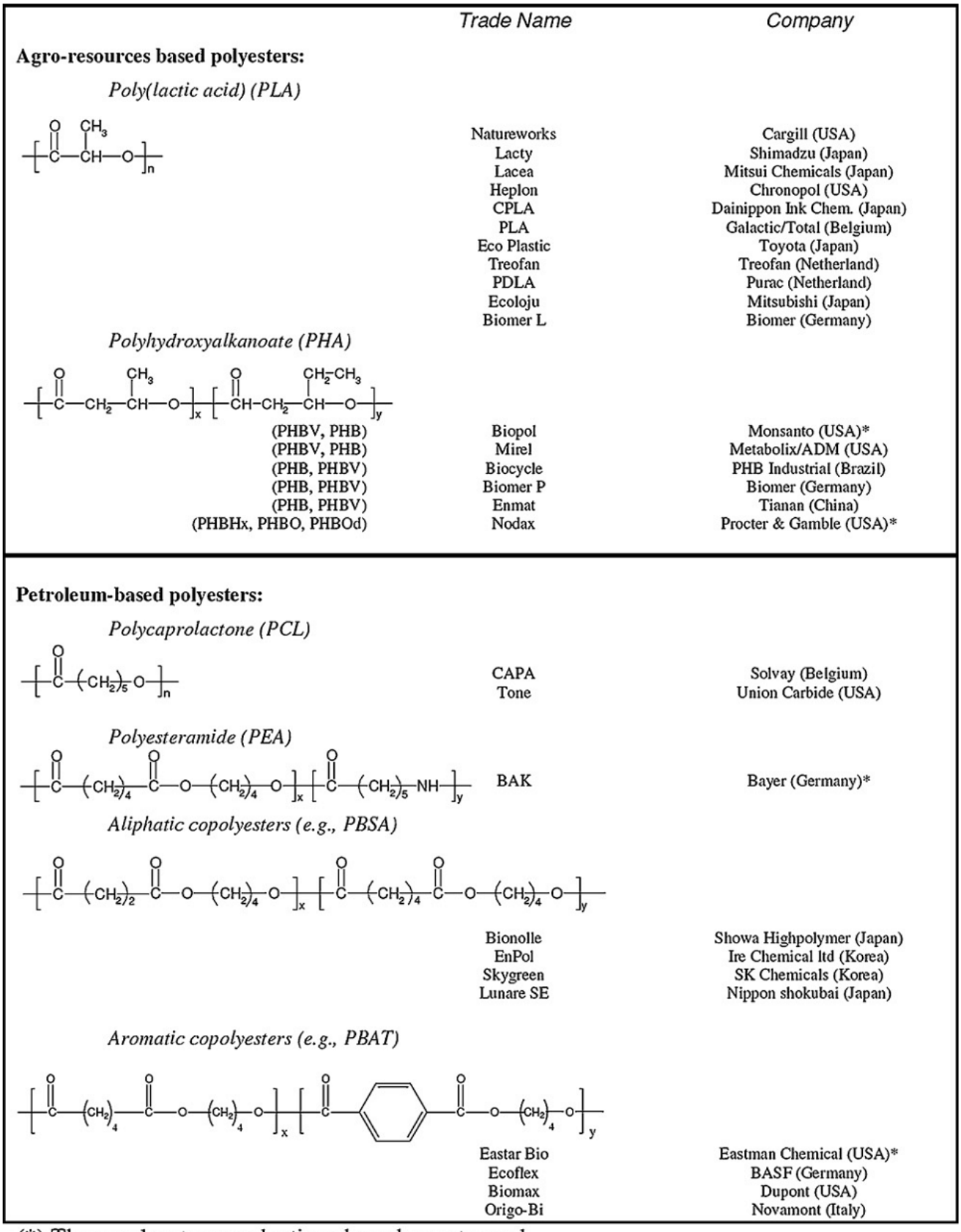

Figure II.21 Structure, Trade Names and Suppliers of Main Biodegradable Polyesters Commercially Available. **[110]**

Table II.10 Physical Data of Some Commercial Biopolyesters.**[110]**

	PLA Dow–Cargill (NatureWorks)	PHBV Monsanto (Biopol D400G – HV = 7 mol%)	PCL Solvay (CAPA 680)	PEA Bayer (BAK 1095)	PBSA Showa (Bionolle 3000)	PBAT Eastman (Eastar bio 14766)
Density	1.25	1.25	1.11	1.07	1.23	1.21
Melting point (°C)[a]	152	153	65	112	114	110–115
Glass transition (°C)[a]	58	5	–61	–29	–45	–30
Crystallinity[b] (in %)	0–1	51	67	33	41	20–35
Modulus (MPa) (NFT 51-035)	2050	900	190	262	249	52
Elongation at break (%) (NFT 51-035)	9	15	>500	420	>500	>500
Tensile stress at break or max. (MPa) (NFT 51-035)	–	–	14	17	19	9
Biodegradation[c] (mineralization in %)	100	100	100	100	90	100
Water permeability WVTR at 25 °C ($g/m^2/day$)	172	21	177	680	330	550
Surface tension (γ) (mN/m)	50	–	51	59	56	53
γ_d (dispersive component)	37	–	41	37	43	43
γ_p (polar component)	13	–	11	22	14	11

[a] Measured by DSC.

[b] Determined on granules, before processing.

[c] After 60 days in controlled composting according to ASTM 5336.

Aliphatic polyesters from agro-resources are the most promising biodegradable polymers with high potentials to substitute for long-lasting polymers. PLA has been the focus of much attention because it is derived from renewable resources such as starch. Beside its inherent biocompatibility, biodegradability, this polyesters present comparable properties to those durable polymers.

II-8 Poly(lactic acid): Synthesis, Structure, Properties and Applications

II-8-1 Poly(lactic acid) Precursor: Lactic Acid

Lactic acid (2-Hydroxy propionic acid, CH_3-CHOHCOOH), a naturally occurring organic hydroxy acid is the sole monomeric precursor for PLA production which was first isolated in 1780 from sour milk by the Swedish chemist Scheel and first produced commercially in 1881.**[116]** Lactic acid (milk acid) finds large applications such as in food, pharmaceutical, textile, leather and chemical industries and of course as the monomer for the synthesis of PLA. As shown in **Figure II.22** the structure of the lactic acid is characterized by an asymmetric carbon, indicating that is

a chiral molecule which exists as two optically active enantiomers i.e. L-lactic acid and D-lactic acid, and an optically inactive D,L form or the so called meso-lactic acid formed from a racemic/equimolar mixture (50/50 mixture) of the L and D configuration forms.

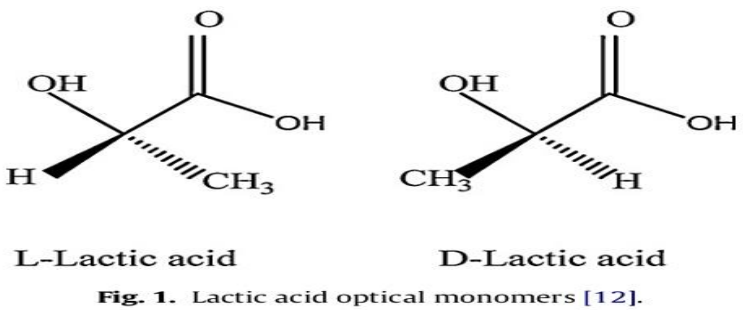

Fig. 1. Lactic acid optical monomers [12].

Figure II.22 Lactic Acid Optical Monomers.**[117]**

Lacitic acid can be commercially produced via chemical synthesis or renewable carbohydrate fermentation. The first technique provides only the racemic mixture of L- and D-lactic and uses fossil-derived products as raw materials. Consequently, the commercial fermentative batch process which takes three-six days to complete is preferred because it allows producing optically pure L- (99.5%) and D-lactic acid (0.5%) and is environmentally benign bioprocess which uses low cost renewable (biomass) feedstock as carbon source for the fermentation at low temperature and consumes low energy. Because of these advantages, approximately 90% of the total lactic acid produced worldwide is made by bacterial fermentation and the remaining portion is produced synthetically by the hydrolysis of lactonitrile by a strong acid. However, lactic acid from the microbial process is difficult to recover and its purification is a long multistep process (ultra-filtration, nano-filtration, electro-dialysis and ion exchange) which makes lactic acid more expensive. Depending on the type of the bacteria strain, two fermentation methods can be distinguished. The first is the hetero-fermentative process and the second known as homo-fermentative method is the more extensively used in industry which gives lower levels of by-products and greater raw material conversion (~90%). The raw materials (carbon source) for the fermentation can be refined sugar (glucose, sucrose etc.) or any carbohydrates containing sugar from agricultural production and residues. For example,

NatureWorks®, the worldwide leading producer of PLA, exclusively uses corn starch as raw material for lactic acid production via lactic fermentation.**[117]**

II-8-2 Polyl(actic acid) Production Techniques

As depicted in **Figure II.23**, the conversion of lactic acid monomer to high molecular weight (Mw) PLA can be accomplished either by direct condensation polymerization or azeotropic dehydration and condensation. The ring opening polymerization (ROP), as a third synthesis method, uses the lactide (lactic acid cyclic dimer) as the monomer, therefore it requires an intermediate step necessary for the preparation of the monomer. All of these three methods are discontinuous, and none of these is simple or easy to conduct; they all require rigorous control of conditions (temperature, pressure and pH), the use of catalysts and long polymerization times, which implies high energy consumption.**[118]** Nowadays, direct azeotropic dehydration and condensation polycondensation and ROP are the most used production routes. Depending on the stereo purity of the starting monomer, a family of polymers may be synthesized : pure poly-L-lactic acid (PLLA), pure poly-D-lactic acid (PDLA), and poly-D,L-lactic acid (PDLLA).**[119]** Poly(lactic acid) and polylactide describe the same chemical product. Poly(lactic acid) defines polymers obtained from direct polycondensation reaction of the lactic acid monomer and polylactide those derived from the ring opening polymerization of the intermediary lactide precursor, while the abbreviation “PLA” is used to describe both.

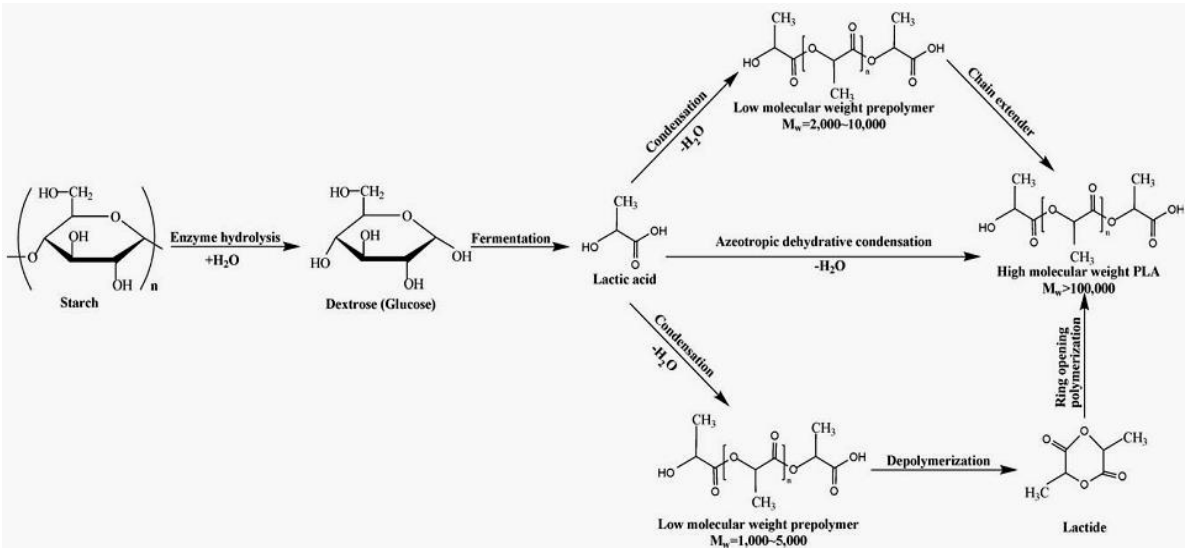

Figure II.23 Synthesis Routes of Poly(lactic acid).**[118]**

II-8-2-1 Direct Condensation Polymerization

A direct condensation polymerization (polycondensation) in bulk of lactic acid to obtain PLA is possible thanks to the presence of both hydroxyl and carboxyl groups on the monomer (**Figure II.24**). Even though it is the least expensive method involving solvents under high vacuum and high temperature, it is not common in the commercial manufacture of PLA because only low to intermediate Mw polymers (oligomers) can be achieved arising from the presence of impurities, viscosity build up during polymerization and mainly from the difficulty to remove water from the condensation equilibrium reaction responsible of decrease in conversion and depolymerization.**[116]** To increase the Mw, esterification-promoting adjuvants (bis(trichloromethyl) carbonate, dicyclohexylcarbodiimide, and carbonyl diimidazole) or chain extenders (epoxides such as butyl glycidyl ether, or isocyanates) are used, which obviously increase the steps and complexity of the production and also the cost of the final product.**[109,116,119]** In addition to these disadvantages, the final polymer may contain impurities and unreacted chain extenders which may be nonbiodegradable or nonbioresorbable additives.

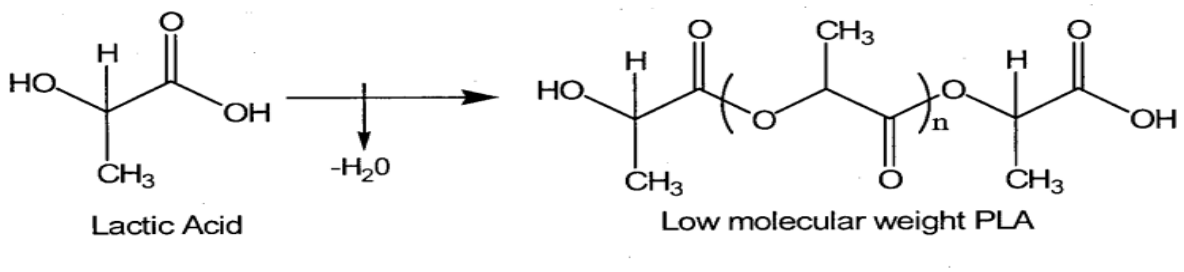

Figure II.24 Synthesis of Low Molecular Weight PLA via Direct Polycondensation of Lactic Acid Monomer.**[120]**

II-8-2-2 Azeotropic Condensation Polymerization

This is a solvent-based technique developed and patented by Mitsui Toatsu Chemicals (Japan). In this process, schematically illustrated in **Figure II.25**, high Mw PLA is achieved by direct condensation of lactic acid without the use of coupling agents or esterification-promoting adjuvants and their associated drawbacks.**[109]** Because the polymerization takes place in solution, water of condensation is continuously and readily removed by azeotropic condensation of the lactic acid and the

catalyst (Sn compounds: Sn, SnO or $SnCl_2$) in a refluxing, high boiling, aprotic solvent (diphenyl ether) under reduced pressure.**[109,116,121]** However, this technique suffers from the high content of catalyst used to achieve acceptable monomer conversion which has to be removed or at least deactivated otherwise it causes degradation of the product during processing, and toxicity especially in the packaging and biomedical applications. In addition the excess use of solvent (fresh and dehydrated) during polymerization and non-solvent to collect the final polymer makes this technique sound non-environmental, involving different steps thus laborious and expensive.**[109,121]**

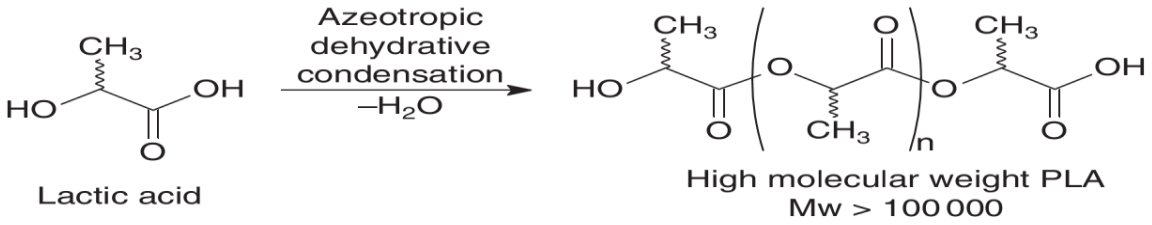

Figure II.25 Manufacturing Route of Poly(Lactic Acid) According to Mitsui Process.**[114]**

II-8-2-3 Ring Opening Polymerization (ROP)

The first ring opening polymerization of lactide that produced low Mw PLA was first reported by Wallace Hume Carothers et al. after their pioneering work as early as 1932. It was until 1954 that Dupont patented a method to obtain high molecular weight PLA after improvements in lactide purification. At the early stage of PLA discovery, its high cost confined its application to the biomedical field. This method produces pure high Mw PLA (>100 000) but necessitates first the preparation of the lactide and then its purification by vacuum distillation accomplished at high temperature without the use of solvent which increases the overall cost of the polymerization.**[104,122]** Again, owing to the stereoisometric nature of the lactic acid, three stereoforms of lactide are generated: L-Lactide, D-Lactide, and meso-Lactide as shown on (**Figure II.26**). Stereo pure lactides are obtained by distilling water from lactic acid under mild conditions and vacuum without solvent through a combined process of oligomerization and cyclization achieved by the catalytic depolymerization of the low Mw (oligomer) PLA under reduced pressure which leads a mixture of L-, D-, or meso-lactides (**Figure II.26**).

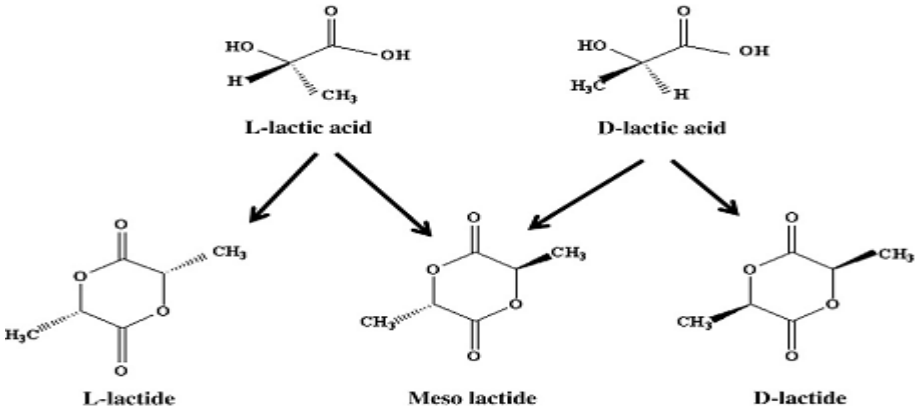

Figure II.26 Stereoforms of Lactides.**[101]**

ROP polymerization, schematically shown in **Figure II.27**, can be carried out on large scale by melt polymerization which is the most used technique due to its simplicity and reproducibility, but bulk, solution, and suspension polymerization techniques are also possible. The polymerization mechanism can be cationic, anionic, or coordination-insertion type depending on the catalyst and initiator concentration system. The polymerization is generally catalyzed by organo-metallic compounds such as the most used tin octoate (Sn(II) diethyl-2-hexanoate) which is a Lewis-acid type catalyst which was reported as the most efficient with low degree of racemization and accepted by the US Food and drug Administration (FDA) due to its low toxicity.**[123]** The other group of catalysts is the metal alkoxides especialy Mg, Sn, Ti, Zr, Zn, and Al-alkoxides.**[122]**

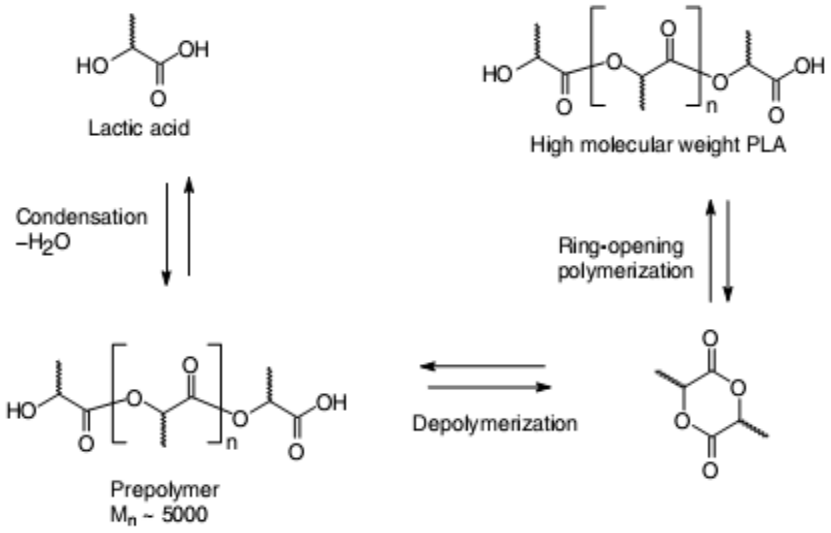

Figure II.27 Schematic of PLA Production via Ring Opening Polymerization Using Lactide Monomer.**[121,124]**

A solvent free and low-cost continuous process that permits the production of both the lactide and the PLA in the melt was developped and pattented by Cargill Dow LLC (**Figure II.28**) . This environmentally friendly process involves different steps starting from preparation of PLA oligomer from continuous condensation operation followed by its conversion to a mixture of lactide stereo isomers using tin catalysis to promote rate and selectivity of interamolecular cyclization reaction. Thereaftere the lactide is purified and undego a ring opening polymerizaton using tin based catalyst to give a range of high Mw PLA polymers in pellets form.**[124,128]**

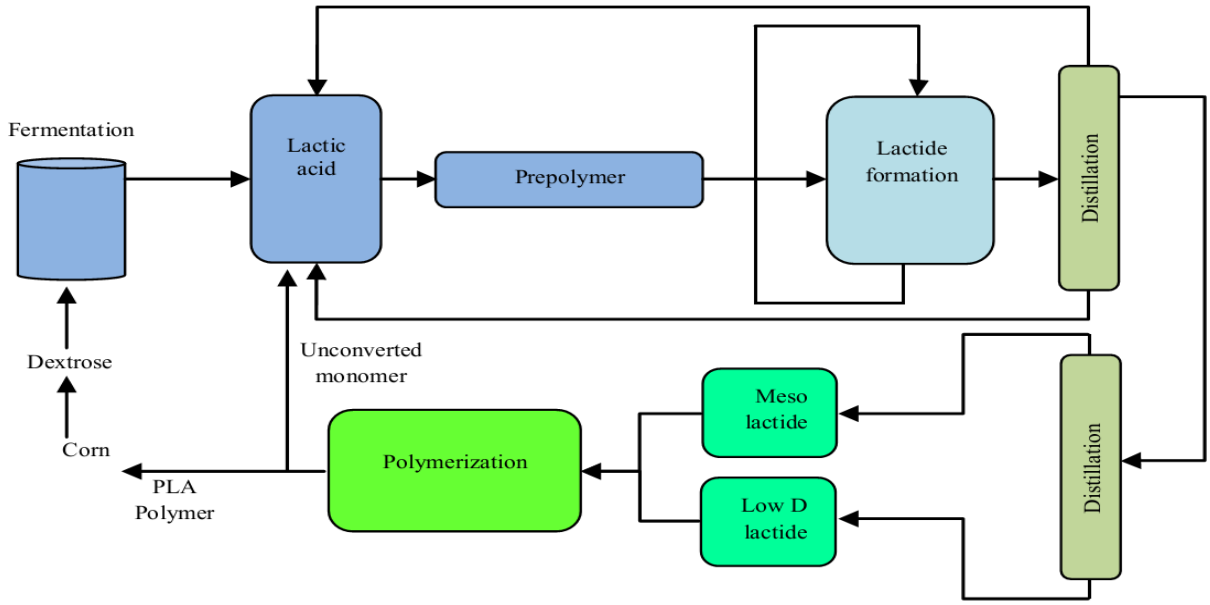

Figure II.28 Nonsolvent Process to Prepare Polylactic Acid.**[124]**

This process is actually used by NatureWorks LLC the world wide leader in PLA production. Cargill Dow LLC which was a joint venture between Cargill Inc. and Dow Chemical Co. commercialized their PLA polymer under the trade name NatureWorks™ and their fiber Ingeo™ spun from their polymer. Dow sold its share to Cargill in 2005, which renamed their PLA business NatureWorks LLC.**[101,121]** Many companies have expressed interest in producing PLA for biodegradable plastics on commercial scale; some of these worldwide major companies that are now involved in PLA manufacturing are listed in **Table II.11**.

Table II.11 Some of Worldwide Polylactic Acid Resin Producers. **[114]**

Producer	Capacity (MT/year)	Location
NatureWorks	140,000	Nebraska, USA
Purac–Sulzer Chemtech–Synbra Technology	5,000	The Netherlands
Galactic–Total Petrochemicals: Futerro	1,500	Belgium
Zhejiang Hisun Biomaterial	5,000	Zhejiang, China
Shanghai Tong-jie-liang Biomaterial	300	Shanghai, China
Mitsui Chemical—LACEA®	No data	Japan
Unitika–Terramac	5,000	Japan
Nantong Jiuding Biological Engineering	1,000	Jiangsu, China
Piaoan Group	10,000 (in planning)	Henan, China
Purac–Toyobo	No data	Japan
Toray Industries	5,000	Kyungsangbuk-do, South Korea
Pyramid Bioplastics Guben GmBH	60,000 (in planning)	Guben, Germany
Teijin Limited	1,200	Matsuyama, Ehime Prefecture, Japan

II-8-3 PLA Properties

The chirality of lactic acid monomer makes PLA an interesting polymer. The stereochemical composition of PLA polymer backbone is one of the most important factors which determine its properties. By varying the chemical composition in terms of L- and D- isomers during synthesis, a large spectrum of PLA polymers with different physical, mechanical and thermal properties can be tailored to match performance requirements for various applications. Furthermore as for other polymers, the properties of PLA are significantly dependent on other factors such as Mw and molecular weight distribution, orientation, thermal history and processing conditions. **[101,102,125]**

II-8-3-1 Crystallization

Crystallinity governs most of the polymer properties including stiffness, hardness, modulus, tensile strength, melting point etc., so it deserves great attention. PLA can be either crystalline or amorphous, depending on the stereochemistry and thermal history.**[109]** The crystallinity of PLA, as a determinant factor in PLA performance, can be modified by adjusting the stereochemical composition of the polymer to produce semi-crystalline or amorphous PLA.**[114,125]** Polymerization of optically pure L,L-lactide or D,D-lactide leads semicrystalline up to 40% PLLA or

PDLA polymers due to their isotactic/syndiotactic stereo regular microstructures.**[101,109]** However, an amorphous atactic polymer is produced from the meso-lactide monomer polymerization owing to the dual presence of the L- and D-stereoforms in the mesolactide, that disturbs the structure stereoregularity.**[125]** The most common commercial polymers of PLA are optical copolymers of predominantly L-lactide, with small amounts of meso-lactides.**[124,126]** The crystallization ability of polylactides decreases with chain stereoirregularity, accordingly resins containing more than 90% L-lactic acid are semicrystalline, when it contains 50-90% it is entirely amorphous and below 43% optical purity crystallization is no longer possible.**[101,109]** Depending on preparation conditions PLLA crystallizes in different forms (α, β and γ-form with the more stable one being the α form. As for PET, the crytstallization kinetics was reported to be rather slow,**[114]** and nucleating agent are very often used to increase the nucleation rate of PLA.**[101,126]**

II-8-3-2 Thermal Properties

As for any semicrystalline polymer, PLA exhibits both glass transition temperature (T_g) and a melting temperature (T_m) but with relatively high T_g and low T_m as compared to other thermoplastics (**Figure II.29**). The T_g and T_m of PLA are dependent on both the Mw and the optical purity of the polymer **(Table II.12)**. Typical value of T_g reported in literature ranges from 50°C to 80°C which also depends on thermal history, quenching and annealing. The reported T_m is in the range 130°C to 180°C, and 93 J/g is the most referred PLA melt enthalpy for 100% crystallinity used to estimate the degree of crystallinity by differential scanning calorimetry (DSC).**[126,127,128]** The presence of a double melting point in PLLA is generally found and attributed to slow rates of crystallization and recrystallization.**[114]**

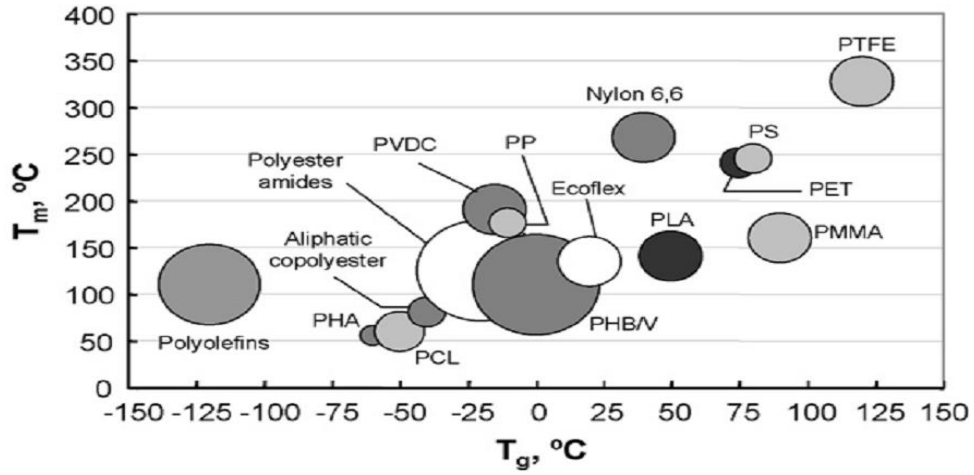

Figure II.29 Comparison of Glass Transition and Melting Temperatures of PLA with Other Thermoplastics.**[126]**

Table II.12 Primary Transition Temperatures of Selected PLA Copolymers.**[126]**

Copolymer ratio	Glass transition temperature (°C)	Melting temperature (°C)
100/0 (L/D,L)-PLA	63	178
95/5 (L/D,L)-PLA	59	164
90/10 (L/D,L)-PLA	56	150
85/15 (L/D,L)-PLA	56	140
80/20 (L/D,L)-PLA	56	125

PLA also suffers from low heat distortion temperature (HDT) and vicat softening point mainly due to its low Tg. HDT values of PLA are not influenced neither by the Mw nor by crystallinity, however those of the vicat softening point are influenced by crystallinity. HDT values of amorphous and crystalline PLA are in the ranges 55-57 °C and 60-66°C, respectively, while those of vicat penetration are in the intervals 59°C-60°C and 157-165C for amorphous and crystalline PLA respectively.**[125]** In terms of thermal stability, PLA is considered a less stable polymer exhibiting rapid loss of Mw during processing in the molten state. The ester linkage of PLA tends to degrade during thermal processing under hydrolytic conditions. The decomposition temperature of PLA lies between 230°C and 260°C attributed to various reactions of different mechanisms including (a) hydrolysis by trace amounts of water, (b) zipper-like depolymerization, (c) oxidative, random main-chain scission, (d) intermolecular transesterification to monomer and oligomeric esters, and (e) intramolecular transesterification resulting in formation of monomer and oligomer lactides of low Mw.**[101,104,114,126]** Thermal degradation of PLA is

reported to be affected by the process temperature, residence time, presence of impurities of residual catalysts, moisture, crystallinity, % isomer, residual lactic acid, Mw and Mw distribution.**[104]** The decomposition of PLA leads to formation of CO, CO_2, acetaldehyde and to volatile lactide which can result in fuming and/or fouling the processing equipment.**[129]**

II-8-3-3 Degradation

The primary mechanism of PLA degradation is hydrolysis of the ester bond, followed by bacterial attack on the fragmented residues. In the environment, PLA degrades within several months of exposure to moisture, whereas in compost under high temperature and high humidity conditions it may degrade within several weeks.**[118,124]** The environmental degradation of PLA is a two-step process. First the high Mw molecules are reduced to lower Mw species by random chain scission of the ester bonds. In the second stage the Mw reductions proceeds until lactic acid and low Mw oligomers are formed which are then metabolized by microorganisms to yield carbon dioxide and water.**[118]** The degradation has been found to be an autocatalyzed process due to the increasing amount of compounds containing carboxylic end-groups and also to depend on a range of factors and just to name some of them these are: temperature, crystallinity, moisture, dimension of the article and metal impurities from catalyst.**[118,124]**

II-8-3-4 Solubility in solvents

In general, polylactides are soluble in dioxane, aceto-nitrile, methylene chloride, 1,1,2-trichloroethane and dichloroacetic acid, but a good solvent for PLA and for most of the corresponding copolymers is chloroform. Amorphous PLA is soluble in organic solvents, while crystalline PLA is soluble in chlorinated solvents and benzene at elevated temperatures. Poly(meso-lactides) are soluble in many other organic solvents like acetone, pyridine, ethyl lactate, tetrahydrofuran, xylene, ethyl acetate, dimethylformamide, methyl ethyl ketone. All polylactides are insoluble in water, some alcohols and alkanes.**[101,109,114,125]**

II-8-3-5 Physical and Mechanical Properties

The density of PLA is 1.25 g/cm^3 and 1.29 g/cm^3 for amorphous and crystalline PLA which is lower than that of PET (1.34 g/cm^3), but higher than that of other conventional polymers with densities in the range of 0.8-1.1 g/cm^3.**[101,102,118,125]** Physical and mechanical properties of PLA are dependent on a range of parameters, such as crystallinity, polymer structure, molecular weight and material formulation (plasticization, blending, reinforcing etc.).**[102,109,114]** PLA is a clear, colorless and glossy polymer showing good appearance and transparency with high gloss (105-200%) compared to those of PET (60-110%) and PP (75-90%).**[101]** Because of its high Tg (above room temperature), PLA behaves as a glassy polymer just like PS. When subjected to tensile testing, PLA exhibits poor plastic behavior and fails in a brittle fashion with little strain softening (**Figure II.30**).**[130]** Concerning its resistance to impact, PLA is notch sensitive and its impact strength is greatly affected by crystallinity. For low crystallinity (3-9%), the notched Izod impact strength of PLLA is in the range 2.0-3.0 kJ/m^2 while at higher crystallinity (45-70%) it is in the interval 3.0-7.0 kJ/m^2. PDLA exhibits lower impact resistance in the range 1.5-2 kJ/m^2. The unnotched impact strength for PLLA of low and high crystallinity is the range 13-20 kJ/m^2 and 18-35 kJ/m^2 respectively indicating higher differences than those observed for the notched counterparts.**[125]**

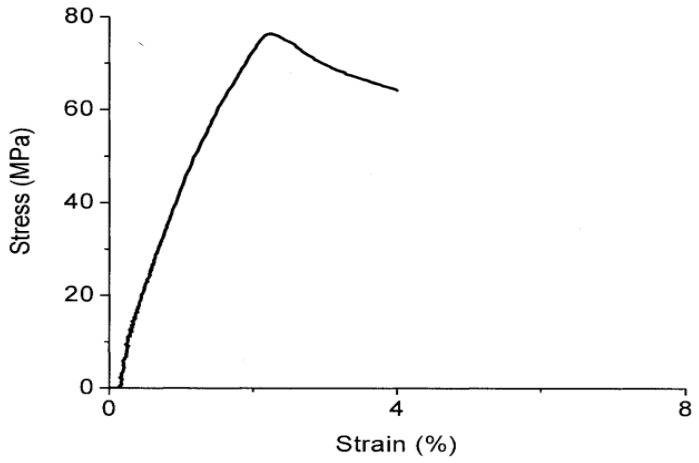

Figure II.30 A Typical Stress-Strain Curve of PLA.**[130]**

Overall PLA has good mechanical properties which are comparable to other commodity thermoplastics like PS and PET (**Table II.13**). As shown on this table, PLA has high modulus (3-4 GPa) and tensile strength (45-60 MPa), but suffers from low T_g, low elongation (ductility) (4-10%) and impact strength which are even lower than those of its homologous glassy polystyrene. Consequently these are the chief culprits for its limited commercial applications.**[114,125]**

Table II.13 Comparison of Typical PLA Properties with Several Petroleum-Based Commodity Thermoplastic Resins. **[118]**

	PLA	PET	PS	HIPS	PP
T_g (°C)[a]	55	75	105	–	–10
Tensile strength @ break (MPa)[a]	53	54	45	23	31
Tensile modulus (GPa)[a]	3.4	2.8	2.9	2.1	0.9
Elongation @ break (%)[a]	6	130	7	45	120
Notched Izod IS (J/m)[a]	13	59[1]	27	123	27[6] (i-PP)
Gardner impact (J)[a]	0.06	0.32	0.51	11.30	0.79
Cost ($/lb)[b]	1–1.5	0.70–0.72	0.99–1.01	1.01–1.03	1.15–1.17

PET: poly(ethylene terephthalate); PS: polystyrene; HIPS: high-impact polystyrene; PP: polypropylene; i-PP: isotactic polypropylene homopolymer; IS: impact strength.
[a] Data mainly cited from ref. 7.
[b] Cost cited from "Plastics News", March 31, 2011 except PLA resin.

II-8-3-6 Rheology and Processing

The actual commercial PLA resins can be processed like all other thermoplastics into various products using conventional technologies of processing including extrusion, injection molding, blow molding, thermoforming, fiber spinning and film forming. The products can be recycled by re-processing or even hydrolyzed into lactic acid, the basic chemical of PLA. **[72,122]** PLA is characterized by low melt strength and poor shear-sensitivity of its melt viscosity, which can be overcome by introducing branching into its backbone either during compounding by adding peroxides or during polymerization by introducing monomers or multifunctional initiators.**[121]** Branched PLA displays high viscosity (melt-strength) at low shear rates, making it more suitable for operations such as extrusion coating, extrusion blow-molding, and foaming **(Figure II.31)**.**[121,125]**

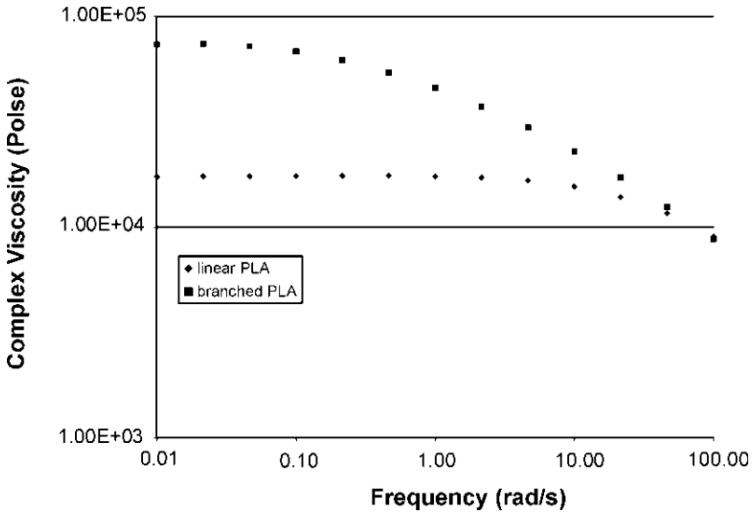

Figure II.31 Rheological Properties of Linear and Branched NatureWorks PLA.**[121]**

II-8-3-7 Other Properties

PLA is generally recognized as safe (GRAS) owing to its low toxicity. Nowadays, PLA resins are approved by the US FDA and European regulatory authorities for all food and medical applications.**[118]** PLA has good barrier properties to flavors and aromas with permeation properties to all gases similar to those of PS.**[104,121,131]** In addition PLA has good crease-retention and crimp, excellent grease and oil resistance, easy low-temperature heat sealability making it appropriate for numerous packaging applications and a good candidate to replace traditional polymers used in this area.**[121,125]**

Optical properties are very important in protecting and preserving products that are sensitive to visible and UV light. Compared to other traditional packaging materials, LDPE shows the highest transmission of UV light followed by PLA (**Figure II.32**). Therefore UV absorbers are needed in the case of PLA to protect packed products.**[132]**

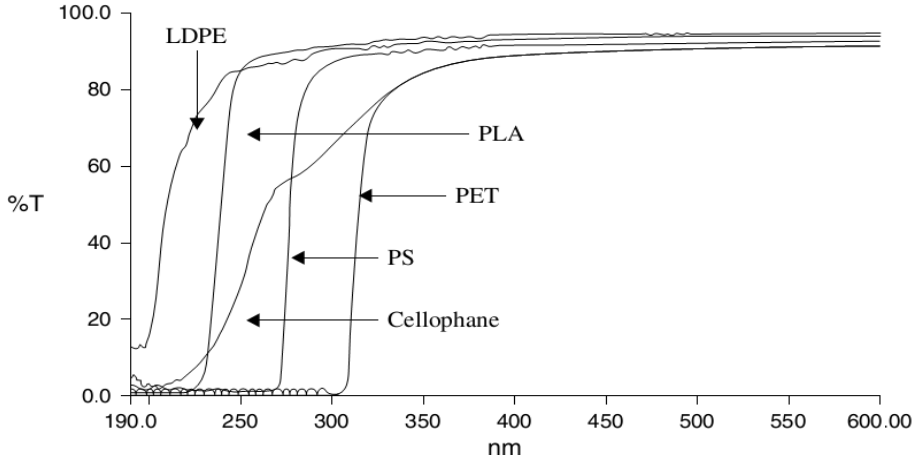

Figure II.32 Percent Transmission Versus Wavelength for PLA, PS, LDPE, PET, and Cellophane Films.**[132]**

II-8-4 PLA Applications

In spite of its excellent properties, the commercial use of PLA has been historically confined in the biomedical applications owing to its high production cost.**[121]** Breakthrough and new innovations accomplished in the production of lactide monomer and the change of polymerization technique from batch to continuous process helped to decrease the PLA price.**[122,131]** In addition, the joint venture between Cagill LLC and Dow Chemical Company in 1997 allowed the large scale production of PLA under the trade name NatureWorks LLC which permitted PLA to change status from an engineering resin to a commodity plastic.**[123]** The cost-performance balance helped PLA to compete well with general purpose petrochemical-based plastics.**[122,131]** and to forge roles in a wide range of end-use applications namely, the packaging and the textile (fiber) sectors and even in the automotive, building sector, cosmetics and electronics which require more durable PLA products.**[42,125] Table II.14** Summarizes some of the application sectors for PLA together with some examples.

Table II.14 Main Applications for PLA.**[133]**

Sector	Examples
Packaging	Food packaging, films, rigid thermoformed food and beverage containers, carrier bags and labels, coated papers and boards, battery packaging, windows for envelopes
Agriculture	Sheet or moulded forms for time-release fertilizers, plant clips
Transportation	Parts of automobile interiors (head liners, upholstery, spare tyre covers)
Electric appliances and electronics	CD, computer keys, cases for Walkmans, wrappers for CD
Houseware	Carpets
Other (fibres and fabrics)	Textiles and non-wovens

II-8-4-1 Medical, Biomedical and Pharmaceutical Applications

For several decades PLA and its copolymers have been extensively used in biomedical field for various applications because of their bioresorbability and biocompatible properties in the human body as well as their ability to degrade both in vivo and in vitro. The main reported examples on medical or biomedical products are bone fracture internal fixation devices in surgery like screws, resorbable prostheses and resorbable surgical sutures which do not need to be removed with a second operative procedure, degradable implants and tissue engineering porous skafolds as reconstructive matrices for damaged tissues and organs.**[109,123]** In recent times, these biomedical applications have been extended to pharmaceutical and medical fields as microspheres and microcapsules which have been widely applied in drug delivery systems for the prolonged administration of a wide variety of medical agents.**[29,104]**

II-8-4-2 Packaging Applications

In the packaging domain (food and nonfood sector) which represents its second market, PLA complies with most requirements for packaging applications and provides excellent physical and mechanical properties at low price. When plasticized it mimics and challenges conventional polymers used in this field such as PP, PET, LDPE, PVC and PS, and is considered as their main alternative and as one solution to alleviate solid waste disposal problems from this application stream which is up to

now considered as the main source of environmental concerns due to the use of these nonbiodegradable polymers.**[101,124]**

Low toxicity, clarity, high gloss and transparency, reasonable barrier properties, good heat sealability and ease of printability and conversion into different forms as well as degradation in biological environment such as soil or compost, has made PLA an ideal and viable material for packaging.**[126,134]** In commercial packaging PLA performs better than PS but it compares more or less to PET.**[109]** In high clarity packaging roles, PLA is a good alternative to PET and some cellulosics which is being used as candy wrap, optically enhanced films, and shrink labels as well as the sealant layer in form-fill coextrusion.**[123]**

PLA is being used as a food packaging for fresh and short shelf-life products, such as fruit and vegetables and those whose quality is not damaged by PLA oxygen permeability.**[104,109]** The initial use of PLA as a packaging material has been in high value films.**[109]** PLA Films, produced by blown double bubble technology, are transparent and have acceptance by customers for food contact. Cast films have very low haze, excellent gloss, and moderate gas (O_2, CO_2, and H_2O) transmission rates desirable for consumer food packaging.**[124]** Other popular package applications include, compostable and loose-fill bags, drinking cups, rigid thermoforms, food and beverage containers, lamination films (paper coatings), blister packages and single-use-bottles because of their resistance to fats and oils, as well as their ability to "block" flavors and aromas.**[109,131]**

II-8-4-3 Fiber and Textiles

Fiber is one of the largest potential application areas for PLA. PLA is readily melt spinnable, and can be designed for many fiber applications. Some of the current fiber uses include hollow fiber-fill for pillows and comforters, bulk continuous filament for carpet, filament yarns, and spun yarns for apparel, spunbond, and other nonwovens and bicomponent fibers for binders and self-crimping fibers and nappies.**[109,124]**

PLA fiber can be combined with natural or regenerated fibers including cotton, wool, silk, viscose, lyocell, and others along with synthetic fibers made from PET, nylon, and other petroleum-based synthetics. PLA can be included as a minor component (5-15%) or as the major fiber, depending on the balance of properties and appearance desired. Some of the beneficial characteristics of PLA fiber products include its natural soft feel, ease of processing, good resistance to UV, reduced flammability, and unique stain and soil resistance and facile dyeability.**[124]**

REFERENCES

[1] Hull, D., An Introduction to Composite Materials, Cambridge University Press, Cambridge UK **(1981)**.

[2] Akovali G., 'Handbook of Composite Fabrication', Rapra Tehnology Limited, Shawbury UK **(2001)**.

[3] Kaw A.K., Mechanics of Composite Materials, 2nd Edition, CRS Press, Boca Raton, Fla. USA **(2006)**.

[4] Karian H.G., Handbook of Polypropylene and Polypropylene Composites, Marcel Dekker Incorporated, New York USA **(1999)**.

[5] Chung D.L., Composite Materials: Science and Applications, Springer-Verlag, London UK **(2003)**.

[6] Deborah C., Composite Materials: Science and Applications, Functional Materials for Modern Technologies, Springer-Verlag London Limited, London UK **(2004)**.

[7] Matthews F.L. and Rawlings R.D., Composite Materials: Engineering and Science, First Edition, Chapman & Hall Inc., London UK **(1993)**.

[8] Callister, Jr.W.D., "Materials Science and Engineering: An Introduction", 7th edition, John Wiley & Sons, Inc. USA **(2007)**.

[9] Fried, J.R., "Polymer Science and Technology", 2nd edition, Prentice Hall PTR, New Jersey USA **(2003)**.

[10] Why Composites? available at http://www.unitedcomposites.net/usapages/whycomposites2.htm

[11] Dülgerbaki, Ç., Master Thesis, "Synthesis and Characterization of Polythiophene/Montmorillonite and Polythiophene/Polypropylene Composites", the Graduate School of Natural and Applied Sciences, Middle East Technical University, Ankara Turkey **(2006)**.

[12] William Gacitua, E.; Aldo Ballerini, A.; Zhang, J., Maderas Ciencia y tecnología, Vol. 7(3), pp 159 **(2005)**.

[13] Xanthos M.,"Functional Fillers for Plastics",Wiley-VCH, Weinheim, Germany **(2005)**.

[14] Pandey, J.K.; Reddy, K.R.; Kumar, A.P.; Sing, R.P., Polym. Degrad. Stab., Vol. 88, pp 234 **(2005)**.

[15] Chrissopoulou, K.; Anastasiadis, S.H., Eur. Polym. J., Vol. 47, pp 600 **(2011)**.

[16] De Azeredo, H.M.C., Food Res. Int., Vol. 42, pp 1240 **(2009)**.

[17] Thostenson, E.T.; Li, C.; Chou, T.W., Comp. Sci. Tech., Vol. 65, pp 491 **(2005)**.

[18] Bikiaris, D.N., Polym. Degrad. Stab., Vol. 98, pp 1908 **(2013)**.

[19] Darder, M.; Aranda, P.; Ruiz-Hitzky, E., Adv. Mater., Vol. 19, pp 1309 **(2007)**.

[20] Kumar, A.P.; Depan, D.; Tomer, N.S.; Singh, R.P., Prog. Polym. Sci., Vol. 34, pp 479 **(2009)**.

[21] Chen, W., PhD Thesis, "Multiwall Carbon Nanotubes Reinforced Epoxy Nanocomposites", Faculty of the Graduate School, University of Southern California USA **(2009)**.

[22] Kojima, Y.; Usuki, A.; Kawasumi, M.; Okada, A.; Fukushima, Y.; Kurauchi, T.T.; Kamigaito, O., J. Mat. Res., Vol. 8, pp 1179 and pp 1185 **(1993)**.

[23] Kojima, Y.; Usuki, A.; Kawasumi, M.; Okada, A.; Kurauchi, T.T.; Kamigaito, O., J. Polym. Sci. Part A: Polym. Chem., Vol. 31, pp 983 **(1993)**.

[24] Vaia R.A.; Ishii, H.; Giannelis, E.P., Chem. Mater., Vol. 5, pp 1694 **(1993)**.

[25] Annabi-Bergaya, F., Microp. Mesop. Mat., Vol. 107, pp 141 **(2008)**.

[26] Paul, D.R.; Robeson, L.M., Polymer, Vol. 49, pp 3187 **(2008)**.

[27] Ahmadi, S.J.; Huang, Y.D.; Li, W., J. Mat. Sci., Vol. 39, pp 1919 **(2004)**.

[28] Hussain, F.; Hojjati, M.; Okamoto, M.; Gorga, R.E., J. Comp. Mat., Vol. 40 (17), pp 1511 **(2006)**.

[29] Sorrentino, A.; Gorrasi, G.; Vittoria, V., Trends F. Sci. Tech., Vol. 18, pp 84 **(2007)**.

[30] Lai, S.M., Wu, S.H., Lin, G.G., Don, T.M., Eur. Polym. J., Vol. 52, pp 193 **(2014)**.

[31] Xu, W.; Raychowdhury, S.; Jiang D.D.; Retsos, H., Giannelis E.P., Small, Vol. 4, pp 661 **(2008)**.

[32] Silva, A.A.; Dahmouche, K.; Soares, B.G., Appl. Clay Sci., Vol. 47, pp 414 **(2010)**.

[33] Wang, B.; Zhou, K.; Jiang, S.; Shi, Y.; Wang, B.; Gui, Z.; Hu, Y., Mat. Res. Bull., Vol. 56, pp 107 **(2014)**.

[34] Herrera, N.; Mathew, A.P.; Oksman, K., Comp. Sci. Tech., Vol. 106, pp149 **(2015)**.

[35] Inuwa, I.M.; Hassan, A.; Wang, D.Y.; Samsudin, S.A.; Mohamad Haafiz, M.K.; Wong, S.L.; Jawaid, M., Polym. Degrad. Stab., Vol. 110, pp 137 **(2014)**.

[36] Bras, J.; Hassan, M.L.; Bruzesse, C.; Hassan, E.A.; El-Wakil, N.A.; Dufresne, A., Ind. Crops Prod., Vol. 32, pp 627 **(2010)**.

[37] Etmimi, H.M.; Mallon, P.E.; Sanderson, R.D., Eur. Polym. J., Vol. 49, pp 3460 **(2013)**.

[38] Moczo, J. and Pukanszky, B., J. Ind. Eng. Chem., Vol. 14, pp 535 **(2008)**.

[39] Tjong, S.C., Mat. Sci. Eng., R. 53, pp 73 **(2006)**.

[40] Laoutid, F. ; Bonnaud, L.; Alexandre, M.; Lopez-Cuesta, J.M.; Dubois, P., Mat. Sci. Eng. R. 63, pp 100 **(2009)**.

[41] Lee, L.J.; Zeng, C.; Cao, X.; Han, X.; Shen, J.; Xu, G., Comp. Sci. Tech., Vol. 65, pp 2344 **(2005)**.

[42] Raquez, J.M.; Habibi,Y.; Murariu, M.; Dubois, P., Prog. Polym. Sci., Vol. 38, pp 1504 **(2013)**.

[43] Yıldırım, Y.; Oral, A., Rad. Phys. Chem., Vol. 96, pp 69 **(2014)**.

[44] Murariu, M.; Dechief A.L.; Bonnaud, L.; Paint, Y.; Gallos, A.; Fontaine, G.; Bourbigot, S.; Dubois, P. Polym. Degrad. Stab., Vol. 95, pp 889 **(2010)**.

[45] Souza, D.H.S.; Andrade, C.T.; Dias, M.L., Mat. Sci. Eng. : C, Vol. 33, pp 1795 **(2013)**.

[46] Katiyar, V.; Gerds, N.; Koch, C.B.; Risbo, J.; Hansen, H.C.B.; Plackett, D., Polym. Degrad. Stab., Vol. 95, pp 2563 **(2010)**.

[47] Katiyar, V.; Gerds, N.; Koch, C.B.; Risbo, J.; Hansen, H.C.B.; Plackett, D., J. Appl. Polym. Sci., Vol. 122, pp 112 **(2011)**.

[48] Yan S.F.; Yin J.B.; Yang J.Y.; Chen, X.S., Materials Letters, Vol.61, pp 2683 **(2007)**.

[49] Fukushima, K.; Tabuani, D.; Abbate C.; Arena, M.; Rizzarelli, P., Eur. Polym. J., Vol. 47, pp 139 **(2011)**.

[50] Nakayama, N.; Hayashi, T., Polym. Degrad. Stab., Vol. 92, pp 1255 **(2007)**.

[51] Zheng, X.; Zhou, S.B.; Xiao, Y.; Yu, X.J., Li, X.H., Wu, P.Z., Colloids and Surfaces B: Biointerfaces, Vol. 71, pp 67 **(2009)**.

[52] Jiang, L.; Zhang, J.; Wolcott, M.P., Polymer, Vol. 48 , pp 7632 **(2007)**.

[53] Kumar, V.; Dev, A.; Gupta, A.P., Composites: Part B, Vol. 56, pp 184 **(2014)**.

[54] Yu, J.; Qiu, Z., ACS Appl. Mat. Interf., Vol. 3, pp 890 **(2011)**.

[55] Zhang, X.; Sun, J., Fang, S.; Han, X.; Li, Y.; Zhang, C., J. Appl. Polym. Sci., Vol. 122, pp 296 **(2011)**.

[56] He, L.; Sun, J.; Wang, X.; Fan, X.; Zhao, Q.; Cai, L.; Song, R.; Ma, Z.; Huang, W., Mat. Chem. Phys., Vol, 134, pp 1059 **(2012)**.

[57] Mai, F.; Habibi, Y.; Raquez, J.M.; Dubois, Ph.; Feller, J.F.; Peijs, T.; Bilotti, E., Polymer, Vol. 54, pp 6818 **(2013)**.

[58] Liu, M.; Zhang, Y.; Zhou, C. Appl. Clay Sci., Vol. 75, pp 52 **(2013)**.

[59] W.Y. Lin; Shih, Y.F.; Lin, C.H.; Lee, C.C.; Yu, Y.H., J. Taiwan Inst.Chem. Eng., Vol. 44, pp 489 **(2013)**.

[60] Maniar, K.K., Polym.–Plast. Tech. Eng. Vol. 43, pp. 427 **(2004)**.

[61] Singh, R.P.; Zhang M.; Chan, D., J. Mater. Sci., Vol. 37, pp 781**(2002)**

[62] Giannelis, E. P.; Krishnamoorti, R.; Manias, E., Adv. Polym. Sci., Vol.138, pp 107 **(1999)**.

[63] Masami Okamoto, "Biodegradable Polymer/Layered Silicate Nanocomposites: A Review; in: Mallapragada, S. and Narasimhan, B. "Handbook of Biodegradable Polymeric Materials and Their Applications", American Scientific Publishers, Vol.1, Chapter 8, pp 1-45 **(2005)**.

[64] Chivrac, F.; Pollet, E.; Avérous, L., Mat. Sci. Eng., R. 67, pp 1 **(2009)**.

[65] *Seyidoğlu, T., PhD Thesis,* "Purification and Modification of Bentonite and its use in Polypropylene and Linear Low Density Polyethylene Matrix Nanocomposites", *the Graduate School of Natural and Applied Sciences,* Middle East Technical University, Ankara Turkey **(2010)**.

[66] Bordes, P.; Pollet, E.; Avérous, L., Prog. Polym. Sci., Vol. 34, pp 125 **(2009)**.

[67] Rhim, J.W.; Park, H.M.; Ha, C.S., Prog. Polym. Sci., Vol. 38, pp 1629 **(2013)**.

[68] Powell, C.E. and Beall, G.W., Cur. Opin. Sol. St. Mat. Sci., Vol. 10, pp 73 **(2006)**.

[69] Verbeek, C.J.R., "Products and Applications of Biopolymers", InTech, Rijeka Croatia **(2012)**.

[70] Sinha Ray, S.; Okamoto , M., Prog. Polym. Sci., Vol. 28, pp 1539 **(2003)**.

[71] Choudalakis, G.; Gotsis, A.D., Eur. Polym. J., Vol. 45, pp 96 **(2009)**.

[72] Balakrishnan, H.; Hassan, A.; Imran, M.; Wahit, M.U., Polym.-Plast. Technol. Eng., Vol. 51, pp 175 **(2012)**.

[73] Sinha Ray, S.; Bousmina, M., Prog. Mat. Sci., Vol. 50, pp 962 **(2005)**.

[74] *Abdallah,W., PhD Thesis,* "Preparation and Characterization of Thermally Stable Organoclays and their Use in Polymer Based Nanocomposites", *the Graduate School of Natural and Applied Sciences,* Middle East Technical University, Ankara Turkey **(2010)**.

[75] Reddy, M.M.; Vivekanandhan, S.; Misraa, M.; Bhatia, S.K. ; Mohanty, A.K., Prog. Polym. Sci., Vol. 38, pp 1653 **(2013)**.

[76] Kiliaris, P.; Papaspyrides, C.D., Prog. Polym. Sci., Vol. 35, pp 902 **(2010)**.

[77] Leszczynska, A.; Njuguna, J.; Pielichowski, K.; Banerjee, J.R., Thermo. Acta, Vol. 453, pp 75 **(2007)**.

[78] Imai, T., "Special Considerations for Clay-Based Materials", in: J.K. Nelson, "Dielectric Polymer Nanocomposites", Springer Science, New York USA, Chapter 3, pp 65-93 **(2010)**.

[79] Wing M.Y. and Zhong-Zhen Y., "Polymer Nanocomposites", Woodhead Publishing and Maney Publishing, Cambridge UK **(2006)**.

[80] Alexandre, M.; Dubois P., Mat. Sci. Eng., R. 28, pp 1-63, **(2000)**.

[81] Suin, S.; Shrivastava, N.K.; Maiti, S.; Khatua, B.B, Eur. Polym. J., Vol. 49, pp 49 **(2013)**.

[82] Hou, L.; Liu, Y., J. Appl. Polym. Sci., Vol. 126, pp 1572 **(2012)**.

[83] Médéric, P.; Pluart, L.L.; Aubry, T.; Madec, P., J. Appl. Polym. Sci., Vol. 127, pp 879 **(2013)**.

[84] Wang, D.; Wilkie, C.A., Polym. Degrad. Stab., Vol. 82, pp309 **(2003)**.

[85] Ojijo, V.; Sinha Ray, S., Prog. Polym. Sci., Vol. 38, pp 1543 **(2013)**.

[86] Pavlidou, S.; Papaspyrides, C.D., Prog. Polym. Sci., Vol. 33, pp 1119 **(2008)**.

[87] Ali Olad, "Polymer/Clay Nanocomposites", in: Boreddy Reddy,"Advances in Diverse Industrial Applications of Nanocomposites", InTech, Chapter 7, pp 113-138 **(2011)** Available from: www.intechopen.com/books/advances-in-diverse-industrial-applications-of-nanocomposites/polymer-clay-nanocomposites *(Last accessed on March **2014**).*

[88] Piscitelli, F.; Posocco, P.; Toth, R.; Fermeglia, M.; Pricl, S.; Mensitieri, G.; Lavorgna, M. J., Colloid Interface Sci., Vol. 351, pp 108 **(2010)**.

[89] Huskić, M.; Žigon, M.; Ivanković, M., Appl. Clay. Sci., Vol. 85, pp 109 **(2013)**.

[90] Bertuoli, P.T.; Piazza, D.; Scienza, L.C.; Zattera, A.J., Appl. Clay. Sci., Vol. 87, pp 46 **(2014)**.

[91] Shen, Z.; Simon, G.P.; Cheng, Y.B., Polymer, Vol. 43, pp 4251 **(2002)**.

[92] Fischer, H.R.; Gielgens, L.H.; Koster, T.P.M., Acta Polym., Vol. 50, pp 122 **(1999)**.

[93] Kouini, B.; Serier, A., Mater. Des., Vol. 34, pp 313 **(2012)**.

[94] Venkatesh, G.S.; Deb, A.; Karmakar, A.; Chauhan, S.S., Mater. Des., Vol. 37, pp 285 **(2012)**.

[95] Lujan-Acosta, R.; Sánchez-Valdes, S.; Ramírez-Vargas, E.; Ramos-DeValle, L.F.; Espinoza-Martinez, A.B.; Rodriguez-Fernandez, O.S.; Lozano-Ramirez, T.; Lafleur, P.G., Mat. Chem. Phys., Vol. 146, pp 437 **(2014)**.

[96] Strawhecker, k; Touny, A.; Wu, L.; Kuppa, V.; Manias, E., "Origins of the Materials Properties Enhancements in Polymer/Clay Nanocomposites", available at: http://zeus.plmsc.psu.edu/nano.html (*Last accessed on* December **2014**).

[97] Ruiz-Hitzkya E. and Meerbeek, A.V., "Clay Mineral and Organoclay-Polymer Nanocomposite, in: Bergaya, F.; Theng, B.K.G.; Lagaly, G., "Handbook of Clay Science", Elsevier, Amsterdam The Netherlands, Chapter 10.3, pp 583 **(2006)**.

[98] Kornmann, X., "Synthesis and Characterization of Thermoset-Clay Nanocomposites., Division of Polymer Engineering, Luleå University of Technology, Sweden **(2001)**.

[99] Fornes, T.D.; Yoon, P.J.; Keskkula, H.; Paul, D.R., Polymer, Vol. 42, pp 9929 **(2001)**.

[100] Zeng, Q.H.; Yu, A.B.; Lu, G.Q.; Paul D.R., J. Nanosci. Nanotech., Vol. 5, pp 1574 **(2005)**.

[101] Nampoothiri, K.M.; Nair, N.R.; John R.P., Biores. Techn., Vol. 101, pp 8493 **(2010)**.

[102] Luckachan, G.E.; Pillai, C.K.S., J. Polym. Environ., Vol. 19, pp 637 **(2011)**.

[103] Gross R.A.; Kalra, B., Science, Vol. 297, pp 803 **(2002)**.

[104] Jamshidian, M.; Tehrany, E.A.; Imran, M.; Jacquot, M.; Desobry, S., Compreh. Rev. Food Sci. Food Saf., Vol. 9, pp 552 **(2010)**.

[105] Rizzarelli, P.; Carroccio, S., Analyt. Chim. Acta, Vol. 808, pp 18 **(2014)**.

[106] Ali Shah, A.; Hasan, F.; Hameed, A.; Ahmed, S., Biotech. Adv., Vol. 26, pp 246 **(2008)**.

[107] Imre, B.; Pukánszky, B., Eur. Polym. J., Vol. 49, pp 1215 **(2013)**.

[108] Soroudi, Z.; Jakubowicz, I., Eur. Polym. J., Vol. 49, pp 2839 **(2013)**.

[109] Avérous, L., "Polylactic acid: Synthesis, Properties and Applications", in: Belgacem, M.N. and Gandini, "Monomers, Oligomers, Polymers and Composites from Renewable Resources", Elsevier, Oxford UK, pp 433–450 **(2008)**.

[110] Avérous, L.; J. Macromol. Sci., Polym. Rev., C44, pp 231 **(2004)**.

[111] Yates, M.R. and Barlow, C.Y., Res. Cons. Recy., Vol. 78, pp 54 **(2013)**.

[112] Chen G.Q. and Patel M.K., Chem. Rev., Vol. 112, pp 2082 **(2012)**.

[113] Institute for Bioplastics and Bioplastics, http://en.european-bioplastics.org *(Last accessed on March **2014**).*

[114] Ebnesajjad, S., "Handbook of Biopolymers and Biodegradable Plastics: Properties, Processing, and Applications, Elsevier Inc. USA **(2013)**.

[115] Shen, K.; Haufe, J.; Patel, M.K.; "Final report of Utrecht University to European Bioplastics, Eur. Biopl. **(2009)**.

[116] Donald Garlotta, D., J. Polym. Env., Vol. 9, pp 63 (**2002)**.

[117] Rasal, R.M.; Janorkar, A.V.; Hirt, D.E., Prog. Polym. Sci., Vol. 35, pp 338 **(2010)**.

[118] Liu, H. and Zhang, J., J. Polym. Sci.: Part B: Polym. Phys., Vol. 49, pp 1051 **(2011)**.

[119] Lasprilla, A.J.R.; Martinez, G.A.R.; Lunelli, B.H.; Jardini, A. L.; Filho, R.M., Biotech. Adv., Vol. 30, pp 321 **(2012)**.

[120] Fowlks, A.C., PhD Thesis, "Development of Polylactic Acid-based Materials Through Reactive Modification", Michigan State University USA **(2009)**.

[121] Drumright, R.E.; Gruber, P.R.; Henton, D.E., Adv. Mater., Vol. 12, (23), pp 1841 **(2000)**.

[122] Jacobsen, S.; Degee, Ph.; Fritz, H.G.; Dubois, P.; Jerome, R., Polym. Eng. Sci., Vol. 39, pp 1311 **(1999)**.

[123] Mehta, R.; Kumar, V.; Bhunia, H.; Upadhyay, S.N., J. Macromol. Sci., Part C: Polym. Rev., Vol. 45, pp 325 **(2005)**.

[124] Henton, D.E.; Gruber, P.; Lunt, J.; Randall, J.; "Polylactic Acid Technology, in: Mohanty, A.K.; Misra, M.; Drzal, L.T., "Natural Fibers, Biopolymers, and Biocomposites", CRC Press USA, Vol.1, Chapter 16, pp 527-577 **(2005)**.

[125] Auras, R.; Lim, L.T.; Selke, S.E.M.; Tsuji, H., "Poly(lactic acid): Synthesis, Structures, Properties, Processing, and Applications, John Wiley & Sons, Inc., Hoboken, New Jersey USA **(2010)**.

[126] Lim, L.T.; Auras, R.; Rubino, M. Prog. Polym. Sci., Vol. 33, pp 820 **(2008)**.

[127] Petchwattana, N.; Covavisaruch, S.; Euapanthasate, N. Mater Sci. Eng. Part A, Vol. 532, pp 64 **(2012)**.

[128] Zhang, C.; Man, C.; Pan, Y.; Wang, W.; Jiang, L.; Dan, Y. Polym. Int., Vol. 60, pp 1548 **(2011)**.

[129] Kopinke, F.D.; Remmler, M.; Mackenzie, K.; Moder, M.; Wachsen, O.; Polym. Degrad. Stab., Vol. 53, pp 329 **(1996)**.

[130] Bhardwaj, R., PhD Thesis, Modification of Polylactide Bioplastic Using Hyperbranched Polymer Based Nanostructures, Michigan State University USA **(2008)**.

[131] Anderson, K.S.; Schreck, K.M.; Hillmyer, M.A. Polym. Rev., Vol. 48, pp 85 **(2008)**.

[132] Auras, R.; Harte, B.; Selke, S. Macromol. Biosci., Vol. 4, pp 835 **(2004)**.

[133] Ewa Rudnik, "Compostable Polymer Materials", Elsevier Amsterdam The Netherlands **(2008)**.

[134] Armentano, I.; Bitinis, N.; Fortunati, E.; Mattiolia, S. ; Rescignano, N.; Verdejo, R., Lopez-Manchado, M.A.; Kenny, J.M. Prog. Polym. Sci., Vol. 38, pp 1720 **(2013)**.

Chapter III

PLA Modifications: Litterature Survey and Previous research studies

Chapter III - PLA Modifications: Litterature Survey and Previous Research Studies

III-1 Introduction

PLA is a thermoplastic polyester from renewable resources with superior biocompatibility, biodegradability, recyclability and good processability using conventional processing techniques. Furthermore, its outstanding physical properties comparable to those of many available synthetic polymers and its relatively low cost make it a suitable candidate with high potential to substitute for petroleum-based polymers in various applications such as biomedical, packaging, automotive, and others.**[1, 2]** Despite these attributes, PLA has some important limitations such as poor gas barrier performance and water-permeability, relatively low thermal stability, low toughness and low extensibility. It is, therefore, necessary to improve these properties if PLA is to be used in long-term applications on a large scale where these properties are of paramount importance.**[3]** In this direction, various strategies, including copolymerization, plasticization, addition of fillers, blending with other flexible-tough polymers and rubber-toughening have been adopted to improve the toughness of brittle polylactide bioplastic.**[4-6]**

The low toughness of PLA (characterized by impact strength as low as 2.5-3 kJ/m^2) and its low tensile elongation (less than 4%) have been the major bottle neck for its large applications, consequently significant engineering efforts have been made to overcome PLA brittleness.**[3]** As for any polymer, it has been shown that PLA mechanical properties can be tailored by varying its crystallinity, molecular weight, its stereochemistry and to some extent by using some processing techniques involving orientation and crosslinking. However, it has been demonstrated that these strategies have little effects on toughness improvement.**[6]** Recently a large number of investigations for toughening PLA have been performed by blending PLA in the melt state with ductile or rubbery polymers either biodegradable or non-biodegradable.**[4-6]** In this section, the aforementioned PLA modification techniques are discussed with an emphasis on blending methodology since it constitutes our chosen strategy to toughen PLA in this research work.

III-2 Copolymerization

Copolymerization is a useful blending technique that allows combining two different monomers or oligomers to improve or tailor new properties that are unattainable by homopolymers. This is a powerful technique in the sense that it allows combining immiscible and/or incompatible polymers that are otherwise difficult or impossible to achieve using known blending methods (melt, solution, etc.). By using copolymerization, a wide spectrum of properties can be obtained or adjusted by selecting proper co-monomer, and by just altering the architecture, the sequence (random, block or graft) and the composition/ratio of the monomers forming the synthesized copolymer.**[5,7]**

Toughening PLA with flexible polymers using copolymerization route has been reported as a viable and versatile approach.**[5,7,8]** In this direction, PLA has been copolymerized with numerous flexible monomers using primarily ring-opening copolymerization (ROC) of lactic acid with a range of cyclic polyesters monomers such as glycolide (glycolic acid),**[9,10]** ε-caprolactone,**[11,12]** δ valerolactone,**[13]** trimethylene carbonate,**[14-16]** β-hydroxyalkanoat,**[17]** and other linear monomers like ethylene glycol,**[10,18]** propylene oxide,**[19,20]** and 1,5-dioxepan-2-one.**[21]** ROC is preferred because it offers a precise control of chemistry and the possibility to produce copolymers with high molecular weight as compared to the polycondensation copolymerization technique that is also feasible thanks to the presence of acid and hydroxyl groups in the lactic acid.**[4,5]**

Depending on the architecture of the monomer being copolymerized with PLA, the nature of catalyst and polymerization conditions,**[7,22]** different categories of copolymers can be obtained including linear random copolymers,**[23,24]** star and linear block copolymers,**[25,26]** graft copolymers,**[27-29]** and crosslinked copolymers.**[30]**

Copolymerization is a versatile way to adjust physical and mechanical properties.**[4,5,7,18-22]** However, this method generally requires a complex multi-step synthesis and high toxic organometallic catalysts. It is practically impossible to remove all of the organometallic compounds and residues from these copolymers that

necessitate an additional purification step, adding thus extra cost to the final price.**[31]** Consequently, none of these copolymerization processes is currently economically viable and none is known to produce PLA copolymers on an industrial scale for general purpose applications, therefore the commercial availability of PLA copolymers for commodity uses is very scarce, if not impossible to find, except for medical and biomedical applications where these copolymers have high added value. Even in medical applications, the use of PLA copolymers will be more extensive if their costs come down.**[4]**

In the field of medical and biomedical applications, various number of architectures of biodegradable and/or biocompatible PLA copolymers based on lactic acid have been investigated to serve in this domain.**[5,7]** Considerable amount of PLA copolymers are designed for tissue engineering. In this application, commonly, the monomer of glycolide acid and ε-caprolactone are copolymerized with lactic acid.**[4,5,7]** Other applications include, applications as heart constructs and nerve regeneration guides,**[32]** cartilage implants and wound dressing,**[15]** sustained drug release carrier,**[33]** and stent cover.**[16]** PLA copolymers have also been used as drug carrier such as the best known ZOLADEX which is a polyactide-co-glycolide with a formulation of goserelin as controlled release drug for the treatment of breast cancer.**[22]**

III-3 Plasticization

In addition to copolymerization, PLA modification through the cheap plasticization methodology, has been extensively investigated for toughening PLA to overcome its brittleness and widen its scope of applications in order to compete with more the more flexible and ductile commodity polymers such as polyethylene or polypropylene.**[4-6,34-36]**

Plasticizers are widely used in the plastics industry as additives that when mixed with glassy or rigid plastics enhance their flexibility, processability, toughness and impart them with ductility.**[4-6,34,35,37]** These improvements are mainly due to the ability of the low molecular weight (Mw) plasticizer to mix intimately with the

matrix by penetrating in between the macromolecular chains of the host plastic, and to exchange the intermolecular bonds among the polymer to new bonds between the plasticizer and the macromolecules, promoting thus conformational changes resulting in increased deformability.**[37]** This mechanism weakens the interchain attraction forces between the plastic chains and increases the free volume leading to improved chain mobility and flexibility that are expressed by a depression of the glass transition temperature (T_g) of the plastic.**[5,38-43]** Consequently, this physical property change of the plastic has been widely considered as a powerful tool to measure the efficiency of a plasticizer.**[40,44]**

The choice of plasticizers is limited by the requirement of application and cost to efficiency ratio.**[37]** An effective plasticizer is mainly a low Mw polar compound that should be highly miscible with the matrix, nonvolatile and nontoxic that can significantly lower the (T_g) of the matrix with minimal migration during aging to avoid matrix embrittlement and also minimal environmental and health issues while maintaining the transparency of the material.**[5,34]** In addition to these requirements, a plasticizer for PLA should also be a biodegradable compound to not alter the biodegradability and the eco-friendliness of PLA.**[5]** Furthermore, the selection of a proper plasticizer depends not only on miscibility with the polymer matrix and on the above cited parameters, but also on its concentration and its Mw (monomeric, oligomeric or polymeric).

PLA has been plasticized using various biodegradable and nonbiodegradable plasticizers.**[5]** Among monomeric and oligomeric plasticizers, polyethylene glycol and citrate esters (derived from naturally occurring citric acid) are the most investigated and promising candidates for PLA plasticization.**[4-6,35,36]** Lactide monomer (LA) is known as the plasticizing agent of choice for PLA, however it presents the drawback of readily volatilizing during processing because of its low boiling temperature in addition to fast exudation/migration to the surface.**[45,46]** Oligomeric LA (OLA) has been then studied to solve these two drawbacks, but OLA showed lower efficiency than LA.**[40,45]**

Other monomeric esters than lactide have been investigated as potential plasticizers for PLA including triethyl citrate (TEC),**[47]** tributyl citrate (TBC),**[47,48]** acetyltriethyl citrate (ATEC)**[47],** and acetyltributyl citrate (ATBC)**[47,49,50]**. **Figure III.1** exhibits the chemical structures of some of the most studied oligomeric plasticizers for PLA reported in literature. Migration to the surface and volatilization at low processing temperatures are the main hurdles facing the widespread use of the low Mw plasticizers. Consequently, increasing the Mw of plasticizers has been considered as a possible way to prevent the above mentioned shortcomes (plasticizer volatilization and migration). In this case solubility (mixing) of the plasticizer with the matrix could be maintained through polar interactions.**[51]** Using this strategy, PLA was plasticized with numerous oligomeric or polymeric plasticizing compounds including adipates,**[52,53]** TBC oligomers,**[51,54]** DBM-oligoesters and DBM-oligoesteramides (DBM: diethyl bishydroxymethyl malonate),**[54,55]** PEG,**[56-58]** PLA-*b*-PEG block copolymers,**[59]** poly(propylene glycol) (PPG).**[39,60]**. However, many studies reported a limit to Mw increase. Indeed, increasing the Mw leads to decreasing solubility of the plasticizer and even phase separation due to low saturation concentration of plasticizer.**[50,61]** Therefore, another alternative option that uses mixed plasticizers taking the complementary advantages of low Mw plasticizers with oligomeric and polymeric ones was also attempted.**[62,63]**

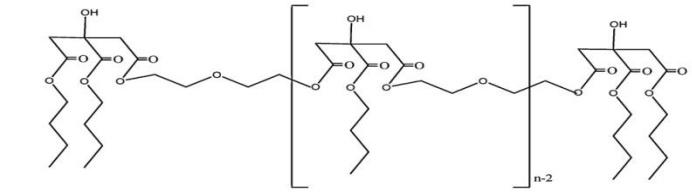

(a) Oligomeric tributyl citrate [82].

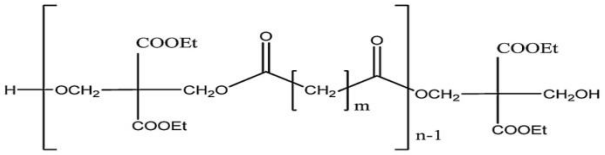

(b) Oligomeric diethyl bishydroxymethyl malonate (DBM) [83].

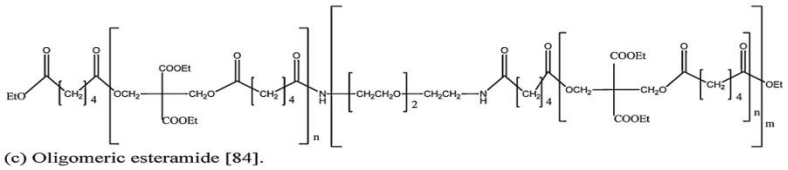

(c) Oligomeric esteramide [84].

Figure III.1 Chemical Structure of Some Common Plasticizers Used For PLA.**[4]**

Recently other types of organic compounds were also identified and tested as possible plasticizers such as bis(2-ethyl-hexyl) adipate (DOA) and glycerin triacetate (GTA),**[49]** epoxidized soybean oil (ESO),**[64,65]** polyester diols,**[66]** ionic liquids,**[67]** sorbitol and glycerol,**[68]** partial fatty acid esters,**[44]** canola oil,**[69]** and N-octyl lactate (NOL).**[70]**

According to all what has been accomplished in the field of PLA plasticization, this strategy has been found to be very effective to endow PLA with flexibility and ductility but still presents some disadvantages. Drawbacks of plasticization have been well summarized by Liu and Zhang in their recent review on toughening modification of PLA.**[5]** It is reported that significant T_g reduction is obtained only at relatively high plasticizers content (15-20%) that is usually accompanied with a substantial undesirable drop in stiffness and strength. In addition other issues are not yet solved, such as embrittlement during aging due to plasticizer exudation, and also limits of both plasticizer loading level (saturation) and plasticizer Mw increase as well as the cold crystallization process related to enhanced chain mobility induced by the plasticizer.**[4-6,35]**

Literature review revealed that considerable efforts have been made to solve problems related to PLA plasticization.**[4-6,35,36]** Many research studies have been attempted to mitigate the stiffness and strength reduction brought about by plasticizer addition through blending with nanofillers to form plasticized PLA nanocomposites,**[71-73]** and also with traditional fillers to form PLA plasticized composites.**[74-76]** Recently, in situ reactive grafting of low molecular weight and functionalized plasticizers onto PLA such as poly(ethylene glycol) and tributyl citrate,**[44,77]** and chemical grafting of plasticizer on PLA molecules via in situ reactive blending have been proposed as a new innovative options to overcome or at least to minimize the migration and phase separation of plasticizers.**[41,78-,79]**

Up to now, despite the tremendous progress made in PLA plasticization, there is no efficient plasticizer that has demonstrated effective balance of PLA properties without exhibiting the above discussed limits. Consequently, research studies are still needed in the PLA plasticization field.

III-4 PLA Modification by Reinforcement "Filling Modification"

Modification of polymers with organic or inorganic fillers has been a traditional approach used to tailor their properties. The achieved developments and the know-how acquired with petroleum-based polymer nanocomposites have been successfully applied to biopolymers to form an emerging class of materials known as bionanocomposites that exhibit impressive enhancements of properties that are promising for numerous applications.**[4-6]** Over the last decade, PLA has been reinforced with various nanoparticles, including montmorillonite (MMT),**[80]** expanded graphite **(**EG),**[81]** mica,**[82]** layered double hydroxide **(**LDH),**[83,84]** SiO_2,**[85,86]** TiO_2,**[87]** and others.**[88-95]** However, among all nanofillers tested with PLA, layered silicates have been the most investigated and reported ones in literature. **[4-6]** PLA nanocomposites have been prepared**]**, by in situ polymerization,**[83]** by solution intercalation,**[80,85,87,88,90,92,93,96,98,99,103,105-107,123,124]** but melt compounding was the most used and the most discussed in literature so far.**[71,74,81,82,84,86,89,91,94,95,97,100-102,104,108-122]**

The first attempt to prepare PLA nanocomposite was certainly that reported by Ogata and coworkers,**[96]** who have prepared the nanocomposite in solution using hot chloroform as solvent in the presence of dimethyldistearylammonium-modified MMT. According to WXRD and SAXS, the authors reported that complete exfoliation was not attained, but rather particular geometrical structures consisting of tactoïdes of several stacked silicate monolayers formed. Despite this low clay dispersion, the obtained structure was responsible of improved Young's modulus.**[207]** Since this pioneering work, a wealth of research studies have been reported on PLA nanocomposites dealing with various PLA modification objectives.

Using a twin screw-extruder, Sinha ray et al.,**[97]** melt mixed 4 wt% of a trimethyl octadecylammonium-modified montmorillonite (MMT) to prepare PLA/OMMT nanocomposite (PLACN4). X-ray diffraction (XRD) and transmission electron microscopy (TEM) confirmed the intercalation of the clay and its homogeneous dispersion. It was also reported that neat PLA properties improved remarkably after nanocomposite preparation. The dynamic mechanical properties

measured at 25°C in tension-torsion mode revealed a significant (2-fold) increase of storage modulus from 1.63 GPa for neat PLA to 2.32 GPa for PLACN4, and the flexural modulus and strength improved from 4.8 GPa and 86 MPa for PLA to 5.5 GPa and 134 MPa for PLACN4 respectively. Thermal investigation also indicated an improvement of nearly 18°C in the heat distortion temperature (HDT) of PLA which increased from 76.2°C to 94°C for the nanocomposite.**[97]**

The effect of the miscibility of three different organic modifiers of the OMMT on clay dispersion in PLA was examined by Krikorian and Pochan.**[98]** It was found that increasing the miscibility of the surfactant/polymer matrix increased the tendency of the system to exfoliate and randomly distribute the silicate layers. The mechanical properties investigation revealed that PLA storage modulus significantly improved with increasing clay content while the transparency of the matrix is maintained due to nanometer-range dispersion of the reinforcement. DSC indicated that the extent of crystallinity was inversely proportional to the extent of modified clay loading in the final nanocomposites, and that the melting temperature (T_m) of PLA was not sensitive to OMMT addition suggesting that the lamellae thickness was constant and not altered by the presence of nanoclay.

The effects of three different types of OMLS on the thermomechanical properties and morphology of PLA nanocomposites were studied by Chang et al..**[99]** The nanocomposites films were prepared by solution technique in which the OMLS contents varied from 0 up to 10 wt%. Clays used in this investigation were two OMLS namely Hexadecylamine–montmorillonite (C16-MMT), dodecyltrimethyl ammonium bromide-montmorillonite (DTA-MMT) prepared from sodium montmorillonite (MMT-Na^+), and the commercially Cloisite®25A (C25A). From morphological studies using XRD analysis, the initial d-spacings of the clays were 11.99, 25.96, 16.85 and 19.63Å for MMT-Na^+, C16-MMT, DTA-MMT and C25A Å respectively indicating that this d-spacing was dependent on the size of the exchanged cation. Interestingly, the d-spacings of all three hybrids had almost the same values, regardless of the clay loading, in contrast to pure organoclays. Exfoliation was not attained, but overall most clay layers were found to be dispersed homogeneously in the matrix polymer, although

some clusters or agglomerated particles were also detected by TEM. For hybrid films, the tensile properties initially increased but then decreased with increasing content of inorganic phase.

Melt blending of an organoclay with PLA to form nanocomposites by using an internal mixer has been considered by Di et al..**[100]** The exfoliation of clay layers was achieved and attributed to the interaction between the organoclay and PLA molecules and also to shearing force during mixing. The crystallization rate of PLA increased at low content of exfoliated clay platelets indicating the role of the clay as nucleating agent, however at higher contents the clay sheets acted as physical barriers to the chain mobility of PLA and reduced the crystallization of PLA. The exfoliation of MMT and its strong interaction with PLA led to improvement of the thermal dynamic mechanical moduli of nanocomposites at low MMT which was observed to decrease at higher organoclay content. The rheological studies showed that the nanocomposites have higher viscosity and more pronounced elastic properties than pure PLA. The authors attributed the improvements to the strong interaction between PLA and exfoliated MMT layers, and concluded that there is an optimum amount of MMT for PLA/MMT nanocomposites for improved properties.

The commercially available Cloisite®25A (C25A) was successfully functionalized by reacting this previously amine modified MMT with (glycodoxypropyl)trimethoxysilane.**[101]** This twice functionalized clay (TFC) with higher organophilicity than C25A was used to prepare PLA/TFC nanocomposites. TEM and Fourier Transform Infrared (FTIR) showed that these nanocomposites exhibited full exfoliation when clay was used up to 5 wt%; however beyond this content an intercalated/exfoliated nanostructure is obtained. PLA/TFC displayed superior tensile modulus, tensile strength and elongation at break as compared to PLA/C25A. The higher degree of exfoliation in the silicate layers in PLA/TFC and the improved mechanical properties compared with those of PLA/C25A were attributed to enhanced compatibility between PLA and TFC that arose from improved interfacial interaction through a chemical reaction between the epoxy groups of the TFC and the end group of the PLA.

In another study, PLA-nanocomposites containing 5 wt% C25A were prepared by twin screw extruder using various masterbatches based on PLLA, PDLLA and PBAT.**[102]** The thermal and mechanical properties of the films prepared by single screw cast films extruder were examined in order to determine the effect of the clay and different carriers on the polymer-clay interactions. The most significant improvements were observed when the nanoclays were incorporated via masterbatch method using a PLLA carrier of the same grade as the PLLA matrix. This nanocomposite exhibited simultaneous strengthening and toughening of the PLA matrix attributed to better molecular interactions between nanoclays and PLLA and to the high level of exfoliation which resulted in increased tensile modulus and elongation at break by 37% and 48% respectively, with an insignificant loss of strength. DSC proved that the clay acted as nucleating agent since it decreased the cold crystallization temperature (T_c) by 15°C. The authors concluded that the improved film properties obtained show the advantage of using masterbatch technology over conventional compounding.

Maleic anhydride grafted PLA (PLA-MAH) was used as a compatibilizer for PLA nanocomposites prepared by solution casting method.**[103]** Two different types of layered silicates were utilized: bentonite and hectorites each one incorporated separately into PLA at a level of 5 wt%. Controversial results were obtained concerning the results of clay dispersion state. X-ray diffraction of the prepared nanocomposites indicated exfoliation of the silicates. However, micrographs from TEM showed the presence of intercalated and partially exfoliated areas. The effect of using PLA-MAH in the two layered silicates was not the same because of the difference between their organic treatments. Tensile testing showed improvements in both the tensile modulus and yield strength for all the prepared nanocomposites, but the bentonite layered silicate exhibited a more distinct improvement in exfoliation and an increase in the mechanical properties because of the addition of PLA-MAH in comparison with the hectorite layered silicate. The results from the dynamic mechanical thermal analysis showed an improvement in the storage modulus over the entire temperature range for both layered silicates together with a shift in the tan δ peak to higher temperatures.

The effects of layered silicate concentration (Cloisite®30B (C30B)) and of the compatibility of PLA with the organoclay were investigated by Pluta et al..**[104]** PLA-based nanocomposites were prepared by melt blending in the presence or absence of an amorphous maleic anhydrite functionalized elastomeric ethylene copolymer as a compatibilizer (Exxelor VA1803). The Mw, measured by SEC, of the processed-unfilled PLA decreased by ~25% (from 126000 to 94400) attributed to the susceptibility of PLA to degradation during melt processing even under non-oxidative atmosphere, while that of the compatibilized PLA (PLA/3wt% Exxelor VA1803) decreased only by ~6% (from 126000 to 118000) as compared to the neat PLA suggesting some stabilizing effect of the compatibilizer towards PLA degradation or some chemical interactions between these components. Furthermore, it was observed that the melt processing in the presence of the nanoclay contributes to further decrease of the Mw, even if the compatibilizer was used. The x-ray diffraction results showed complete exfoliation at low MMT concentration (3 wt%) but at higher MMT concentration (10 wt%) a mixed intercalated and exfoliated nanostructures were detected. It was also found that due to the presence of MMT, the viscosity of the system significantly increased with increasing MMT content, while the viscoelastic spectra from DMA also showed a gradual increase of the storage and loss moduli with the increase of the MMT content and improved dispersion.

Comparaison of PLA/OMMT and PLA/nanoprecipitated calcium carbonate (NPCC) nanocomposites was investigated by Jiang et al..**[89]** OMMT and NPCC showed significantly different effects on the strength, modulus and elongation at break of the PLA nanocomposites. PLA/OMMT showed better mechanical improvements, but the extent of increase in strain at break and decrease in tensile strength was not significant. Different toughening mechanisms were first elucidated for two types of nanocomposites based on the evidence from both macroscopic and microscopic observations. Under uniaxial tension, large quantities of microvoids were created in both PLA nanocomposites. The microvoids in PLA/NPCC caused massive crazing, while in PLA/OMMT they resulted in shear yielding, particularly in the nanocomposite with 2.5 wt% OMMT.

PLA/MMT nanocomposites prepared by solution (toluene) intercalation and melt intercalation methods were investigated by Chow and Lok.**[105]** DSC showed that both T_g and T_m of PLA were not influenced by the addition of MMT, but reduced its T_c. It was also found that PLA/MMT nanocomposites prepared by solution intercalation exhibited higher flexural modulus than PLA/MMT nanocomposites prepared by melt intercalation that was attributed to the better dispersion of MMT layered silicate in PLA. Balanced flexural properties including flexural modulus, yield stress and yield displacement for PLA nanocomposites prepared by both solution and melt intercalation method were obtained at the optimum loading of 1 wt% of MMT. It was concluded that although better clay intercalation and flexural properties were obtained for PLA/MMT nanocomposites prepared by solution intercalation method, melt intercalation method also produced PLA/MMT with comparable flexural properties.

In another study, Rhim et al.,**[106]** prepared PLA nanocomposites by solvent casting method using unmodified MMT "Cloisite®-Na^+" (MMT-Na^+), C20A and C30B. Tensile strength and elongation at break of the composite films prepared with 5 wt% clay decreased by 10-20% and 11-17%, respectively, depending on the clays used. Among the clay types used, C20A was the most effective in improving the water vapor (WVP) barrier property while sacrificing tensile properties the least. The effect of clay concentration tested using C20A showed a significant decrease in Tensile strength and WVP, with increases in clay content.

Cocamidopropylbetaine (CAB) surfactant, a derivative of coconut oil, was used by McLauchlin and Thomas to modify the MMT surface.**[107]** CAB is a quaternary compound that belongs to the betaine group, thus it contains carboxyl moieties which could interact with the polar regions of the PLA chains in the same way as proposed for the hydroxyls of C30B. PLA nanocomposites based on the novel organoclay (CAB-MMT) and on MMT-Na^+ were prepared by solution casting (chloroform), and were compared to PLA/C30B nanocomposites. The nanocomposites were characterized by XRD, TEM and thermogravimetric analysis (TGA). Solubility parameters calculated by three different methods showed that CAB-MMT had the

same solubility parameters as C30B, which had previously been shown to disperse well in PLA. XRD results which were confirmed by TEM analysis showed that PLA readily intercalated both CAB-MMT and C30B to similar extents. Thermal stabilities of the PLA-organoclay composites based on CAB-MMT were higher than those based on the commercial organoclay.

With the perspective of using PLA in biomedical field, Nieddu et al.,**[108]** investigated the reinforcement of PLA by using five types of clays at two concentrations (5 and 10 wt%). The nanocomposites were prepared by melt intercalation method and the mechanical properties of the nanocomposites were dtrmined. Results showed an influence of the type of nanoreinforcement on the interaction with the PLA matrix. Consequently, also the mechanical properties were affected. The nanocomposites showed improved mechanical behavior depending on type and content of clay: the modulus increased, with respect to neat PLA, from 4% to 47% at 10 wt% for the organically modified fluorohectorite content, while strain at break decreased in all composites except in those containing Sepiolite due to its needle-like particles instead of plate-like particles as it is for the other clays.

Fukushima et al.,**[109]** melt blended PLA with expanded graphite (EG) and C30B to produce nanocomposites. The XRD results confirmed by TEM observations showed that C30B was more intercalated by PLA than EG was due to better interaction of PLA with C30B than with EG. Furthermore it was found that co-addition of EG to PLA enhanced the dispersion of C30B as EG content increases. Thermal characterization by DSC indicated that EG accelerated PLA crystallization by increasing the crystallinity from 2% for pristine PLA to 13% and 23% when 6 wt% and 9 wt% EG were added to PLA. However the addition of 3 wt% C30B to the ternary system prevented the inducing effect of EG on polymer crystallization under cooling ascribed to possible restricted segmental motions at the organic-inorganic interface, avoiding PLA crystallization. Significant enhancements in rigidity from 2800 MPa for PLA to 5100 MPa for ternary nanocomposites was achieved after co-addition of 3 wt% and 9 wt% of C30B and EG respectively. With few exceptions, concerning the PLA-EG nanocomposites, the maximum tensile strength remains

practically constant as compared to neat PLA (60-64 MPa). For all compositions containing EG, the nominal strain at break of PLA tends to decrease gradually by increasing the percentage of EG, whereas the PLA-C30B (3 wt%) nanocomposite presents an increase of this parameter with respect to neat polymer matrix, assumed to be due to a slight plasticizer effect conferred by the presence of organomodifier in clay. Notched impact strength of the nanocomposites values were characterized by comparable values (2.6-2.9 kJ/m^2) to those recorded for neat PLA (2.7 kJ/m^2) and noticeable, the ternary compositions do not show relevant decreases in this parameter. It was concluded that the improvement of thermal and mechanical properties obtained by the presence of both nanoparticles in PLA were associated to the good (co)dispersion and to the co-reinforcement effect.**[109]**

Carrasco and coworkers,**[110]** explored the effect of addition of C30B on chemical structure, crystallinity and morphology of PLA. The preparation of the nanocomposites necessitated three extrusion steps followed by injection molding. The results indicated that there was a significant decrease in the average Mw of processed PLA and its nanocomposites with pronounced decrease observed for the nanocomposites especially at higher clay loading which was attributed to significant water absorption by clay that has led to hydrolysis during compounding. The results were confirmed by melt flow index (MFI) measurements which indicated considerable increase in the MFI values, due to a plasticizing effect of the organomodified clays. XRD results confirmed by TEM analysis indicated homogeneous distribution of the clay with exfoliation and some aggregates of clays observed at 0.5 wt% clay content, whereas an intercalated structure was detected at 2.5wt%.

To study the effect of crystallinity degree on the thermal, mechanical, and fracture properties, Gamez-Perez et al.,**[111]** prepared PLA/OMMT nanocomposites at 0.5 wt% and 2.5 wt% OMMT in a twin-screw extruder followed by injection molding and an annealing treatment to increase the percentage of PLA crystallinity. Decrease in the yield stress and an increase in the elongation at break with the addition of OMMT were observed. The elongation at break increased from 4.0% for the PLA to 5.7% and 11% for the nanocomposites with 0.5wt% and 2.5wt%of OMMT respectively.

In another research work, Wang et al.,**[112]** reported an improvement in the mechanical properties measured by dynamic mechanical analysis (DMA) and tensile test for PLA/OMMT nanocomposites prepared by melt-compounding technique. The ductility of PLA was enhanced by addition of only 1 wt% OMMT to PLA, reflected by an increase in the elongation at break from 5.4% to 7.9%, whereas the Young's modulus improved from 1.65 GPa to 1.93 GPa. However, further increase of OMMT loading to 5 wt% induced a significant drop in the elongation at break to a value of 2.9%. Even though the ductility was improved by a factor of 1.5 for the nanocomposites with 1 wt% OMMT; the material still showed brittle behavior.

The study of PLA nanocomposites made up of aluminum hydroxide (ATH) and C30B was reported by Cheng et al..**[113]** The nanocomposites were prepared via direct melt compounding in a twin-screw extruder and the morphology, thermal degradation, and mechanical properties of the PLA/ATH/OMMT composites were investigated by XRD, TEM, TGA and tensile testing. XRD investigations showed that the PLA/ATH/OMMT nanocomposite is exfoliated-intercalated, which was verified by TEM observations. Thermal stability measurements under air atmosphere (oxidative conditions) indicated that the thermal degradation temperature and activation energy of PLA were increased after addition of ATH and further thermal stability was observed when OMMT was incorporated into PLA/ATH to form PLA/ATH/OMMT. Regarding the mechanical properties it was found that addition of ATH increased the stiffening but induced brittleness by decreasing elongation at break and tensile strength as ATH increases. However, addition of OMMT helped to counterbalance the observed low mechanical performance especially the loss in strength and stiffness.

Considerable thermo-mechanical improvements in PLA were obtained by preparing PLA nanocomposites based on two different clays montmorillonite (C30B) and fluorohectorite (SOMMEE) at 5 and 10 wt% clay loading using co-rotating twin screw extruder.**[114]** It was found that both clays have a good interaction with the PLA matrix and their corresponding nanocomposites with PLA at 5 and 10 wt% loadings showed a good level of clay dispersion as detected by XRD and confirmed by

TEM and SEM. However some reduced C30B dispersion was noticed as compared to SOMMEE. According to DSC results, both clays acted as nucleating agents, especially for SOMMEE, by inducing PLA crystallization and promoting its kinetics which was more pronounced at 10 wt%. The highest thermo-mechanical and mechanical improvements were obtained at 10 wt% of clay ascribed to the enhanced clay dispersion and increased crystallinity at this clay loading level. With respect to PLA, the nanocomposites, especially that with higher aspect ratio SOMMEE clay, exhibited the highest thermo-mechanical and mechanical improvements at 10 wt% of clay which was associated with the good clay dispersion level as well as to the high clay content and with increased polymer crystallinity, sustained by XRD, SEM, DSC and DMTA analysis.

Lai et al.,**[115]** developed PLA nanocomposites using C30B clay with loadings of 1, 3 and 5 wt% processed in an internal mixer. At 1 wt% clay, the nanocomposites showed the highest level of exfoliation as compared to the other investigated clay loadings. In addition this nanocomposite had the lowest tensile modulus but exhibited significant stress-whitening and necking behavior with a large extension reflected by an elongation at break increase from 5.61% to 208%, representing up to 37-fold increment compared to the neat PLA while maintaining almost constant its tensile strength (~51MPa). However, at higher loading (2 wt% and 5 wt%) the nanocomposites had intercalated structures in which C30B acted as rigid filler, that had raised the modulus but caused premature failure of the nanocomposites. The deformation mechanism of tensile bars of the nanocomposites was also discussed using SEM and TEM and it was revealed that the well dispersed clay resulted in a highly plasticized interfacial region which brought about multiple shear-banding that induced plastic deformation and substantial shear yielding. DSC results indicated that T_g of PLA was slightly decreased by addition of clay but in general it was found that the effects of chain degradation and plasticization by clay surfactant outweigh the reinforcing effect of the rigid clay at low clay loading. It was also revealed that PLA crystallinity increased at high clay loadings suggesting the nucleating effect of the clay.

In spite of the excellent results obtained with PLA bio-nanocomposites, it is generally found that the incorporation of the nanofillers into PLA leads to its stiffening.**[4-6]** Consequently, and with the objective of preparing toughened PLA materials with balanced properties, nano-biocomposites based on plasticized PLA has been proposed as a way to improve PLA ductility and to expand its applications window.**[71,74,116-125]** In this regard addition of a plasticizer to PLA nano-biocomposites has been considered by several authors.**[116,117]** For example, agglomerated structures were obtained when PLA/OMMT nanaocomposite was plasticized with poly(ethylene glycol) (PEG) that resulted in low elongation at break (< 5%). Moreover, the shear thinning properties of the nanocomposites were independent of the addition of PEG.**[116]** The effects of the addition of different amounts of four types of modified C20A, C25A and C30B and unmodified (MMT-Na^+) clays on PLA plasticized with 20 wt% of PEG 1000 nanocomposites prepared in an internal mixer were investigated by Paul et al..**[117]** XRD revealed that both PLA and PEG intercalate in the clay galleries, depending on the clay modifications. It also appeared that PEG was even able to intercalate between clay interlayers of unmodified MMT. These results were confirmed by DSC analyses indicating that there was a real competition between PEG 1000 and PLA for the intercalation into the clay interlayers. At constant filler level, among all the clays studied, C30B brought the greater effect in terms of thermal stability and a delay in the onset of thermal degradation of the plasticized PLA was obtained with increasing clay content. No mechanical properties investigation was reported in this study.**[117]** It was also found by the same authors that addition of PEG plasticizer reduced T_g of PLA by ~26°C from 49.7°8C to 23.4°C; however, this decrease was slightly smaller (2-5 °C) for plasticized nanocomposites without clear relation to the filler type and related content, and below T_g, PEG acted as a reinforcement than as a plasticizer as reflected by a gradual increase of storage modulus with filler loading. XRD results revealed that PLA intercalates better in C30B than in C20A and C25A owing to its higher affinity to C30B than to the other clays (affinity to PLA: C30B > C20A > and C25A). However the authors did not report on the mechanical properties.**[118,119]**

PLA blown films obtained by mixing 10 wt% of acetyltriethyl citrate ester plasticizer and 5 wt% MMT to PLA showed improved barrier properties and 20% increase in modulus as compared to the neat PLA films without scarifying the ultimate ductility of the nanocomposites.**[120]** However, the plasticizer acted more as a processing aid than a toughening agent as the elongation at break of the materials remained below 10%. DSC measurements demonstrated that the thermal properties namely T_g, cold crystallization and melting point temperatures were not significantly influenced by the presence of MMT.

Shibata et al.,**[121]** studied the thermal and mechanical properties of PLA nanobiocomposites plasticized with diglycerine tetraacetate (PL-710) and ethylene glycol oligomer containing 2 types of MMT modified with octadecylamine and poly(ethylene glycol) stearylamine i.e., ODA-M and PGS-M respectively. Better clay dispersion was observed for PLA/ODA-M and plasticized PLA/ODA-M composites than for PLA/PGS-M and plasticized PLA/PGS-M composites. The PLA and PLA/PL-710 composites containing ODA-M showed a higher tensile strength and modulus than the corresponding composites with PGS-M. The PLA/PL-710 (10 wt%) composite containing ODA-M showed considerably higher elongation at break than the pristine plasticized PLA, and had a comparable tensile modulus to pure PLA. T_g of the composites decreased with increasing plasticizer and the addition of the clays did not cause a significant increase of T_g.

Multifilaments yarns were prepared from filaments melt-spun using PLA nanocomposites made up of PLA melt blended with various contents of C30B. Plasticized PLA nanocomposite containing 10 wt% dioctyl adipate (DOA) plasticizer and 4 wt% C30B was also prepared.**[122]** XRD diffractograms and TEM observations performed only for unplasticized and plasticized PLA/4wt% C30B showed good dispersion of C30B in the PLA with intercalate/exfoliated structure. DSC analysis indicated that the slow crystallization of PLA occurs only above 100°C and was slow even above 120°C, and the crystallization kinetics enhanced with clay content increase due to the nucleating effect of the clay. It was also noted that addition of the plasticizer decreased the T_g, T_c and T_m of PLA by increasing chain mobility. Accordingly, DOA

promotes faster and more intensive crystallization. A decrease of the tensile properties is observed when the quantity of C30B increases, but an improvement of the thermal and shrinkage properties was highlighted. The decrease in mechanical properties especially elongation at break demonstrated the necessity of using dioctyl adipate (DOA) plasticizer to spun the blend with 4 wt% C30B. The obtained filaments had better elongation properties (86.4%) compared to filaments from PLA (46.8%), so they could be used to produce knitted fabrics.

High performance PLA composites composed of melt-blended carbon black (CB) and PLA plasticized with acetyl tributyl citrate (ATBC) and poly(1,3-butylene adipate) (PBA) as plasticizers were reported by Wang et al..**[74]** Interaction between PLA and CB was evidenced by FTIR spectroscopy which was improved thereafter by the co-addition of ATBC and PBA plasticizers. Mechanical properties investigated by tensile test showed that both ATBC and PBA decreased the tensile strength of PLA, but improved its elongation at break. Interestingly, the elongation at break of PLA containing 30 wt% PBA was above 600% and higher than that of PLA plasticized with the same amount of ATBC. However; the incorporation of CB increased stiffness but had an adverse effect on elongation at break which decreased for both composites plasticized by ATBC and PBA. Moreover, it was also found that T_g increased with increasing CB content and addition of plasticizer was found to enhance dispersion of CB as was evidenced by SEM.

With the aim of reducing the dependence on petroleum-based surfactants, Al-Mulla et al.,**[123]** modified MMT-Na^+ with three fatty nitrogen compounds (FNCs), fatty amides (FA), fatty hydroxamic acids (FHA), and carbonyl difatty amides (CDFA) synthesized from vegetable oils. The clays were used in the preparation by solution casting of epoxidized soybean oil (ESO) plasticized PLA nanocomposites at PLA/ESO ratio of 80/20 (w/w) which was found to have the highest elongation at break.**[124]** The XRD and TEM results confirmed the production of nanocomposites of higher thermal stability than PLA/ESO compound. Concerning the mechanical properties, the highest tensile strength, modulus, and elongation at break of the FA-MMT, FHA-MMT, and CDFA-MMT nanocomposites were obtained when 3 wt% of

the FA-MMT or the FHA-MMT and 2 wt% the CDFA-MMT loadings were used which was attributed to increased intercalation of PLA/ESO in the clays and to enhanced interactions of the intercalated PLA/ESO chains with the silicates surface layers. However; above these clay concentrations, it was reported that the tensile properties decreased due to the decrease of the PLA/ESO chains interacting with the clay as the clay coagglomerates.

Martino et al.,**[71]** combined the effect of 15 wt% of polymeric adipates with different molar masses (from 1500 to 2500 Da), with 3 wt% C30B. The clay was swelled in liquid polyadipates prior to their blending with PLA to facilitate chains intercalation and nanofiller exfoliation during melt-blending. When the organoclays were previously mixed with low molecular weight liquid polyadipates, swelling occurred and facilitated intercalation of PLA chains into C30B galleries. Thus the prepared materials showed enhanced ductility and barrier properties. The addition of 15 wt% of polyadipate led to an increase of the elongation at break of up to 300%. A loss of ductility was observed with the addition of 3 wt% of C30B but elongation at break still remained above 200%.

III-5 Modification of PLA by Blending with Polymers and Rubbers

The largest amount of research on toughening PLA has occurred in the blending field because toughening is usually an integral part of blend design, especially for those blends involving rigid polymers like PLA.**[5,6]** Blending PLA with existing polymers is a potentially cost effective way of addressing its toughness issue using available processing facilities. With the aim of improving toughness, PLA has been blended with a variety of flexible polymers or rubbers either biodegradable or non-biodegradable.**[4-6,35]** Because of immiscibility, blending PLA with most polymers requires generally either addition of premade compatibilizers,**[125-129]** or their in situ formation at interface through reactive compatibilization.**[130-135]**

PLA/biodegradable polymer blends were the most studied and extensively investigated than PLA/non-biodegradable polymer blends due to their property improvements without compromising biodegradability.**[136]** Numerous biodegradable

polymers were reported to have been melt blended with PLA including various aliphatic and aliphatic-aromatic polyesters such as poly(ε-caprolactone) (PCL),**[125-135,137-139]** poly(ethylene succinate) (PES),**[140]** poly(tetramethylene-co-adipateterephthalate) (PTAT),**[141]** Poly(butylene succinate-co-L-lactate) (PBSL),**[142]** poly(butylene succinate) (PBS),**[142-146]** poly(butylene succinate-co-adipate) (PBSA),**[147,148]** poly(butylene adipate) (PBA),**[149]** poly(butylene adipate-co-terephtalate) (PBAT),**[150-153]**, poly(propylene carbonate) (PPC),**[154,155]** and others.**[156-166]**

The blend system of PLA with the more flexible biodegradable PCL has been probably the most studied biodegradable blend.**[125-135,137-139]** Marginal improvement in toughness is obtained by simple blending PLA and PCL owing to their immiscibility.**[126,137-139]** Consequently, in most cases PLA and PCL have been blended in the presence of a compatibilizer,**[125-129]** or by using reactive compatibilization.**[130-135]** An increase in tensile strain was possible only when PCL content was above 60 wt% that was accompanied with a significant reduction in modulus and tensile strength.**[139]** Addition of a small amount of an ethylene oxide and propylene oxide copolymer did not offer significant ductility improvement,**[126]** but addition of 4 wt% of PLA-PCL-PLA tri-block copolymer to PLA/PCL (70/30, w/w) blends enhanced the ductility of the blend expressed by an increase in elongation at break from 2% for PLA/PCL (70/30, w/w) blend to 53% for the ternary blend which was attributed to better PCL domains dispersion and reduction in their size from 10-15 to 3-4μm as evaluated by SEM.**[127]** An increase of the elongation at break from 175% to 300% was reported when 10 wt% of the PLA-PCL diblock copolymer was incorporated in PLA/PCL (80/20, w/w) blend.**[128]** Improved compatibility was reported between PLA and PCL when these were reactively melt blended in the presence of lysine triisocyanate (LTI) as a compatibilizer. Significant impact fracture toughness was reported attributed to the strengthening structure of the blend owing to the crosslinking reactions that occurred between the isocyanate groups of LTI and hydroxyl and carboxyl groups of PLA.**[135]** Recently, a block copolymer of poly(ethylene glycol) and poly(propylene glycol) (PEG-PPG) was used as new copolymer for PLA/PCL (80/20, w/w) blends. The resultant blends were characterized

in terms of morphology, mechanical, and thermal properties. SEM observations revealed better miscibility between PLA and PCL for compatibilized blends which exhibited a significant enhancement in tensile strain at break compared to that of the neat PLA/PCL blend, in which the highest strain was obtained at 7.5 phr of block copolymer, but tensile stress of the blends slightly declined.**[129]**

Fully biodegradable polymer blends were prepared by blending PLA with poly(ethylene succinate) (PES).**[140]** DSC revealed that PLA was immiscible with PES, and its crystallization rate accelerated with the increase of PES in the blends while the crystallization mechanism did not change. The elongation at break was only around 5.3% for neat PLA, but significantly increased to around 15.2% for PLA/PES (80/20, w/w), and further increased tremendously to around 143.7% for PLA/PES (60/40, w/w). The elongation at break of PLA increased by around 2 and 26 times in comparaison to PLA-rich blends, while the Young's modulus of PLA only decreased by 25 and 30%.

PLA/PTAT biodegradable membranes prepared by solvent casting method using chloroform were investigated by Liu et al..**[141]** The asymmetric blends (75/25 and 25/75 w/w PLA/PTAT) exhibited better compatibility and hence better mechanical performance than the 50/50 (w/w) blend. Compared to pristine PLA which had a tensile strength at break of 28 MPa and an elongation at break 19%, the 75 wt% PLA and the 25 wt% PLA blends had a tensile strength and an elongation at break of 24 MPa and 97%, and 11MPa and 285% respectively, while the 50/50 (w/w) blend had lower tensile strength (7 MPa) and elongation at break (34%).

Shibata et al.**[142]** melt mixed PLA with poly(butylene succinate) (PBS) and poly(butylene succinate-co-L-lactate) (PBSL). Dynamic viscoelasticity and SEM measurements of the blends revealed that PBSL and PBS exhibited almost the same extent of compatibility with PLA. PBSL and PBS were homogenously dispersed as 0.1-0.4µm particles in the blends when their content in the blend is in the range 5-20 wt%. All the blends showed considerably higher elongation at break than pure PLA, PBSL, and PBS. DSC analysis of the blends revealed that crystallization of the PLA component is promoted by the addition of a small amount of PBSL, while the addition

of PBS was much less effective. Similarly, Wang et al.**[143]** also published physical properties comparison of PLA/PBS and PLA/PBSL blends. These systems had similar compatibility and higher elongations at break than their parent polymers as was found by **Shibata** et al.**[142]** but not as high as was expected because of the low Mw of PBS and PBSL.**[143]** PLA/PBS blends for possible packaging applications were also examined by Bhatia et al..**[144]** Rheological results indicated miscibility between the two polymers for blends containing less than 20 wt% PBS. Brittleness of PLA was mitigated, but elongation at break, stiffness and strength decreased with PBS content. In another study conducted by Yokohara et al.,**[145]** PLA and PBS were found immiscible in the molten state and their blends exhibited phase-separated structure. However, it was reported that PBS accelerated the crystallization of PLA, indicating that PBS droplets acted as crystallization nuclei for PLA. Uncompatibilized melt mixed blend of PLA/PBS (90/10, w/w) exhibited slightly higher elongation and almost the same unnotched impact strength (18 KJ/m^2) as neat PLA.**[146]** Incorporation of 0.5 wt% of Lysine triisocyanate (LTI) or 0.15 wt% of lysine diisocyanate LDI as reactive compatibilizers in the PLA/PBS (90/10, w/w), significantly increased to more than 150%, and the impact strength increased to 50-70 kJ/m^2 in the presence of 0.5 wt% LTI which was then affected by the concentration of LTI and PBS. The MFI value of PLA/PBS (90/10 wt%) decreased from 25 g/10 min at 200°C in the absence of LTI to ~3 g/10 min in the presence of LTI indicating that isocyanate groups of LTI reacted with both terminal hydroxyl or carboxyl groups of the polymers. Laser scanning confocal microscopy (LSCM) observations revealed spherical particles at 1 μm in the presence of LTI and particle dimensions were not affected by the content of LTI of PBS. The result of this research demonstrated that LTI was more effective as reactive processing agent than LDI to increase the compatibility of PLA/PBS blend composites and to increase the toughness (impact strength) of PLA.**[146]**

Ojijo et al.**[147]** reported melt blending of PLA with the flexible and tough poly(butylene succinate-co-adipate) (PBSA) at various compositions. FTIR investigation revealed the absence of any chemical interaction between the two polymers, resulting thus in a phase-separated morphology as was also observed by SEM. The interfacial area of PBSA droplets per unit volume of the blend reached a

maximum in the PLA/PBSA blend (70/30, w/w) which allowed maximum intermingling of PLA and PBSA chains near the interface and resulted in optimal synergies of properties between the two polymers.**[147]** Very recently the same authors, prepared PLA/PBSA blends by in situ reactive compatibilization using triphenyl phosphite (TPP). The resultant compatibilized blends showed improved toughness, depending on the quantities of TPP and PBSA and the sequence and duration of mixing. For the blends containing 30 and 10 wt% PBSA the impact strength increased from 6 kJ/m^2 for PLA to 11 and 16 kJ/m^2, respectively, whereas the elongation at break increased from 6% for PLA to 20 and 37% for the same blends without considerable loss in tensile strength.**[148]**

To maintain PLA transparency, Meng et al..**[149]** prepared PLA/poly(butyl acrylate) (PBA). Dynamic rheology, SEM and DSC results showed that the PLA is partially miscible with PBA. The PBA component improved the crystallization ability of PLA and the crystallinity of PLA increased with content of PBA (<15 wt%). There was slight decrease in the transparency with increasing PBA content, and the tensile toughness and elongation at break of the PLA blends were greatly improved from 2.13 MJ/m^3 to 47.02 MJ/m^3 and from 4% to 31% respectively for PLA/PBA blend (85/15, w/w) without severe loss in tensile strength and modulus. Rheological results revealed that PBA enhanced the processability of PLA by decreasing the viscosity and the melt elasticity of the blends indicating thus its plasticizing effect.**[149]**

Several research groups investigated toughening of PLA with poly(butylene adipate-co-terephthalate) (PBAT) using various compatibilization techniques.**[150-153]** Jiang et al reported that addition of 5 wt% PBAT to PLA increased the elongation at break from 3.7 for neat PLA to 115%, but owing to weak interfacial adhesion between the phases, the impact strength of the PLA (2.6 KJ/m^2) was only slightly improved to 4.4 KJ/m^2 for PLA/PBAT (80/20, w/w) blend. Elongation at break of PLA improved from 3.7% to 200% after addition of 20 wt% PBAT but tensile strength and modulus significantly decreased.**[150]** Addition of 2 or 5 wt% of a random terpolymer of ethylene, acrylate ester, and glycidyl methacrylate (denoted as ‘‘T-GMA’’) as a reactive compatibilizer in PLA/PBAT melt compounding dramatically

improved the tensile toughness of the PLA/PBAT blend without severe loss in tensile strength.**[151]** The impact strength of the blend improved by 2-fold (30-40 KJ/m^2) at 2 wt% of T-GMA compared to uncompatibilized blends, but impact strength ultimately tended to be saturated with increasing T-GMA. SEM micrographs revealed that better misciblility and more shear yielding mechanism were involved in the toughening of the blend.**[151]**

Al-Itry et al.,**[152]** melt processed PLA and PBAT in the presence of various amounts of chain extension/branching agent, containing nine glycidyl methacrylate (GMA) functions, named Joncryl. The elongation at break of PLA/PBAT (80/20, w/w) blends with 0.25 and 0.5 % wt Joncryl achieved 116% and 135% respectively, higher than that for pure PLA (14%). The tensile modulus increased with the incorporation of GMA functions from 1350 MPa for neat PLA to 1095 MPa for PLA/PBAT/0.5 which indicated a reactivity control at the interface due to the formation of ester linkages between PLA, PBAT and Joncryl. The reactive compatibilization on the PLA/PBAT blends in tis study has been confirmed by TEM and SEM.**[152]**

The compatibility and interactions between PLA and PBAT was improved via a transesterification reaction using tetrabutyl titanate (TBT).**[153]** The mechanical properties of PLA/PBAT (70/30, w/w) blends were significantly improved after the incorporation of TBT; the blends with 0.5% TBT concentration gave values of tensile strength, elongation at break and impact strength of 45 MPa, 298% and 9 kJ/m^2, respectively. These results were supported by SEM observations which revealed that interfacial deboning, pullout of PBAT, and yielding deformation were the most important mechanisms to improve toughness. **[153]**

Toughening PLA by using poly(propylene carbonate) (PPC) was investigated for a range of compositions, but PLA was the continuous phase only for blends with 30 wt% PPC or less. These blends exhibited improved tensile properties compared to PLA but strength and stiffness were decreased.**[154]** In a recent publication, Gao et al.**[155]** used poly(vinyl acetate) (PVAc) to compatibilize the partially biodegradable blends of PLA and PPC. DSC revealed that the difference in the values of T_g between PPC and PLA clearly decreased with the introduction of PVAc, indicating that PVAc

acted as a good compatibilizer for the PPC/PLA blends. SEM micrographs showed that PVAc was selectively localized in the PLA phase and at the interface between PPC and PLA phases which bridged the phases and enhanced their interfacial bonding. Both of these were mainly responsible for the significant increase in the mechanical properties, especially the PLA/PPC/PVAc (70/30/10, w/w) which exhibited 10-fold improvement of the elongation at break of PLA (40 vs. 4%) while relatively both stiffness (1960 vs. 2164 MPa) and strength (50.7 vs. 59.8 MPa) of the matrix were maintained. **[155]**

The possibility of toughening PLA using a novel biodegradable aliphatic-aromatic copolyester (random poly(butylene succinate-co-glutarate-co-adipate-co-terephtalate)) (PBSGAT) was explored by Kowalczyk et al..**[156] PLA/**PBSGAT formed phase separated blend where the copolyester formed particles in the blends as observed by SEM, and exhibited a separate glass transition as obtained by DSC and confirmed by DMTA. 20-fold increase of the ultimate strain (0.4 to 2.73%) and 2.5-fold increase of the tensile impact strength (57.9 to 136.2 KJ/m^2) with respect to neat PLA was achieved in the blends with 25-35 wt% of PBSGAT. TEM and SEM studies of drawn specimens evidenced that the main toughening mechanism was cavitation inside the copolyester particles, which promoted shear yielding and further plastic deformation of PLA matrix.**[156]**

In an effort to improve PLA toughness, a thermoplastic polyester elastomer (TPEE) was melt mixed with PLA and a diisocyanate modifier (MDI) was used as a reactive compatibilizer.**[157]** DSC indicated that PLA/TPEE formed an immiscible mixture and addition of TPEE did not affect the thermal properties of PLA. It was also observed that PLA/TPEE/Modifier blend was also an immiscible system with a two-phase morphology and the addition of MDI decreased PLA crystallinity. PLA/TPEE exhibited increased elongation at break up to 240% but decreased stiffness and strength compared to neat PLA. For PLA/TPEE/MDI, MDI content had significant effect on elongation at break which improved as MDI content increased, but MDI had little effect on modulus and tensile strength; for instance the elongation at break, tensile strength and modulus of PLA/TPEE (80/20, w/w) were 80%, 32 MPa and 850

MPA respectively and those of PLA/TPEE/MDI (80/20/5, w/w) were 340%, 36 MPa and 890 MPa. The fractured surfaces and tensile tested fractured surfaces revealed that the debonding initiated shear yielding mechanism was involved in the toughening of the blend.**[157]**

Polyhydroxyalkanoates and their copolyesters were also used to modify PLA.**[158-163]** To alleviate PLA brittleness, Schreck et al.,**[158]** admixed PLA with NodaxH6, a commercially available Polyhydroxyalkanoat (PHA). A 2-fold increase in impact strength from 22 J/m for neat PLA to 44 J/m for PLA/NodaxH6 (85/15, w/w) was obtained. The addition of 5 wt% of PLA-b-NodaxH6 block copolymer for further improvement of in impact strength failed. Melt blending of PLA with polyhydroxybutyrate (PHB) at various concentrations was found a viable method to improve PLA properties.**[159]** PLA/PHB blends were immiscible but exhibited molecular interactions. The incorporation of the highly crystallizable PHB increased PLA crystallization and improved its mechanical properties. PLA/PHB (75/25, w/w) blend exhibited significantly improved tensile properties compared with pure PLA that was attributed to the finely dispersed PHB crystals acting as a filler and nucleating agent in PLA.**[159]**

Plasticized PLA/PHB (75/25, w/w) blends were examined by Abdelwahab et al..**[160]** Addition of 25% PHB did not improve the elongation at break of PLA (7%) but rather the tensile strength reduced from 42 to 16 MPa. When a plasticizer was added, the elongation at break of the PLA/PHB (75/25) blends was increased to 15%.**[160]** In another study reactive compounding of PLA and Poly(hydroxyoctanoate) (PHO) in the presence of dicumyl peroxide (DCP) and triallyl trimesate (TAM) trifunctional coagent resulted in a finer morphology compared to the unreacted blend, which was attributed to a compatibilizing effect possibly arising from copolymer formation at the interface. Accordingly the elongation at break and impact properties of the blends were improved compared to neat PLA.**[161]**

The influence of poly(ethylene glycol) (PEG) plasticizer on the tensile and impact strengths of PLA/poly(hydroxybutyrate-co-hydroxyvalerate) (PHBV) blends was investigated by Wang et al..**[162]** Toughness and elongation at break of the

PDLA/PHBV (70/30, w/w) blends were greatly improved by the addition of PEG. The notched impact strength increased about 400% from ~15 J/m for neat PLA to ~65 J/m for PLA/PHBV/PEG (70/30/20, w/w), and the elongation at break increased from 5.03% for neat PLA to 237.0% for the blend PLA/PHBV/PEG (70/30/20, w/w). However these improvements were accompanied with a concomitant reduction of strength and stiffness.**[162]** In another report it was indicated that PLA ductility and toughness were effectively improved by incorporation of 10-30 wt% of PHBV to PLA as evidenced by the structure-property study achieved by Ma et al..**[163]** The thorough investigation of deformation mechanism by SEM revealed that fibrillation, partial interfacial debonding, PHBV domain cavitation and matrix yielding were involved in the toughening mechanism of the PLA/PHBV blends under impact and tensile testing conditions.**[163]**

To reduce the inherent brittleness of PLA, Bhardwaj et al.**[164]** developed a new approach in which a hydroxyl functional hyperbranched polymer (HBP) was in-situ cross-linked with a polyanhydride (PA) in the PLA matrix during melt processing. The crosslinking reaction was proved by FTIR and by DMTA. TEM and atomic force microscopy (AFM) revealed the sea-island morphology of PLA-cross-linked HBP blend in which the domain size of cross-linked HBP particles in the PLA matrix was less than 100 nm as observed by TEM. The presence of cross-linked hyperbranched polymer in the PLA matrix exhibited ~570% and ~847% improvements in toughness and elongation at break, respectively, as compared to unmodified PLA. The increase in the ductility of modified PLA was related to stress whitening and multiple crazing initiated in the presence of cross-linked HBP particles. **[164]**

A biodegradable hyperbranched poly(ester amide) (HBP) was used to alleviate the brittleness of PLA.**[165]** The presence of intermolecular hydrogen bonds between PLA and HBP was confirmed by FTIR. DSC showed that good miscibility was found below 10 wt% HBP above which the blends exhibited two T_gs. It was also found that HBP decreased the crystallinity from 30.99% for neat PLA to 18.58% for the blend containing 20 wt% HBP. Significant increase in elongation at break values was attained and accompanied with a slight increase of tensile strength. Especially, the

blend with 10 wt% HBP exhibited good tensile strength 48.81 MPa and elongation at break of about 43.06 % as compared to PLA (46.58 MPa and 5%). Above this concentration the mechanical properties sharply dropped. SEM revealed that the particle size of the dispersed phase increased from 0.3-0.6 μm to 1-4 μm when HBP content increased from 5 wt% to 15 wt% respectively but the particles became partially connective at 20 wt% HBP which was the cause of decreased mechanical properties.**[165]**

Hydroxyl-terminated hyperbranched poly(ester amide) (HBP) and isocyanate-terminated prepolymer of butadiene (ITPB) alone and in combination, were investigated as two potential toughening agents for PLA.**[166]** Synergistic effects in impact strength were observed in PLA/HBP/ITPB ternary blends. Impact strength of the ternary blend was improved by over 86%, while the elongation at break was increased by over 100% with good stiffness-toughness balance. Physical and chemical interactions between the hydroxyl-terminated HBP and the ITPB were responsible for the observed synergistic effect and improvements in impact strength. SEM images showed evidence of stretched polymer which indicated that the fracture behavior of PLA changed from brittle to ductile in the PLA/HBP/ITPB ternary blends. DSC data revealed that the addition of the HBP/ITPB alone or in combination decreased the degree of crystallinity, but had no significant influence on T_g.**[166]**

Several other biodegradable fully-biobased resins have also been used to toughen PLA.**[167-169]** The melt blend of PLA with soybean oil derivative (PLA/polySOY) in the presence of Poly(isoprene-b-L-lactide) block copolymers as compatibilizers exhibited tensile toughness and strain at break as high as 4 times and 6 times than that of unmodified PLA, respectively.**[167]** In another work it was indicated that the reactive blending of functionalized PLA (F-PLA) with 5 wt% conjugated soybean oil (CSO) resulted in an elongation at break of more than 17-fold that of neat F-PLA and more than 133% compared to the nonreactive F-PLA/CSO blend of the same composition.**[168]** PLA/Castor oil melt blend was considered by Robertson et al..**[169]** The binary PLA/castor oil blend exhibited a tensile toughness 7 times greater than neat PLA. The addition of a synthesized bio-based poly(ricinoleic acid)-PLA

diblock copolymer allowed for control over the morphology of the blends, and even further improvement in the tensile toughness was realized that is an order of magnitude larger than that of neat PLA.**[169]**

Currently, blending PLA with biodegradable polymers is hampered by the expensiveness of the final product as biodegradable polymers are of high price. Therefore using commercially available cost effective nonbiodegradable polymers would be preferred and advantageous even if it does not sound an environmentally and friendly long-term solution.**[4,5]** Modification of PLA was examined using various polymers that are neither biobased nor biodegradable, like for instance polyolefin,**[170-181]** thermoplastic polyurethanes (PU),**[182-186]** and rubbers such as polyisoprene (PIP),**[187,188]** polyamide elastomer (PAE),**[189,190]** natural rubber (NR),**[191-195]** acrylonitrile-butadiene-styrene copolymers (ABS)**[196-198]** ethylene vinyl acetate (EVA),**[199-201]** hydrogenated styrene-butadiene-styrene block copolymer (SEBS),**[202,203]** and others**[204-226]**. To improve compatibility and to control the interface, reactive blending is achieved by incorporating additional reactive components to the system such as polyethylene-g-glycidyl methacrylate (PE-g-GMA)**[174]** or glycidyl methacrylate grafted poly(ethylene octane) (PEO-g-GMA),**[175]** or other maleic anhydride grafted polymers or rubbers like LDPE-g-MAH**[176]** and SEBS-g-MAH.**[178]**

Mixing PLA with rubbers or polymers bearing appropriate chemical functionality(ies) able to react with carboxyl or hydroxyl end groups of PLA during processing has been also considered as a viable approach to toughen the brittle PLA. Typical examples are functionalized elastomers such as natural rubber grafted glycidyl methacrylate (NR-g-GMA),**[191]** epoxidized NR (ENR),**[193,194]** natural rubber grafted poly(vinyl acetate) (NR-g-PVAc),**[195]** ethylene glycidyl methacrylate grafted acrylonitrile-butadiene-styrene (ABS-g-GMA),**[197]** PEO-g-GMA,**[206,207]** ethylene glycidyl methacrylate (EGMA),**[209-211]** and ethylene-butyl acrylate glycidyl methacrylate (E-BA-GMA).**[212-214]** When EGMA polymers are used to toughen PLA, it is demonstrated that the epoxy group of the glycidyl methacrylate (GMA) can react in situ with the carboxyl and hydroxyl end groups of PLA during melt blending

and can lead to GMA-grafted PLA copolymer that can compatibilize the blend.**[208,210]** Other rubbers containing GMA, such as ABS-g-GMA and PEO-g-GMA have also been used to toughen PLA by the same mechanism.**[197,206,207]**

Blends of PLA with polyolefin are expected to have significant practical and economic interests due to the ease of processing and availability. High toughness, good impact performance, and low cost make polyethylene (PE), and polypropylene (PP) promising polymers to toughen PLA and enlarge its use for commercial applications such as packaging.**[4-6]** Numerous research studies reported on blends of PLA with PE.**[170-176]** Linear low density polyethylene (LLDPE) was used to toughen amorphous (aPLA) and semi-crystalline PLA (sPLA).**[172]** Compared to s-PLA, toughening effect for the aPLA blend (aPLA/LLDPE-80/20, w/w) required the use of PLA-PE block copolymer. The authors ascribed this to the differences in interfacial interactions between a-PLA and s-PLA with LLDPE. The impact strength of the blends aPLA/LLDPE and aPLA/LLDPE/PLA-PE (80/20/5, w/w) were nearly the same (34 vs. 36 J/m), but when PLA-PE (30/30, w/w) with high critical entanglement Mw was used, the impact strength drastically increased to 460 J/m that is ~38 times that of aPLA (12 J/m). Higher impact strength values were recorded for sPLA (20 J/m) and its blends at the same compositions, namely sPLA/LLDPE (350 J/m) and sPLA/LLDPE/PLA-PE with PLA-PE (30/30, w/w) (660 J/m). The same authors, compared PLA/LLDPE and PLA/High density polyethylene blends (PLA/HDPE).**[173]** It was found that flexible LLDPE which relieved impact stress by cavitation resulted in high levels of toughness compared to HDPE which likely dissipated impact energy by debonding at the particle-matrix interface.

Ethylene-acrylic acid (EAA) and two different polyethylenes with glycidyl methacrylate (PE-g-GMA) were used as reactive compatibilizers for LDPE/PLA blends (80/20, w/w).**[174]** Ethylene acrylic acid copolymer (EAA) was not effective in compatibilizing immiscible PLA/LDPE blend, whereas PE-g-GMA8 (8 wt% GMA) reduced the domain size of dispersed phase by reducing the immiscibility between the two phases and resulted in enhanced tensile properties. Adding PE-g-GMA8 at 5 wt% to LDPE/PLA (80/20, w/w) blend provided a maximum stress of 0.94 kgf/mm^2 and

strain at break of 77.9 % compared to 3.26 kgf/mm^2 and 4.0 % for the blend with 5 wt% PE-g-GMA25 (25 wt% GMA). ^{1}H-NMR analysis of the extracted reaction product between PLA and PE-g-GMA formed during melt-mixing, confirmed the compatibilizing chemical reaction that occurred between PLA and PE-g-GMA8, and the chemical linked copolymers which were considered to act as reactive compatibilizers were formed.**[174]**

The effects of PEO-g-GMA (denoted as mPEO) compatilizer on phase structure of PLA/LLDPE were studied by spreading coefficient calculation prediction, SEM, DSC, and wide-angle x-ray diffraction (WAXD) analysis.**[175]** The spreading coefficient calculations based on experimental and calculated surface tension data showed that mPEO would spread on LLDPE extensively to encapsulate LLDPE completely, which was in good agreement with the results of DSC, SEM, and WAXD analysis. In this sense, LLDPE may be dissolved partially in the mPEO phase and act as an mPEO component, thus the toughness of the ternary blends system would be expected to be improved since the content of elastomer increased with the addition of the LLDPE. The compatibilized LLDPE/PLA blends exhibited smaller domain sizes from 1.6-3.2 to < 0.5 μm, lower crystallization temperature (T_c) (from ca. 103 to 96°C), and less crystallinity (from 34.2% to 24.1%) compared to physical blends. However, no mechanical properties of the blends were given in this study.**[175]**

Films of PLA/LLDPE compatibilized with LDPE-g-MAH and uncompatibilized were prepared in the whole range of composition by Singh et al..**[176]** Mechanical properties of the polymer blends depended on the component polymer ratios and the compatibilizer content. Among the investigated samples, PLA/LLDPE (20/80, w/w) and PLA/LLDPE/LDPE-g-MAH (20/80/4, w/w) blends exhibited the optimum tensile strength and elongation at break. The FTIR analysis evidenced the specific interactions that occurred in the compatibilized system. The result of this study indicated that LDPE-g-MAH can be used in PLA/LLDPE to improve interfacial adhesion between PLA and LLDPE.**[176]**

Polypropylene was also investigated to endow PLA with toughness.**[177-181]** One study, revealed that the elongation at break of PLA/PP increased, while stiffness

and biodegradability deteriorated with addition of PP.**[178]** A mixture of PP-*g*-MAH (5 phr) and SEBS-*g*-MAH (5 phr) effectively increased the impact strength of the PP/EPDM/PLA (64/16/20) blends (6.3 vs. 23.7 kgf cm/cm) without adverse effect on tensile strength (241.1 vs. ~239 Kgf/cm^2).**[179]** This result was consistent with the morphological and rheological properties of the PP/EPDM/PLA blends. The increase in viscosity and decrease in interfacial tension of the compatibilized PP/EPDM/PLA (64/16/20) blends was interpreted with the qualitative picture of the Palierne emulsion model. The interfacial tension calculated from the emulsion model was consistent with the mechanical and morphological properties of the PP/EPDM/PLA (64/16/20, w/w) blends.**[179]** Mechanical, morphological, and rheological properties of PLA/PP blend impact modified with Biomax® strong 120 and compatibilized with PP-g-MAH, PE-g-GMA and their mixture (PP-g-MAH/PE-g-GMA) was examined by Lee et al.**[180]** The results of the tensile strength, flexural strength, and impact strength of the ternary blends confirmed that the mechanical properties of ternary blends containing the mixture of compatibilizers (3 phr) have better mechanical properties than the blend containing a single compatibilizer. Conversely, the tensile strength and flexural strength of the ternary blend were decreased by incorporating PE-g-GMA as a single compatibilizer. The rheological studies indicated that the ternary blends with mixture of compatibilizers had higher viscosity than that of the blends with single compatibilizer. Furthermore the ternary blends using the hybrid compatibilizer and that using the single compatibilizer PP-g-MAH exhibited a single-phase microstructure, which is unusual for such a complex mixture.**[180]** Very recently, PP/PLA blend films compatibilized with PP-g-MAH prepared by melt mixing technique and cast film extrusion were studied in the whole range of composition.**[181]** Morphological observation showed that the blend was a two phase system and FTIR investigation revealed improved interactions between the polymers in the presence of the compatibilizer. Increasing PLA content from 40 to 60 wt% resulted in decreased melting temperature and crystallinity from 158°C to 154°C and 38% to 31%, respectively. Modulus and tensile strength increased with increasing the PLA content, while elongation at break was drastically decreased from 500% (polypropylene) to less than 50% (blends).**[181]**

Toughening brittle polymers by modifying them with rubber and rubber like particles is a widely accepted approach for thermoplastics and thermosets. Similar brittleness problems encountered with PLA had been solved before by using rubber toughening methodology such as in the case of the brittle polystyrene (PS) which was toughened by chemical mixing with polybutadiene rubber to form high impact polystyrene (HIPS) which showed increased impact strength of PS from 13-25 J/m to 50-400 J/m when the rubber ratio was 10-20 wt%. HIPS and other prominent examples of styrene copolymers produced by this technique such as acrylonitrile-butadiene-styrene copolymers (ABS) and styrene-acrylonitrile copolymers (SAN) are now largely commercialized.**[6]** Inspired from these rubber-toughened polymers, addition of suitable rubbery polymer "known as rubber toughening" was also investigated as an effective way to enhance PLA toughness without reduction of T_g, unlike in the case of plasticization. It is well known that in rubber toughened systems the dispersed particles of the immiscible rubber interfere with the failure mechanisms. The spherical rubber particles act as stress concentrators, initiating and terminating crazes in the brittle polymer matrices, which are responsible for the enhanced fracture energy absorption.**[182]**

Many research work have been reported in literature dealing with PLA toughening using polyurethanes.**[182-186]** Dynamic mechanical test (DMA) demonstrated that PLA/poly(ether)urethane (PEU) formed partially immiscible mixture in which the PU elastomer particles in sub-micron scale were dispersed in PLA matrix (SEM).**[182]** DSC results indicated that addition of the elastomer not only accelerated the crystallization rate of PLA, but also decreased the PLA crystallinity. Mechanical tests showed that the fracture of PLA transformed from brittle to ductile upon addition of PEU proving its toughening effects on PLA matrix. Significant elongation at break (4% to 363%) and impact strength (64 to 315 J/m^2) were imparted to PLA, but at the expense of stiffness and strength which were reduced. The toughening-mechanism investigation by SEM revealed that shear yielding occurs in the PLA matrix as induced by the PEU domains.**[182]**

Feng et al.,[183] observed transition of PLA fracture from brittle to ductile by blending PLA with biodegradable thermoplastic polyurethane (TPUE) elastomer. The blends were partially miscible systems because of the hydrogen bonding between the molecules of PLA and TPUE. Investigation of mechanical properties indicated that with increasing TPUE content, the blends exhibited increasing tough failure evidenced by an increase in elongation at break (350%) and notched impact strength (25 KJ/m^2) for the PLA/20 wt% TPUE blend without an obvious drop in the tensile strength.**[183]**

In another study, it was found that TPUE spherical particles dispersed in the PLA matrix, and the uniformity decreased with increasing TPUE content.**[184]** Addition of TPUE improved the toughness of the PLA as stress whitening appeared on fractured samples. For the blend with 30 wt% TPUE, the elongation at break of the blend reached 602.5%, and samples could not be broken in the notched impact tests at room temperature.**[184]**

PLA was also successfully toughened by blending with a poly(lactic acid) based poly(ester-urethane) (PEU), which contained poly(butylene succinate) as a flexible segment.**[185]** Ductility and toughness steadily increased with increasing content of PEU. When the weight fraction of PEU reached 10 wt%, the strain at the break dramatically increased to 308% and impact strength reached 2.6 KJ/m^2 compared to those of neat PLA, i.e. 7.2% and 1.87 KJ/m^2 respectively. The degree of crystallinity of toughened PLA component was hardly changed regardless of the content of PEU but its T_g decreased with an increasing content of PEU, suggesting that the blends showed limited miscibility.**[185]**

Recently Imr et al.**[186]** compared toughening PLA with TPUE using reactive and physical blending. The analysis and comparison of the structure and properties of physical and reactive blends proved the successful coupling of the phases. Coupling resulted in more advantageous structure and superior mechanical properties compared to those of physical blends as confirmed by morphology, macroscopic properties and the quantitative estimation of interfacial interactions. Structural studies and the composition dependence of properties indicated the formation of a submicron, phase-in-phase structure which positively influenced properties at large PU contents. The

results strongly support that reactive processing is a convenient, cost-effective and environmentally friendly technique to obtain blends with superior properties.**[186]**

The solution blending of a synthesized star shaped PLA with rubbery Poly(cis-1,4-isoprene) (PIP) formed an immiscible mixture witnessed by the appearance of two T_gs each stemming from PLA and PIP domains.**[187]** Because of the known compatibility of PVAc with PLA, PIP-g-PVAc was prepared and blended with PLA. PLA/PIP-g-PVAc exhibited two T_gs and the analysis of mechanical properties showed that the tensile properties of the PLA/PIP-g-PVAc blend were much superior to those of the PLA/PIP blend. The mechanical properties of PIP-g-PVAc/star-shaped PLA (20/80, w/w) increased, especially its elongation at break which improved from 10.2% for neat PLA to 14.3%, and its toughness measured as the area under stress-strain curve enhanced from 7.4 to 18.2 but with a loss of stiffness from 1582.5 MPa to 1065 MPa. Kowalczyk et al.,**[188]** reported that incorporation of as low as 5 wt% PIP into PLA increased the strain at break of compression molded film during uniaxial drawing, and also improved its tensile impact strength by 80% (58 to 105 KJ/m^2). SEM, TEM and small angle x-ray scattering (SAXS) investigation of the mechanism responsible of PLA toughening revealed that the rubbery particles initiated crazing at the early stages of deformation, that is immediately followed by cavitation inside rubber particles, which further promoted shear yielding of PLA.**[188**

Zhang et al.,**[189]** melt mixed PLA with biodegradable polyamide elastomer (PAE). PLA and PAE have good compatibility as was attested by DMA results, and the PAE particles were found uniformly dispersed with domains at sub-micron scale as was observed by SEM. These results were attributed to the compatibility of the polyether soft segments with PLA, and to hydrogen bonds between the PA hard segments with PLA. Increasing PAE contents (5-30 wt%) changed the deformation behavior of PLA from brittle to ductile and resulted in significant increase of elongation at break of blends (5.1% to 367%) but decreased tensile strength (46.8 to 24.6 MPa). Interestingly, when the PAE content is 10 wt% the elongation significantly increased to 194.6%, while the tensile strength of the blend is maintained similar to neat PLA. Stoclet et al.**[190]** considered melt blending of PLA with biosourced

Polyamide11 in the whole composition range. PLA/PA11 blends were immiscible but a self-compatibilization behavior of the PLA/PA11 system was evidenced via SEM. In the case of PLA-rich blends, the crystallization of PA11 from the melt displayed a contribution of "homogeneous nucleation" corroborating the high degree of dispersion of the minor phase. The non-symmetric structural behavior of the blends over the whole composition range was found to influence the mechanical properties. More particularly in the PLA-rich range, the thread-like dispersion of the stiff PA11 component plays the role of in situ fibrillar reinforcement of the soft PLA matrix.**[190]**

Several publications reported on melt blending of PLA with natural rubber (NR) and (NR)-based polymers for toughening objectives.**[191-195]** PLA/NR constituted an immiscible blend as observed by SEM which showed coarse morphology as the NR content increased.**[191]** The impact strength and elongation at break of PLA/NR blend underwent dramatic improvement with increasing NR content up to the optimum content of 10 wt%. Further improvement of impact strength and elongation at break of PLA/NR blend was achieved with addition of NR-g-GMA compatibilizer content up to 1wt%. Moreover, with increasing % grafting up to 4.35 wt% GMA in NR-g-GMA, the impact strength of the (90/9/1) PLA/NR/NR-g-GMA(4.35 wt%) blend was 2.5 times higher than that of PLA (19.06 to 54.24 KJ/m^2) and the elongation at break was 2 times higher than that of uncompatibilized PLA/NR (74.51 to 159.08%). With the addition of NR-g-GMA, better dispersion and distribution of NR in PLA matrix was observed by SEM micrographs. These results were attributed to the efficient reaction between the PLA functional groups and the epoxy reactive group of the rubber which was evidenced by FTIR study.**[191]**

PLA toughening with natural rubber (NR)-based polymers was undertaken by Jaratrotkamjorn and co-workers.**[192]** The study focused on the effect of rubber polarity, rubber viscosity and molecular weight on mechanical properties of the blends. Three types of rubbers were used: NR, natural rubber grafted with poly(methyl methacrylate) (NR-g-PMMA), and epoxidized natural rubber with epoxidation degree of 25 and 50 (ENR25 and ENR50). It was found that all blends showed higher impact strength than PLA. Rubber mastication method was more effective than chemical

modification method in toughening PLA, that is, among all modifiers; masticated NR was the best in toughening PLA. The tiny particles observed by SEM for ENR and NR-g-PMMA in the blends designated higher miscibility to PLA than virgin NR, but these particles might have been too small to promote toughening and were also structurally more rigid than NR ones. DSC indicated no significant change in T_g of PLA but rather a cold crystallization peak appeared and was associated with the nucleating effect of the rubber.**[192]**

In another research work, PLA was successfully toughened by melt blending with an epoxidized natural rubber (ENR).**[193]** The impact strength and elongation at break of the blends were enhanced with ENR content but tensile strength and modulus were reduced. The impact strength of the 20 wt% degree of epoxidation (PLA/ENR20) and that of 50 wt% (PLA/ENR50) blends increased to 6-fold and 3-fold, respectively, compared to that of pure PLA attributed to the interfacial adhesion/reaction between ENR and PLA. The elongation at break of the PLA/ENR20 and the PLA/ENR50 blends increased from 9.3% for pure PLA to 32% and 27%, respectively, and the PLA/ENR50 blend showed much higher tensile strength and lower elongation at break than the PLA/ENR20 blend. This was attributed to possible enhanced molecular interactions and crosslinking for ENR preventing immediate rubber detachment from the PLA matrix causing thus larger plastic deformation zones near the fracture margin compared to PLA/ENR20. DSC results showed that T_g of PLA was not influenced by the presence of ENR, and PLA/ENR blends were amorphous after melt blending, but once annealed at 100°C for one hour, they crystallized and revealed two melting peaks on their thermograms. Moreover it was found that ENR hindered the crystallization of PLA due to the crosslinking between ENR and PLA molecular chains. Rheological studies revealed that PLA/ENR20 exhibited very strong shear thinning behavior compared to PLA/ENR50 which showed higher melt viscosity due to extensive molecular and crosslinking reactions at this higher rubber epoxidation content.**[193]**

Pongtanayut introduced NR and ENR by melt blending in PLA for toughening purpose.**[194]** SEM revealed that PLA/NR resulted in an immiscible blend with coarse particles of NR dispersed in PLA, but PLA/ENR was partially immiscible with finer

morphology. Moreover phase inversion occurred at high rubbers contents for both blends. The T_g of PLA decreased by the same extent ca. 6-8°C but its melting temperature was not influenced in both blends. Incorporation of NR enhanced the crystallization ability of PLA better than ENR did showing thus the nucleating ability of the rubbers towards PLA. NR was found a better tougher agent for PLA than ENR. The ductility of PLA was significantly improved by blending with NR with optimum mechanical properties obtained at 10 wt% beyond which all properties significantly deteriorate.**[194]**

NR-g-PVac was used as a toughening agent for PLA and as a compatibilzer for PLA/NR blends.**[195]** The presence of PVAc in the NR-g-PVAc copolymer increased the miscibility of PLA and NR. NR-g-PVAc, especially the one with 12 wt% PVac content (NR-g-PVac12), was a good toughening agent for PLA and was better than NR and NR-g-PMMA as reported previously.**[192]** There was 4-fold and 2-fold increase in impact strength for the optimal composition of PLA/NR/NR-g-PVAc (90/50/5, w/w) compared to PLA (2.85 vs.12.49 KJ/m^2) and to PLA/NR (6.36 vs. 12.49) respectively, while the elongation at break showed a higher value (16.10%) than the PLA (5.44%) and PLA/NR (4.25%) blend showing approximately 3-fold and 4-fold increase, respectively. It was also found that NR and NR-g-PVAc acted as nucleating agents for PLA illustrated by the induced cold crystallization and the increased crystallinity. Furthermore NR mastication was found an efficient method for increasing the toughness and ductility of the blends containing NR-g-PVAc which depended on the blend composition and the number of mastications.**[195]**

In addition to the above discussed biodegradable rubbers, PLA was also toughened using nonbiodegradable rubbers including ABS, EVA, SEBS, PEO and others.**[195-226]** Simple melt blending of PLA with ABS formed thermodynamically immiscible blend with deteriorated mechanical properties.**[196]** In situ compatibilization of PLA/ABS blends with the reactive styrene-acrylonitrile-glycidyl methacrylate copolymer (SAN-GMA) in the presence of ethyltriphenyl phosphonium bromide (ETPB) as a catalyst led to significantly decreased ABS domains dispersed in PLA matrix attributed to the reaction between the epoxy group of SAN-GMA and

reactive groups of PLA as identified by FTIR. Compatibilized blends exhibited balanced satisfactory stiffness-toughness, i.e., enhanced impact strength and elongation at break with a slight loss in stiffness and strength, and increased ABS content significantly improved impact strength of the reactive blends. For example, addition of 5 wt% SAN-GMA to the PLA/ABS (70/30, w/w) blend increased elongation from 3.1% to 20.5% and impact strength from 63.8 to 81.1 kJ/m^2. By further incorporating 0.02 phr ETPB, the elongation and impact strength of the blend increased to 23.8% and 123.9 kJ/m^2, respectively.**[196]**

In another work dealing with PLA toughening by ABS based-polymers, **Sun** et al.**[197]** prepared a series of functionalized acrylonitrile-butadiene-styrene (ABS-g-GMA) by emulsion polymerization at different grafting concentrations of GMA (1-7 wt%) and used them to improve PLA toughness. The reaction between the PLA functional groups and GMA of ABS-g-GMA was evidenced by torque measurements which indicated an increase of the viscosity (increased torque) of PLA/ABS-g-GMA blend as the GMA content increased in ABS-g-GMA. Chemical reactions taking place between PLA and ABS-g-GMA were thoroughly discussed and schematically represented **(Figure III.2)**. SEM observations revealed uniform dispersion of the rubber particles indicating sufficient compatibilization when only 1 wt% GMA was grafted on ABS which resulted in maximum toughness reflected by notched impact strength of 540 J/m that is 27 times that of PLA and an elongation at break of ~170%. Grafting GMA above this degree resulted in agglomeration of ABS-g-GMA particles and decline in mechanical properties.**[197]**

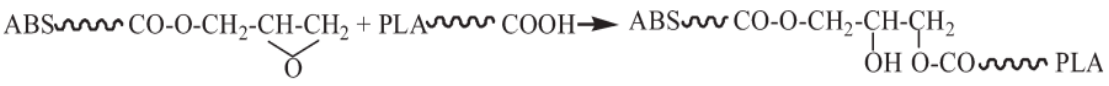

Reaction 1

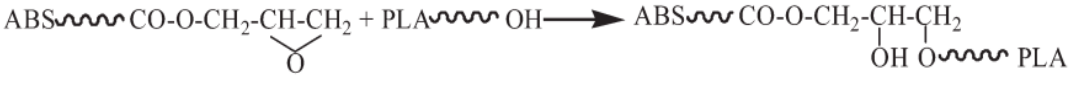

Reaction 2

Figure III.2 Reactions in PLA/ABS-g-GMA blends.**[197]**

The incorporation of G-ABS, ABS with 58% butadiene rubber (BD), enhanced the impact strength of PLA/ABS(BD25%) (50/50, w/w) blend astonishingly.**[198]** The mechanical properties of the PLA/ABS blends were further improved by the addition of SAN-GMA compatibilizer, which was more effective than either polycarbonate (PC), PE-epoxy, EPR-MAH, or SAN-MAH. The PLA/ABS (50/50, w/w) added with G-ABS and 5phr of SAN-GMA exhibited the tensile and impact strength higher than 40 MPa and 80 J/m, respectively. Further incorporation of a heat stabilizer in the range of 0.0-1.0 phr contributed to the stabilization of PLA during the compounding process and raised the impact strength significantly without affecting the tensile strength, flexural strength, and flexural modulus.**[198]**

Li et al.,**[199]** first reported on PLA toughening using ethylene-co-vinyl acetate (EVA) with various VA content. PLA/EVA blends' morphology changed from sea-island to co-continuous for the blends with VA content 40 wt% (EVA40). The interfacial interaction between PLA and EVA was investigated by FTIR and rheological measurements. The stronger interfacial interaction in PLA/EVA28, which exhibits homogeneous and smaller dispersed particle size, was supported by the rheological results. DSC and polarized optical microscope showed that all the samples were mainly in amorphous state during the injection molding process. However, annealing promoted the second crystallization of PLA matrix, leading to the improvement of the crystalline structure. As expected, with the addition of EVA, the ductility and fracture toughness are improved and the decreased tensile modulus and strength was enhanced by annealing. The study conducted by Ma et al.**[200]** supported that of Li et al.**[199]** in that PLA/EVA blends' compatibility and phase morphology was controlled by the ratio of vinyl acetate and ethylene in the random copolymers. A significant increase in the impact toughness was found at 15 wt% of EVA with a vinyl acetate content of approximately 50 wt% (EVA50). Further increasing the EVA50 content, super-tough PLA/EVA50 blends (notched impact toughness > 60 kJ/m^2) was obtained. The impact toughness of PLA is improved by a factor of ~30 after addition of 30 wt% EVA50 and elongation at break reached 400%. The local deformation mechanism studied by TEM, SAXS and SEM revealed that internal rubber cavitation

in combination with matrix yielding is the dominant toughening mechanism for the PLA/EVA blends under both impact and tensile testing conditions.**[200]**

Said et al.,**[201]** reported the tensile properties of PLA/EVA18 (VA 18 wt%) before and after gamma irradiation. The degree of crystallinity of PLA phase indicated that PLA and EVA were immiscible over the composition range investigated. However, there was a sharp decrease in the crystallinity with increasing EVA and irradiation dose. Tensile properties were greatly dependent on the ratio of EVA content in the mixture and PLA/EVA (80/20, w/w) blend exhibited the maximum tensile strength and ductility compared with other blends. On the other hand, strain at break was gradually increased up to 50 wt% EVA ratio and then suddenly increased at 80 wt% of EVA. After being irradiated by 50 kGy, the tensile strength and modulus were greatly enhanced, whereas the elongation at break was slightly reduced.**[201]**

PLA toughening by hydrogenated styrene-butadiene-styrene block copolymer (SEBS) and EGMA as compatibilizer was reported by Hashima et al..**[202]** The as molded compatibilized blend PLA/SEBS/EGMA (70/20/10, w/w) exhibited better mechanical performance than uncompatibilized PLA/SEBS (70/30, w/w). However, both blends underwent significant deterioration of their mechanical properties after annealing at 80°C for 8h. For the compatibilized blend, the tensile elongation at break and impact strength decreased from 185 to 100% and from 92 to 32 KJ/m^2 respectively, while those of the uncompatibilized blends dropped from 178 to 98% and from 16 to 7 KJ/m^2 respectively. The high temperature property and thermal aging resistance were improved by further incorporation of polycarbonate (PC) that resulted in maximum notched impact strength of about 60 KJ/m^2 for PLA/PC/SEBS/EGMA (40/40/15/5, w/w). Based on TEM, DSC and DMA the authors associated this outstanding toughness with the negative pressure effect of SEBS that dilates the plastic matrix consisting of PLA and PC to enhance the local segmental motions. In another research investigation Qi et al.**[203]** successfully synthesized SEBS-g-PLA copolymer at different grafting ratios by solvothermal method. SEBS-g-PLA possessed two-phase structure with vague phase boundaries and when incorporated into SEBS/PLA system, the phase boundaries between SEBS and PLA in PLA/SEBS blend disappeared

indicating its potential as a compatibilizer. It was also demonstrated that SEBS-g-PLA could be used as a good toughening agent for PLA. The PLA/SEBS-g-PLA blends exhibited improved notched impact strength and elongation at break but lower tensile strength with increasing SEBS grafting.**[203]**

Functionalized and non-functionalized thermoplastic polyolefin elastomers (POE) such as Poly(ethylene-co-octane) (PEO) copolymer have also been used as toughening agents for PLA.**[204-208]** Nijenhuis et al.[**204]** demonstrated that all PLA/PEO blends containing up to 50 wt% PEO were miscible and showed single T_gs. Changes in mechanical properties were small in blends with less than 10 wt% PEO, but at higher PEO concentrations the materials became very flexible, and an elongation at break of more than 500% was observed for a blend with 20 wt% PEO.**[204]**

A series of PEO graft PLA (PEO-g-PLA) was successfully synthesized and used to compatiblize PLA/PEO blend (80/20, w/w).**[205]** A Molau test, SEM observations of cyro-fractured surface morphology and particle size analysis of PLA/PEO blend system demonstrated that this new copolymer, significantly improved the compatibility of the PLA/PEO (80/20, w/w) blend. PEO-g-PLA up to 2.5 wt% was effective in reducing the PEO dispersed phase domain size (from 6.2 to 4.5-2.1μm), increasing elongation at break (from 15.4% to 99.1-181.9%) and impact strength (from 137 J/m to nonbreak) without significant decreases of tensile strength (from 34.7 to 30.1-35.6MPa) or tensile modulus (from 1.46 to 1.10-1.21GPa) compared to PLA/PEO blend, however, beyond the critical content of 2.5wt% all properties declined. The study also showed that PEO-g-PLA was more efficient than PEO-g-MAH to compatibilize and to increase the mechanical properties of PLA/PEO (80/20, w/w) blend.**[205]**

Su et al.**[206]** employed PEO and a glycidyl methacrylate grafted poly(ethylene-co-octane) (PEO-g-GMA denoted as mPEO) to toughen PLA. The immiscibility between PLA and mPEO decreased as mPEO ratio increased in the blend. Both the elongation at break and impact strength of the PLA were increased with increasing PEO or mPEO contents, but mPEO results in better improvements.

PLA/PEO (85/15, w/w) showed impact strength of 19.4 kJ/m^2 and elongation break of 67%. Whereas the impact strength and elongation at break of PLA/mPEO (85/15, w/w) were nearly 7 times (29.80 vs. 4.0 kJ/m^2) and 6 times (133 vs. 21%) those of PLA respectively. At this composition PLA/mPEO had finer particle dispersion (0.4 µm) than PLA/PEO (1.2-2.5 µm). When the mPEO content was as high as 45 wt%, the impact strength of the PLA/mPEO blends was 54.7 kJ/m^2 but stiffness and strength underwent significant decrease due to excessive amount of rubber. These improved results were attributed to the reaction of the epoxy groups of the mPEO with the functional groups of PLA which was also responsible of an increase of the viscosity of the blends.**[206]**

The blend of PLA/PEO-g-GMA (0.8% GMA) was also studied by Feng et al.**[207]** PLA/PEO showed no change in impact strength, however the impact strength of the reactive blend enhanced slowly and then exhibited a sharp brittle-ductile transition at 20 wt% PEO-GMA at which super-toughness with good stiffness balance was attained. This super-tough blend exhibited an impact strength of 87 KJ/m^2 representing 11-fold over that of PLA/PEO blends with the same elastomer content and almost 22-fold higher than that of pure PLA with 40% reduction in tensile strength (71.4 to 42.1 MPa) and modulus (2.1 to 1.3 GPa) compared to PLA. Furthermore, SEM permitted the identification of the critical interparticle ligament (Lc=0.5µm) at which the brittle-ductile transition occurred for this super-tough blend. This super-toughness was attributed to the interfacial compatibilization and not to crystallization of PLA as its level in the blends measured by DSC was very low (< 6%).**[207]**

Another reactive strategy in which PLA/PEO blend was compatibilized using an EGMA was developed by Li et al..**[208]** It was found that the PEO particle size was significantly decreased by the addition of EGMA, and the PEO particle size and distribution decreased with the increase of the EGMA content up to 2 wt%, beyond which the PEO particle size and distribution remained unchanged. Rheological results revealed that the melt elasticity and viscosity of the PLA blends increased with the incorporation of PEO and EGMA. The failure mode changed from brittle fracture of neat PLA to ductile failure of the PLA/PEO blends. Elongation at break and impact

strength of PLA/PEO blends increased significantly with the increase of EGMA content up to 2 wt% and the optimal composition for the PLA/PEO/EGMA blend was (80/20/2, w/w).**[208]**

A super-tough PLA was prepared by reactive blending of PLA with poly(ethylene-co-glycidyl methacrylate) (EGMA) (80/20, w/w) followed by annealing at 90°C for 2.5 hr.**[209]** Chemical compatibilization happened in the system and the as molded blend showed an elongation at break 40 times higher than that of neat PLA (200% vs. 5%) and notched impact strength twice to three times that of PLA which was then improved by annealing process to 72 kJ/m^2 ca. about 50 times that of PLA and exceeding that of an ABS resin (21 kJ/m^2), but Elongation of the blends was reduced to below 35% after annealing process. The rubber decreased the crystallization temperature of PLA attributed to the nucleating activity of the rubber that facilitated crystal growth at numerous locations. It was concluded that interface control in multicomponent materials and crystallinity played a key role in significant improvement in toughness.**[209]**

Blown films of PLA/EGMA were prepared by Yeh et al..**[210]** DMA and morphological analysis by SEM of PLA/EGMA blends revealed compatibility between EGMA and PLA at EGMA contents equal to or less than 2 wt%. This compatibility is due to reaction between the reactive groups of PLA and the epoxy group of EGMA and/or to the self-reacted EGMA molecules, respectively as evidenced by the appearance of ester and ether absorption bands in FTIR spectra. Thermal analysis by DSC and DMA of PLA and PLA/EGMA specimens revealed that the percentage crystallinity, peak melting temperature, and onset recrystallization temperature values of PLA/EGMA specimens reduce gradually as their EGMA contents increased. In contrast, the T_gs of PLA/EGMA specimens increase gradually in conjunction with their EGMA contents. The tensile and tear strength values of PLA/EGMA blown film specimens in machine and transverse directions improved significantly, and reached their maximal values as their EGMA contents approached an optimum value of 6 wt%.**[210]**

Melt blending of PLA with various rubbers was considered by Jiang et al..**[211]** Morphological study by TEM and SEM of injection molded samples indicated that EGMA is highly compatible due to its reaction with PLA (0.5-2μm), and maleic anhydride grafted poly(styrene-ethylene/butylene-styrene) triblock elastomer (mSEBS) is less compatible (5-6μm) with PLA and poly(ethylene-co-octane) (EOR) is incompatible with PLA (20-30μm). Furthermore, compared to EOR system, it was found that the orientated microstructure in flow direction (FD) in PLA/mSEBS system is much more remarkable and finer due to its better compatibility with PLA. However for PLA/EGMA system, a fine co-continuous microlayer structure is formed due to elongation and orientation along the FD and the transverse direction to flow (TD) of both PLA and rubber phases. All blends exhibited higher toughness than PLA; however PLA/EGMA was a super-tough blend with notched impact strength of 87.8 kJ/m^2, ca. over 20 times higher than that of neat PLA. In contrast to mSEBS, EGMA and EOR decreased the cold crystallization of PLA ascribed to their nucleating effect, but in all PLA/rubber blends, the crystallinity of PLA is at the same low level (<10%) indicating that the crystallinity of PLA matrix does not appear to be a contributing factor resulting in the significant dependence of impact toughness, especially in the higher rubber loadings region. **[211]**

Blending of ethylene/n-butylacrylate/GMA terpolymer elastomer (E-BA-GMA) and zinc ionomer (EMAA-Zn) with PLA with simultaneous dynamic vulcanization of E-BA-GMA rubber resulted in salami structure of the blend in which the EMAA-Zn phase evolved from occluded sub-inclusions into continuous phase with decrease in the E-BA-GMA/EMAA-Zn ratio.**[212,213]** Blending temperature greatly affected impact strength of the ternary blend but not tensile properties. At 240°C PLA ternary blends displayed super-toughness with moderate strength and stiffness. Further toughness improvement was possible when the elastomer/ionomer weight ratio was equal to or larger than one (≥ 1) such as the ternary blend with 15 wt% E-BA-GMA which displayed impact strength of 860J/m and elongation at break greater than 200%.**[212]** super-toughness was thought to be due to the effective interfacial compatibilization between PLA and E-BA-GMA at elevated blending temperatures which was found to be promoted by the zinc ions of the ionomer. The investigation of

micromechanical deformation process of the ternary blends by SEM observations of impact-fractured surfaces suggested that the low cavitation resistance of dispersed particles in conjunction with suitable interfacial adhesion was responsible for the optimum impact toughness observed.**[213]** The same authors developed innovative reactive blend system involving dual reactions to toughen PLA.**[214]** The dual reactions comprised simultaneous vulcanization (crosslinking) of E-BA-GMA and interfacial reactive compatibilization between PLA and E-BA-GMA. The ionomer was prepared by ZnO neutralization of the ionomer precursor ethylene/methacrylic acid copolymer (EMAA). The detailed study of the interfacial compatibilization pointed out that it greatly enhanced with increases in degree of neutralization and/or functionality of EMAA-Zn (content of EMAA) both of which also influenced, but to a much lesser extent, the crosslinking level of E-BA-GMA as was found by DMA analyses. Consequently, toughness depended on these two factors i.e. impact strength of the resulting PLA ternary blends increased with increased degree of ionomer neutralization and higher functionality as was revealed by fractography (SEM) and FTIR analyses. Combination of a relatively low extent of crosslinking of the E-BA-GMA phase and a strong interfacial adhesion was found to favor the achievement of super-toughness. Morphological analysis by TEM analyses revealed that particle size and polydispersity correlated with impact strength, a finer and more uniform particle size and distribution tended to yield superior impact strength of the PLA blends.**[214]**

In view of toughening PLA, ethylene-propylene copolymer (EPR), ethylene-acrylic rubber (EAR), acrylonitrile-butadiene rubber (NBR), and isoprene rubber (IR) were added separately to PLA.**[215]** All blends showed partial miscibility between PLA and rubber. Toughness was achieved by the more polar NBR which exhibited the smallest particle size (3-4 μm) than the other three rubbers in the blends and impact strength two times higher than that of PLA. Tensile tests showed that the NBR and IR blends possessed a high ability to induce plastic deformation before the break as well as high elongation properties. **[215]**

The brittleness of PLA was alleviated by the addition of an ethyl acrylate ultrafine powdered rubber particles (EA-UFPR) to PLA.**[216]** At the optimum rubber

content of 10 wt% both elongation at break and toughness underwent nearly 50 times (3.5 vs. 200%) and 4 times (24 vs. 100 J/m) increase respectively compared to neat PLA, but these improvements were accompanied with a significant drop in tensile (45%) and flexural (20%) moduli. Microscopic observation revealed good rubber particles dispersion and adhesion to PLA, and plastic deformation of PLA matrix occurred owing to multiple crazes induced by the rubber particles indicating that crazing was the major toughening mechanism responsible of energy dissipation and thus of the obtained mechanical properties enhancements. Furthermore the introduction of the ultrafine acrylate rubber particles by only 0.5 wt% helped increasing the degree of crystallinity indicating the nucleating activity of the rubber particles.**[216]** When fully-vulcanized EA-UFPR particles were used, considerable improvement in tensile toughness (~220%) was successfully achieved with the incorporation of only 1 wt% EA-UFPR, without sacrificing PLA stiffness and strength.**[217]** The mechanism of deformation in this system was debonding cavitation at the PLA/EA-UFPR interfaces during stretching, that is responsible of extensive energy dissipation and superior tensile toughness.

Based on our literature survey, it clearly appears that numerous research work have been carried out in the field of PLA toughening using various polymers and rubbers, however little information is available on toughening PLA using impact modifiers.**[218]** Impact modifiers can provide an interesting alternative to plasticizers to reduce PLA brittleness, while maintaining acceptable stiffness. These modifiers are either linear elastomers of low T_g or crosslinked core-shell polymers.**[5]** Some companies have commercialized impact modifiers specifically designed for PLA. Some of these impact modifiers are ethylene-based copolymers and are generally used at an overall content of 10 wt% maximum for industrial applications.**[3,5]** Some examples of these commercially available impact modifiers specifically designed for PLA include Sukano® PLA im S550 series from Sukano Co. and OnCap™ BIO Impact T from PolyOne that are designed for transparent applications. Biomax® 100 and 120 are two commercial modifiers for PLA from DuPont Company for food and non-food applications respectively. Both modifiers are said to be ethylene-acrylate copolymers and are designed to improve the toughness of PLA in packaging and

industrial applications with minimal impact on transparency. Paraloid™ BPM-500 acrylic-based impact modifier from Rohm and Haas have minimal effect on PLA films clarity. Biostrength™130, 150, 200, 280 and 700 are grades of core-shell impact modifiers for PLA launched in the market by Arkema.**[5,218]** Several research studies tested some of these commercial impact modifiers.**[219-221]** Toughening effects of Biomax® Strong 100 on PLA and highly-filled PLA/calcium sulfate anhydrite composites indicated that notched impact strength of PLA with 5 and 10 wt% Biomax® Strong 100 increased from 2.6 kJ/m^2 of the neat PLA to 4.6 and 12.4 kJ/m^2, respectively and that elongation was above 25% for the blend with 10 wt% of the impact modifier, while tensile strength and modulus of PLA gradually decreased with addition of the impact modifier. PLA modified films using either Biomax® Strong 100 or Sukano® PLA im S550 as a toughener had maximum elongation of 255% for the former at 12 wt% loading and 240% for the latter at 8 wt% loading, while elongation of neat PLA was about 90%. Sukano® PLA im S550 gave clearer films, but the clarity of films decreased with concentration for both tougheners. In another study the toughening effects of Biomax® Strong 100 on semicrystalline and amorphous PLA were compared. Biomax® Strong 100 achieved superior toughening on semicrystalline PLA over amorphous PLA.**[219-221]** Recently, Biomax® Strong 100 and other masterbatchs for PLA packaging applications were also tested.**[222]** PLA films containing Biomax® Strong showed significant increase of impact force resistance (90 to 380N) representing 4-fold increase compared to PLA alone with relatively low adverse effect on mechanical strength as PLA tensile strength reduced by only 3-5%. Mat Taib et al.,**[218]** reported a detailed study on Biomax® Strong 100 toughened PLA. It was found that addition of impact modifier decreased the ability of PLA to crystallize and/or recrystallize and the degree of crystallinity of PLA decreased with increasing impact modifier content. Addition of the impact modifier did not result in noticeable change in the T_g of the amorphous PLA suggesting immiscibility between blend components, a fact that was also confirmed by DMA tests. Toughening effect of the impact modifier was evidenced by tensile tests which showed improvement in elongation at break and notched impact strength but at the expense of yield stress and tensile modulus. Better enhancement was observed at impact modifier ratio of 30 wt%

with comparable yield stress and tensile modulus to those of polypropylene. SEM micrographs revealed that the toughening mechanisms among others involved shear yielding or plastic deformation of the PLA matrix induced by interfacial debonding between the PLA and the impact modifier domains.**[218]**

To maintain the transparency of PLA, Zhang et al.**[223]** considered melt blending of PLA with methyl methacrylate-butadiene-styrene (MBS) that is a well-known transparent core-shell impact modifier largely used for PVC. PLA/MBS blends were compatible and exhibited a single T_g and MBS acted as an effective heterogeneous nucleating agent for PLA and significantly improved the degree of crystallinity of PLA. With an increase of MBS content, the tensile strength of the blends decreased; however, the elongation at break and impact strength increased significantly indicating the toughening effects of the MBS on PLA. The impact strength of the PLA/MBS (75/25, w/w) blend was about 21 times that of neat PLA. The improvements were ascribed to the large plastic deformation (shear yielding) in PLA matrix that is an important energy-dissipation process triggered by the cavitation of MBS particles.**[223]** Very recently, two premade transparent impact modifiers poly(butadiene-co-methylmethacrylate-co-butylacrylate-co-hydroxyethylmethacrylate) (BMBH) and poly(butadiene-co-lactide-co-methylmethacrylate-co-butylmethacrylate) (BLMB) that are based on copolymers of polybutadiene (for absorbing energy) and methylmethacrylate (for optical transparency) were tested with PLA. Interestingly compound of BLMB copolymer could enhance impact strength up to 25% compared to virgin PLA, while retaining films optical transparency of the PLA matrix. However, compound of BMBH copolymers with butyl acrylate as component could only increase impact strength up to 12% compared to virgin PLA.**[224]**

SAN-g-MAH, PEO-MAH and EGMA were used to compatibilize PC/PLA (70/30, w/w) blends. Mechanical, morphological and rheological properties suggested that SAN-g-MAH is the most effective compatibilizer. The maximum value of the mechanical properties such as impact, tensile and flexural strengths of the PC/PLA (70/30, wt%) blend was observed when the SAN-g-MAH was used at the amount of 5 phr.**[225]** With the perspective of toughening PLA with minimum loss in heat

resistance and stiffness, PLA/PC (50/50, w/w) blends compatibilized by PBSL and epoxy (EP) were investigated by Wang et al..**[226]** DSC of PLA/PBSL and PC/PBSL blends showed that individual components were immiscible. The notched impact strength of PLA/PC/PBSL ternary blends increased with PBSL content up to 10 phr PBSL due to enhanced interfacial interaction and proper domain size of the dispersed phase on the basis of DMA, DSC, and SEM analysis. PLA/PC/EP (50/50/10, w/w) exhibited slight improvement of impact strength (10.8 J/m) compared to PLA/PC/PBSL of same composition (65.1 J/m) and to neat PLA (7.5 J/m) which then drastically decreased below that of PLA (7.2 J/m) after addition of 1 phr tetrabutylammonium bromide (TBAB) catalyst. A combination of PBSL and EP improved toughness of PLA/PC blend (25.5 J/m). However, adding both modifiers with the TBAB catalyst in the PLA/PC blend only resulted in moderate improvement in impact strength (34 J/m).**[226]**

III-6 Toughened PLA Nanocomposites

Copolymerization, plasticization, and blending with flexible polymers and rubbers are viable toughening techniques that are generally aimed at improving either the impact strength (toughness) and/or the tensile ductility of PLA. However, improvements in either often come at the expense of concomitant substantial reductions in stiffness and/or strength of the material. Consequently a balance among stiffness, strength and toughness has to be attained to achieve desirable material performance.**[1-7,35]** It has been demonstrated that applying nanocomposites technology to the above strategies would improve the toughness without significant adverse effects on stiffness-strength balance of the designed materials.**[35]** Our literature survey revealed that while investigations on PLA blends with flexible polymers and rubbers are rather largely well documented, their ternary nanocomposites studies are very scarce. An attempt is made here to summarize the most available and relevant studies found in open literature by focusing mainly on layered silicates based ternary nanocomposites.

Various nanofillers including silica,**[227,228]**cellulose nanocrystal,**[229,230]** cellulose microfibers,**[231]** carbon nanotubes,**[232,233],** and layered silicates**[236-256]** have been incorporated in toughened PLA blends in the aim to counterbalance the negative softening effect of the added flexible or rubbery polymers and/or to endow PLA with other functional properties. In some other cases composites are prepared using micro- and macro-fillers such as $CaCO_3$,**[234]** and basalt fibers.**[235]**

Chen at al.**[236,237]** studied PLA/PBS nanocomposites containing a twice functionalized orgnoclay (TFC) prepared using commercial Cloisite®25A (C25A) functionalized with an organosilane. The silicate layers of PLA/PBS/TFC were exfoliated to a larger extent than PLA/PBS/C25A attributed to the increased interfacial interaction between the polyesters and the TFC clay through chemical reaction. XRD results indicated that TFC was more compatible with PLA than with PBS. At low content, TFC was exfoliated and encapsulated inside PLA, but at higher contents, TFC dispersed in both PLA and PBS with coexistence of intercalated/exfoliated morphology. Increasing TFC (0-10 wt%) decreased the domain size of the PBS dispersed phase (ca. 1.8-0.2mm). When located inside the PLA phase, the reactive TFC did not hinder the coalescence of the dispersed PBS domains; however at higher contents, TFC acted as a compatibilizer in the PLA/PBS blend and sharply decreased the particle size of PBS. Incorporation of 10 wt% TFC in PLA/PBS (75/25, w/w) not only improved Young's modulus from 1075 MPa to1990 MPa but also the elongation at break from 72% to 118% compared to unfilled PLA/PBS blend. Whereas addition of 10 wt% C25A to the same blend increased the tensile modulus to 1940 MPa but at the expense of elongation at break which deceased to 3.6% which was even lower than that of PLA (6.9%).**[236,237]** The same authors obtained similar results when TFC was used in PLA/PBSA (75/25; w/w) blend. Compared to PLA/PBSA/C25A, incorporation of TFC resulted in comparable moduli (1.78 vs.1.75 MPa), and improved elongation at beak (5 vs. 46%) which was however lower than that of PLA/PBSA binary blend (154%).**[238]** In another study Biodegradable PLA/PBSA/OMMT nanocomposites (70/30/6, w/w) were prepared using OMMT modified with four different surfactants.**[239]** Addition of organoclay reduced dispersed PBSA domain size and the extent of this reduction was dependent on the

type of the clay modifier and on interaction between the clay surface and the polymer blend. The fine morphology and the improved adhesion between the phases contributed to the improvement of the thermal and the mechanical properties of nanocomposites over the binary blends, but enhancement in elongation at break was not attained, probably due to the crystallinity of the blends.**[239]**

PLA/OMMT nanocomposites toughened with EPR-g-MAH and prepared with both solution and melt intercalation methods were investigated by Chow and Lok.**[240]** XRD results revealed the formation of exfoliated nanocomposites using solution technique while partially intercalated/exfoliated structure was observed for melt intercalated nanocomposite. For both techniques, EPM-g-MAH successfully facilitated clay dispersion by intercalating into the gallery of the OMMT. FESEM micrographs showed that more fibrillated structure was observed from the fractured surface of PLA/OMMT/EPM-g-MAH nanocomposites prepared by melt intercalation method. The flexural modulus and flexural yield stress of PLA/OMMT nanocomposites were decreased by addition of EPM-g-MAH. Melt intercalation method was able to produce PLA/OMMT/EPM-g-MAH nanocomposites with relatively higher flexural yield stress and flexural yield displacement. On the other hand, solution intercalation method was able to produce PLA/OMMT/EPM-g-MAH nanocomposites with relatively higher flexural modulus.**[240]** Further study using melt intercalation method indicated that thermal properties of PLA were greatly influenced by the addition of OMMT and EPM-g-MAH.**[241]** Addition of OMMT and EPM-g-MAH did not influence much on the T_g and T_m of PLA. However OMMT acted as nucleating agent by decreasing the crystallization temperature (T_c). The degree of crystallinity slightly increased for PLA/OMMT but dropped after addition of EPM-g-MAH attributed to the encapsulation of OMMT by the rubber that hindered the nucleating activity of the heterogeneous clay.**[241]**

Toughening PLA nanocomposites with PCL was explored by different researchers.**[242-244]** PLA/PCL/OMMT nanocomposites were prepared using PCL with different Mw. In comparison to PLA, it was found that the Young's modulus and tensile strength increased by 19% and by 17% for the PLA/PCL/OMMT (90/5/5, w/w)

respectively; whereas, the elongation remained below 4%.**[242]** Clay reinforced PLA/PCL Blend (90/10, w/w) was studied by Yu et. al..**[243]** The obtained nanocomposites showed enhanced tensile strength, modulus and elongation at break than that of PLA/PCL blends. 1wt% OMMT was the optimum concentration beyond which all tensile properties drastically decreased. DMA results also showed the increasing mechanical properties with temperature dependence of nanocomposites. Both XRD and TEM attested formation of intercalated/exfoliated nanocomposite. OMMT located mainly in the PLA phase that was confirmed by evaluating the specific interaction between each polymer and OMMT using Flory-Huggins interaction parameter (β). The final values of β showed that PLA was more compatible with OMMT than PCL. SEM images indicated that increasing content of OMMT reduced the domain size of phase-separated particles of the blend from 3-4μm for PLA/PCL blend to 0.2-0.5 μm for PLA/PCL/10 wt% OMMT making, the material more uniform. While the T_m of PLA in the blend was not influenced by OMMT, its T_c dropped and its crystallization degree increased with increasing OMMT loading that is indicative of the nucleating effect of OMMT.**[243]**

Effects of compatibilizer structural parameters and feeding route on the dispersion state of OMMT and its partitioning between the PLA and PCL phases was reported by Shafei et al..**[244]** Both PLA and PLA/PCL nanocomposites exhibited intercalated/exfoliated structure. Highly functionalized PP-g-MAH compatibilizer with a low Mw and batch melt mixing of the compatibilizers and OMMT with PLA or PLA/PCL were much more effective in achieving a high degree of clay exfoliation than direct melt-mixing process. All the PLA/OMMT and PLA/PCL/OMMT hybrids compatibilized with high-molecular-weight PP-g-MAH displayed a higher dynamic melt viscosity. OMMT layers behaved as barriers for the coalescence of the PCL droplets and reduced their size indicating that nanolayers were preferentially wetted by PCL in the blend. Addition of the high Mw compatibilizer induced further domain size decrease compared to lower Mw compatibilizer owing to its lower melt viscosity that resulted in fewer shear breakdowns of the PCL droplets during the melt-mixing process. Mechanical properties were not investigated in this study.**[244]**

To counterbalance the softening effect of PBAT on PLA, OMMT or nanoprecipitated calcium carbonate (NPCC) were introduced in PLA/PBAT blends.**[245]** Results of mechanical testing demonstrated that addition of 10 wt% of PBAT significantly improved the elongation of PLA (43 times) but reduced the strength and modulus to ca. 85% of the values of pure PLA. The addition of OMMT partially restored the strength of the PLA/PBAT binary system and increased its modulus to even higher than that of the pure PLA. On the other hand, NPCC slightly decreased the strength of the binary system and the moduli remained largely unchanged. Both OMMT and NPCC resulted in a substantial elongation decrease of the binary system, with OMMT demonstrating the largest decrease. The elongation of the ternary composites was remarkably increased by using PLA-g-MAH as compatibilizer due to improved dispersion of the nanoparticles. Among these nanocomposites, PLA/PBAT (10/2.5, w/w) OMMT with PLA-g-MAH demonstrated the best overall properties with 87% of the strength of the pure PLA, slightly higher modulus and significantly improved elongation (16.5 times higher than the pure PLA).**[245]**

In an attempt to achieve balanced overall properties, PLA ternary nancomposites containing both PBAT and rigid OMMT nanoparticles were prepared by melt intercalation procedure.**[246]** PLA/PBAT blend (75/25, w/w) exhibited a decrease in tensile strength (62.8%) and tensile modulus (55.1%) respectively as compared with the virgin PLA matrix, but resulted in an increase in the impact strength (21.1 vs. 50 J/m). Addition of 3-5 wt% reactive GMA compatibilizer increased the impact strength of PLA/PBAT blend to the tune of 26.5% (50.44 to 63.85 J/m) and 51.7% (50.44 to 76.56 J/m) while retaining the tensile strength. Incorporation of nanoclay additionally increased tensile modulus from 1841.4 MPa to 2106.7 MPa. XRD results of GMA compatibilized nanocomposites indicated intercalated structure, while TEM observations revealed intercalated as well as exfoliated clay layers in the blend matrix. SEM and TEM investigations showed two phase morphology with efficient dispersion of PBAT within PLA matrix and enhanced miscibility after GMA and clay incorporation. The mechanism of deformation was elucidated, that is, toughening occurred through debonding cavitation followed by

shear yielding of the PLA matrix. DSC and DMA confirmed the two phase morphology of the system and disclosed that addition of GMA enhanced the interfacial adhesion between the individual polymers via reaction with GMA compatibilizer.**[246]**

SEBS-g-MAH was melt mixed with PLA/OMMT with the aim to improve ductility.**[247]** Intercalated structure and homogenous dispersion of the OMMT silicate layers was observed for all nanocomposites with some of the clay encapsulated within the SEBS-g-MAH. Thermal behavior of PLA was greatly influenced by the addition of OMMT and SEBS-g-MAH. OMMT acted as heterogeneous nucleating agent for PLA and substantially decreased its Tc, however coaddition of the rubber encapsulated some of the clay and reduced the nucleating activity of the clay which resulted in an increase in Tc of PLA. T_g of PLA was found unaltered after addition of both modifiers, and the degree of PLA crystallinity steadily increased with increasing rubber loading. Elongation at break increased with increasing rubber loading but at the expense of modulus and tensile strength which decreased. Notched and unnotched impact strength determination revealed the same trend and indicated that the PLA was a notch sensitive material. The processability of PLA/OMMT nanocomposites decreased marginally with the increase of SEBS-g-MAH content. Overall, the PLA/2 wt% OMMT/5 wt% SEBS-g-MAH exhibited balanced in processability, mechanical, and thermal properties.**[247]**

In a recent report it has been demonstrated that PLA/NR blend nanocomposites with different desired properties can be achieved by an appropriate choice of the nanoclays used.**[248]** Location of nanoclays predicted by contact angle measurement and a mathematical model corroborated well with TEM observations. Cloisite®-Na^+ was present in the PLA phase forming big agglomerates, while both organoclays were preferentially located at the PLA/NR interface at low concentration. At high organoclay concentration C15A located at both the interface and NR phase, due to its non-polar surfactant, while C30B was present at both the interface and PLA phase owing to its higher polarity that makes it more compatible with PLA. C15A and C30B, acted as compatibilizers for the PLA/NR blend because of their preferential location at the polymer interface, acting as a solid barrier and preventing the coalescence of NR

droplets resulting thus in finer morphology. However, different properties were obtained depending on the used nanoclays. While C15A allowed a further increase of the elongation at break of the PLA/NR blend, the addition of C30B produced stiffer materials. This behavior was attributed to the different interactions of the nanoclays with the two polymers.**[248]** The crystallization behavior of the system revealed that NR acted as a nucleating agent for the PLA matrix, leading to a decrease of PLA cold crystallization temperature during dynamic DSC measurements and an increase of the crystallization rate followed by rheological measurements during isothermal crystallization. Addition of 3 wt% of organoclays, located at the interface between the two polymers, delayed PLA crystallization by hindering the interfacial nucleating activity of the NR droplets and impeding the migration of small impurities such as fatty acids from the NR droplets to the PLA phase.**[249]**

PLA modified by PMMA and PEO, and reinforced with organically modified vermiculite (OVMT) clay was explored by Auliawan and Woo.**[250]** PLA/PMMA/PEO formed a miscible system at PLA content of 60 wt% and above. Addition of PEO to plasticized PLA enabled chain mobility of PLA at lower temperature, while addition of PMMA suppressed the crystallization process of PLA. Thus with the increase content of PEO and PMMA, the crystallization of PLA can take place at lower temperature and the crystallization extent is suppressed simultaneously. OVMT exhibited good interaction and acceptable dispersion in the ternary polymer blend without altering the crystal structures of PLA/PEO constituents. OVMT acted as nucleating agent by enabling some degree of crystallization and also reduced melting point indicating formation of less perfect crystals than those of the neat ternary polymer blend.**[250]**

Novel toughened PLA nanocomposite based on LLDPE was developed by Balakrishnan et al..**[251]** TEM and XRD analysis provided evidence of intercalated structure in PLA and in LLDPE toughened PLA/OMMT nanocomposites at low OMMT content (2 phr) which contributed to the enhanced mechanical and thermal properties for both PLA and toughened PLA nanocomposites. The Young's and flexural modulus improved with increasing loadings of OMMT and the impact

strength of PLA and PLA/OMMT nanocomposites increased with addition of LLDPE as an impact modifier with a sacrifice of tensile and flexural strength. However, the tensile and flexural strength decreased with addition of OMMT and LLDPE. The impact strength and elongation at break of toughened PLA nanocomposites also declined steadily with increasing loadings of OMMT. Thermal analysis through DSC revealed that the Tc and Tg of PLA in both PLA/OMMT and LLDPE toughened PLA/OMMT nanocomposites decreased with increasing content of OMMT indication nucleating effect of OMMT.**[251]**

PLA/LLDPE nanocomposite based on unmodified sepiolite was prepared using a twin screw extruder.**[252]** PE-g-MAH and SEBS-g-MAH were used as compatibilizers in an effort to increase PLA tensile toughness. Compatibilized blends prepared without clay had higher tensile toughness than those prepared with sepiolite. The nanocomposite blends exhibited, lower tensile strength, and Young's modulus values and increased elongation at break and tensile toughness, compared with those of the PLA nanocomposite. These results were related to the clay dispersion, to the type of morphology of the different blends, to the localization of the sepiolite in the different phases, to the thermomechanical degradation of the PLA matrix phase during melt blending and to the grafting degree of the compatibilizers used. The blend prepared with SEBS-g-MA as compatibilizer agent was the toughest in the tensile test.**[252]**

In an effort to toughen PLA, two types of commercial impact modifiers of core-shell rubber type (Palaroid EXL2330 and EXL2314) and two types of montmorillonites (C30B and C20A) were used.**[253]** PLA/OMMT, PLA/core-shell rubber and PLA/OMMT/core-shell rubber were examined. According to XRD and TEM analyses, both types of PLA/5 wt% nanoclay composites had an intercalated morphology, but the degree of intercalation was higher for C30B than for C20A possibly due to its more hydrophilic nature and thus its compatibility with PLA. In comparison with pure PLA, both types of PLA/5 wt% nanoclay composites had an increased modulus, similar impact strength, slightly reduced tensile strength, and significantly reduced strain at break. Compared to PLA, when the rubber varied in the

range (1-10 wt%) in the binary blends, similar reduction in tensile strength (61 vs. ~53 MPa) and modulus (1800 vs. ~1530 MPa) was recorded for both rubbers. Impact strength improved only with EXL2330 (2.2 vs.4 KJ/m^2), and better enhancement in strain at break was achieved using EXL 2314 (6.5 vs. ~11%). It was found that the simultaneous addition of 5 wt% nanoclay (C30B) and 20 wt% EXL2330 resulted in a PLA composite with a 134% increase in impact strength (2.2 vs. 5.2 KJ/m^2), a 6% increase in strain at break (6.6 vs. 7.0%), a similar modulus (1800 MPa), and a 28% reduction in tensile strength (61 vs. 43.8 MPa) in comparison with pure PLA.**[253]**

An ethylene acrylate based impact modifier from DuPont, Biomax® strong (Biostrong), was used in combination with an OMMT to compensate the loss in stiffness and strength.**[254]** PLA chains were intercalated in OMMT nanocomposites but agglomeration of OMMT at higher loadings (4 wt%) was detected by XRD. A significant improvement in impact strength (ca. 54%) was observed with 2 phr OMMT in PLA/Biostrong (39 vs. 60 J/m), indicating that the OMMT platelets had improved the toughness of the matrix by inducing shear yielding during matrix deformation. The flexural modulus of PLA/Biostrong nanocomposites increased steadily while the flexural strength decreased with increasing amount of OMMT. While T_m was unaltered after addition of both OMMT and Biostrong, the T_g of PLA in PLA/Biostrong increased with addition of OMMT that is indicative of a restriction in chain mobility imposed by OMMT platelets. The drop in T_c of PLA in the presence of Biostrong and OMMT platelets revealed that both additives acted as effective nucleating agents for PLA and considerably promoted its crystallization.**[254]**

With the aim to improve potential use of PLA in automotive applications and to replace the frequently used mineral filled polypropylene (PP) in this area, an innovative strategy in which 10 wt% tributyl citrate (TBC) plasticizer added to the PLA/Biostrong nanocomposite/Cloisite®25A (C25A) (80/10/3, w/w) was developed by Notta-Cuvier et al..**[255]** It was found that a compromise was necessary between high tensile apparent rigidity and strength on the one hand, and levels of ductility on the other. Indeed, plasticization of the polymers always leads to decreased tensile rigidity and strength. In that framework, quaternary composition PLA + 10 wt%

Biomax Strong + 10 wt% TBC + C25A was found of interest because it presented interesting levels of ductility while maintaining rigidity and strength higher than those of a mineral-filled PP. Content of C25A must be determined based on a compromise between optimized strengthening obtained for 1 wt% C25A content and higher ductility and rigidity reached at 3 wt% C25A. I was also found that C25A content had little influence on tensile strength.**[255]**

Recently PLA toughened nanocomposites using 20 wt% of an ethylene-methyl acrylate-glycidyl methacrylate (E-MA-GMA) impact modifier from Arkem (lotader AX 8900) and C20A was explored by Mélo et al..**[256]** The nanocomposites were prepared by twin screw extrusion followed by injection molding at two levels of C25A (2.5 and 5 wt%). XRD results indicated partially exfoliated structure at low C25A concentration (2.5 wt%) but intercalated morphology was detected when OMMT content increased to 5wt%. Addition of the E-MA-GMA terpolymer to PLA substantially increased the impact strength (32 vs. 65 J/m) and further maximum toughness ~85 J/m was obtained after addition of 2 wt% C25A to PLA/E-MA-GMA blend. This improvement in impact strength was attributed to the OMMT compatibilizing effect that reduced interfacial tension between the polymers and suppressed coalescence of E-MA-GMA dispersed phase and also to the good adhesion between the phases owing to the in situ compatibilizing reaction between PLA groups and those of the impact modifier. However, at this composition, tensile modulus was lower than that obtained at 5 wt% C25A.**[256]**

REFERENCES

[1] Raquez, J.M.; Habibi, Y.; Murariu, M.; Dubois, P., Prog. Polym. Sci., Vol. 38, pp 1504 **(2013)**.

[2] Lim, L.T.; Auras, R., Rubino, M., Prog. Polym. Sci., Vol. 33, pp 820 **(2008)**.

[3] Ojijo, V. and Sinha Ray, S., Prog. Polym. Sci., Vol. 38, pp 1543 **(2013)**.

[4] Rasal, R.M.; Janorkar, A.V.; Hirt, D.E., Prog. Polym. Sci., Vol. 35, pp 338 **(2010)**.

[5] Liu, H. and Zhang, J., J. Polym. Sci.: Part B: Polym. Phys., Vol. 49, pp 1051 **(2011)**.

[6] Anderson, K.S.; Schreck, K.M.; Hillmyer, M.A. Polym. Rev., Vol. 48, pp 85 **(2008)**.

[7] Auras, R.; Lim, L.; Selke, S.E.M.; Tsuji, H. Poly(Lactic Acid): Synthesis, Structures, Properties, Processing, and Applications, John Wiley & Sons, Inc., Hoboken, New Jersey USA **(2010)**.

[8] Södergård, A.; Stolt, M. Properties of lactic acid based polymers and their correlation with composition Prog. Polym. Sci., Vol. 27, pp 1123 **(2002)**.

[9] Zhao, Y. M.; Wang, Z. Y.; Wang, J.; Mai, H. Z.; Yan, B.; Yang, F. J. Appl. Polym. Sci., Vol. 91, pp 2143 **(2004**).

[10] Min, C.; Cui, W.; Bei, J.; Wang, S. Polym. Adv. Technol., Vol. 18 (4), pp 299 **(2007)**.

[11] Tsuji, T.; Tezuka, Y. Macromol. Biosci., Vol. 5, pp 135 **(2005)**.

[12] Declerco, H. A.; Cornelissen, M. J.; Gorski, T. L.; Schacht, E. H. J. Mater. Sci., Mater. Med., Vol. 17, pp 113 **(2006)**.

[13] Hiki, S.; Miyamoto, M.; Kimura, Y.; Polymer, Vol. 41, pp 7369 **(2000)**.

[14] Yang, J. ; Liu, F. ; Yang, L. ; Li S. Eur. Polym. J., Vol. 46, pp 783 **(2010)**.

[15] Andronova, N. ; Albetsson, A.C. Biomacromolecules,Vol. 7, pp 1489 **(2006)**.

[16] Asplund, B.; Sperens, J.; Mathisen, T.; Hilborn, J. J Biomat. Sci. Polym. Ed., Vol. 17, pp 615 **(2006)**.

[17] Haynes, D; Abayasinghe, N.K.; Harrison, G.M.; Burg, K.J., Smith, Jr D.W., Biomacromolecules, Vol. 8, pp 1131 **(2007)**.

[18] Shen, P.; Moriya, A.; Rajabzadeh, S.; Maruyama, T.; Matsuyama, H., Desalination, Vol. 325, pp 37 **(2013)**.

[19] Barakat, I.; Dubois, P.; Grandfils, C.; Jerome, R. J. Polym. Sci. Part A, Vol. 39, pp 294 **(2001)**.

[20] Khang, G.; Choee, J. H.; Rhee, J. M.; Le, H. B. J. Appl. Polym.Sci., Vol. 85, pp 1253 **(2002)**.

[21] Watanabe, Y.; Shirahama, H.; Yasuda, H. React. Funct. Polym., Vol.59, pp 211 **(2004)**.

[22] Ebnesajjad, S., Handbook of Biopolymers and Biodegradable Plastics Properties, Processing, and Applications, Elsevier Inc. USA **(2013)**.

[23] Hiljanen, V. M.; Karjalainen, T.; Seppala, J. J. Appl. Polym. Sci., Vol. 59, pp 1281 **(1996)**.

[24] Ruckenstein, E.; Yuan, Y. J. Appl. Polym. Sci., Vol. 69, pp 1429 **(1998)**.

[25] Grijpma, D. W.; Joziasse, C. A. P.; Pennings, A., J. Die Makromol. Chem. Rapid Commun., Vol. 14, pp 155 **(1993)**.

[26] Haynes, D.; Naskar, A. K.; Singh, A.; Yang, C.; Burg, K. J.; Drews, M.; Harrison, G.; Smith, D. W. Macromolecules, Vol. 40, pp 9354 **(2007)**.

[27] Jing, F.; Hillmyer, M. A. J. Am. Chem. Soc., Vol. 130, pp 13826 **(2008)**.

[28] Theryo, G.; Jing, F.; Pitet, L. M.; Hillmyer, M. A. Macromolecules, Vol. 43, pp 7394 **(2010)**.

[29] Guerrouani, N.; Couturaud, B.; Mas, A.; François Schué, F.; Robin, J.J. Eur. Polym. J., Vol. 49, pp 1621 **(2013)**.

[30] Helminen, A. O.; Korhonen, H.; Seppala, J.V. Macromol. Chem. Phys.,Vol. 203, pp 2630 **(2002)**.

[31] Varmaa, I.K.; Albertssonb, A.C.; Rajkhowaa, R. Prog. Polym. Sci., Vol. 30, pp 949 **(2005)**.

[32] Pêgo, A.P.; Van luyn, M.J.A.; Brouwer, L.A.; Van Wachem, P.B.; Poot, A.A.; Grijpma, D.W. et al., J. Biomed. Mater. Res., Vol. 67A, pp 1044 **(2003)**.

[33] Zhu, K.J.; Zhang, J.X.; Wang, C.; Yasuda, H.; Ichimaru, A.; Yamamoto, K. J. Microencapsulation, Vol. 20, pp 731 **(2003)**.

[34] Imre, B. and Pukánszky, B. Eur. Polym. J., Vol. 49, pp 1215 **(2013)**.

[35] Balakrishnan, H.; Hassan, A.; Imran, M.; Wahit, M.U. Polym.-Plast. Technol. Eng., Vol. 51, pp 175 **(2012)**.

[36] Nampoothiri, K.M.; Nair, N. R.; John, R.P., Biores. Tech., Vol. 101, pp 8493 **(2010)**.

[37] Mascia, L. and Xanthos, M., Adv. Polym. Techn., Vol. 11, pp 237**(1992)**.

[38] Bouchareb, B. and Benaniba, T., J. Appl. Polym Sci., Vol. 107, pp 3442 **(2008)**.

[39] Piorkowska, E.; Kulinski, Z.; Galeski, A.; Masirek, R., Polymer, Vol. 47, pp 717 **(2006)**.

[40] Burgos, N.; Martino, V.P.; Jiménez, A., Polym. Degrad. Stab., Vol. 98, pp 651 **(2013)**.

[41] Choi, K.M.; Choi, M.C.; Han, D.H.; Park, T.S.; Ha, C.S., Eur. Polym. J., Vol. 49, pp 2356**(2013)**.

[42] Phuphuak,Y.; Miao, Y. ; Zinck, P.; Chirachanchai, S., Polymer, Vol. 54, pp 7058 **(2013)**.

[43] Lourdin, D.; Coignard L.; Bizot H., Polymer, Vol. 38 (21), pp 5401**(1997)**.

[44] Hassouna, F.; Raquez, J.M.; Addiego, F.; Dubois, P.; Toniazzo, V.; Ruch, D., Eur. Polym. J., Vol. 47, pp 2134 **(2011)**.

[45] Sinclair, R. G., J. Macromol. Sci., Part A: Pure Appl. Chem., Vol. 33, pp 585 **(1996)**.

[46] Jacobsen, S.; Fritz, H. G. Polym. Eng. Sci., Vol. 39, pp 1303 **(1999)**.

[47] Labrecque, L.V.; Kumar, R.A.; Davé, V.; Gross, R.A.; McCarthy, S.P. J. Appl. Polym. Sci., Vol. 66, pp 1507 **(1997)**.

[48] Sierra, J.; Noriega, M.; Cardona, E.; Ospina, S. Proceedings of Annual Technical Conference of the Society of Plastics Engineers (ANTEC), Orlando, Florida, May 16--20, pp 127 **(2010)**.

[49] Murariu, M.; Da Silva Ferreira, A.; Alexandre, M.; Dubois, P., Polym. Adv.Technol., Vol. 19, pp 636 **(2008)**.

[50] Ljungberg, N.; Wesslén, B., J. Appl. Polym. Sci., Vol. 86, pp 1227 **(2002)**.

[51] Ljungberg, N.; Wesslén, B., Polymer, Vol. 44, pp 7679 **(2003)**.

[52] Martino, V.; Ruseckaite, R.; Jiménez, A., J. Therm. Anal. Calorim., Vol. 86, pp 707 **(2006)**.

[53] Martino, V.P.; Jiménez, A.; Ruseckaite, R.A., J. Appl. Polym. Sci., Vol. 112, pp 2010 **(2009)**.

[54] Ljungberg, N.and Wesslén, B., Biomacromolecules, Vol. 6, pp 1789 **(2005)**.

[55] Ljungberg, N. and Wesslen, B., J. Appl. Polym. Sci., Vol. 94, pp 2140 **(2004)**.

[56] Lai, W.C.; Liau, W.B. ; Lin, T.T., Polymer, Vol. 45, pp 3073 **(2004)**.

[57] Kozlowski, M.; Masirek, R.; Piorkowska, E.; Gazicki-Lipman, M., J. Appl. Polym. Sci., Vol. 105, pp 269 **(2007)**.

[58] Li, H.; Huneault, M.A., Polymer, Vol. 48, pp 6855 **(2007)**.

[59] Bechtold, K.; Hillmyer, M.A.; Tolman, W.B. Macromolecules, Vol. 34, pp 864 **(2001)**.

[60] Kulinski, Z.; Piorkowska, E; Gadzinowska, K.; Stasiak, M., Biomacromolecules, Vol. 7, pp 2128 **(2006)**.

[61] Ljungberg, N., Andersson, T., Wesslen, B., J. Appl. Polym. Sci., Vol. 88, pp 3239 **(2003)**.

[62] Ren, Z.; Dong, L.; Yang, Y., J. Appl. Polym. Sci., Vol. 101, pp 1583 **(2006)**.

[63] Lemmouchi, Y.; Murariu, M.; Santos, A.M.D.; Amass, A.J.; Schacht, E.; Dubois, P., Eur. Polym. J., Vol. 45, pp 2839 **(2009)**.

[64] Zhan, G.Z.; Zhao, L.; Hu, S.; Gan, W.J., Yu, Y.F., Tang, X.L. ; Polym. Eng. Sci., Vol. 48, pp 1322 **(2008)**.

[65] Ali, F.; Chang, Y.-W.; Kang, S.C.; Yoon, J.Y. , Polym. Bull., Vol. 62, pp 91**(2009)**.

[66] Okamoto, K.; Ichikawa, T.; Yokohara, T.; Yamaguchi, M., Eur. Polym. J., Vol. 45, pp 2304 **(2009)**.

[67] Park, K.I. and Xanthos, M. Polym. Degrad. Stab., Vol. 94, pp 834 **(2009)**.

[68] Li, H. and Huneault, M.A. J. Appl. Polym. Sci., Vol. 119, pp 2439 **(2011)**.

[69] Kumar, R.; Josse C.; Anandjiwala R., Asia-Pacific J. Chem. Eng., Vol. 9, pp 382 **(2014)**.

[70] Wang, Y.; Qin, Y.; Zhang, Y.; Yuan M.; Li, H.; Yuan, M., Int. J. Biol. Macromol., Vol. 67, pp 58 **(2014)**.

[71] Martino, V.P.; Jiménez, A.; Ruseckaite, R.A.; Avérous, L. Polym. Adv. Tech., Vol. 22, pp 2206 **(2011)**.

[72] Gumus, S.; Ozkoc G.; Aytac, A., J. Appl. Polym. Sci., Vol. 123, pp 2837 **(2012)**.

[73] Scatto, M.; Salmini, E.; Castiello, S.; Coltelli, M.B.; Conzatti, L.; Stagnaro, P.; Andreotti, L.; Bronco, S., J. Appl. Polym. Sci., Vol. 127, pp 4947 **(2013)**.

[74] Wang, N.; Zhang, X.; Ma, X.; Fang, J. Polym. Degrad. Stab.,Vol. 93, pp 1044 **(2008)**.

[75] Rahman, M.A.; Santis, D.D.; Spagnoli, G.; Ramorino, G.; Penco, M.; Phuong, V.T.; Lazzeri, A., J. Appl. Polym. Sci., Vol. 129, pp 202 **(2013)**.

[76] Shi, N.; Dou, Q. Polym. Compos., Vol. 35, pp 1570, **(2014)**.

[77] Hassouna, F.; Raquez, J.M.; Addiego, F.; Dubois, P., Toniazzo, V.; Ruch, D., Eur. Polym. J., Vol. 48 (2), pp 404 **(2012)**.

[78] Vidéki, B. ; Klébert, Sz. ; Pukánszky, B. Eur. Polym. J., Vol. 41(8), pp 1699 **(2005)**.

[79] Vidéki, B.; Klébert, Sz.; Pukánszky, B. J. Polym. Sci. Part B: Polym. Phys., Vol. 45(8), pp 873 **(2007)**.

[80] Yıldırım, Y.; Oral, A., Rad. Phys. Chem., Vol. 96, pp 69 **(2014)**.

[81] Murariu, M.; Dechief A.L.; Bonnaud, L.; Paint, Y.; Gallos, A.; Fontaine, G.; Bourbigot, S.; Dubois, P., Polym. Degrad. Stab., Vol. 95, pp 889 **(2010)**.

[82] Souza, D.H.S.; Andrade, C.T.; Dias, M.L., Mat. Sci. Eng. : C, Vol. 33, pp 1795 **(2013)**.

[83] Katiyar, V.; Gerds, N.; Koch, C.B.; Risbo, J.; Hansen, H.C.B.; Plackett, D., Polym. Degrad. Stab., Vol. 95, pp 2563 **(2010)**.

[84] Katiyar, V.; Gerds, N.; Koch, C.B.; Risbo, J.; Hansen, H.C.B.; Plackett, D., J. Appl. Polym. Sci., Vol. 122, pp 112 **(2011)**.

[85] Yan S.F.; Yin J.B.; Yang J.Y.; Chen, X.S., Materials Letters, Vol.61, pp 2683 **(2007)**.

[86] Fukushima, K.; Tabuani, D.; Abbate C.; Arena, M.; Rizzarelli, P., Eur. Polym. J., Vol. 47, pp 139 **(2011)**.

[87] Nakayama, N.; Hayashi, T., Polym. Degrad. Stab., Vol. 92, pp 1255 **(2007)**.

[88] Zheng, X.; Zhou, S.B.; Xiao, Y.; Yu, X.J., Li, X.H., Wu, P.Z., Colloids and Surfaces B: Biointerfaces, Vol. 71, pp 67 **(2009)**.

[89] Jiang, L.; Zhang, J.; Wolcott, M.P., Polymer, Vol. 48 , pp 7632 **(2007)**.

[90] Kumar, V.; Dev, A.; Gupta, A.P., Composites: Part B, Vol. 56, pp 184 **(2014)**.

[91] Yu, J.; Qiu, Z., ACS Appl. Mat. Interf., Vol. 3, pp 890 **(2011)**.

[92] Zhang, X.; Sun, J., Fang, S.; Han, X.; Li, Y.; Zhang, C., J. Appl. Polym. Sci., Vol. 122, pp 296 **(2011)**.

[93] He, L.; Sun, J.; Wang, X.; Fan, X.; Zhao, Q.; Cai, L.; Song, R.; Ma, Z.; Huang, W., Mat. Chem. Phys., Vol, 134, pp 1059 **(2012)**.

[94] Mai, F.; Habibi, Y.; Raquez, J.M.; Dubois, Ph.; Feller, J.F.; Peijs, T.; Bilotti, E., Polymer, Vol. 54, pp 6818 **(2013)**.

[95] Liu, M.; Zhang, Y.; Zhou, C., Appl. Clay Sci., Vol. 75, pp 52 **(2013)**.

[96] Ogata, N.; Jimenez, G.; Kawai, H. ; Ogihara, T., J. Polym. Sci. Part B: Polym. Phys., Vol. 35, pp 389 **(1997)**.

[97] Sinha Ray, S.; Yamada, K.; Okamoto, M.; Ueda, K., Nano. Lett.,Vol. 2, pp 1093 **(2002)**.

[98] Krikorian, V. and Pochan, D.J., Chem. Mater., Vol. 15, pp 4317 **(2003)**.

[99] Chang, J.H.; An, E.U.; Sur, G.S., J. Polym. Sci.: Part B: Polym. Phys., Vol. 41, pp 94 **(2003)**.

[100] Di, Y.; Iannace, S.; Maio, E.D.; Nicolais, L., J. Polym. Sci. Pt. B: Polym. Phys., Vol. 43, pp 689 **(2005)**.

[101] Chen; G.X.; Kim, H.S.; Shim, J.H.; Yoon, J.S., Macromolecules, Vol. 38, pp 3738 **(2005)**.

[102] Lewitus, D.; McCarthy, S.; Ophir, A.; Kenig, S., J. Polym. Environ., Vol, 14, pp171 **(2006)**.

[103] Petersson, L.; Oksman, K.; Mathew, A.P., J. Appl. Polym. Sci., Vol. 102, pp 1852 **(2006)**.

[104] Pluta, M.; Jeszka, J.K.; Boiteux, G., Eur. Polym. J., Vol. 43, pp 2819 **(2007)**.

[105] Chow, W.S.; Lok, S.K., Polym. Polym. Comp., Vol. 16, pp 263 **(2008)**.

[106] Rhim, J.W.; Hong, S.I.; Ha, C.S., LWT-Food Sci. Techn., Vol. 42, pp 612 **(2009)**.

[107] McLauchlin, A.R. and Thomas, N.L., Polym. Degrad. Stab., Vol. 94, pp 868 **(2009)**.

[108] Nieddu, E.; Mazzucco, L.; Gentile, P.; Benko, T.; Balbo, V.; Mandrile, R.; Ciardelli, G., React. Funct. Polym., Vol. 69, pp 371 **(2009)**.

[109] Fukushima, K.; Murariu, M.; Camino, G.; Dubois, P., Polym. Degrad. Stab., Vol. 95, pp 1063 **(2010)**.

[110] Carrasco, F.; Gámez-Pérezb, J.; Santana, O.O.; Maspoch, M.Ll., Chem. Eng. J., Vol. 178, pp 451 **(2011)**.

[111] Gamez-Perez, J., Nascimento, L., Bou, J.J., Franco-Urquiza, E., Santana, O.O., Carrasco, F., Maspoch, M.Li., J. Appl. Polym. Sci., Vol. 120, pp 896 **(2011)**.

[112] Wang, B.; Wan, T.; Zeng, W., J. Appl. Polym. Sci., Vol. 125, pp E364 **(2012)**.

[113] Cheng; K.C.; Yu, C.B., Guo, W.; Wang, S.F.; Chuang,T.H.; Lin, Y.H., Carbohydrate Polymers, Vol. 87, pp 1119 **(2012)**.

[114] Fukushima, K.; Tabuan, D.; Arena, M.; Gennari, M.; Camino,G., React. Funct. Polym., Vol. 73, pp 540 **(2013)**.

[115] Lai, S.M., Wu, S.H., Lin, G.G., Don, T.M., Eur. Polym. J., Vol. 52, pp 193 **(2014)**.

[116] Tanoue, S.; Hasook, A.; Iemoto, Y.; Unryu, T., Polym. Comp., Vol. 27, pp 256 **(2006)**.

[117] Paul, M.A.; Alexandre, M.; Degee, P.; Henrist, C.; Rulmont, A.; Dubois, P., Polymer, Vol. 44, pp 443 **(2003)**.

[118] Pluta, M.; Paul, M.A.; Alexandre, M.; Dubois, P., J. Polym. Sci. Part B: Polym. Phys., Vol. 44, pp 299 **(2006)**.

[119] Pluta, M., Paul M.A.; Alexandre, M.; Dubois, P., J. Polym. Sci.: Part B: Polym. Phys., Vol. 44, pp 312 **(2006)**.

[120] Thellen, C.; Orroth, C.; Froio, D.; Ziegler, D.; Lucciarini, J.; Farrell, R.; D'Souza, N.A.; Ratto, J.A., Polymer, Vol. 46, pp 11716 **(2005)**.

[121] Shibata, M.; Someya, Y.; Orihara, M.; Miyoshi, M., J. Appl. Polym. Sci., Vol. 99, pp 2594 **(2006)**.

[122] Solarski, S.; Mahjoubi, F.; Ferreira, M.; Devaux, E.; Bachelet, P.; Bourbigot, S.; Delobel, R.; Coszach, P.; Murariu, M.; Ferreira, A.; Alexandre, M.; Degee, P.; Dubois, P., J. Mater. Sci., Vol. 42, pp 5105 **(2007)**.

[123] Al-Mulla, E.A.J.; Suhail, A.H.; Aowda, S.A., Indust. Crops Prod., Vol. 33, pp 23 **(2011)**.

[124] Al-Mulla, E.A.J.; Yunus, W.M.Z.; Ibrahim, N.A.; Rahman, M.Z., J. Mater. Sci., Vol. 45, pp 1942 **(2010)**.

[125] Choi, N.S.; Kim, C.H.; Cho, K.Y.; Park, J.K., J. Appl. Polym. Sci., Vol. 86, pp 1892 **(2002)**.

[126] Chen, C.C.; Chueh, J.Y.; Tseng, H.; Huang, H.M.; Lee, S.Y., Biomaterials, Vol.24, pp 1167 **(2003)**.

[127] Maglio, G; Migliozzi, A.; Palumbon, R.; Immirzin, B.; Volpen, M.G., Macromol. Rapid. Commun., Vol. 20, pp 236 **(1999)**.

[128] Tsuji, H.; Yamada, T.; Suzuki, M.; Itsuno, S., Polym. Int., Vol. 52, pp 269 **(2003)**.

[129] Chavalitpanya, K.; Phattanarudee; S., Energy Procedia 34, pp 542 **(2013)**.

[130] Monticelli, O.; Calabrese, M.; Gardella, L.; Fina, A.; Gioffredi, E., Eur. Polym. J., Vol. 58, pp 69 **(2014)**

[131] Wang, L.; Ma, W.; Gross, R.A.; McCarthy, S.P., Polym. Degrad. Stab., Vol. 59, pp 161 **(1998)**.

[132] Semba, T.; Kitagawa, K.; Ishiaku, U. S.; Hamada, H., J. Appl. Polym. Sci., Vol. 101, pp1816 **(2006)**.

[133] Semba, T.; Kitagawa, K.; Ishiaku, U. S.; Kotaki, M.; Hamada, H. J. Appl. Polym. Sci., Vol. 103, pp 1066 **(2007)**.

[134] Takayama, T.; Todo, M.; Tsuji, H.; Arakawa, K., J. Mater. Sci.,Vol. 41, pp 6501 **(2006)**.

[135] Harada, M.; Iida, K.; Okamoto, K.; Hayashi, H.; Hirano, K., Polym. Eng. Sci., Vol. 48, PP 1359 **(2008)**.

[136] Verbeek, C.J.R., "Products and Applications of Biopolymers", InTech, Rijeka Croatia **(2012)**.

[137] Lopez-Rodriguez, N.; Lopez-Arraiza, A.; Meaurio, E.; Sarasua, J.R., Polym. Eng. Sci., Vol. 46, pp 1299 **(2006)**.

[138] Vilay, V.; Mariatti, M.; Ahmad, Z.; Pasomsouk, K.; Todo, M., J. Appl. Polym. Sci., Vol. 114, 1784 **(2009)**.

[139] Broz, M.E.; VanderHart, D.L.; Washburn, N.R., Biomaterials, Vol. 24, pp 4181**(2003)**.

[140] Lu, J.; Qiu, Z.; Yang, W., Polymer, Vol. 48, pp 4196 **(2007)**.

[141] Liu, T.Y.; Lin, W.C.; Yang, M.C.; Chen, S.Y. , Polymer, Vol. 46, pp 12586 **(2005)**.

[142] Shibata, M.; Inoue, Y.; Miyoshi, M., Polymer, Vol. 47, pp 3557 **(2006)**.

[143] Wang, R.Y.; Wang, S.F.; Zhang, Y.; Wan, C.Y.; Ma, P.M., Polym. Eng. Sci., Vol. 49, pp 26 **(2009)**.

[144] Bhatia, A.; Gupta, R.K.; Bhattacharya, S.N.; Choi H.J., Kor.-Aus. Rheol. J., Vol. 19, pp 125 **(2007)**.

[145] Yokohara, T. and Yamaguchi, M., Eur. Polym. J., Vol. 44, pp 677 **(2008)**.

[146] Harada, M.; Ohya, T.; Iida, K.; Hayashi, H.; Hirano, K.; Fukuda, H., J. Appl. Polym. Sci., Vol. 106, pp 1813 **(2007)**.

[147] Ojijo, V.; Sinha Ray, S.; Sadiku, R., ACS Appl. Mater. Interf., Vol. 4, pp 6690 **(2012)**.

[148] Ojijo, V.; Sinha Ray, S.; Sadiku, R., ACS Appl. Mater. Interf., Vol. 5, pp 4266 **(2013)**.

[149] Meng, B.; Deng, J.; Liu, Q.; Wu, Z., Yang, W., Eur. Polym. J., Vol. 48, pp 127 **(2012)**.

[150] Jiang, L.; Wolcott, M.P.; Zhang, J., Biomacromolecules, Vol. 7, pp 199 **(2006)**.

[151] Zhang, N.; Wang, Q.; Ren, J.; L. Wang, J. Mater. Sci., Vol. 44, pp 250 **(2009)**.

[152] Al-Itry, R.; Lamnawar, K.; Maazouz, A., Polym. Degrad. Stab., Vol. 97, pp 1898 **(2012)**.

[153] Lin, S.; Guo, W.; Chen, C.; Ma, J.; Wang, B., Mater. Des., Vol. 36, pp 604 **(2012)**.

[154] Ma, X.; Yu, J.; Wang, N., J. Polym. Sci., Part B: Polym. Phys., Vol. 44, pp 94 **(2006)**.

[155] Gao, J.; Bai, H.; Zhang, Q.; Gao, Y.; Chen, L.; Fu, Q. , eXPRESS Polym. Lett., Vol.6, pp 860 **(2012)**.

[156] Kowalczyk, M.; Piorkowska, E.; Dutkiewicz, S.; Sowinski, P., Eur. Polym. J., Vol. 59, pp 59 **(2014)**.

[157] Zaman, H.U.; Song, J.C.; Park, L.S.; Kang, I.K.; Park, S.Y.; Kwak, G., Park, B.S.; Yoon, K.B., Polym. Bull., Vol. 67, pp 187 **(2011)**

[158] Schreck, K.; Hillmyer, M., J. Biotechnol., Vol. 132, pp 287 **(2007)**.

[159] Zhang, M., and Thomas, N.L., Adv. Polym. Techn., Vol. 30, pp 67 **(2011)**.

[160] Abdelwahab M.A., Flynn A., Chiou B.S., Imam S., Orts W., Chiellini E., Polym. Degrad. Stab., Vol. 97, pp 1822 **(2012)**.

[161] Nerkar, M.; Ramsay, J.A.; Ramsay, B.A.; Vasileiou, A.A.; Kontopoulou, M., Polymer, Vol. 64, pp 51 **(2015)**.

[162] Wang, S.; Ma, P.; Wang, R.; Wang, S.; Zhang, Y.; Zhang, Y., Polym. Degrad. Stab., Vol. 93, pp 1364 **(2008)**.

[163] Ma, P.; Spoelstra, A.B.; Schmit, P.; Lemstra, P.J., Eur. Polym. J., Vol. 49, pp 1523 **(2013)**.

[164] Bhardwaj, R. and Mohanty, A.K., Biomacromolecules**,** Vol**.** 8, pp 2476 **(2007)**.

[165] Zhang, W.; Zhang, Y.; Chen, Y., Iran. Polym. J., Vol. 17, pp 891 **(2008)**.

[166] Nyambo, C.; Misra, M.; Mohanty, A.K., J. Mater. Sci., Vol. 47, pp 5158 **(2012)**.

[167] Robertson, M.L.; Chang, K.; Gramlich, W.M.; Hillmyer, M.A., Macromolecules, Vol. 43, pp 1807 **(2010)**.

[168] Gramlich, W.M.; Robertson, M.L.; Hillmyer, M.A., Macromolecules, Vol. 43, pp 2313 **(2010)**.

[169] Robertson, M.L.; Paxton, J.M.; Hillmyer, M.A., ACS Appl. Mater. Interf., Vol. 3, pp 3402 **(2011)**.

[170] Wang, Y. and Hillmyer, M.A., J. Polym. Sci. Part. A: Polym. Chem., Vol. 39, pp 2755 **(2001)**.

[171] Wang, Y. and Hillmyer, M.A., Polym. Mater. Sci. Eng., Vol. 85, pp 597 **(2001)**.

[172] Anderson, K.S.; Lim, S.H.; Hillmyer, M.A., J. Appl. Polym. Sci., Vol. 89, pp 3757 **(2003)**.

[173] Anderson, K.S. and Hillmyer, M.A., Polymer, Vol. 45, pp 8809 (2004).

[174] Kim, Y.F.; Choi, C.N.; Kim, Y.D.; Lee, K.Y.; Lee, M.S., Fibers and Polymers, Vol. 5, pp 270 **(2004)**.

[175] Su, Z., Li, Q.; Liu, Y.; Xu, H.; Guo, W., Wu, C., J. Macromol. Sci., Part B: Physics, Vol. 48, pp 823 **(2009)**.

[176] Singh, G.; Bhunia, H.; Rajor, A.; Choudhary, V., Polym. Bull., Vol. 66, pp 939 **(2011)**.

[177] Wojciechowska, E.; Fabia, J.; Slusarczyk, C.; Gawlowski, A.; Wysocki, M.; Graczyk, T., Fibres Text. East. Eur., Vol. 13, pp 126 **(2005)**.

[178] Reddy, N.; Nama, D.; Yang, Y.Q., Polym. Degrad. Stab., Vol. 93, pp 233 **(2008)**.

[179] Park, D.H.; Kim, M.S.; Yang, J.H.; Lee, D.J.; Kim, K.N.; Hong, B.K.; Kim, W.N., Macromol. Res., Vol. 19, Vol. 2, pp 105 **(2011)**.

[180] Lee, H.S. and Kim, J.D., Polym. Compos., Vol. 33, pp 1154 **(2012)**.

[181] Ploypetchara, N.; Suppakul, P.; Atong, D.; Pechyen, C., Energy Procedia, Vol. 56, pp 201 **(2014)**.

[182] Li, Y. and Shimizu, H., Macromol. Biosci., Vol. 7, pp 921 **(2007)**.

[183] Feng, F.; Ye, L., J. Appl. Polym. Sci., Vol. 119, pp 2778 **(2011)**.

[184] Han, J.J.; Huang, H.X., J. Appl. Polym. Sci., Vol. 120, pp 3217 **(2011)**.

[185] Zeng, J.B.; Li, Y.D.; He, Y.S.; Li, S.L.; Wang, Y.Z., Ind. Eng. Chem. Res.,Vol. 50, pp 6124 **(2011)**.

[186] Imre, B.; Bedo, D.; Domján, A.; Schön, P.; Vancso, G. J.; Pukánszky, B., Eur. Polym. J., Vol. 49, pp 3104 **(2013)**.

[187] Jin, H.J.; Chin, I.J.; Kim, M.N.; Kim, S.H.; Yoon, J.S., Eur. Polym. J., Vol. 36, pp 165 **(2000)**.

[188] Kowalczyk, M. and Piorkowska, E., J. Appl. Polym. Sci., Vol. 124, pp 4579 **(2012)**.

[189] Zhang, W.; Chen, L.; Zhang, Y., Polymer, Vol. 50, pp 1311 **(2009)**.

[190] Stoclet, G.; Seguela , R.; Lefebvre, J.M., Polymer, Vol. 52; pp 1417 **(2011)**.

[191] Juntuek,P.; Ruksakulpiwat, C.; Chumsamrong, P., Ruksakulpiwat, Y., J. Appl. Polym. Sci., Vol. 125, pp 745 **(2012)**.

[192] Jaratrotkamjorn, R.; Khaokong, C.; Tanrattanakul, V., J. Appl. Polym. Sci., Vol. 124, pp 5027 **(2012)**.

[193] Zhang, C.; Wang, W.; Huang, Y.; Pan, Y.; Jiang, L.; Dan, Y.; Luo, Y.; Peng, Z., Mater. Des., Vol. 45, pp 198 **(2013)**.

[194] Pongtanayut, K.; Thongpin, C.; Santawitee, O., Energy Procedia, Vol. 34, pp 888 **(2013)**.

[195] Chumeka, W.; Tanrattanakul, V.; Pilard , J.F.; Pasetto, P., J Polym Environ, Vol. 21, pp 450 **(2013)**.

[196] Li, Y. and Shimizu, H., Eur. Polym. J., Vol. 45, pp 738 **(2009)**.

[197] Sun, S.; Zhang, M.; Zhang, H.; Zhang, X., J. Appl. Polym. Sci., Vol. 122, pp 2992 **(2011)**.

[198] Jo, M.Y., Ryu, Y.J.; Ko, J.H.; Yoon, J.S. J. Appl. Polym. Sci., Vol. 125, E231 **(2012)**.

[199] Li, Y.; Liu, L.; Shi, Y.; Xiang, F.; Huang, T.; Wang, Y.; Zhou, Z., J. Appl. Polym. Sci., Vol. 121, pp 2688 **(2011)**.

[200] Ma, P.; Hristova-Bogaerds, D.G.; Goossens, J.G.P.; Spoelstra, A.B.; Zhang, Y.; Lemstra, P.J., Eur. Polym. J., Vol. 48, pp 146 **(2012)**.

[201] Said, H.M., J. Rad. Res. Appl. Sci., Vol. 6, pp 11 **(2013)**.

[202] Hashima, K.; Nishitsuji, S.; Inoue, T., Polymer, Vol. 51, pp 3934 **(2010)**.

[203] Qi, R.; Luo, M.; Huang, M., J. Appl. Polym. Sci., Vol. 120, pp 2699 **(2011)**.

[204] Nijenhuis, A.J.; Colstee, E.; Grijpma, D.W.; Pennings, A.J., Polymer, Vol. 37, pp 5849 **(1996)**.

[205] Ho, C.H.; Wang, C.H.; Lin, C.I.; Lee, Y.D., Polymer, Vol. 49, pp 3902 **(2008)**.

[206] Su, Z.; Li, Q.; Liu, Y.; Hu, G.H.; Wu, C., Eur. Polym. J., Vol. 45, pp 2428 **(2009)**.

[207] Feng, Y.; Hu,Y., Yin, J., Zhao, G.; Jiang, W., Polym. Eng. Sci., Vol. 53, pp 389 **(2013)**.

[208] Li, D.; Shentu, B.; Weng, Z., J. Macromol. Sci., Part B: Physics, Vol. 50, pp 2050 **(2011)**.

[209] Oyama, H. T., Polymer, Vol. 50, pp 747 **(2009)**.

[210] Yeh, J.; Tsou, C.; Li, Y.; Xiao, H.; Wu, C.; Chai, W.; Lai, Y.; Wang, C. J. Polym. Res., Vol. 19, pp 9766 **(2012)**.

[211] Jiang, J.; Su, L.; Zhang, K.; Wu, G., J. Appl. Polym. Sci., Vol. 128, pp 3993 **(2013)**.

[212] Liu, H.; Chen, F.; Liu, B.; Estep, G.; Zhang, J. Macromolecules, Vol. 43, pp 6058 **(2010)**.

[213] Liu, H.; Song, W.; Chen, F.; Guo, L.; Zhang, J. Macromolecules, Vol. 44, pp 1513 **(2011)**.

[214] Song, W.; Liu, H.; Chen, F.; Zhang, J., Polymer, Vol. 53, pp 2476 **(2012)**.

[215] Ishida, S.; Nagasaki, R.; Chino, K.; Dong, T.; Inoue, Y., J. Appl. Polym. Sci., Vol. 113, pp 558 **(2009)**.

[216] Petchwattana, N.; Covavisaruch, S.; Euapanthasate, N., Mater. Sci. Eng., Vol. A 532, pp 64 **(2012)**.

[217] Zhao, Q.; Ding, Y.; Yang, B.; Ning, N.; Qiang, Fu, Polym.Test., Vol. 32, pp 299 **(2013)**.

[218] Taib, R.M.; Ghaleb, Z.A.; Mohd Ishak, Z.A., J. Appl. Polym. Sci., Vol. 123, pp 2715 **(2012)**.

[219] Murariu, M.; Ferreira, A.D.S.; Duquesne, E.; Bonnaud, L.; Dubois, P. Macromol. Symp., Vol. 272, pp 1 **(2008)**.

[220] Zhu, S.; Rasal, R.; Hirt, D. Proceedings of Annual Technical Conference of the Society of Plastics Engineers (ANTEC 2009), Chicago, Illinois, June 22-24, pp 1616 **(2009)**.

[221] Afrifah, K.A. and Matuana, L.M., Macromol. Mater. Eng., Vol. 295, pp 802 **(2010)**.

[222] Byrne, F.; Ward, P.G.; Kennedy, J.; Imaz, N.; Hughes, D.; Dowling, D.P., J. Polym. Environ., Vol. 17, pp 28 **(2009)**.

[223] Zhang, H.; Liu, N.; Ran, X.; Han, C.; Han, L.; Zhuang, Y.; Dong, L., J. Appl. Polym. Sci., Vol. 125, E550 **(2012)**.

[224] Choochottiros, C.; and Chin, I.J., Eur. Polym. J., Vol. 49, pp 957 **(2013)**.

[225] Lee, J.B.; Lee, Y.K.; Choi, G.D.; Na, S.W., Park, T.S.; Kim, W.N., Polym. Degrad. Stab., Vol. 96, pp 553 **(2011)**.

[226] Wang, Y.; Chiao, S.M.; T.F. Hung, Yang, S.Y., J. Appl. Polym. Sci., Vol. 125, pp E402 **(2012)**.

[227] Chen, B.K.; Shih, C.C.; Chen, A.F.; Composites: Part A, Vol. 43, pp 2289 **(2012)**.

[228] Li, D.; Shentu, B.; Weng, Z., J. Macromol. Sci. , Part B: Phys., Vol. 51, pp 1766 **(2012)**.

[229] Bitinis, N.; Verdejo, R.; Bras, J.; Fortunati, E.; Kenny, J.M.; Torre, L.; López-Manchado, M.A., Carbohyd. Polym.: Part I: Vol 96, pp 611 **(2013)**.

[230] Bitinis, N.; Fortunati, E.; Verdejo, R.; Bras, J.; Kenny, J.M.; Torre, L.; López Manchado, M.A., Carbohyd. Polym.: Part II: Vol 96, pp 621 **(2013)**.

[231] Fortunati, E.; Puglia, D.; Kenny, J.M.; Minhaz-Ul Haque, Md.; Pracella, M., Polym. Degrad. Stab., Vol. 98, pp 2742 **(2013)**.

[232] Shi, Y.; Li, Y.; Wu, J.; Huang, T.; Chen, C.; Peng, Y.; Wang, Y., J. Polym. Sci.: Part B: Polym. Phys., Vol. 49, pp 267 **(2011)**.

[233] Raja, M.; Ryu, S.H.; Shanmugharaj, A.M., Eur. Polym. J., Vol. 49, pp 3492 **(2013)**.

[234] Suksut, B. and Deeprasertkul, C., J. Polym. Environ., Vol. 19, pp 288 **(2011)**.

[235] Liu, T.; Yu, F.; Yu, X.; Zhao, X.; Lu, A.; Wang, J., J. Appl. Polym. Sci., Vol. 125, 1292 **(2012)**.

[236] Chen, G.X.; Kim, H.S.; Kim, E.S.; Yoon, J.S., Polymer, Vol. 46, pp 11829 **(2005)**.

[237] Chen, G.X. and Yoon, J.S., Polym. Degrad. Stab., Vol. 88, pp 206 **(2005)**.

[238] Chen, G.X.; Yoon, J.S., J. Polym. Sci., Part B: Polym. Phys., Vol 43, pp 478 **(2005)**.

[239] Ojijo, V.; Cele, H.; Ray, S.S., Macromol. Mat. Eng., Vol. 296, pp 865 **(2011)**.

[240] Chow, W.S.; Lok, S.K., J. Thermo. Comp. Mater., Vol. 21, pp 265 **(2008)**.

[241] Chow, W.S.; Lok, S.K., J. Therm. Calorim., Vol. 95, pp 627 **(2009)**.

[242] Hasook, A.; Tanoue, S.; Iemoto; Y., Unryu, T., Polym. Eng. Sci., Vol. 46, pp 1001 **(2006)**.

[243] Yu, Z.; Yin, J.; Yan, S.; Xie, Y.; Ma, J.; Chen, X., Polymer, Vol. 48, pp 6439 **(2007)**.

[244] Shafiei Sabet, S. and Katbab, A.A., J. Appl. Polym. Sci., Vol. 111, 1954 **(2009)**.

[245] Jiang, L.; Liu, B.; Zhang, J., Ind. Eng. Chem. Res., Vol. 48, pp 7594 **(2009)**.

[246] Kumar, M.; Mohanty, S.; Nayak, S.K.; Rahail Parvaiz, M., Biores. Techn., Vol. 101, pp 8406 **(2010)**.

[247] Leu, Y.Y.; Mohd Ishak, Z.A.; Chow, W.S., J. Appl. Polym. Sci., Vol. 124, pp 1200 **(2012)**.

[248] Bitinis, N.; Verdejo, R.; Maya, E.M.; Espuche, E.; Cassagnau, P.; Lopez-Manchado, M.A., Compos. Sci. Tech., Vol. 72, pp 305 **(2012)**.

[249] Bitinis, N.; Fortunati, E.; Verdejo, R.; Armentano, I.; Torre, L.; Kenny, J.M.; López-Manchado, M.A., Appl. Clay Sci., Vol. 93-94, pp 78 **(2014)**.

[250] Auliawan, A. and Woo, E.M., Polym. Compos., Vol. 32, pp 1916 **(2011)**.

[251] Balakrishnan, H.; Hassan, A.; Wahit, M.U.; Yussuf, A.A.; Abdul Razak, S.B., Materialsand Design, Vol. 31, pp 3289 **(2010)**.

[252] Nunez, K.; Rosales, C.; Perera, R.; Villarreal, N.; Pastor, J.M.; Polym. Eng. Sci., Vol. 52, pp 988 **(2012)**.

[253] Li, T.; Turng, L.S.; Gong, S.; Erlacher, K., Polym. Eng. Sci., Vol. 46, pp 1419 **(2006)**.

[254] Balakrishnan, H.; Masoumi, I.; Yussuf, A. A.; Imran, M.; Hassan, A.; Wahit, M.U., Polym-Plast. Technol., Vol. 51, pp 19 **(2012)**.

[255] Notta-Cuvier, D.; Odent, J.; Delille, R.; Murariu, M.; Lauro, F.; Raquez, J.M.; Bennani, B.; Dubois, P., Polymer Testing, Vol. 36, pp 1 **(2014)**

[256] Mélo, T.J.A.; Araújo, E.M.; Brito, G.F.; Agrawal, P., J. Alloys Comp., Vol. 615, S389 **(2014)**.

Chapter IV

MATERIALS AND EXPERIMENTAL PROCEDURES

Chapter IV - Materials and Experimental Procedures

The objective of this chapter is to present the raw materials used in this research work and the prepared formulations. In addition, equipments and conditions used to prepare the mixtures and the techniques and procedures adopted for their characterization are also explained in details.

Recall that for both research studies conducted in the present work, the raw materials, the characterization techniques and the injection molding processes were the same but only the melt compounding procedures of the mixtures were different. Consequently, and for convenience matter, it was judged that it would be preferable to write only one experimental procedure for both parts.

IV-1 Materials

IV-1-1 Polymer Matrix

A Commercial grade of PLA (PLI 005) was obtained from NaturePlast (Caen, France) and was used as the matrix for the binary blends and the ternary nanocomposites. PLI 005 is a yellowish-transparent thermoplastic resin produced from genetically modified organisms-free corn (GMO-free corn) that is a renewable vegetable resource.**[1]** This resin is an injection grade that could be easily processed on conventional injection molding equipments. Drying is necessary before processing because moisture can bring about hydrolytic degradation to PLA resins. According to the manufacturer, moisture content should be less than 0.025% (250 ppm) and drying conditions are 80°CC in vacuum conditions. Furthermore, PLA resins are sensitive to thermal degradation that can cause a loss of mechanical properties, to avoid this drawback the manufacturer recommends to process PLI 005 at temperatures less than 240°C and to thoroughly purge the extruder before and after extruding PLI 005.**[1-4]** Typical properties as given by the manufacturer are presented in **Table IV.1.**

Table IV.1 Properties of PLA (PLI 005) Matrix.**[1]**

Physical Properties	**Value**	**ISO**
Density **(g/cm^3)**	1.25 (±0.05)	1183
Melt Flow Index (MFI), **g/10 min** (190°C, 2.16g)	10-30	1133
Optical Properties	Transparent	---
Shrinkage **(%)**	0.15	---
Mechanical Properties	**value**	**ISO**
Tensile yield strength, **MPa**	55	3527
Tensile yield elongation, **%**	2	527
Tensile strength at break, **MPa**	47	527
Tensile elongation at break, **%**	3	527
Tensile Modulus**, MPa**	3300	527
Charpy Impact (unnotched) 4J, **KJ/m^2**	21	179
Thermal Properties	**value**	**ISO**
HDT A (1.8 MPa) **(°C)**	50	75-2
Melt temperature **(°C)**	145-155	---
Degradation temperature **(°C)**	240-250	---

IV-1-2 Impact Modifier

The Lotader®AX8900 rubber, an extrusion and blow molding grade in pellet form, was purchased from Arkema Inc. (Puteaux, France) and was used as a reactive impact modifier for PLA. This is a random terpolymer of ethylene-methyl acrylate and glycidyl methacrylate (E-MA-GMA), and according to the datasheet of the manufacturer of the material, methyl acrylate (MA) and glycidyl methacrylate (GMA) contents are 24 and 8 wt% respectively.

On one hand the presence of the ethylene groups in the structure of the impact modifier brings flexibility, and that of the acrylic ester provides softness, polarity and

thermal stability. On the other hand the dual functionality (acrylic and epoxy) of the GMA groups endows the rubber with high reactivity towards hydroxyl (OH), carboxyl (COOH), amine (NH_2) and anhydride groups containing materials.**[5,6]** Both acrylic and epoxy groups provide enhanced impact resistance and strength, and improved acid and heat resistance.**[7]** The general specifications of the impact modifier provided by the manufacturer are given in **Table IV.2** and its chemical structure is shown in **Figure IV.1**.

The epoxy groups react with terminal carboxyl (COOH) and hydroxyl (OH) groups of the PLA and also with the OH groups present on the organophilic clay, while polar interactions are also possible between the ester groups of the E-MA-GMA and those of the PLA.**[8]** In this sense the E-MA-GMA acts as an impact modifier for PLA and as a compatiblizer between the PLA and the organoclay.**[9]**

Table IV.2 General Specifications of Lotader®AX8900 (E-MA-GMA).**[5]**

Characteristics	Unit	value	Test method
Methyl Acrylate Content	wt%	24	FTIR
Glycidyl Methacrylate Content	wt%	8	FTIR
Density (23 °C)	g/cm^3	0.94	ISO 1183
Melting Point	°C	65	DSC
Vicat Softening Point (1 Kg)	°C	< 40	ASTM D1525 / ISO 306
Young's Modulus [1]	MPa	8	ASTM D 638 Type IV
Elongation at Break [1]	%	1100	ASTM D 638 Type IV
Tensile Strength at Break[1]	MPa	4	ASTM D 638 Type IV
Flexural Modulus	MPa	< 30	ASTM D 790 / ISO 178
Hardness Shore A [1](1 second)	---	64	ASTM D 2240
Hardness Shore D [1](1 second)	---	18	ASTM D 2240

[1] On compression molded samples.

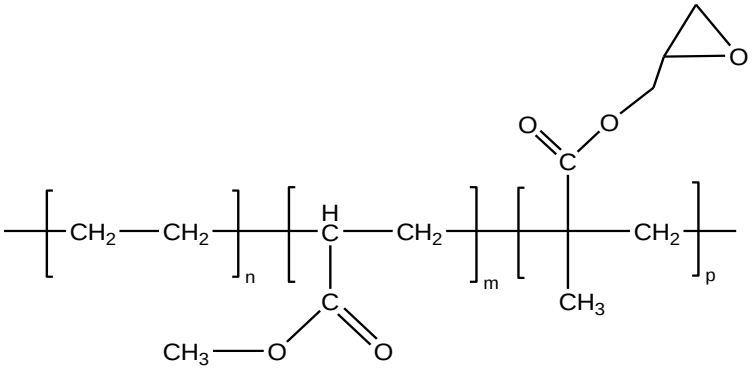

Figure IV.1 Chemical Structure of the Impact Modifier (Lotader®AX8900) (E-MA-GMA).**[6,7]**

IV-1-3 Reinforcement (Organoclay)

The layered silicate used in this study as a nanoscale reinforcing agent was Cloisite®30B obtained from Southern Clay Products (Gonzales, Texas, USA). Cloisite®30B (referred hereafter as OMMT) is an off-white fine powder of a natural montmorillonite modified with a quaternary ammonium salt. The cation of the organic modifier of the organoclay is methyl, tallow, bis-2-hydroxyethyl, quaternary ammonium (MT2EtOH) used at a concentration of 90 meq/100g clay, and the anion is chloride. The tallow structure depicted in **Figure IV.2** is made up of long alkyl chain constituting primarily of almost 65% of carbon chains of 18 carbons and the remaining components are made up of chains of 16 carbons (~30%) and chains of 14 carbons (~5%).**[10]** Some physical characteristics of Cloisite®30B as given by the supplier are summarized in **Table IV.3.**

The choice of the type of organoclay and its weight ratio in the nanocomposites has been made according to our literature survey. Cloisite®30B has been chosen according to previous research studies which have demonstrated that this organoclay disperses better in PLA than other organoclays**.[3,4,11-13]** All along the present study, the amount of clay was kept constant at 2 wt% of the total weight of the ternary nanocomposites formulations, which was also made according to different research works which have reported that 2 wt% is an optimum amount.**[7,9]**

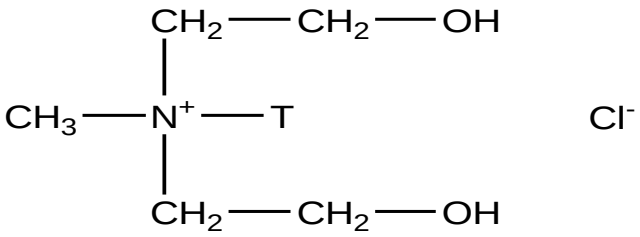

T: tallow (~65% C18; ~30% C16; ~5% C14)

Figure IV.2 Chemical Structure of the Organic Modifier of the Cloisite®30B.**[10]**

Table IV.3 Some Characteristics of Cloisite®30B.**[10]**

Properties	**Values**	**Units**
Modifier Concentration	90	meq/100g clay
Moisture Content	< 2	%
Weight Loss on Ignition	30	%
Color	off-white	---
d-spacing (x-ray)	18.5	Å
Density		
Loose Bulk Density	14.25	lbs/ft^3
Packed Bulk Density	22.71	lbs/ft^3
Specific Gravity	1.98	lbs/ft^3
Typical Dry Particle Sizes		
10%	< 2	µ, volume
50%	< 6	µ, volume
90%	< 13	µ, volume

IV-2 Blends and Nonocomposites Preparation Procedure

To accomplish the experimental part, four steps were necessary. These include drying of the raw materials, production of the mixtures through extrusion melt compounding according to specified formulations and process conditions, grinding step, sample preparation by injection molding and finally testing and characterization experiments. Compositions of binary blends and ternary nanocomposites are given in **Table IV.4**, and flowchart of the experimental procedure is given in **Figure IV.3**.

Table IV.4 Compositions of Studied Formulations.

		Materials Concentrations (wt%)		
N°	**Composition**	**PLA**	**E-MA-GMA**	**Organoclay**
1	PLA	100	----	---
2	E-MA-GMA	----	100	---
3	PLA + OMMT	98	---	2
	Binary Blends (PLA/E-MA-GMA)			
4	PLA + E-MA-GMA	95	5	---
5	PLA + E-MA-GMA	90	10	---
6	PLA + E-MA-GMA	85	15	---
7	PLA + E-MA-GMA	80	20	---
8	PLA + E-MA-GMA	75	25	---
9	PLA + E-MA-GMA	70	30	---
	Ternary Nanocomposites (PLA/E-MA-GMA/Organocaly)			
10	PLA + E-MA-GMA	93	5	2
11	PLA + E-MA-GMA	88	10	2
12	PLA + E-MA-GMA	83	15	2
13	PLA + E-MA-GMA	78	20	2
14	PLA + E-MA-GMA	73	25	2
15	PLA + E-MA-GMA	68	30	2

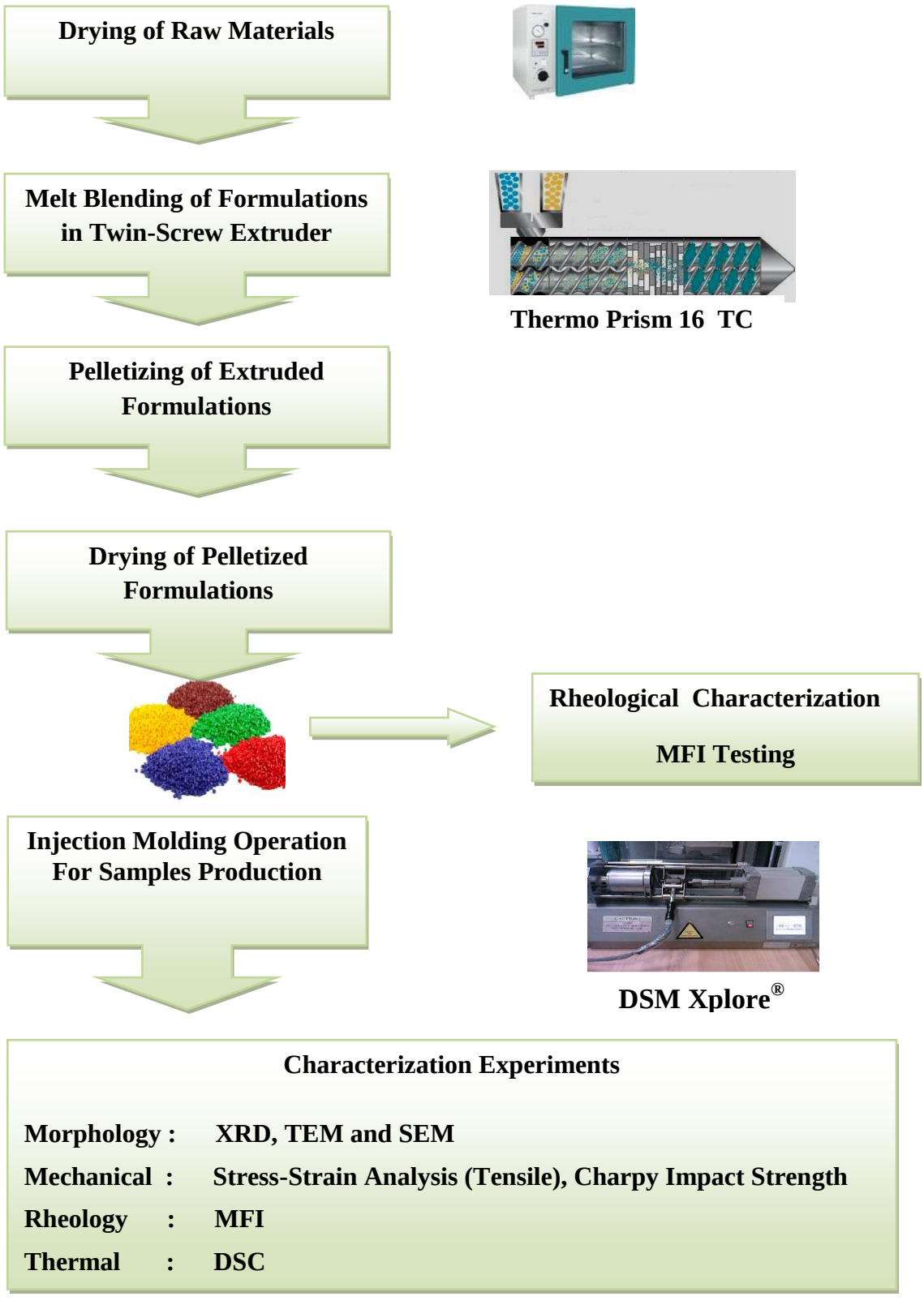

Figure IV.3 Flowchart of the Experimental Work.

IV-2-1 Melt Compounding for the Study of PLA Toughening

Because all the ingredients used in this study i.e. the PLA matrix, the reinforcing organoclay (OMMT) and the impact modifier (E-MA-GMA) are highly hydrophilic, a drying step of these components was necessary before melt compounding. PLA and the organoclay were dried overnight at 80°C in a vacuum oven and the rubber was dried overnight at 45°C in a conventional oven. Drying was necessary to get rid of trapped moisture to avoid PLA degradation by hydrolysis and also to prevent presence of air bubbles in the specimens.

In the binary and ternary nanocomposites, the weight percent of the rubber was varied in the range of 5-30 wt%, and the amount of clay in the nanocomposites was kept constant at 2 wt%. Formulations of the different mixtures were prepared by melt compounding using a Thermo Prism TSE 16 TC, co-rotating, fully intermeshing twin-screw extruder (screw diameter (D)=16 mm and screw length (L)=384 mm (L/D=24)). Throughout the experiments, the extrusion speed was adjusted constant at 250 rpm and the total feeding rate of the extruder was set to 25 g/min according to previous works.**[7,9]** Because PLA was an injection grade resin that was very difficult to handle at the extrusion speed of 250 rpm, a preliminary optimization of extrusion temperature was performed to achieve an acceptable high melt strength that facilitates the extrusion process. The optimum processing zone temperatures of the extruder barrel were set to 150-170-170-170-170°C from the hopper to the die. The dry mixtures were tumbled in a plastic bag and fed directly into the hopper equipped with a mixer. Before each extrusion, it was necessary to calibrate the total feeding rate to 25 g/min for each formulation owing to the differences between the densities of the mixtures.

The extruded rods of the formulations were collected on aluminum plates and were cooled at ambient temperature to avoid hydrolysis of PLA by water cooling. For comparison, PLA was extruded at the same conditions as for the blends and ternary nanocomposites to serve as reference. Thereafter, a pelletizer was used to grind all the

extrudates and the obtained granules were stored in sealed plastic bags and kept in desiccators to avoid moisture uptake.

IV-2-2 Melt Compounding for the Study of the Effects of Mixing Protocols on PLA Toughening.

In this part, the formulations of the nanocomposites were produced by melt intercalation method using the same twin screw extruder under the same processing conditions as in the previously described procedure. Also, the drying conditions of the different materials were kept the same as described previously. To prepare the nanocomposites, the weight percent of the rubber was varied in the range of 5-20 wt%, and the amount of clay was kept constant at 2 wt%.

Four addition orders (PC-I, PI-C, CI-P and ALL-S) were considered to investigate the effects of addition method of the components on the final structure and properties of the nanocomposites. In the first three modes: P, C and I stand for PLA, clay and the impact modifier respectively. For instance, in the PC-I sequence the PLA and the clay were compounded in the first extrusion process, and the rubber modifier was added to the obtained mixture in the subsequent second run. In the ALL-S, all of the ingredients of the nanocomposite were fed simultaneously into the hopper. Because in the first three modes of addition at least two of the ingredients experienced extrusion twice, the All-S mixture was also extruded twice so that its components experience more or less the same thermal and mechanical history as for the other mixtures. Neat PLA was also extruded twice under the same conditions to serve as a control material. Hereafter, the materials are referred to according to their sample codes.

IV-2-3 Injection Molding Process

Specimens for different characterization tests were prepared using mini-injection molding equipment (DSM Xplore®, 10 cm^3 shot volume). The injection process consists of 5 steps for each one the pressure and injection time can be set. For good quality specimens, the injection parameters i.e. melt and mold temperatures, pressure and time of the injection molding process have all been optimized. The melt and mold temperatures

were set at 170°C and 60°C, respectively and the other injection parameters are listed in **Table IV.5**. Note that the injection parameters were kept constant throughout all experiments and no mold release agent was used because it may affect the results of x-ray experiments. Tap water was used as a cooling liquid for the mold to keep its temperature constant.

Prior to injection molding, all materials were dried overnight in a vacuum oven at 80°C. In a typical injection sequence, the injection cylinder was filled in 10 seconds with an appropriate amount of material (~7g), then the material was allowed to melt for 3 minutes, finally the injection process was accomplished. Each injection cycle, including de-molding time, lasted nearly 5 minutes and produced one dog-bone specimen for tensile properties determinations and one rectangular bar for impact strength measurements.

After production, the specimens were stored in hermetic sealed plastic bags and stored in a desiccator. The time between the storage and testing has been scrupulously respected to avoid the effects of crystallization fluctuations on the obtained values of the physical or mechanical properties.

Table IV.5 Injection Molding Parameters.

	Pressure (bar)	**Time (sec)**
Step 1	10	1
Step 2	10	5
Step 3	12	15
Step 4	12	15
Step 5	2	60

IV-3 Testing and Characterization Techniques

To investigate the effects of the rubber, the organoclay and their concentrations and addition sequences on PLA properties, the prepared formulations were characterized using x-ray diffraction (XRD), transmission electron microscopy (TEM) and scanning electron microscopy (SEM) for morphological characterization. Mechanical performance

of the produced mixtures was evaluated using tensile measurements (Young's modulus, tensile strength and elongation at break) and Charpy impact strength determinations. Thermal behavior (melting and crystallization) of the compounds was studied using differential scanning calorimetry (DSC). Finally, flow behavior of the materials was investigated using melt flow index (MFI) measurements.

IV-3-1 Morphological Characterization

In this study complementary XRD and TEM analyses were used to investigate the degree of organoclay dispersion in the nanocomposites, and SEM was used to investigate dispersion and coalescence of the rubber phase in the blends and the nanocomposites.

IV-3-1-1 X-rays Diffraction Analysis (XRD)

Experimental Technique

Due to its easiness and availability, x-ray diffraction is a versatile non-destructive technique that has been commonly used in determining the structure of materials. In the field of nanocomposites it is widely used to evaluate the extent of clay dispersion as it allows measuring the interlayer spacing between the basal layers of an ordered layered silicates i.e. intercalated structures.**[2-4,7,9,11-13]**

As shown in **Figure IV.4**, when an incident x-ray beam strikes at an angle θ an orderly arrangement of successive plans of atoms of a material or of clay layers separated by a distance "d", the wave "2" will travel farther than wave "1". If the extra distance traveled by wave "2" (2 d sinθ) is equal a whole number of wavelengths of the radiation (λ), the x-rays would be in phase upon leaving the crystal, thus constructive interference takes place and diffraction occurs creating a maxima/peak on the diffractogram.**[14,15]** This essential condition for diffraction to occur can be expressed mathematically by **equation 3.1**, known as Bragg's law of diffraction. A schematic representation of this theory is illustrated in **Figure IV.4**.

$$\mathbf{n\,\lambda = 2\,d\,\sin\theta} \qquad \mathbf{(3.1)}$$

where **d** is the spacing between successive identical planes of atoms in a crystal or planes in the case of layered materials (referred to as the d-spacing), **θ (°)** and **λ (**Å) are the incidence angle and the wavelength of the x-rays beam, and **n** is an integer known as the order of reflection.**[14,15]**

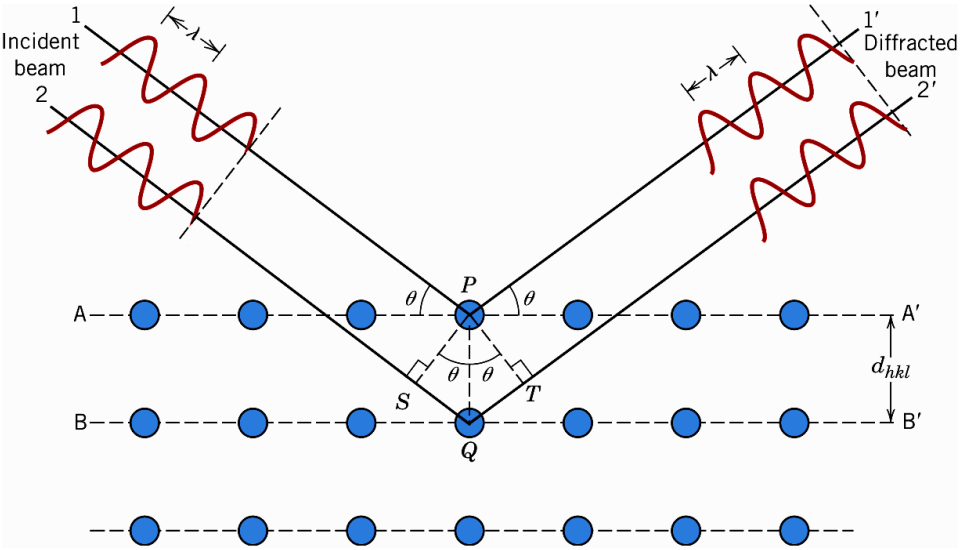

Figure IV.4 Diffraction of X-ray by Plans of Atoms (A-A' and B-B').**[14]**

For nanocomposites structures analysis, intercalated (ordered) and/or exfoliated (disordered) structures of nanocomposites can be identified by observing the position, shape, and intensity of the basal reflections from the dispersed silicate sheets. In the case of phase separated composites, the polymer is unable to penetrate into the clay galleries leading thus to no change in the shape, position and intensity of the original clay peak that is indicative of no change in the clay basal spacing. Intercalation of polymer chains between silicate sheets (increase of interlayer spacing) is indicated by the shift of the diffraction peak of the clay towards lower angles in the XRD plots, while disappearance of x-ray diffraction peaks in the diffractogram reflects an exfoliated structure due to extensive interlayer spacing as a consequence of disordered silicate layers and loss of structural registry.**[2-4,7,9,11-13]**

Method

The nanocomposite samples for XRD tests were cut from dog-bone tensile bars. X-ray diffraction (XRD) measurements were performed at room temperature using a Rigaku D/MAX 2200/PC x-ray diffractometer operating in reflection mode. Diffractograms of the organoclay pristine powder and the molded nanocomposites were acquired with a step size of 0.02° from 2θ=1° to 10° and 1°/min scan rate using a monochromatic CuKα x-ray radiation (λ=1.5418 Å) generated at 40 kV and 40 mA. The basal spacing (d_{001}-reflection) of the OMMT nanosheets in the samples was derived from the peak position in the XRD diffractograms according to Bragg's law ($n\lambda=2d\sin\theta$).

IV-3-1-2 Transmission Electron Microscopy (TEM)

Experimental Technique

XRD results may be misinterpreted giving thus incorrect conclusions about nanocomposite structure. For example absence of registry in XRD patterns of a nanocomposite does not always confirm an exfoliated structure, therefore TEM is widely used as a complementary tool to ascertain and validate the results obtained by XRD investigation.**[2,4,7,9,12]**

TEM is a valuable imaging technique widely used to probe the internal structure of nanocomposites at the atomic level. This analytical method provides a qualitative evaluation of filler spatial distribution and dispersion level through a direct visual observation of the samples. Basically this technique is based on transmission of electrons through an ultrathin specimen (less than 100 nm). When a beam of electrons strikes a specimen, the unscattered electrons are transmitted across the specimen and hit a fluorescent screen, which gives rise to a shadow image of the specimen with its parts displayed in various darkness shades according to their electron density differences, and the image is then detected by a charge coupled device (CCD) camera and digitalized.**[16-18]**

Method

Ultrathin sections (70-80 nm) of the nanocomposites were produced from freeze fractured impact test bars. Sections were trimmed perpendicular to the molding direction at cryogenic temperature using Leica® EM UC6 ultra-microtome (Leica Microsystems, Wetzlar, Germany) equipped with a diamond knife. Sections were received in a water bath and then transferred to coper grids and finally dried and stored in dessicator until examination time.

TEM micrographs were acquired using a FEI Tecnai® Spirit G^2 Biotwin transmission electron microscope operating under an accelerating voltage of 80 KV in bright field mode (FEI Company, OR, USA). The TEM images were obtained at different positions from different sections at various magnifications to ensure that the images were representative for each sample. Images were captured using a CCD camera, and then they were recorded on photographic plates and digitalized.

IV-3-1-3 Scanning Electron Microscopy (SEM)

Experimental Technique

Scanning electron microscopy is a microscopic technique that can give pictorial topographical view and morphological examination of the surface of materials at magnification that extends between that of optical microscopy and that of TEM (10 to 100 000 times).**[17]** High magnification capability, high imaging resolution, and ease of sample preparation make SEM a powerful instrument. In SEM, the conductive surface of a sample is scanned with a beam of incident electrons. The backscattered or secondary electrons emitted from the surface of the sample are collected by a detector and form an image on the screen representing the features of the sample surface that can be then photographed. Characterization of nonconductive materials requires surface coating using a metal such as gold, silver or platinum to avoid buildup of trapped charge that results in loss of resolution,**[17,18]** and for the investigation of multiphase systems, staining technique using OsO_4 or RuO_4 can be applied to increase contrast between phases.**[18]**

Method

A Jeol JSM-6400 (Jeol, Tokyo, Japan) low-voltage scanning electron microscope (SEM) was used to examine the morphology of the prepared materials. Cryofractured samples were obtained from injected molded impact test bars immersed and kept in liquid nitrogen for 5 minutes and subsequently broken. The etched surfaces, from which the rubber was selectively removed at 45°C using liquid n-Heptane until the surfaces of the specimens whitened, were prepared with the aid of a sonicator. The surfaces were coated with thin layer of gold film to avoid electrostatic charging during observation. SEM photographs were taken at X250 and X3000 magnifications. The impact modifier droplet size in all of the formulations was evaluated by the image processing software "ImageJ".**[19]** Typically, a number of particles (approximately 250-300) from three to four independent SEM micrographs were analyzed by the program to estimate first the average area (A_i) of each individual particle (i). This obtained cross-sectional area (A_i) was then converted into equivalent diameter (d_i) of a sphere using **equation 3.2**, and the number-average particle diameter (D_n) was computed by using **equation 3.3**.

$$d_i = 2\sqrt{(A_i/\pi)} \qquad \textbf{(3.2)}$$

$$D_n = \frac{\sum n_i d_i}{\sum n_i} \qquad \textbf{(3.3)}$$

where n_i is the number of the dispersed domains having the apparent particle diameter d_i counted from the SEM images. Particles whose sizes were too small to be properly measured at the magnification chosen were neglected.

IV-3-2 Mechanical Characterization

IV-3-2-1 Tensile Properties

Experimental Technique

Among the myriad number of mechanical properties that characterizes plastics, tensile properties are the most frequently evaluated, reported and considered

characteristics in selecting or designing products made up of plastics.**[15]** Tensile test is a measurement of the ability of a material to withstand forces that tend to pull it apart and to determine to what extent the material stretches before breaking. This test involves elongation of a dumbbell shaped sample properly aligned and firmly gripped between two mechanical jaws that pull the sample at a constant deformation rate with gradual increase of extension load that is measured simultaneously as a function of time until sample failure. The instantaneous force F (N) versus elongation ε (mm) (Load-displacement) curve obtained from the uniaxial tensile testing machine is plotted and then converted to stress-strain curve.**[15,20-22]**

Method

The tensile properties were investigated at room temperature using injected molded dog-bone specimens previously dried overnight (45°C). The shape of a typical tensile specimen and its dimensions are illustrated in **Figure IV.5** and summarized in **Table IV.6** respectively.

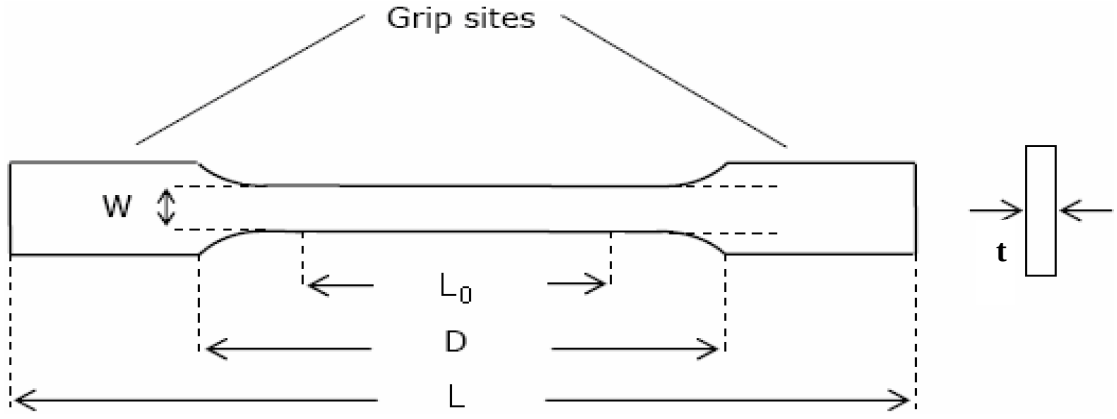

Figure IV.5 Schematic of a Tensile Test Specimen**.**

Table IV.6 Dimensions of Tensile Test Specimen.

Symbol	Abbreviation	Value (mm)
W	Width of narrow section	4.0
D	Distance between grips	50.0
L	Total length	75.0
L_0	Gauge length	30.0
t	Thickness	02.0

Tensile tests were performed according to ISO 527 by means of a Shimadzu Autograph AG-IS 100 KN universal testing machine equipped with a computerized data acquisition system (Shimadzu Corporation, Tokyo, Japan). The crosshead speed was set constant at 3 mm/min calculated based on gauge length of the sample of 3 mm and a strain rate of 0.1 min^{-1} as specified by the standard.**[23]** The obtained stress-strain diagrams from the test were analyzed by using Microsoft Excel® software, and tensile properties namely, Young's modulus (E), tensile strength (σ) and percent elongation at break (ε_b), were calculated using standard procedures and formulae.

a) Tensile strength

$$\sigma = \frac{F}{A_0} \qquad \textbf{(3.4)}$$

where σ is the engineering stress (MPa), $\boldsymbol{F}$ is the instantaneous applied force (N) on the sample and $\boldsymbol{A_0}$ (m^2) is the original cross-section area of the sample.

c) Elongation at break

$$\varepsilon = \frac{L - L_0}{L_0} = \frac{\Delta L}{L_0} \qquad \textbf{(3.5)}$$

where $\boldsymbol{\varepsilon}$ is the engineering strain , $\boldsymbol{L}$ (m) and $\boldsymbol{L_0}$ (m) are the instantaneous length and the initial gauge length of the sample respectively, and $\Delta\boldsymbol{L}$ (m) is the change in sample length.

b) Modulus

$$E = \frac{\sigma}{\varepsilon} \qquad \textbf{(3.6)}$$

where E (MPa) is the Young's modulus measured as the slope of the stress-strain curve within the proportional range.

At least five specimens were tested for each set of samples, and the values were averaged and reported together with their respective standard deviations (SD). Deviations

of the individual values of each property (E, σ, and ε) from the average value was estimated using standard deviation calculation as given by **equation 3.7**.

$$SD = \sqrt{\frac{\sum X^2 - n(\bar{X})^2}{n-1}} \qquad \textbf{(3.7)}$$

where **SD** is the estimated standard deviation, **X** is the value of a single observation, **n** is the number of observations, and $\bar{X}$ is the arithmetic mean of the set of observations.

IV-3-2-2 Charpy Impact Strength

Experimental Technique

Another important method for testing the mechanical properties of plastics is to evaluate their toughness through a standardized impact test that determines their impact strength. An impact test is a destructive test that measures the energy required to break a standard specimen under rapid stress loading conditions. Impact strength of plastics can be measured by a number of techniques including the Charpy test method. **[15,20-22]**

In the Charpy test procedure, the sample in the form of a rectangular beam is mounted horizontally and supported near its both ends. An appropriate chosen hammer-like pendulum (of known weight) is raised to a given angle from the vertical and then released to strike the sample at its middle point and broke it into two separate halves. The energy required to break the specimen in a single swing of the pendulum is determined from the loss of its kinetic energy that equals that absorbed by the sample. During the test, only the specimens that break completely are considered acceptable, and the Charpy impact strength is calculated by dividing the energy read from the apparatus by the broken thickness or surface of the sample, and the result is expressed in terms of energy absorbed per unit thickness or per unit area of the sample (KJ/m or KJ/m^2). Note that for the notched impact test, the notch is pointing on the side opposite to the direction of the swing of the pendulum.**[15,20-22]**

Method

Notched and unnotched Charpy impact strength (IS) were assessed at room temperature using a Ceast Resil Impactor 6967 impact testing apparatus and a hammer-like pendulum of 7 Joules. The test was performed according to the procedure described in ISO 179 standard, using injection molded samples having dimensions of 80x10x4 mm representing length (L), width (W) and thickness (t).**[24]** A sharp "V" notch was cut from one side in the middle of the test specimen using a manual "V" notch cutter. **Figure IV.6** illustrates a schematic drawing of **(a)** a Charpy impact instrument, and **(b)** the "V" notch shape and its specifications.**[25]**

Impact tests were performed on notched and unnotched specimens previously dried overnight at 45°C. At least five specimens were tested for each set of samples, and the values were averaged and reported together with their respective standard deviations (SD).

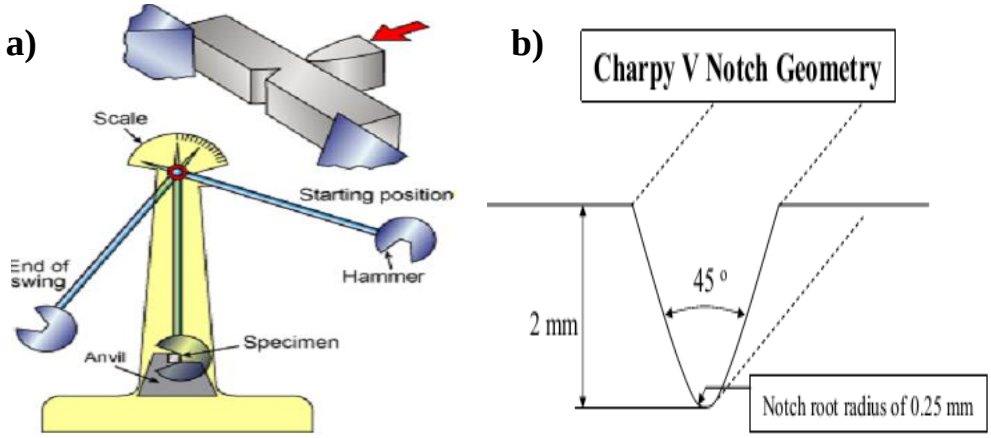

Figure IV.6 Schematic Drawing of **(a)** the Charpy Impact Apparatus and **(b)** Shape of the "V" Notch Cut and its Dimensions.**[25]**

IV-3-3 Rheological Characterization: Melt Flow Index (MFI) Measurements

Experimental Technique

Melt flow index (MFI), also known as melt flow rate (MFR), measures the plastic's ability to flow. The MFI test apparatus, schematically shown in **Figure IV.7,** is a simple ram extruder and the principle of the MFI test consists of measuring the extrusion

rate of a thermoplastic material through a capillary die with specific length and diameter under prescribed temperature and load (pressure) that depend on standard requirements.**[21]**

In a typical MFI test, a dried thermoplastic is introduced into the barrel of the MFI instrument and preheated to a required specified temperature. After packing, a dead weight is mounted on the top of the ram (piston) and the melt is allowed to flow through the die. The extrudate is collected at specified time intervals and weighed. Finally, the MFI is calculated and reported as the average weight in grams of the extrudate per 10 minutes (g/10min).**[3,6,7,9,21]**

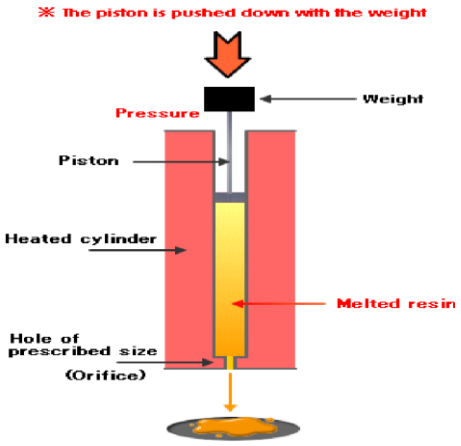

Figure IV.7 Schematic Drawing of a Melt Flow Index Apparatus.**[6]**

Method

Melt flow index (MFI) of the neat components and the mixtures was measured using Omega Melt Flow Indexer (Omega, Turkey). The measurements were carried out according to ISO 1133 at a temperature of 190°C under a load of 2.16 kg as specified by the standard.**[26]** The weight of the extruded sample collected in 10 minutes, defined as the MFI, was determined for at least five repeated runs, and the results were averaged to obtain a mean value and together with its standard deviation.

IV-3-4 Thermal Characterization: Differential Scanning Calorimetry (DSC)

Experimental Technique

Differential scanning calorimetry (DSC) is a rapid thermoanalytical experimental technique used to determine the thermal transitions of a polymer when heated at a constant heating rate within temperature range. These include glass, melt and crystallization transitions and beside these, other important physical properties can also be assessed by this technique such as heat capacity and degree of crystallization.**[27]**

In a typical DSC analysis, the temperature is measured continuously throughout the experiment and the heat flow rate is equalized by a differential technique between a sample placed in a hermitically sealed pan and a reference sample (in general an empty pan) while both are subjected to a controlled temperature program. The outcome of the analyses is a curve known as a thermogram representing the heat flow/energy difference between the samples as a function of temperature in which significant deviations in the difference between the two heat flows appear as peaks. The DSC experiment can be conducted in air or under inert atmosphere using an inert gas such as nitrogen, helium or argon.**[21,27]**

Method

Thermal properties of the materials were investigated with the aid of a Shimadzu DSC-60 differential scanning calorimeter (DSC) (Shimadzu Corporation, Tokyo, Japan). For instrument calibration, indium was used to calibrate thermal response due to heat flow as well as the temperature before analysis. Samples of 9-10 mg were cut from injection molded tensile bars, sealed in aluminum pans and heated from room temperature to 220°C at a heating rate of 10 °C/min under constant nitrogen flow of 50 cm^3/min to avoid moisture and oxidative degradation. The following events were determined from this scan: the glass transition temperature (T_g), crystallization temperature (T_c), melting temperature (T_m), crystallization enthalpy (ΔH_c), and melting enthalpy (ΔH_m).

The degree of crystallinity (χ_c) of PLA in the compounds was estimated by normalizing the observed heat of fusion to that of 100% crystalline PLA sample by using the following **equation 3.8[2]:**

$$\chi_c(\%) = \left(\frac{\Delta H_m - \Delta H_c}{\Delta H_f \times \varphi_{PLA}}\right) \times 100 \quad \textbf{(3.8)}$$

where χ_c (%) is the degree of crystallinity, ΔH_m and ΔH_c are the heats of fusion and crystallization of the sample respectively. ΔH_f is the heat of fusion of 100% crystalline PLA, and φ_{PLA} is the weight fraction of the PLA in the sample.

REFERENCES

[1] Datasheet of PLA (PLI 005) from NaturePlast (NaturePlast, Caen, France): "http://www.natureplast.eu/fr/" (Last accessed; February **2014**).

[2] Murariua, M.; Dechief, A. L.; Bonnaud, L.; Paint, Y.; Gallos, A.; Fontaine, G.; Bourbigot, S.; Dubois, P., The Production and Properties of Polylactide Composites Filled with Expanded Graphite, Polym. Degrad. Stab. ,Vol. 95, pp 889 **(2010)**.

[3] Zhou, Q.; Xanthos, M., Nanoclay and crystallinity effects on the hydrolytic degradation of polylactides, Polym. Degrad. Stab. ,Vol. 93, pp 1450 **(2008)**.

[4] Bhatia A., Master Thesis, Experimental Study of Structure and Barrier Properties of Biodegradable Nanocomposites, School of Civil, Environmental and Chemical Engineering RMIT University: Melbourne, Australia **(2008)**.

[5] Datasheet of Lotader®AX8900 from Arkema (Puteaux, France), available on website at: "http://www.arkema.com/export/shared/.content/media/downloads/productsdocumentations/ceca/pof/lotader/tds-lotader-ax8900.pdf" (Last accessed; March **2014**).

[6] Ersu D., Master Thesis, Preparation and Characterization of Nanocomposites with a Thermoplastic Matrix and Spherical Reinforcement, The Graduate School of Natural and Applied Sciences of Middle East Technical University: Ankara, Turkey, **(2006)**.

[7] Cengiz, F., Master Thesis, **Preparation and Characterization of Recycled Polypropylene Based Nanocomposites**, The Graduate School of Natural and Applied Sciences of Middle East Technical University: Ankara, (Turkey) **(2008).**

[8] Taib, R. M.; Ghaleb, Z. A.; Mohd Ishak, Z. A., Thermal, Mechanical, and Morphological Properties of Polylactic Acid Toughened with an Impact Modifier, J. Appl. Polym.Sci., Vol. 123, pp 2715 **(2012)**.

[9] Coskunses, F. I., Yilmazer, U., J. Appl. Polym. Sci. ,Vol. 120, pp 3087 (**2011).**

[10] Datasheet of Cloisite® 30B from Southern Clay Products (Gonzales, Texas, USA), available on website at: "http://www.scprod.com/". (Last accessed; March **2014**).

[11] Pluta, M. ; Paul, M. ; Alexandre, M. ; Dubois, P., J. Polym. Sc. Part B: Polym. Phys., Vol. 44, pp 299 **(2006)**.

[12] McLauchlin, A. R.; Thomas, N. L., Polym. Degrad. Stab. ,Vol. 94, pp 868 **(2009)**.

[13] Molinaro, S.; Romero, M. C.; Boaro, M.; Sensidoni, A.; Lagazio, C.; Morris, M.; Kerry, J., J. Food Eng., Vol. 117, pp 113 **(2013)**.

[14] Callister, Jr. W. D., Materials Science and Engineering-An Introduction, 7th edition, John Wiley & Sons, Inc. USA, **(2007)**.

[15] David, D. J. and Misra A., Relating Materials Properties to Structure, Handbook and Software for Polymer Calculations and Materials Properties, Technomic Publishing Company Inc. Lancaster, Pennsylvania, USA **(1999)**.

[16] Williams D. B. and Carter C.B., Transmission Electron Microscopy : A Textbook for Materials Science, Springer Science, New York USA **(2009)**.

[17] Goodhew, P.J.; Humphreys, J.; Beanland R., Electron Microscopy and Analysis, 3rd edition, Taylor and Francis, Inc., London and New York **(2001)**.

[18] Michler G. H., Electron Microscopy of Polymers, Springer-Verlag Berlin Heidelberg Germany **(2008)**.

[19] Rasband, W.S., ImageJ, U. S. National Institutes of Health (NIH), Bethesda, Maryland,
USA, available on website at: "http://imagej.nih.gov/ij/", (Last accessed; June **2014**).

[20] Alfredo Campo E., Selection of Polymeric Materials: How to Select Design Properties from Different Standards, William Andrew Inc., Norwich, New York USA **(2008)**.

[21] Shah V., Handbook of Plastics Testing and Failure Analysis, 3rd edition, John Wiley & Sons, Inc., Hoboken, New Jersey USA **(2007)**.

[22] Brown R., Handbook of Polymer Testing: Short-Term Mechanical Tests, Rapra Technology Limited, Shawbury, United Kindom **(2002)**.

[23] International Standard IS0 527-1: Plastics-Determination of Tensile Properties-Part1: General principles, ISO **(1993)**.

[24] International Standard IS0 179-1: Plastics-Determination of Charpy Impact Properties Part1: Non-Instrumented Impact Test, AMENDMENT 1, ISO **(2005)**.

[25] Brittle Fracture and Impact Tests, Chapter12, Suranaree University of Technology, Tapany Udomphol, Bangkok Thailand, available on website at: http://www.sut.ac.th/engineering/Metal/pdf/MechMet/14_Brittle%20fracture%20and%20impact%20testing.pdf, (Last accessed on March **2014**).

[26] International Standard IS0 1133-2: Plastics. Determination of the melt mass-flow rate (MFR) and melt volume-flow rate (MVR) of thermoplastics. Method for materials sensitive to time-temperature history and/or moisture, ISO **(2011)**

[27] Gabbott P., Principles and Applications of Thermal Analysis, Blackwell Publishing Ltd., Oxford United Kindom, **(2008)**.

Chapter V

Ethylene-Methyl Acrylate-Glycidyl Methacrylate Toughened Poly(lactic acid) Nanocomposites

Chapter V - Ethylene-Methyl Acrylate-Glcidyl Methacrylate Toughened Poly(lactic acid) Nanocomposites

V-1 Introduction

Biodegradable polymers are promising alternatives to petroleum-based polymers to reduce pollution caused by their long lasting wastes and also to limit the depletion of the nonrenewable fossil resources. Poly(lactic acid) (PLA) produced from renewable resources is a linear aliphatic thermoplastic polyester with outstanding potential to substitute for conventional polymers owing to its biodegradability, renewability, processability, and climate naturality.**[1,2]** PLA found use in various applications,**[1,3]** nevertheless its inherent brittleness evidenced by its low T_g, impact strength, strain at break, and tensile toughness, has limited its widespread implementation. Many efforts have been devoted to improve PLA properties including copolymerization,**[2-6]** plasticization,**[7,8]** nanoreinforcement.**[9-17]** However melt blending PLA with biodegradable and nonbiodegradable flexible polymers has attracted the greatest interest owing to its ease of application and its economical implementation.**[2,18-25]** PLA Rubber toughening has also been attempted, using biodegradable**[3,26]** and nonbiodegradable rubbers**[27-33]** were used to toughen PLA. Despite these efforts, little information is available on toughening PLA using impact modifiers. Furthermore, while PLA blends with flexible polymers and rubbers are rather largely well documented, their ternary nanocomposites studies are very scarce. In this regard, our present work is a mere contribution to fill in this gap.

In this chapter, the results concerning PLA toughening with an ethylene-methyl acrylate-glycidyl methacrylate (E-MA-GMA) impact modifier by reactive blending in a twin screw extruder are presented. Moreover, to counterbalance the loss in modulus of these blends, the ternary nanocomposites of the already prepared blends were synthesis using an organomontmorillonite clay at 2 wt%. The structure of the materials was investigated by XRD, TEM, and SEM. Thermal properties of the materials were studied by DSC, and their mechanical performance was evaluated by impact and tensile testing. Melt Flow Index (MFI) measurements were carried out to determine the rheological properties of the mixtures.

RESULTS AND DISCUSSION

V-2 Morphology

V-2-1 X-ray Diffraction (XRD) Analyses

The structure of a nanocomposite, i.e. the extent of intercalation and exfoliation govern its properties. Thus, it is of paramount importance to determine the degree to which polymers intercalate the silicate sheets of the clay. TEM and XRD techniques have been widely used to evaluate the dispersion state of the clay platelets in polymer/clay nanocomposites.**[2,12,15]** The structure of a nanocomposite is usually established using XRD analysis at low angles ($2\theta < 10°$).**[2,14,15]** The interlayer spacing, called also "d-spacing", of the clay platelets can be evaluated from the primary diffraction peak position of the organoclay in the XRD diffractogram and Bragg's law ($n\lambda = 2d\sin\theta$). The disappearance of the characteristic peak, its shift to lower diffraction angle and the broadening of the peak suggest exfoliation, intercalation and partial exfoliation respectively.**[34]**

In this study Cloisite®30B and its amount in the nanocomposites has been chosen according to previous research studies which also have shown that this organoclay disperses better in PLA than other organoclays.**[35-41]** In many research reports it has been demonstrated that C30B can give exfoliated nanocomposites either in melt processing or in in situ intercalative polymerization.**[35-38]** For instance, Pluta et al.,**[39]** used Cloisite®20A, Cloisite®25A and Cloisite®30B to prepare plasticized PLA nanocomposites. It was found that the series of organo-modified montmorillonites with decreasing affinity to PLA is Cloisite®30B, Cloisite®20A, and Cloisite® 25A, respectively. Zhou et al.,**[40]** also found that C30B shows better dispersion and more exfoliation in PLA than 15A, the latter being mostly intercalated. In another research work the degree of intercalation of PLA in Cloisite®30B was found higher than that in Cloisite®20A indicating that it was relatively easier for PLA molecules to penetrate between Cloisite®30B layers than between those of Cloisite®20A.**[41]** This was attributed to the hydrophilic nature of Cloisite®30B which is more compatible with hydrophilic PLA in comparison with hydrophobic

Cloisite20A. The better dispersion of C30B in PLA is ascribed to the efficient interactions between the carbonyl functions of PLA chains and hydroxyl functions of C30B and those of its surfactant modifier, which are responsible for the improved dispersion of this clay mineral in the PLA matrix.**[20]** Very recently, mélo et al.**[33]** produced toughened PLA nanocomposites using the same E-MA-GMA rubber (Lotader®AX8900) as in the present study and Cloisite®20A at 2.5 wt% and 5 wt% as reinforcement. The nanocomposites prepared in counter-rotating twin screw extruder showed partially exfoliated intercalated structures at 2.5 wt%. However clay dispersion deteriorated when clay was increased to 5 wt% and the nanocomposites exhibited intercalated structures with re-appearance of the original peaks of the clay. All of these results justify our choice of Cloisite®30B as reinforcement at 2wt%.

XRD traces recorded for pristine materials i.e. OMMT, PLA and the E-MA-GMA rubber are presented in **Figure V.1**. The OMMT weight fraction in the nanocomposites was maintained constant at 2 wt%. PLA and the rubber displayed no characteristic peak in the range of observation, while the reference diffractogram of OMMT clay in pure powder form exhibited a strong peak at a diffraction angle of ($2\theta=4.78°$), which corresponds to an interlayer spacing of 1.85 nm. This value corroborates with that reported in the manufacturer's data sheet.

When compounded with PLA, the characteristic diffraction peak of the organoclay shifted to lower diffraction angle ($2\theta=2.58°$) and the intensity decreased suggesting that the d-spacing (d_{001}) increased to 3.42 nm (**Figure V.1**). The distance between the clay platelets in the binary PLA/OMMT nanocomposite is larger than that in the neat clay indicating intercalation. The intercalated structure might be attributed to the affinity of PLA to the organoclay through favorable interactions between the carboxyl end groups of PLA with the hydroxyl groups on the surface of OMMT and to possible interactions that might have also occurred between the terminal carboxyl groups of PLA with the hydroxyl groups of the surfactant present in the OMMT.**[20]** The original peak of the clay still appears in the diffractogram of this nanocomposite with lower intensity suggesting that some of the clay layers were not intercalated.

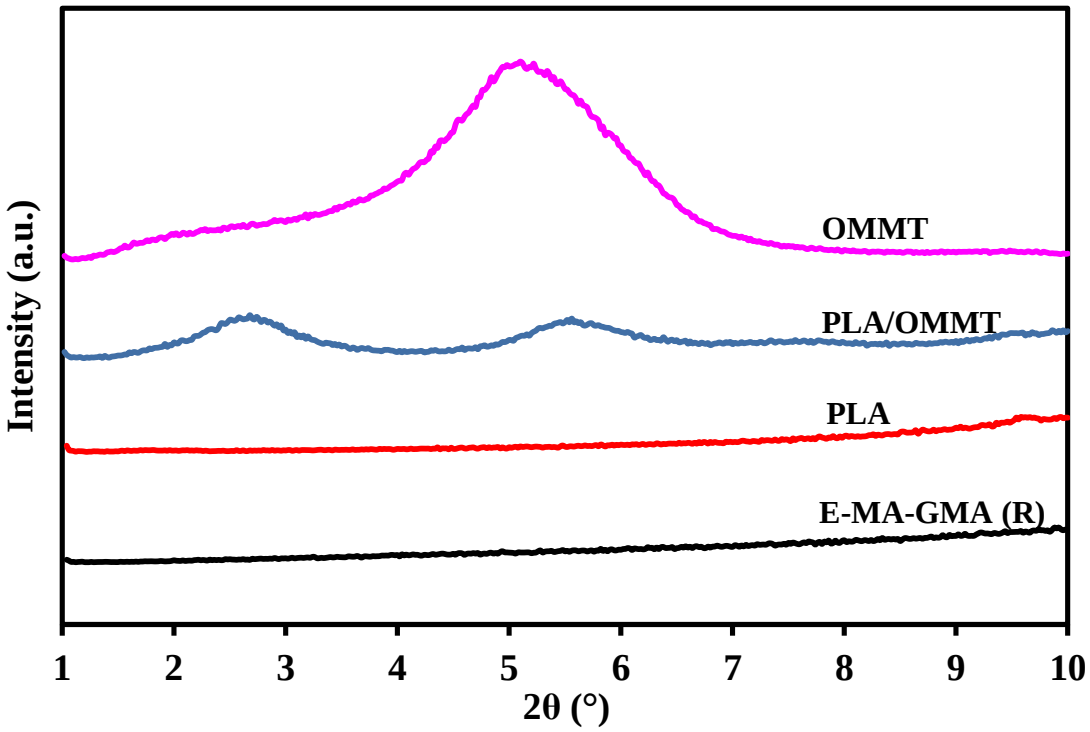

Figure V.1 X-Ray Patterns of E-MA-GMA Rubber, PLA, OMMT and PLA/OMMT Nanoocomposites prepared with 2 wt% OMMT.

Addition of 5 wt% rubber to PLA/OMMT did not significantly affect the structure of the nanocomposite (**Figure V.2**). As it can be observed, the original peak of the organoclay at (2θ=4.78°) still exists, but is smaller and broader implying intercalation and partial exfoliation due to additional intercalation of the rubber between the galleries of the clay. When the rubber content was increased to 10 wt%, both peaks disappeared from the diffractogram indicating complete exfoliation of the organoclay. This may be attributed to the affinity of the reactive rubber to the modifier of the clay. The rubber contains glycidyl reactive groups and ester moieties that might have interacted with both the clay modifier and PLA. In this sense, the rubber modifier also played the role of a compatibilizer and promoted dispersion of the OMMT.**[15,34]** Similar results were obtained by Chow et al..**[14]** In their study, they reported an incremental increase in the d-spacing when EPM-g-MAH was added to the PLA/OMMT system that was attributed to the diffusion of the rubber into the galleries of clay. Furthermore, addition of the rubber increased the shear intensity applied on

the clay during processing owing to its high viscosity. Hence, more clay platelets were delaminated and dispersion and intercalation were improved.**[34]**

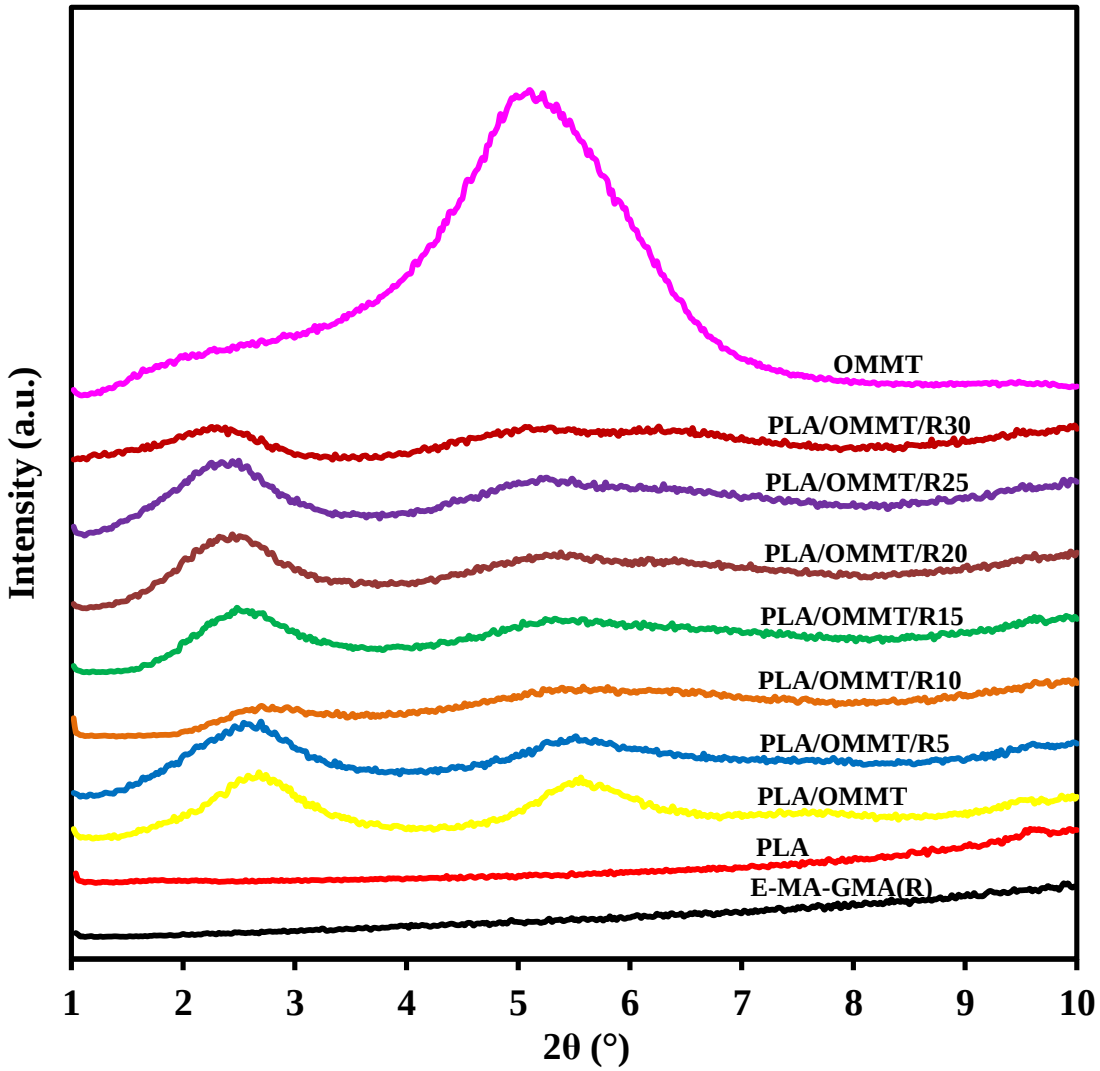

Figure V.2 X-Ray Patterns of PLA, Rubber and the Nanocomposites at 2 wt% OMMT. (The R Indicates the Rubber, and the Number Following R Indicates the wt% of the Rubber). The Curves are Shifted Vertically for Clarity.

Except for the 10 wt% rubber content, it can be seen that the original peak of the clay still existed with a slight shift to lower angle, but it became broader and decreased in intensity, implying the presence of ordered tactoids.**[34]** It should be noted that at 10 wt% rubber content, an optimum balance of the mechanical properties was obtained. Beyond 10 wt% rubber content, the two peaks reappeared at approximately the same diffraction angles (2θ=2.44°) and (2θ=5.08°) corresponding to basal spacings of 3.62 nm and 1.74 nm respectively, and no further enhancement was

observed in the intercalation/exfoliation process. This might be explained by the competitive interaction between the PLA and the rubber, in comparison to that between the polymers and the clay. Another possibility is that the rubber might have bonded to the edges of the clays through interactions of the hydroxyl groups of the clay and no further penetration into the clay galleries took place.

V-2-2 Transmission Electron Microscopy (TEM) Analyses

XRD results do not give complete information about the spatial distribution of the clay. Thus, transmission electron microscopy (TEM) is generally used as a complementary technique to get a direct visualization of the dispersion state in the nanocomposites.**[2,15,34]** Typical TEM micrographs of the nanocomposites are shown in **Figure V.3** and **Figure V.4**. The TEM micrographs in these two figures reveal the formation of nanocomposites that corroborate with the XRD results discussed earlier. The dark bundles and ribbons represent the clay particles and the light grey areas show the polymer matrix.

Figure V.3(a) is a TEM micrograph of binary PLA/OMMT at low magnification illustrating that the clay nanoplatelets were dispersed quite homogeneously. **Figure V.3(b)** is the TEM micrograph of the PLA/OMMT nanocomposite at high magnification exhibiting the formation ofintercalated/exfoliated structure in this nanocomposite, and **Figure V.3(c)** displays the TEM image of the ternary PLA/OMMT/Rubber nanocomposite with 10 wt% rubber content.

Isolated exfoliated platelets, intercalated clay and small tactoids can be clearly observed in **Figures V.3(b) and V.3(c)** indicating that addition of the rubber did not negatively influence the melt intercalation process of the PLA/OMMT nanocomposite. All of the ternary nanocomposites exhibited partial exfoliation, intercalation and small tactoids. It is also clearly observed from **Figure V.4(a-c)** that addition of more rubber did not further improve exfoliation. These observations are consistent with the results of XRD analysis.

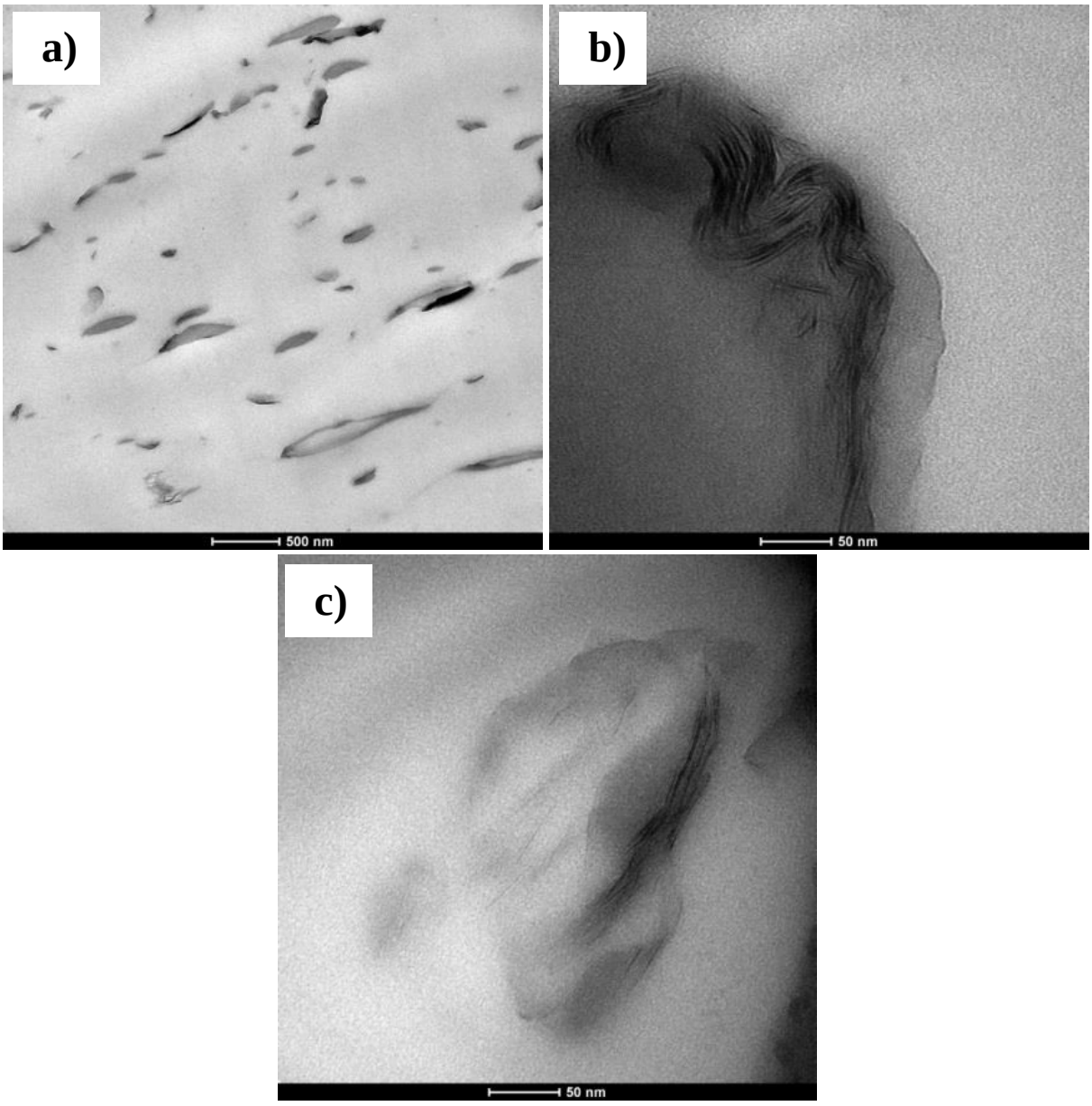

Figure V.3 TEM Micrographs of the Nanocomposites Containing 2 wt% clay: **(a)** PLA/OMMT (500 nm), **(b)** PLA/OMMT (50 nm) and **(c)** PLA/OMMT/R10 (50 nm). (The R Indicates the Rubber, and the Number Following R Indicates the wt% of the Rubber).

It is reported that the location of the clay in a rubber-toughened nanocomposite affects the particle size of the dispersed phase and thus the performance of the mixture. There are controversial reports on the effects of organoclay location on toughness in rubber-toughened nanocomposites. Some reports point out that the highest toughness was achieved when the clay was dispersed in the continuous phase, whereas others claim that the highest improvement in toughness was obtained when the clay was at the interface or dispersed inside the minor phase.**[42]**

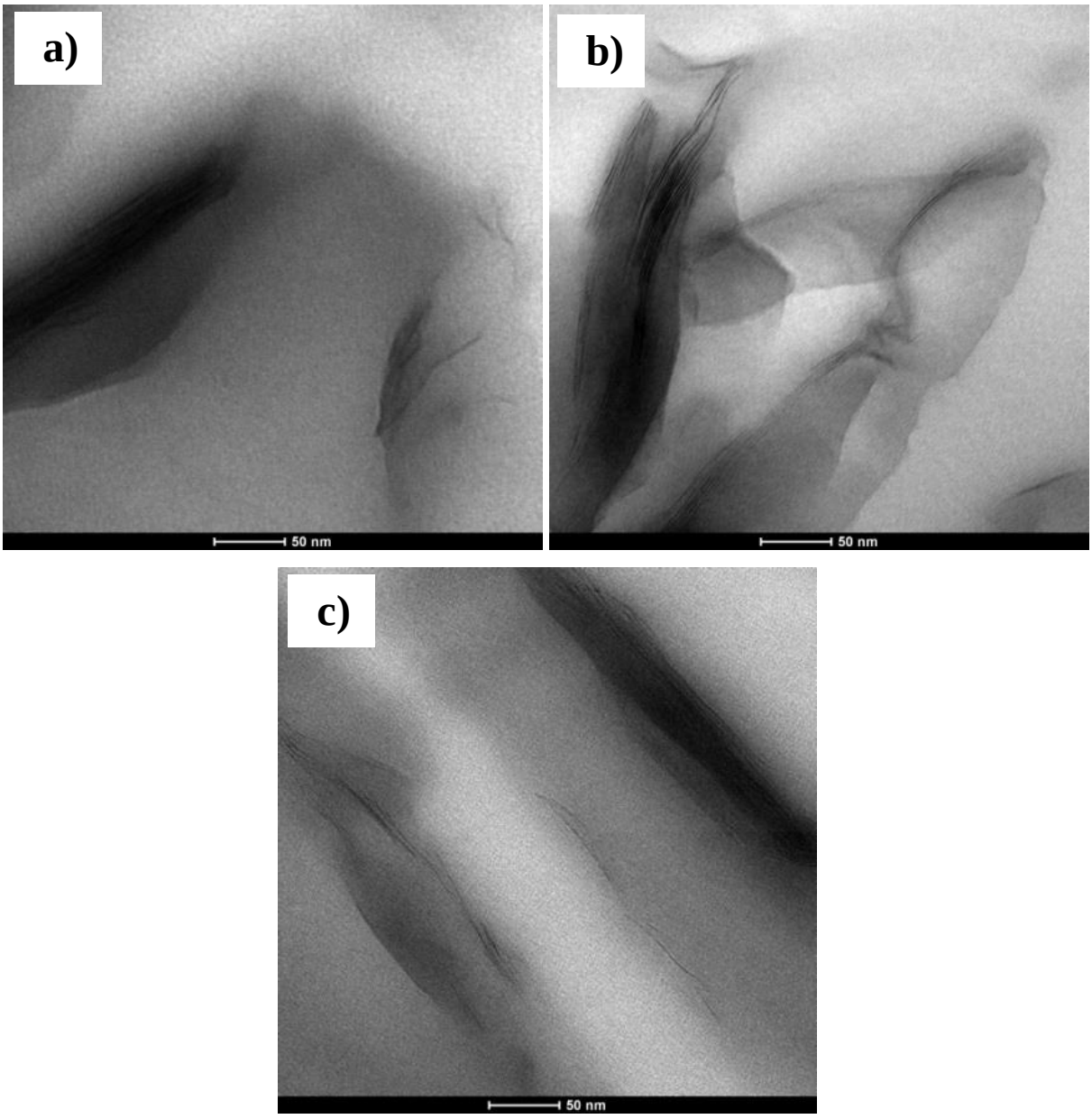

Figure V.4 TEM Micrographs of the Nanocomposites Containing 2 wt% clay: **(a)** PLA/OMMT/R15 (50 nm), **(b)** PLA/OMMT/R20 (50 nm), **(c)** PLA/OMMT/R30 (50 nm). (The R Indicates the Rubber, and the Number Following R Indicates the wt% of the Rubber).

It was not possible to determine the position of the clay particles in the mixtures by the TEM micrographs owing to the low contrast difference between the PLA and the rubber. To obtain better contrast between the rubber phase and the PLA continuous phase in TEM and SEM images, staining the rubber phase was attempted using both osmium tetroxide (OsO_4) and ruthenium tetroxide (RuO_4) but this procedure failed after lot of trails. Clay particles are more likely to be located in the PLA matrix, since

it is more polar than the rubber, and it has lower viscosity than the rubber. However, scanning electron microscopy and mechanical properties analyses that are discussed later suggest that most of the clay particles might be embedded in the rubber phase and some were located at the interface of the rubber and PLA as well as in the PLA matrix. This could be due to the fact that during melt compounding, the rubber melted first (T_m≈53°C) and encapsulated most of the clay before PLA started melting at approximately 152°C.

V-2-3 Scanning Electron Microscopy (SEM) Analyses

SEM micrographs of the unetched surfaces of PLA and PLA/OMMT are displayed in **Figures V.5(a) and V.5(b)** respectively. As can be observed from **Figure V.5(a)**, PLA exhibits a typical fractured surface of a brittle material with rather a smooth surface with no plastic deformation. Few straight parallel lines of crack propagation are clearly noticeable with no deviations of the cracks implying easy crack initiation and propagation and rapid progress of catastrophic cracks responsible for premature fracture with low energy dissipation.**[15,24]**

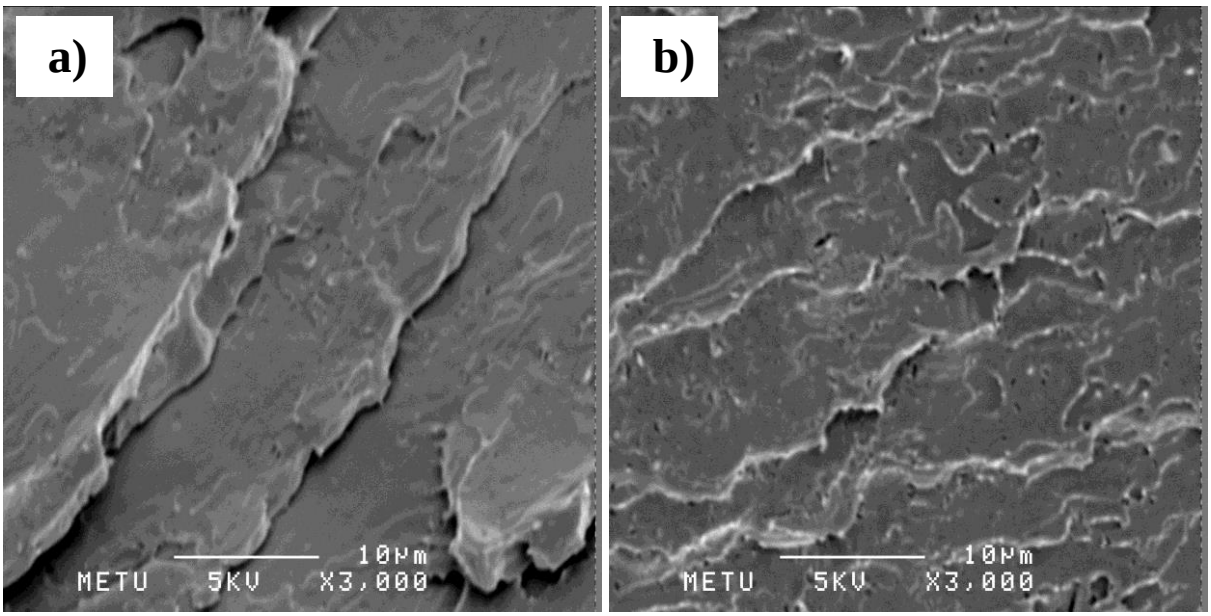

Figure V.5 SEM Micrographs of the Fractured Surfaces of the Unetched Injection Molded Specimens of **(a)** PLA and **(b)** PLA/2 wt% OMMT.

PLA/OMMT micrograph shows a rougher fractured surface with multiple small and long crack lines developed in different directions due to the presence of the clay (**Figure V.5(b)**). This suggests that clay particles deflected the cracks and increased their path. This mechanism that is responsible for roughness and low energy absorption before failure was also observed in Reference12 for PLA/OMMT. The SEM observations of these materials are consistent with the low impact strength and toughness results obtained in mechanical characterization.

Figure V.6(a-c) shows typical SEM images of the etched surfaces of the binary blends of PLA/Rubber. The vacuoles left after etching reflect the morphology of the dispersed phase. The morphology of the mixtures is that of a two-phase binary blend where PLA formed the continuous phase and the rubber was segregated as spherical domains typical of an immiscible blend, supporting the DSC results discussed later. The rubber particles are evenly dispersed at all concentrations used with narrow size distribution. Their sub-micron mean size (0.4µm-0.8µm) suggests low interfacial tension owing to the efficient reaction during compounding between the epoxy groups of the rubber and the hydroxyl and carboxyl terminal groups of the PLA,**[1,4,28,31]** as well as other possible polar interactions between the ester groups of PLA and those of rubber. Such reaction was proved by Fourrier Transform Infrared Spectroscopy by Su et al.**[1]** in their study of blends of PLA and glycidyl methacrylate grafted poly(ethylene octane) (PLA/mPOE). As also observed in **Figure V.6(a-c)** the domain size increased with increasing rubber content. The viscosity of the dispersed phase increased with increasing rubber content, consequently the droplet coalescence rate increased at the expense of the droplet break up rate, thus large particles were formed.**[4]** The craters observed are deformed and shaped like ellipsoids with irregular surfaces indicating that the rubber phase shared the impact load with the matrix and was tightly bonded to the PLA. This might also be ascribed to the reaction between the PLA functional groups and the reactive groups of the rubber as mentioned earlier. The copolymer formed at the interface leads to better spatial distribution of the dispersed phase and plays the role of an emulsifier by reducing interfacial tension. Thus, the droplet breakup rate is increased and phase coalescence rate is retarded during melt

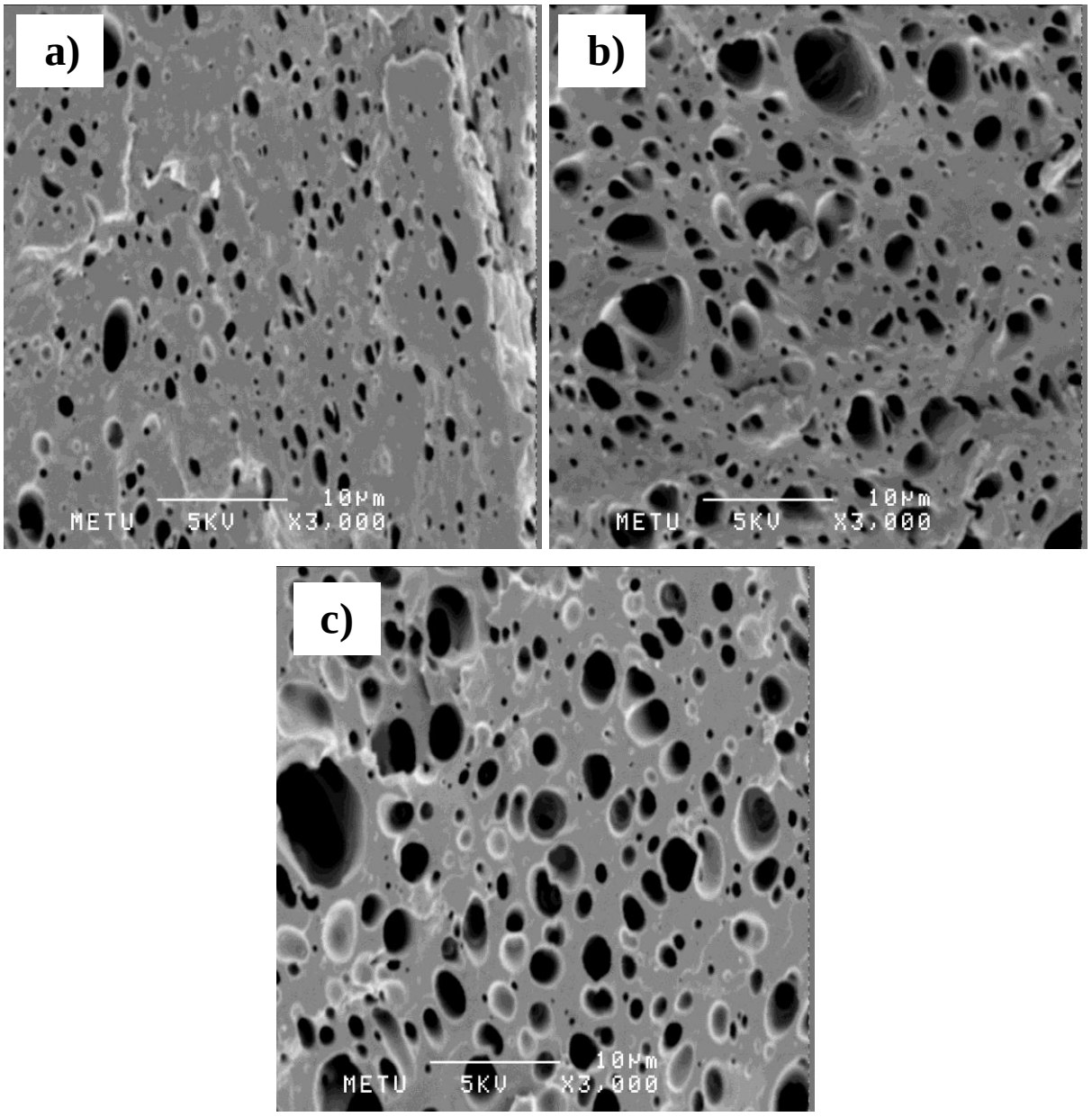

Figure V6 SEM Micrographs of the Fractured Etched Surfaces of the Injection Molded Specimens of the Binary Blends **(a-c)** at 10 wt%, 20 wt% and 30 wt% Rubber Content Respectively.

compounding, consequently small particle size is generated.**[4]** This copolymer is also efficient in bridging the two components of the blend for efficient load transfer responsible for toughness improvement that is consistent with the results of the mechanical properties.**[34]** The function of the rubber domains is not only to share the load with the matrix, but to contribute to energy dissipation by initiating multiple crazing in the matrix and to stop and/or divert cracks to prevent their development to rapid catastrophic cracks.**[27]** Few cracks are also visible in **Figure V.6(a)** with

tortuous path due to the presence of the rubber. This indicates that the rubber domains were able to deflect the propagation of the cracks, and the long crack propagation paths absorbed considerable energy contributing to energy dissipation that is responsible for toughness improvement.

Figure V.7(a-c) displays the SEM morphology of the etched surfaces of the ternary nanocomposites. The observed craters had the same morphological features as

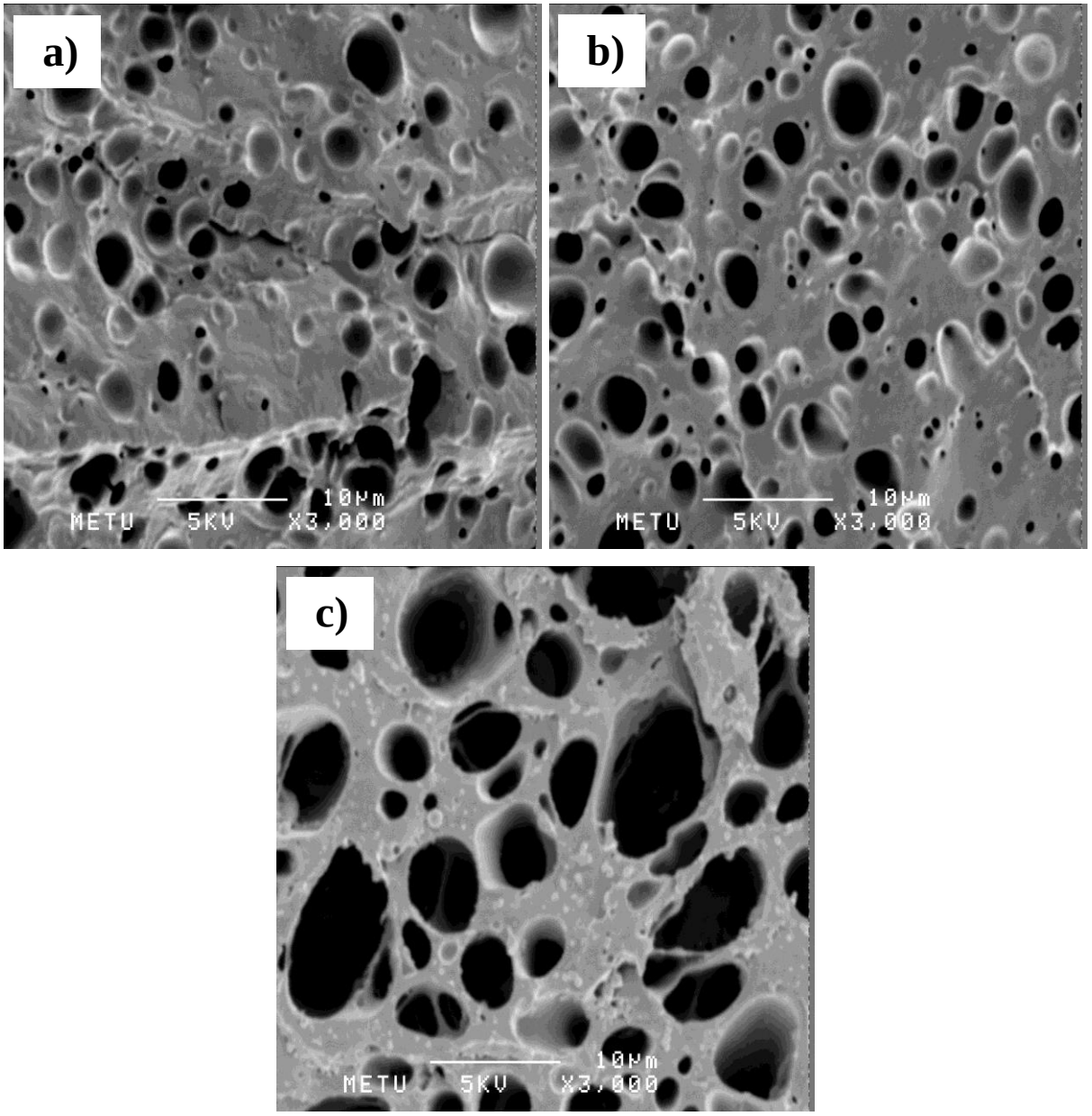

Figure V.7 SEM Micrographs of the Fractured Etched Surfaces of the Injection Molded Specimens of the Ternary Nanocomposites **(a-c)** at 10 wt%, 20 wt% and 30 wt% Rubber Content Respectively.

those of the binary compounds suggesting that the clay did not interfere with the reaction between the rubber and the PLA, but influenced the size of the rubber domains. As observed in these figures, the mean domain size of the nanocomposites increased with increasing rubber content (0.4µm-1.5µm) and was mostly larger than that of the binary blends (0.4µm-0.8µm). The higher domain size in the nanocomposites suggests that the clay particles did not act as barriers for coalescence, but enlarged the rubber phase domains by affecting the viscosity ratio between the rubber and PLA matrix.**[32,34,42]**

Figures V.8(a) and V.8(b), show the morphology of the non-etched fractured surfaces of the binary blends and ternary nanocomposites at 10 wt% rubber content respectively. Surfaces of both materials are rough owing to the presence of the rubber and the clay indicating that high energy was necessary to failure. It is also observed that some of the rubber particles were ejected out from their previous positions in the PLA matrix and some were still embedded and surrounded with voids after the fracture process indicating that debonding and/or cavitation of the rubber took place at the interface due to its low strength compared to that of PLA.**[2]** Debonding and/or cavitation are believed to play a major role in toughening mechanism in rubber-toughened blends. Since the rubber has different elastic properties than PLA, its particles act as stress concentrators and debonding and/or cavitation occur at the interface. The high triaxial stress raised in the rubber particles is then released to the PLA matrix neighboring the voids and debonding progress, consequently the matrix between the rubber particles is easily deformed and shear yielding occurs. Cavitation and shear yielding mechanisms are energy dissipation mechanisms retarding crack initiation and propagation and thus responsible of the improved mechanical properties.**[2,26]**

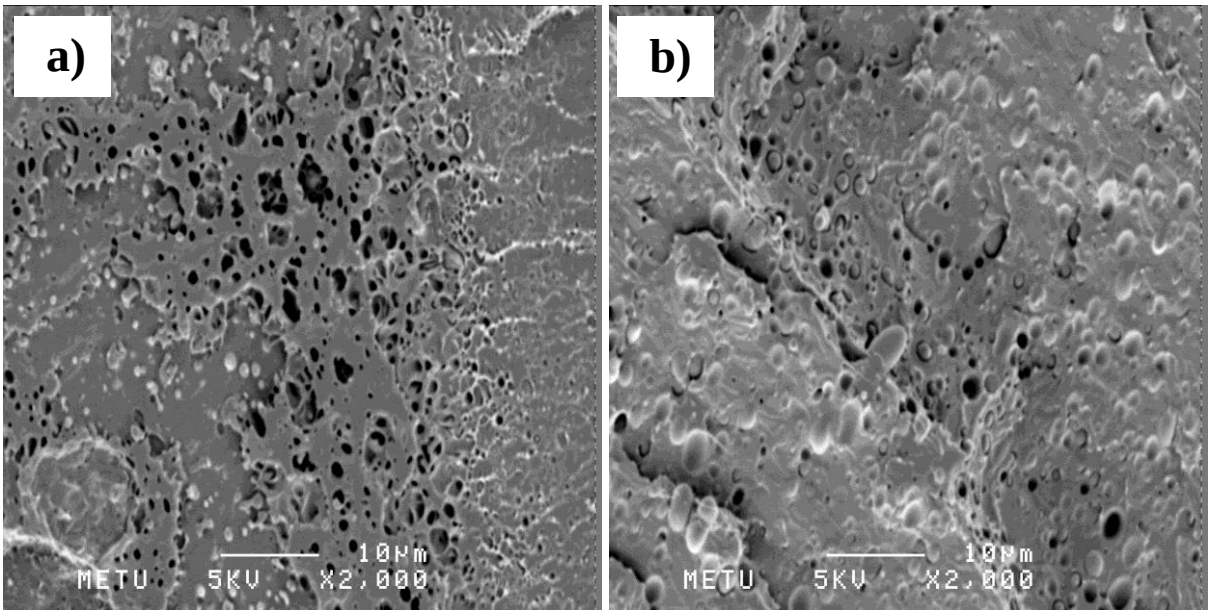

Figure V.8 SEM Micrographs of the Fractured Surfaces of the Unetched Injection Molded Specimens at 10 wt% Rubber Content of **(a)** the Binary Blend and **(b)** the Ternary Nanocomposite.

V-3 Mechanical Properties

In general, rubber-toughening of polymers leads to reduced strength and stiffness and enhanced toughness provided that a strong interface exists between the phases. However, addition of rigid nanofillers into polymers to form nanocomposites increases strength and stiffness, but may decrease toughness. Combining the two techniques may lead to balanced properties or even to simultaneous improvement in all the three properties.**[42,43]** It is reported that in both polymer blends and nanocomposites, the interfacial interactions and the level of dispersion of the components are the key factors that govern the final properties.**[34]**

V-3-1 Tensile Properties

Figures V.9 and V.10 display typical stress-strain curves of pristine PLA, and its binary blends and ternary nanocomposites, and **Figures V.11, V.12 and V.13** show the effect of the rubber and the OMMT on Young's modulus, tensile strength and elongation at break of these materials respectively.

As can be observed in **Figure V.9**, PLA shows the behavior of a typical rigid and brittle material. During stretching, PLA deformed with a steep linear increase in stress, followed by a yield point and a very short necking. Finally, it fractured catastrophically at very low elongation (ca. 5%) due to lack of crack deviation and cavitation mechanisms as reported by He et al..**[44]** Slight stress-whitening were visible on specimens indicating that PLA deformed by crazing mechanism.**[25]** PLA deformation behavior was not significantly affected by the addition of 2 wt% OMMT, and the same mode of deformation was observed. However, more stress-whitening was noticed after the failure of PLA/OMMT. Addition of the rubber induced a substantial change in the tensile behavior of PLA (**Figure V.9**). The failure mode changed from brittle to ductile with a noticeable yield point, longer necking and increased plastic deformation followed by stress softening before failure.

All of the stress-strain curves of the binary blends (**Figure V.9**) and nanocomposites (**Figure V.10**) exhibited the same pattern.

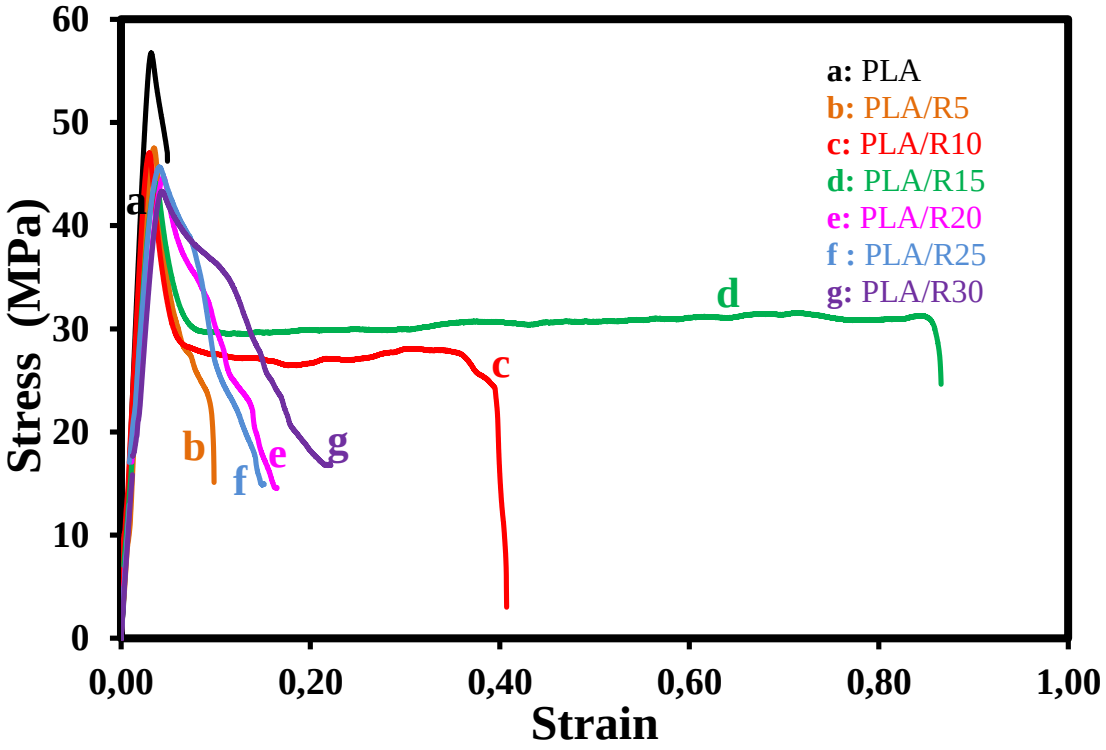

Figure V.9 Typical Stress-Strain Curves of the Binary Blends.

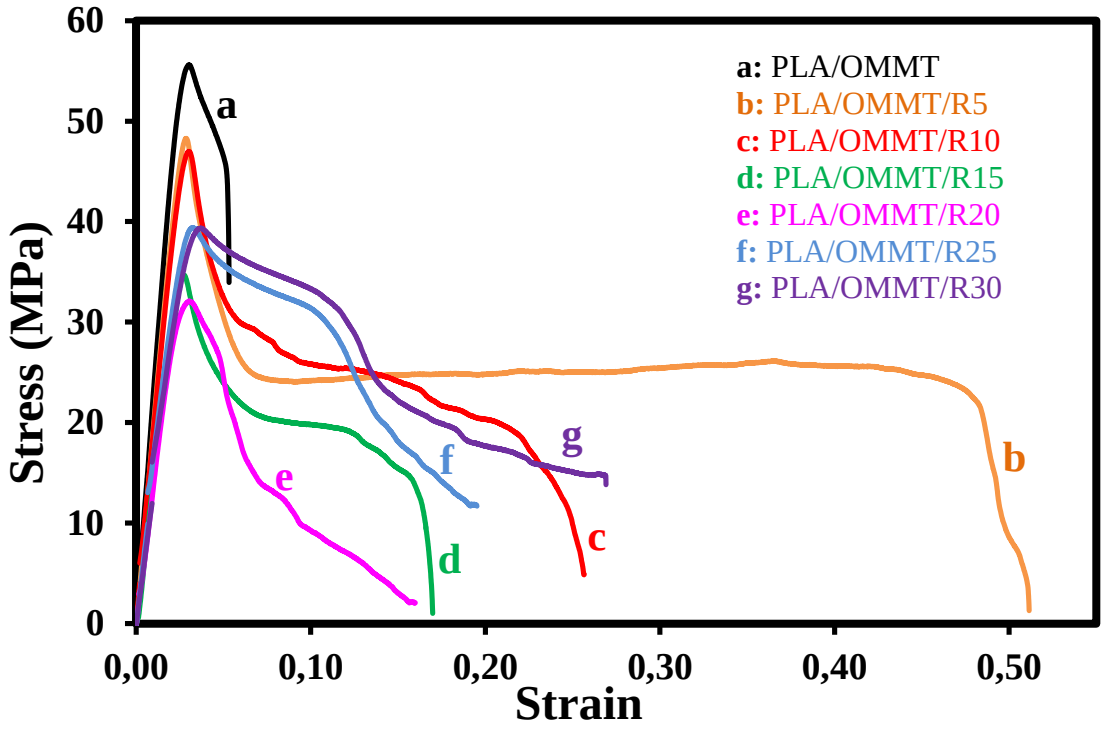

Figure V.10 Typical Stress-Strain Curves of the Ternary Nanocomposites.

V-3-1-1 Young's Modulus

Addition of 2 wt% organoclay resulted in increase of the tensile modulus of PLA from 2068.0 MPa to 2290.8 MPa (**Figure V.11**). The enhancement in modulus with the addition of OMMT corroborates with the results of other research studies.**[2,15,20,29,32]** The increase in tensile modulus may be ascribed to the stiffening effect of the dispersed rigid clay layers, as well as the reduced chain mobility of PLA by the surface of the clay.**[2,15,20,29]** The intercalated/exfoliated structure of the OMMT results in high contact surface area favorable for enhanced interfacial interactions between the carboxyl end groups of PLA and the hydroxyl groups on the organoclay and contributes to chain immobilization.**[15,20,29]** These interactions are responsible for enhanced adhesion between the PLA matrix and the filler. As a result, an effective stress transfer from the matrix to the filler is established leading to increased elastic modulus.**[20]**

In the binary blends the modulus dropped steadily as the rubber content is increased (**Figure V.11**) owing to the elastomeric nature of the rubber with low

modulus.**[2,32,44]** The decrease in the modulus was in the range of 10-40 % in the composition interval studied. For example, at 20 wt% rubber content, the decrease is around 26% which is lower than the 31% reduction reported for the PLA/poly(ethylene-glycidyl-methacrylate) (PLA/EGMA) blend.**[28]** This might be ascribed to the presence of methyl acrylate groups in the rubber of the present study. Compared to other findings, the reduction in modulus is similar to the 25% decrease obtained in PLA/NR-g-PBA blend,**[27]** but far less than the 50 % decrease in PLA/TPO blend containing 5 phr TPO-PLA as compatibilizer.**[30]** Our decrease was also lower than that reported by Mélo et al.**[33]** for their PLA/E-MA-GMA/2 wt% Cloisite®20A which was 38%.

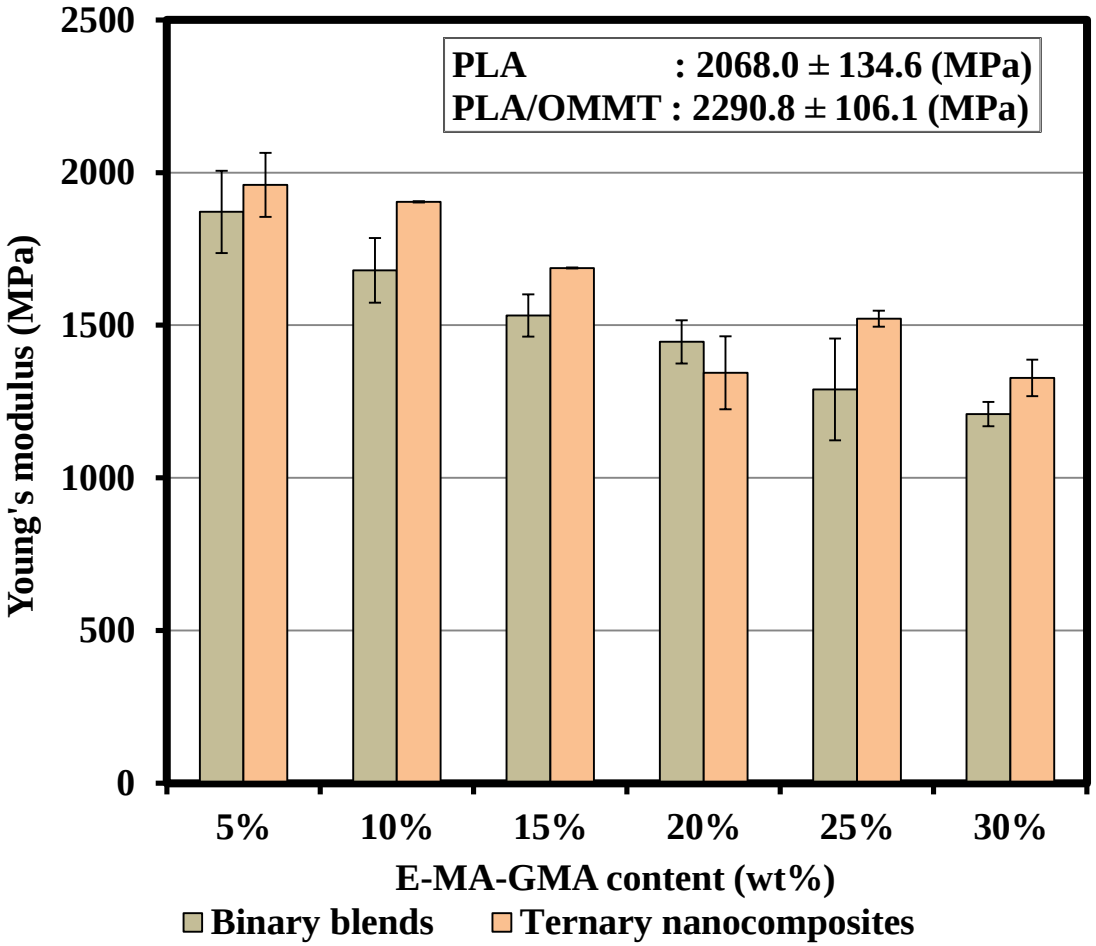

Figure V.11 Effect of the Rubber Content on the Young's Modulus of the Binary Blends and Ternary Nanocomposites at 2 wt% Clay.

In **Figure V.11** it can also be observed that incorporation of 2 wt% OMMT induced a substantial increase in the modulus for all the nanocomposites owing to the stiffening effect of the OMMT that induced chain immobilization as discussed for the PLA/OMMT nanocomposite.**[2,15,20,29,32]**

V-3-1-2 Tensile Strength

Figure V.12 shows the tensile strength of the blends and nanocomposites. A slight decrease in the tensile strength from 56.3 MPa to 55.7 MPa was observed after addition of 2 wt% OMMT to PLA.

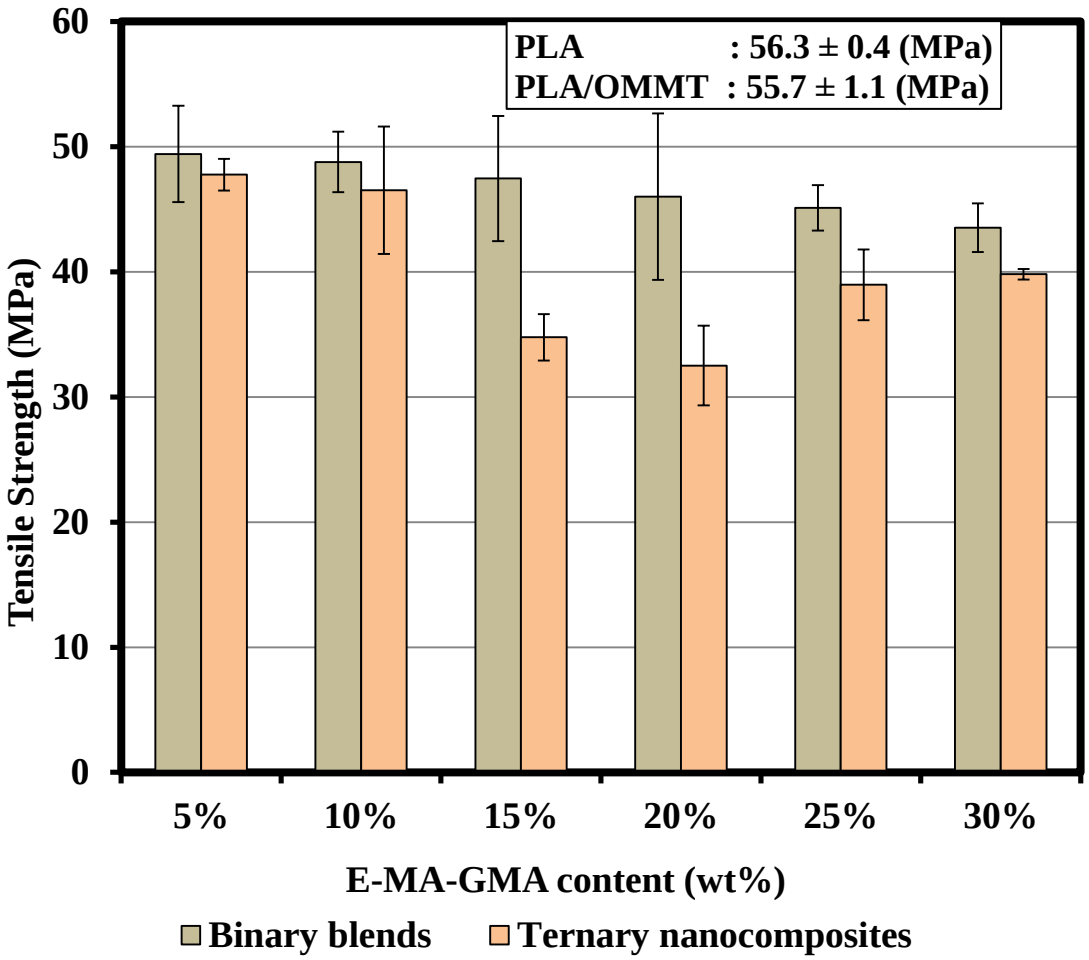

Figure V.12 Effect of the Rubber Content on the Tensile Strength of the Binary Blends and Ternary Nanocomposites at 2 wt% Clay.

In the binary blends, the tensile strength decreased from 49.4 MPa to 43.5 MPa as the rubber content increased from 5 to 30 wt% owing to the elastomeric nature of the rubber.**[1,15,29]** It should be noted that the tensile strength was affected less by the

rubber than the elastic modulus was. The addition of the OMMT to the binary blends also decreased the tensile strength of the binary blends. Similar decrease in tensile strength was observed in a recent study of PLA/SEBS-g-MAH/OMMT nanocomposites.**[29]** The OMMT counteracted the negative effect of the rubber on the tensile strength only when the rubber content was less than 15 wt% owing to its low content (2 wt%).

V-3-1-3 Elongation at Break

PLA is a hard and brittle material reported to elongate not more than 10 %.**[3]** **Figure V.13** shows the effect of the rubber on PLA and its binary blends and ternary nanocomposites. As expected, the elongation at break of pure PLA was very low (≈ 5%) owing to its rigid nature. Addition of 2 wt% OMMT did not significantly affect the elongation at break of the PLA, but induced stress whitening upon extension.

Addition of the rubber up to 15 wt% increased the elongation at break of the blends to reach a maximum value of 46% representing 9 fold increase in comparison to that of pristine PLA. Thus, the rubber changed the deformation of PLA from brittle to ductile. This implies that high energy was dissipated during crack propagation before failure owing to the elastic nature of the rubber and to the strong interface developed through the interactions of the ester groups of the rubber and PLA, and the reaction of the epoxy groups of the dispersed rubber phase and hydroxyl and carboxyl end groups of the PLA matrix leading to the formation of PLA-g-rubber at the interface.**[2]** In addition, this copolymer might have reduced the stress concentration around the dispersed rubber particles by local plastic deformation favorable for increased elongation at break.**[15]** Beyond 15 wt% rubber content, the elongation at break underwent a drastic reduction and attained a value of approximately 16 % in the range of 20-25 wt% rubber loading. This may be attributed to chain entanglements formed at the interface that might have reduced the chain mobility.**[45]** Beyond 25 wt% rubber, the elongation at break increased due to high rubber fraction.

The elongation at break of the ternary nanocomposites exhibited the same trend as that of the binary blends. Up to 20 wt% rubber loading, the values of elongation at

break of the ternary nanocomposites were lower than those of the binary compositions, due to the constraining effect of OMMT on the molecular mobility.**[20,29]** Beyond this rubber content, the elongation at break increased owing to higher rubber content.

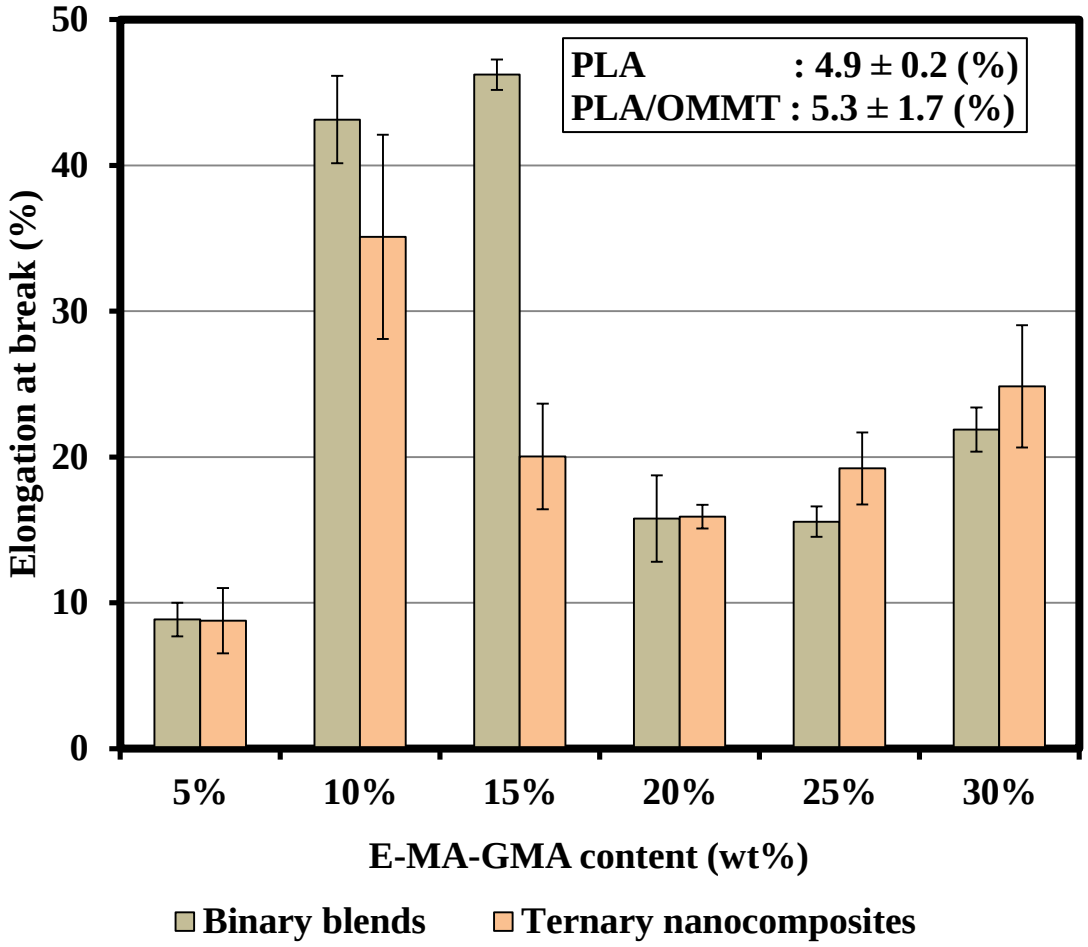

Figure V.13 Effect of the Rubber Content on the Elongation at Break of the Binary Blends and Ternary Nanocomposites at 2 wt% Clay.

V-3-2 Impact Strength

Notched impact strength is a measure of the energy necessary to propagate an existing notch (resistance to crack propagation), while unnotched impact strength is a measure of the energy to initiate and propagate a crack (resistance to crack initiation and propagation).**[46]**

Rubbers containing glycidyl moieties were generally used as impact modifiers and/or as compatibilizers with different success.**[2,4,28,47]** In rubber-toughened

polymer blends numerous factors such as the extent of mixing, rubber content, viscosity ratio, interfacial adhesion, and rubber particle size affect the final morphology and hence the final properties.**[23,24]**

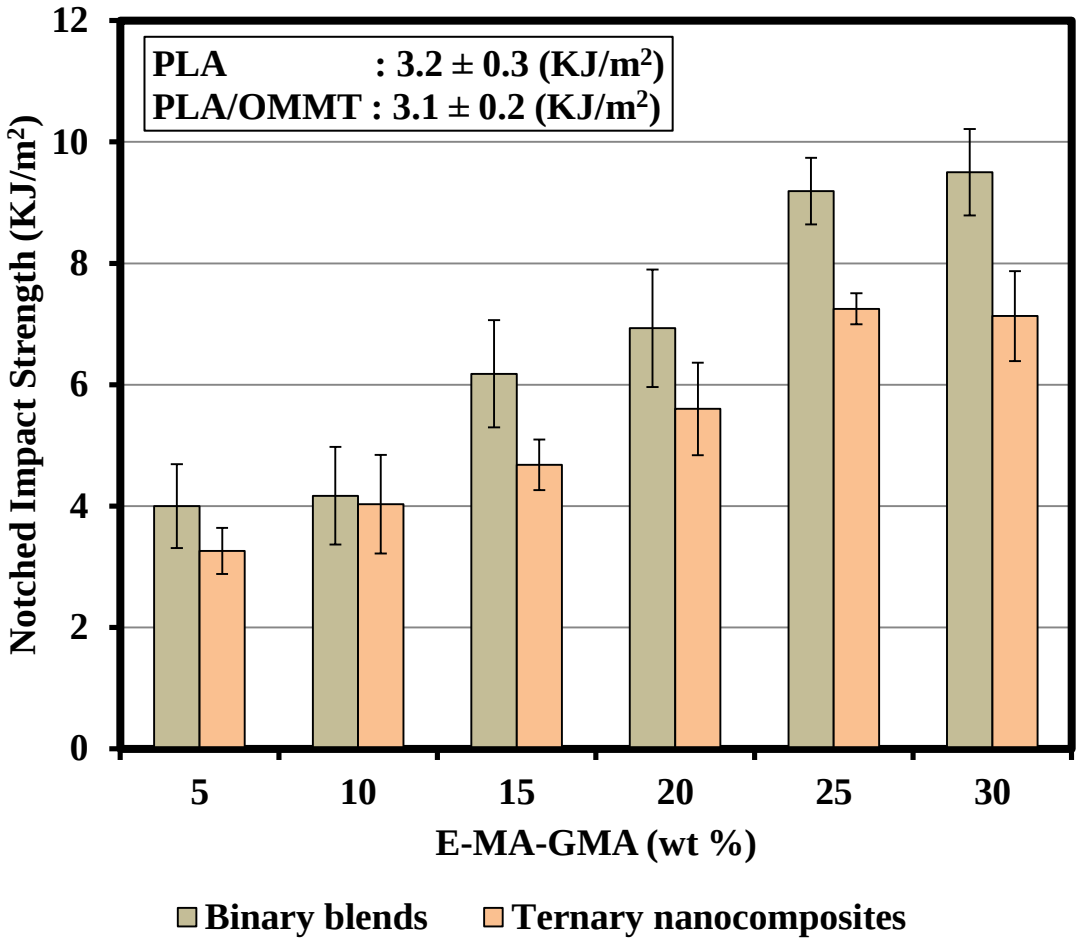

Figure V.14 Effect of the Rubber Content on the Notched Charpy Impact Strength of the Binary Blends and Ternary Nanocomposites at 2 wt% Clay.

The effects of the OMMT and the rubber on notched Charpy impact strength (IS) of neat PLA are reported in **Figure V.14**. PLA subjected to impact load failed in a brittle manner typical of a glassy polymer and the low impact strength recorded was only 3.2 KJ/m^2. Broken specimens showed intense stress whitening especially near the notch tip characteristic of local crazing. The incorporation of the clay imparted a negligible decrease (≈3%) in the IS of plain PLA which is within the experimental error. Similar results were obtained for nylon-clay nanocomposites.**[48]** The IS was maintained relatively constant owing to the efficient interactions between PLA and the OMMT and to the intercalation/exfoliation as revealed by XRD and TEM. However,

no improvement could be obtained owing to the absence of deformation mechanisms to absorb and dissipate energy such as crazing, cavitation and shear yielding.**[15]**

The addition of the rubber significantly enhanced the impact strength of the PLA. The IS increased steadily from 4 KJ/m^2 at 5 wt% rubber content to reach a maximum of 9.5 KJ/m^2 at 30 wt% rubber content. This is attributed to the elastomeric nature of the rubber and its fine and homogeneous dispersion, as well as to the strong interface developed during compounding as discussed earlier.**[4,15]** The reactions led to the formation of a grafted copolymer (PLA-g-rubber) located at the interface that acted as an emulsifier and reduced the interfacial tension between the two phases resulting in high level of dispersion, fine particle size and low polydispersity as observed by SEM. The rubber inclusions acted as stress concentrators during impact deformation and transformed the behavior of the PLA from brittle to ductile by changing the mechanism of deformation. Such mechanisms of deformation might include crazing, cavitation, shear bending, crack bridging and shear yielding that are well known in toughened polymer blends.**[2]**

At 10 wt% rubber content, the binary blend and the ternary nanocomposite exhibited nearly the same IS value, probably due to the highest exfoliation state observed in this nanocomposite. At other rubber contents, the IS values of the ternary nanocomposites were lower than those of the corresponding binary blends. This could be attributed to their larger particle size (0.4µm-1.5µm). It was reported that well dispersion of clay into a blend might suppress coalescence. **[32]** However, the opposite result was obtained in the present study that might indicate that most of the clay was encapsulated in the rubber phase with some clay residing at the interface between the PLA and the rubber and in the PLA matrix as discussed earlier in the XRD and TEM sections. Yu et al.**.[49]** reported that high toughness is obtained when maximum quantity of exfoliated clay is dispersed in the continuous phase of a functionalized rubber-toughened blend. In conclusion, in this study, the organoclay was more effective for improvement of modulus than for improvement of impact toughness. At 2 wt% OMMT, balanced stiffness-toughness was observed at 10 wt% rubber content that exhibited the highest level of exfoliation.

V-4 Rheological Characterization: Melt Flow Index (MFI) Measurements

Rheological measurements are widely used as a mean to determine the extent of interactions in reactive polyblends.**[15,44]** The rheological properties of the pristine materials, the blends and the nanocomposites were determined using melt flow index measurements (MFI).

Figure V.15 shows the MFI of the starting materials and the compounds. The MFI of the injection grade PLA increased from 47.2 to 51.1 g/10min after extrusion indicating that its molecular weight has been decreased as expected, since PLA is known to be a shear sensitive material.**[13]**

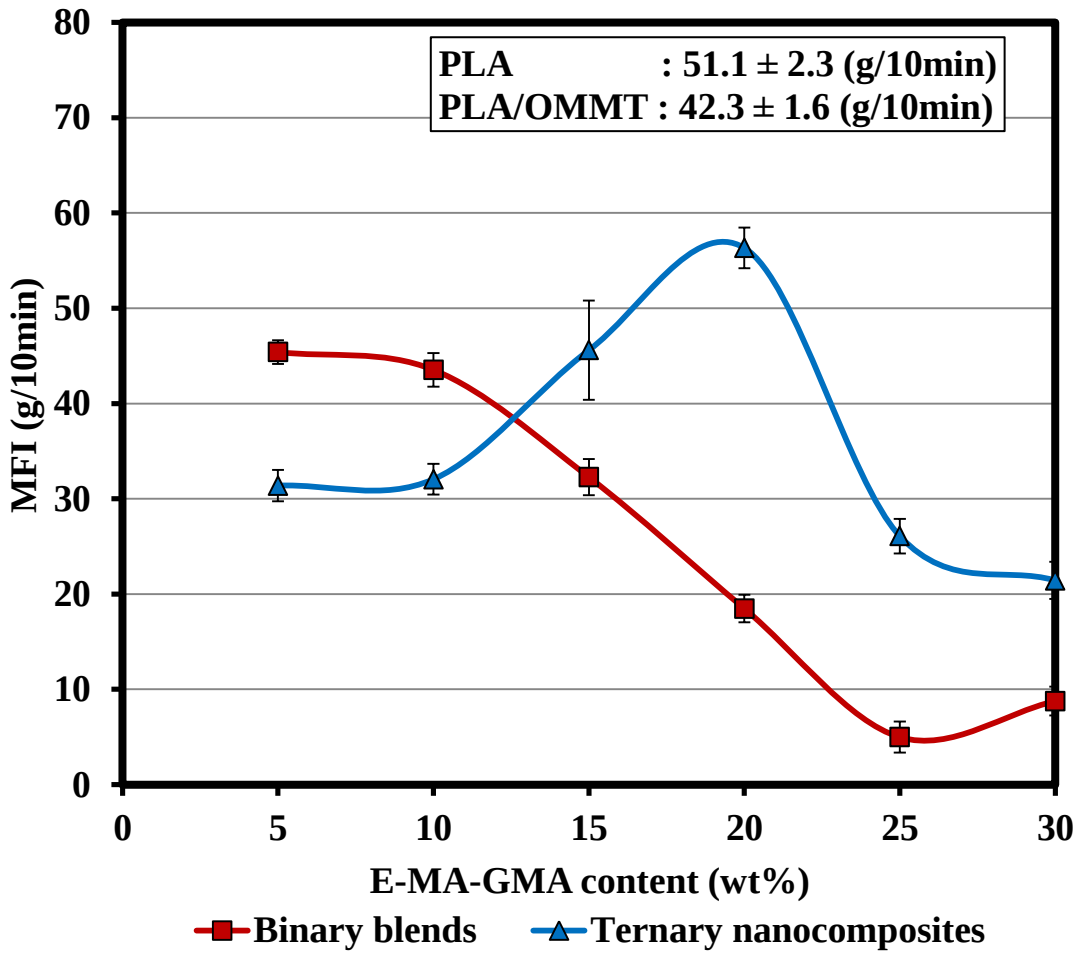

Figure V.15 Effect of the Rubber Content on the MFI of the Binary Blends and the Ternary Nanocomposites at 2 wt% Clay.

Addition of 2 wt% clay to PLA decreased the MFI to 42.3 g/10min. The decrease in the MFI (increase in viscosity) is attributed to the "filler effect", as well as to the enhanced interactions of the modified clay and the PLA through possible interactions of the carboxyl and hydroxyl terminal groups of the PLA with the hydroxyl groups of the surfactant of the clay that constrain chain mobility.**[15,20]** Also, the aspect ratio of clay increases through delamination of the clay agglomerates and exfoliation as observed by XRD and TEM giving rise to larger surface area for interactions that restrict the flowability of the material.**[20]**

In the binary blends of PLA/Rubber, addition of the rubber up to 25 wt% to PLA decreased the MFI. The decrease in MFI is attributed to the high viscosity of the rubber and to the reaction of the epoxy groups of the rubber with the hydroxyl and carboxyl end groups of the PLA and the likely polar interactions of their ester groups. The reaction might lead to formation of a graft copolymer at the PLA and the rubber interface that would strengthen the interfacial adhesion, restrict chain mobility and reduce slippage of the chains at the interface.**[15,20]** In the literature, interfacial interactions are reported to result in increase in viscosity (decrease in MFI) in several polymer systems.**[1,29,30]** For example, Kusmono et al.**[15]** reported a decrease in MFI after addition of SEBS-g-MAH to compatibilize a PA6/PP blend. They attributed such a decrease to the formation of SEBS-g-PA6 copolymer at the interface due to reaction of PA6 amine groups with maleic anhydride groups of SEBS-MAH. At 30 wt% rubber content, the MFI of the blend increased to reach approximately the MFI of the neat rubber measured as 8.3 g/10min.

In the ternary nanocomposites, the MFI increased up to the composition containing 20 wt% of rubber. This increase might be due to plasticizing effect of the dissolved clay surfactant. As the viscous rubber content is increased, more of the clay platelets are delaminated and some of the surfactant of the clay dissolves in the matrix inducing plasticization and increasing the MFI.[**13,20**] At even higher rubber contents, the plasticization effect of the clay surfactant was hindered by the high content of the highly viscous rubber, consequently the MFI decreased.

V-5 Thermal Characterization: Differential Scanning Calorimetry (DSC)

Differential scanning calorimetry was performed from room temperature to 220°C using samples from tensile injected dog-bones to evaluate the effects of the organoclay and the rubber on the phase transition behavior of the PLA and the mixtures. Thermograms of PLA and its binary blends and ternary nanocomposites exhibited three main transitions namely: a glass transition temperature (T_g), a crystallization exotherm (characterized by T_c and ΔH_c), and a melting endotherm (characterized by T_m and ΔH_m) **(Figures V. 16 and V.17)**. The values of the calorimetric parameters and the degree of crystallization of PLA are summarized in **Tables V.1 and V.2**. The degree of crystallization was calculated from equation 3.8 of chapter 3 using a value of 93 J/g for the heat of fusion of 100% crystalline PLA.**[24,27,28]**

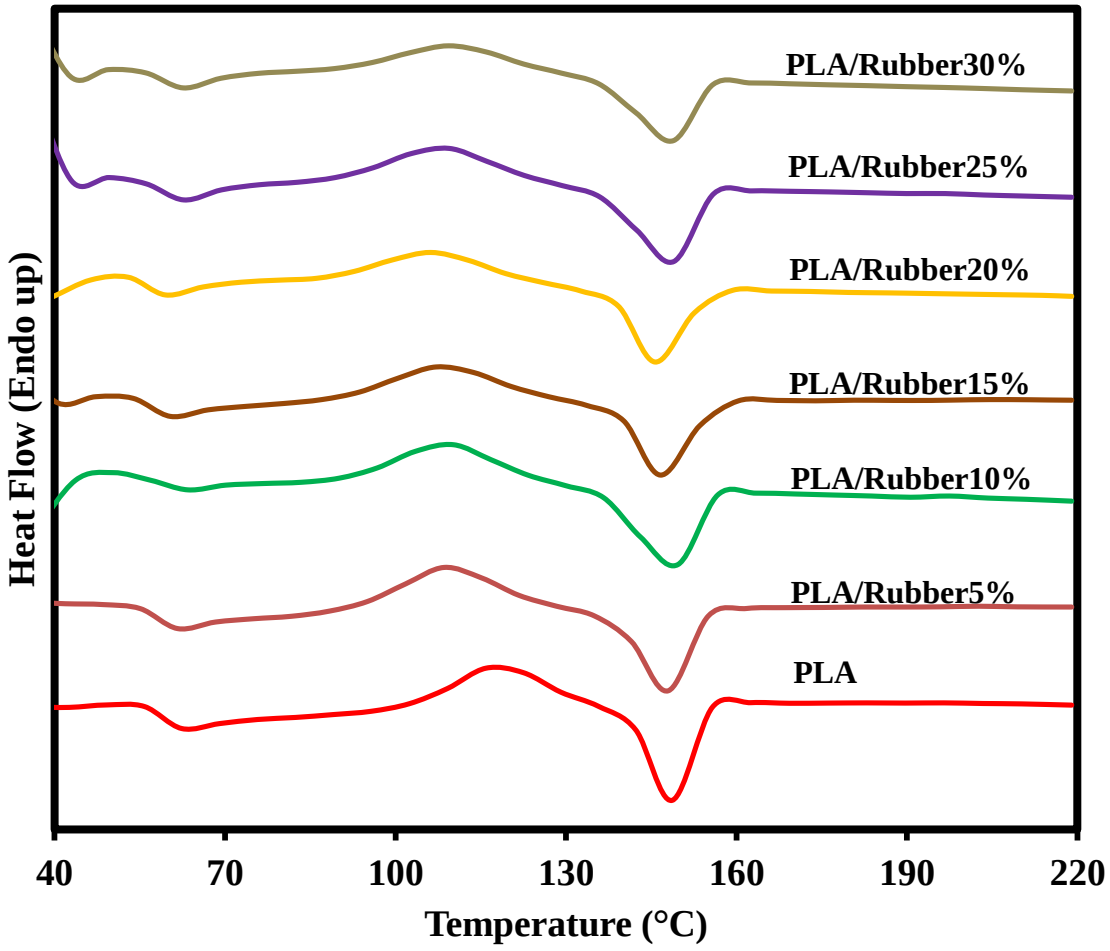

Figure V.16 DSC Thermograms of PLA an the Binary Blends at Different E-MA-GMA Rubber Concentrations.

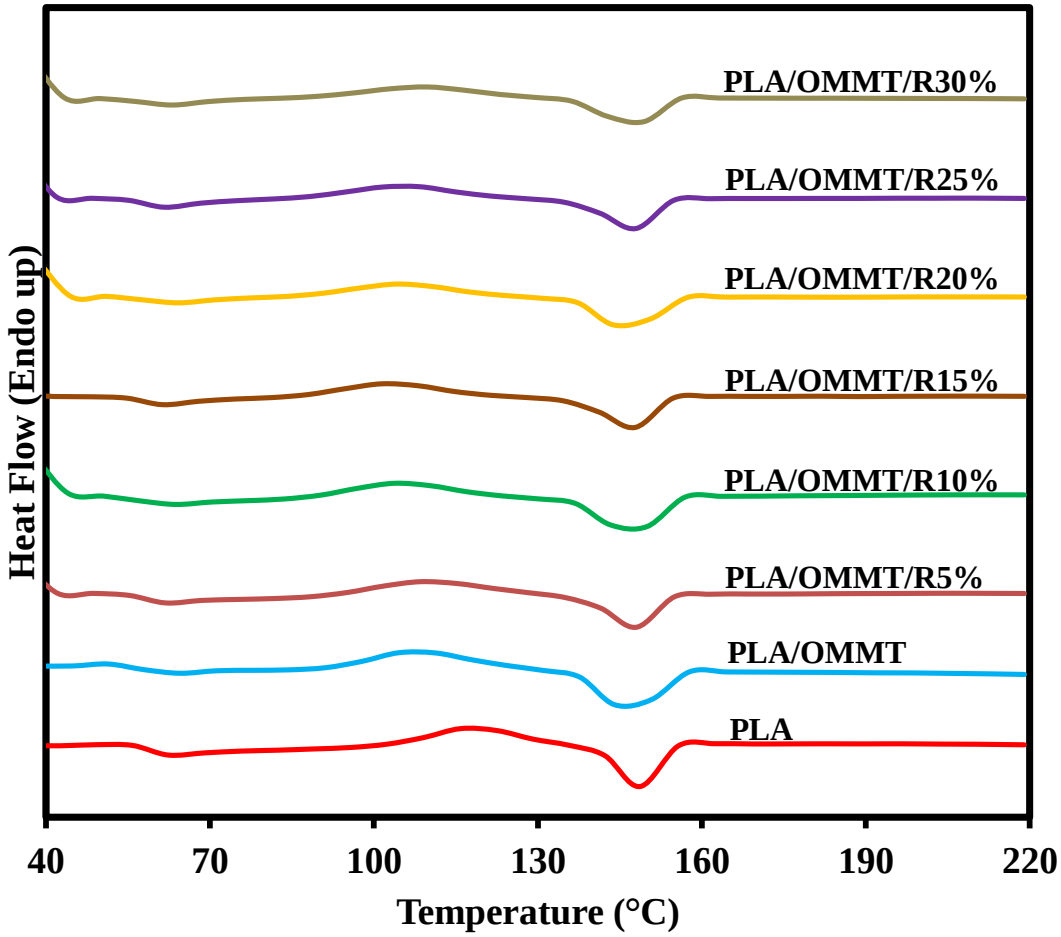

Figure V.17 DSC Thermograms of PLA an the Ternary Nanocomposites at different E-MA-GMA Rubber Concentrations.

The melting temperature of the rubber was recorded as 53.1°C, and its glass transition temperature that is below room temperature was not studied here. The thermogram of pure PLA is characterized by a glass transition temperature at 58.9°C, a crystallization exotherm at T_c=118.2°C, and a melting endotherm at T_m=152.7°C (**Table V.1**). As shown in this table, and considering the experimental error of the measurements, PLA in the binary blends and ternary nanocomposites exhibited the same glass transition temperature as the pure PLA, suggesting that PLA and the rubber were immiscible in the composition range studied. Similarly, Ishida et al. studied toughening of PLA with different types of rubbers, and the DSC thermograms of all the blends exhibited a single glass transition temperature, thus it was concluded that the compounds were immiscible.**[23]**

TABLE V.1
Thermal Parameters of PLA and the Binary Blends

SAMPLE	T_g (°C)	T_c (°C)	ΔH_c(J/g)	T_m (°C)	ΔH_m(J/g)	χ_c (%)
PLA	58.9	118.2	20.2	152.7	25.6	5.8
PLA/R5	57.3	109.5	23.3	152.4	27.7	5.0
PLA/R10	57.4	108.4	19.8	152.8	24.4	5.5
PLA/R15	57.6	107.8	19.4	152.6	24.9	6.9
PLA/R20	57.5	106.5	15.9	152.1	23.9	10.8
PLA/R25	57.9	108.2	13.8	152.2	22.4	12.3
PLA/R30	58.1	109.3	13.6	151.9	21.3	11.8

In the binary blends, the addition of the rubber had no significant effect on the melting temperature of the PLA. This suggests that the incorporation of the rubber did not change the crystal structure of PLA as also observed by Zeng et al. **[3]**. On the other hand, the crystallization temperature decreased substantially, after addition of only 5 wt% of rubber, and it dropped from 118.2 to 109.5°C due to the nucleating effect of the rubber that favors initiation and crystal growth at many sites. In a recent study, Petchwattana et al.**[24]** reported that addition of only 0.5 wt% ultrafine acrylate rubber did not affect the melting temperature of PLA, but it decreased the crystallization temperature. This result was attributed to the rubber particles that might have acted as nucleating sites for crystallization. It was also found that further increase of the rubber content inhibited crystallization. Oyama**[28]** reported that the dispersed poly(ethylene-glycidyl-methacrylate) rubber (EGMA) in PLA played the role of nucleating agent and promoted the crystallization of PLA, and further annealing of the blends for 2.5 hours at 90°C resulted in super-tough PLA blends. **Table V.1** shows that in general the degree of crystallization of the binary blends increased with higher rubber loading, possibly due to the chemical reaction between the epoxy groups of the rubber and the carboxyl and hydroxyl terminal groups of PLA and the likely polar interactions of their ester groups that increased the viscosity of the system. According

to Oyama,**[28]** the high viscosity causes a high shear force during mixing and pulls out the copolymer formed by the reaction of PLA and EGMA at the interface, to the PLA matrix. In the present study, it is believed that this phenomenon has also occurred in our PLA based blends and the pull out of the copolymer from the interface to the bulk of the matrix induced the chain mobility necessary for crystallization, thus the degree of crystallization increased.

Table V.2 indicates that the incorporation of 2 wt% OMMT into PLA did not significantly affect the melting temperature and glass transition temperature of PLA as also found by Chow et al..**[16]** On the other hand, the crystallization temperature was drastically decreased from 118.2 to 107.6°C. This is ascribed to the nucleation effect of the clay owing to its large surface area.**[20,29]** The intercalated/exfoliated structure as observed by XRD and TEM could also have contributed to the increase in the nucleating sites as reported by Balakrishnan et al..**[20]** Similar results were also reported by other research groups.**[12,16]** The degree of crystallinity of PLA/OMMT was lower than that of the neat PLA. This might be due to the hindrance caused by exfoliated/intercalated structure of the organoclay that reduced the mobility of polymer chains.**[15,29]**

TABLE V.2
Thermal Parameters of PLA and the Ternary Nanocomposites

SAMPLE	T_g (°C)	T_c (°C)	ΔH_c(J/g)	T_m (°C)	ΔH_m(J/g)	χ_c (%)
PLA	58.9	118.2	20.2	152.7	25.6	5.8
PLA/OMMT	57.5	107.6	23.2	151.7	26.2	3.3
PLA/OMMT/R5	57.0	109.7	21.3	151.9	26.6	6.1
PLA/OMMT/R10	57.7	105.2	17.1	151.8	25.6	10.4
PLA/OMMT/R15	57.8	103.2	16.5	151.1	23.1	8.6
PLA/OMMT/R20	58.5	104.9	15.9	151.3	20.4	6.3
PLA/OMMT/R25	58.5	105.5	14.4	151.4	19.8	8.0
PLA/OMMT/R30	58.1	108.8	14.4	151.2	19.2	7.6

The crystallization temperatures of the ternary nanocomposites are generally lower in comparison to the crystallization temperatures of the binary blends that have the same quantity of rubber (**Tables V.1 and V.2**). This is also attributed to the nucleating effect of the nanofiller.**[20,29]** In the ternary nanocomposites with 5-10 wt% rubber, the viscosity increased (MFI decreased) in comparison to that of PLA/OMMT as shown in **Figure V.15** The degree of crystallization increased owing to the effect described by Oyama**[28]** overcoming the hindrance effect of the clay. In the ternary nanocomposites with 15-20 wt% rubber, the viscosity decreased (**Figure V.15**), thus the chain mobility is expected to be enhanced. However, in this range, the degree of crystallization decreased that might be attributed to immobilization of the polymer molecules by clay. In the ternary nanocomposites with 20-30 wt% of rubber, the degree of crystallization levels up owing to high viscosity and the constraining effect of the clay. Both of these factors reduce chain mobility needed for crystallization. The effect described by Oyama**[28]** did not take place at this high level of rubber content possibly due to saturation of the interface corresponding to maximum interactions.**[46]**

V-6 CONCLUSIONS

PLA was successfully toughened by melt blending with E-MA-GMA rubber in the range of 5 to 30 wt% using a twin screw extruder. Organoclay was added at 2 wt% to compensate the decrease in other mechanical properties. XRD and TEM showed that PLA/OMMT binary nanocomposite exhibited intercalated/exfoliated structure with some remaining tactoids. Addition of the rubber promoted dispersion of the OMMT by intercalating with PLA molecules into the clay galleries. At 10 wt% rubber content exfoliation was observed. Beyond this rubber content, intercalated/exfoliated structure reappeared and no further enhancement in dispersion was observed.

The morphology revealed by SEM showed that PLA and E-MA-GMA were immiscible in the range of rubber content studied, and the rubber formed the dispersed phase. The addition of rubber changed the brittle behavior of PLA to ductile by inducing debonding and/or cavitation. The rubber domain size increased with

increasing rubber content in both the blends and nanocomposites. The nanocomposites exhibited coarser morphology suggesting that the clay did not act as a barrier for the coalescence owing to its likely preferential location in the rubber.

The impact strength and the elongation at break were improved in the binary blends and ternary nanocomposites at the expense of stiffness and strength. In the ternary nanocomposites, the best balance of these properties was observed at 10 wt% rubber content.

The viscosity of the blends and nanocomposites, evaluated by MFI measurements, was highly influenced by the rubber and the clay. The MFI of the binary blends decreased with increasing rubber content up to 25 wt% rubber. In the ternary nanocomposites, an increase of the MFI was observed up to 20 wt% rubber content owing to the plasticization effect of the dissolved organoclay surfactant, and beyond this rubber content, the MFI decreased owing to the highly viscous rubber content.

DSC analysis showed that the T_g of PLA in the blends and nanocomposites was not significantly influenced by the presence of the rubber confirming the immiscibility of the mixtures. Both the clay and the rubber decreased the crystallization temperature of PLA and acted as nucleating agents for PLA and affected its crystallization.

REFERENCES

[1] Su, Z.; Li, Q.; Liu, Y.; Hu, G.; Wu, C. Eur. Polym. J., Vol. 45, pp 2428 **(2009)**.

[2] Kumar, M.; Mohanty, S.; Nayak, S. K.; Parvaiz, M. R. Biores. Techn., Vol. 101, pp 8406 **(2010)**.

[3] Zeng, J.; Li, Y.; He, Y. ; Li, S.; Wang, Y. Ind. Eng. Chem. Res., Vol. 50, pp 6124 **(2011)**.

[4] Sun, S.; Zhang, M.; Zhang, H.; Zhang, X. J. Appl. Polym. Sci., Vol. 122, pp 2992 **(2011)**.

[5] Liu, H.; Zhang, Z. J. Polym. Sci. Part B: Polym. Phys., Vol. 49, pp 1051 **(2011)**.

[6] Meng, B.; Tao, J.; Deng, J.; Wu, Z.; Yang, M. Mater. Lett., Vol. 65, pp 729 **(2011)**.

[7] Ljungberg, N.; Andersson, T.; Wesslén, B. J. Appl. Polym. Sci., Vol. 88, pp 3239 **(2003)**.

[8] Martino, V. P.; Jiménez, A.; Ruseckaite, R. A. J. Appl. Polym. Sci., Vol. 112, pp 2010 **(2009)**.

[9] McManus, A. J.; Doremus, R.; Siegel, R.; Bizios, R. J. Biomed. Mater. Res., Vol. 72A, pp 98 **(2005)**.

[10] Kasuga, T.; Maeda, H.; Kato, K.; Nogami, M.; Hata, I.; Ueda M. Biomaterials, Vol. 24, pp 3247 **(2003)**.

[11] Kasuga, T.; Ota, Y.; Nogami, M.; Abe, Y. Biomaterials, Vol. 22, pp 19 **(2001)**.

[12] Marras, S. I.; Zuburtikudis, I.; Panayiotou, C. Eur. Polym. J., Vol. 43, pp 2191 **(2007)**.

[13] Carrascoa, F.; Gamez-Perez, J.; Santanac, O. O.; Maspoch, M. Ll. Chem. Eng. J., Vol. 178, pp 451 **(2011)**.

[14] Chow, W. S. ; Lok, S. K. J Thermo. Comp. Mat., Vol. 21, pp 265 **(2008)**.

[15] Kusmono; Ishak, Z.; Chow, W. S.; Takeichi, T.; Rochmadi Euro. Polym. J., Vol. 44, pp1023 **(2008)**.

[16] Chow, W. S.; Lok, S. K. J. Therm. Calorim., Vol. 95, pp 627 **(2009)**.

[17] Chang, J.H.; An, Y . U.; Cho, D.; Giannelis, E. P. Polymer, Vol. 44, pp 3715 **(2003)**.

[18] Yokohara, T.; Yamaguchi, M. Eur. Polym. J., Vol. 44, pp 677 **(2008)**.

[19] Broz, M. E.; VanderHart, D. L.; Washburn, N. R. Biomaterials, Vol. 24, pp 4181 **(2003)**.

[20] Balakrishnan, H.; Hassan, A.; Wahit, M. U.; Yussuf, A. A.; Abdul Razak, S. B. Mat. Des., Vol. 31, pp 3289 **(2010)**.

[21] Lee, J. B.; Lee, Y. K.; Choi, G. D.; Na, S. W.; Park, T. S.; Kim, W. N. Polym. Degrad. Stab., Vol. 96, pp 553 **(2011)**.

[22] Nijenhuis, A.J.; Colstee, E.; Grijpma, D. W.; Pennings, A. J. Polymer, Vol. 37, pp 5849 **(1996)**.

[23] Ishida, S.; Nagasaki, R.; Chino, K.; Dong, T.; Inoue, T. J. Appl. Polym. Sci., Vol. 113, pp 558 **(2009)**.

[24] Petchwattana, N.; Covavisaruch, S.; Euapanthasate, N. Mat. Sci. Eng. A., Vol. 532, pp 64 **(2012)**.

[25] Theryo, G.; Jing, F.; Pitet, L. M.; Hillmyer, M. A. Macromolecules, Vol. 43, pp 7394 **(2010)**.

[26] Li, Y.; Shimizu, H. Macromol Biosci, Vol.7, pp 921 **(2007)**.

[27] Zhang, C.; Man, C.; Pan, Y.; Wang, W.; Jiang, L.; Dan, Y. Polym. Int., Vol. 60, pp 1548 **(2011)**.

[28] Oyama, H. T. Polymer, Vol. 50, pp 747 **(2009)**.

[29] Leu, Y. Y.; Mohd Ishak, Z. A.; Chow, W. S. J. Appl. Polym. Sci., Vol. 124, pp 1200 **(2012)**.

[30] Ho, C.; Wang, C.; Lin, C.; Lee, Y. Polymer, Vol. 49, pp 3902 **(2008)**.

[31] Hashima, K.; Nishitsuji, S.; Inoue, T. Polymer, Vol.51 , pp 3934 **(2010)**.

[32] Bitinis, N.; Verdejo, R.; Maya, E. M.; Espuche, E.; Cassagnau, P.; Lopez-Manchado, M.A. Comp. Sci. Tech., Vol. 72, pp 305 **(2012)**.

[33] Mélo, T.J.A.; Araújo, E.M.; Brito, G.F.; Agrawal, P., J. Alloys Comp., Vol. 615, S389 **(2014)**.

[34] Yeniova, C.; Yilmazer, U. Polym. Comp., Vol. 31, pp 1853 **(2010)**.

[35] Paul, M.A.; Delcourt, C.; Alexandre, M.; Degee, P.; Monteverde, F.; Rulmont, A. ; Dubois, P., Macromol. Chem. Phys., Vol. 206, pp 484 **(2005)**.

[36] Di, Y.; Iannace, S.; Maio, E.D.; Nicolais, L.; J. Polym. Sci. Part B: Polym. Phys., Vol. 43, pp 689 **(2005)**.

[37] Paul, M.A.; Delcourt, C.; Alexandre, M.; Degee, P.; Monteverde, F. ; Dubois, P., Polym. Degrad. Stab., Vol. 87, pp 535 **(2005)**.

[38] McLauchlin, A.R. and Thomas, N.L., Polym. Degrad. Stab., Vol. 94, pp 868 **(2009)**.

[39] Pluta, M.; Paul, M.A.; Alexandre, M.; Dubois, P., J. Polym. Sci. Part B: Polym. Phys., Vol. 44, pp 299 **(2006)**.

[40] Zhou, Q. and Xanthos, M., Polym. Degrad. Stab., Vol. 93, pp 1450 **(2008)**.

[41] Li, T.; Turng, L.S.; Gong, S.; Erlacher, K., Polym. Eng. Sci., Vol. 46, pp 1419 **(2006)**.

[42] Martins, C. G.; Larocca, N. M.; Paul, D. R.; Pessan, L. A. Polymer, Vol. 50, pp 1743 **(2009)**.

[43] Alyamac, E.; Yilmazer, U. Polym. Comp., Vol. 28, pp 251 **(2007)**.

[44] He, S.; Wu, W.; Wang, R.; Pu, W.; Chen, Y. Polym.-Plast. Technol. Eng., Vol. 50, pp 719 **(2011)**.

[45] Chow, W. S.; Neoh, S. S. Polym.-Plast. Technol. Eng., Vol. 49, pp 62 **(2010)**.

[46] Baouz, T.; Fellahi, S. J. Appl. Polym. Sci., Vol. 98, pp 1748 **(2005)**.

[47] Coskunses, F. I.; Yilmazer, U. J Appl. Polym. Sci., Vol. 120, pp 3087 **(2011)**.

[48] Okada, A. Mater. Sci. Eng. C, Vol. 3, pp 109 **(1995)**.

[49] Yu, Z. Z.; Hu, G. H.; Varlet, J.; Dasari, A.; Mai, Y. W. J. Polym. Sci. Part B: Polym. Phys., Vol. 43, pp 1100 **(2005)**.

Chapter VI

Effects of Mixing Protocols on Impact Modified Poly(lactic acid) Layered Silicate Nanocomposites

Chapter VI - Effects of Mixing Protocols on Impact Modified Poly(lactic acid) Layered Silicate Nanocomposites

VI-1 Introduction

PLA is at the forefront of biopolyesters that competes well with many available synthetic polymers owing to its good mechanical and physical properties, biocompatibility, ease of processability and much more importantly its renewability. However, the low toughness of PLA and its low tensile elongation have been the major bottle neck for its large applications, consequently significant engineering efforts have been made to overcome PLA brittleness and to widen its window of applications.**[1-3]**

Toughening of PLA by flexible polymers has gained much attention.**[1-10]** To compensate the softening effect of the toughener, addition of nanofillers, mostly organomodified montmorillonite (OMMT), was considered to form nanocomposites.**[11-17]** It is generally known that the performance of toughened blends depends on various parameters such as components ratios and their properties, interfacial adhesion between the components, rubber particle size and shape, processing conditions and preparation methods, etc.**[6,8]** In this context, the effect of addition procedure on the performance and properties of ternary nanocomposites has been examined for many systems, including PA6/EPR-g-MAH/OMMT,**[18]** LDPE/E-MA-GMA/OMMT,**[19]** PS/SEBS-g-MAH/OMMT,**[20]** PET/E-MA-GMA/OMMT,**[21]** PP/PP-g-AA/EVA/OMMT,**[22]** and others.**[23-26]** Borah et al.**[23]** studied LLDPE/EMA/OMMT using three different compounding protocols and two types of OMMT. It was found that the morphology and the properties of the nanocomposites were dependent on the blending sequence and on the type of the clay used. The Cloisite®25A clay migrated from the LLDPE phase to the EMA phase at a surprisingly high rate and the corresponding nanocomposites exhibited high impact strength as compared with the neat blend. However, Cloisite®30B clay was mainly located at the interface of LLDPE and EMA, and the compound exhibited low impact strength. In PA6/ABS/OMMT using SMA as a compatibilizer, the OMMT was

preferentially located in the PA6 matrix in exfoliated state irrespective of the compounding mode, and the morphology of ABS dispersed phase was reported to be highly altered by the mixing sequence, which in turn affected the mechanical properties.**[24]** The x-ray diffraction (XRD) results of PA66/SEBS-g-MAH/OMMT showed exfoliated structure regardless of the preparation order, whereas TEM observations indicated that OMMT location was affected by the mixing procedure.**[25]** Moreover, the OMMT in the matrix or at the interface was found in the exfoliated state, but the clay that was enclosed in the rubber was only intercalated as a result of the high affinity of clay to PA66, suggesting that clay dispersion cannot be determined solely on the basis of XRD, but needs to be complemented by visual tools such as TEM. Dasari et al.**[26]** found that the microstructure and mechanical properties of PA66/SEBS-g-MAH/OMMT ternary nanocomposite were extremely influenced by order of mixing of nanocmoposite components. They concluded that for PA66/SEBS-g-MAH/OMMT, it is beneficial in terms of impact strength to have the maximum amount of the exfoliated organoclay in the PA66 matrix, because the presence of OMMT in the rubber phase decreases its cavitation ability as a result of the stiffening effect of OMMT and accordingly it reduces the toughening efficiency

This chapter reports, the results concerning the effects of four different melt compounding protocols on the performance of rubber-toughened PLA nanocomposites prepared using ethylene-methyl acrylate glycidyl methacrylate (E-MA-GMA) impact modifier and 2 wt% OMMT melt mixed in co-rotating twin screw extruder. The structure and the morphology of the nanocomposites were observed by XRD, transmission electron microscopy (TEM) and scanning electron microscopy (SEM), their mechanical performance was evaluated by tensile and impact tests and their thermal characteristics were measured by differential scanning calorimetry (DSC).

RESULTS AND DISCUSSION

VI-2 Morphology

VI-2-1 X-ray Diffraction (XRD) Analyses

X-ray diffraction patterns of the PLA and the rubber did not show any characteristic basal diffraction peak in the studied range of 2θ=1-10°. However, the pure OMMT powder displayed a single strong characteristic peak at 2θ=4.78° corresponding to an interlayer spacing d=1.85 nm (OMMT in **Figure VI.1**).

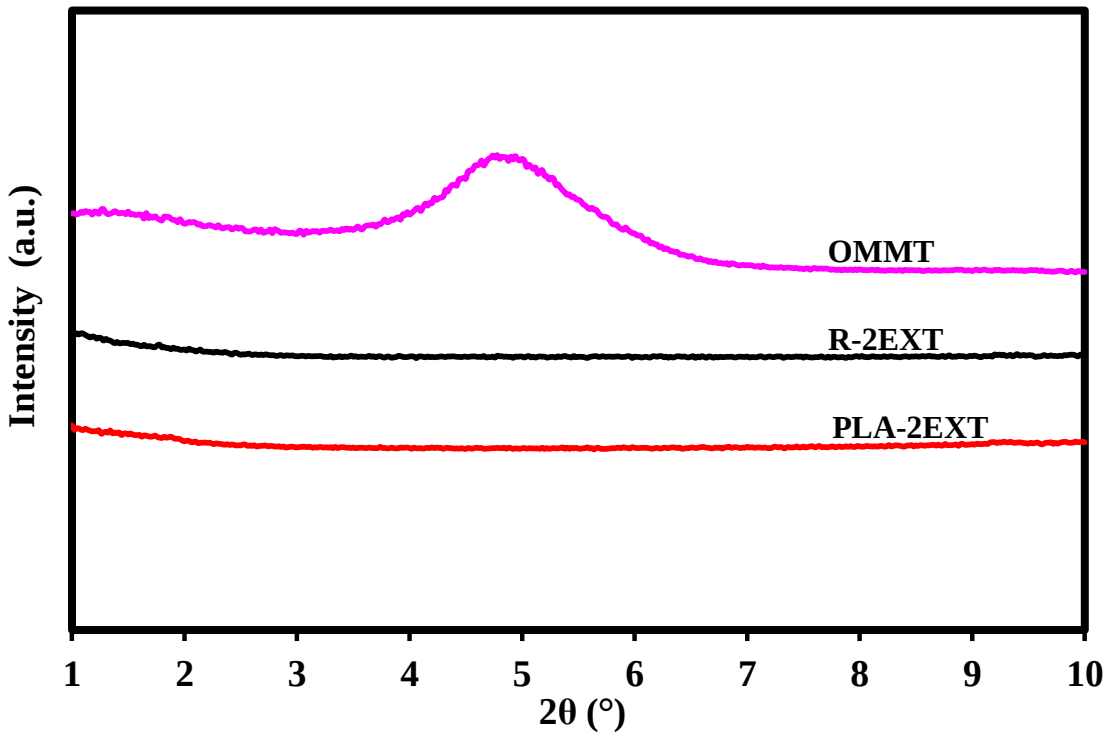

Figure VI.1 X-ray Patterns of PLA extruded twice (PLA-2EXT), Rubber "E-MA-GMA" extruded twice (R-2EXT) and Cloisite®30B (OMMT).

The characteristic peak of the OMMT in the binary PLA/OMMT nanocomposite extruded once was shifted to a lower angle 2θ=2.56° (d=3.45 nm) (PLA/OMMT-1EXT in **Figure VI.2**). This increase in the reflection spacing of the clay indicates intercalation of the PLA molecules between the clay galleries that disrupt and decrease the electrostatic attraction between the clay nanosheets giving rise to expansion of their parallel interlayer distances.**[19]** This PLA intercalation between

clay nanoplatelets is attributed to the favorable interactions of the PLA carboxyl (COOH) end groups with the hydroxyl (OH) entities of the clay surfaces and those of its surfactant modifier.**[6,12,19]** Another OMMT peak with low intensity was observed at a higher angle 2θ=5.36° (d=1.65 nm) than that of pure clay, because of the presence of tactoids (PLA/OMMT-1EXT in **Figure VI.2**). Clays are generally modified with an excess of surfactants**[27]**, thus the decrease in the original interlayer spacing of the OMMT is believed to be due to the collapse of the clay galleries resulting from the dissolution of some surfactant parts from clay galleries into polymer matrix**[22,23]** and/or to rearrangement of the alkyl ammonium chains of the OMMT.**[19]** Another possible reason to the collapse of the clay, is the thermal degradation of the clay surfactant**[22,23]**, but this has been ruled out because the organoclay is reported to be stable at the processing temperature of 170°C used in this study. In fact, in their study of PET/clay nanocomposites and based on their TGA measurements, Ghasemi et al.**[28]** reported that Cloisite® 30B degrades at 233°C recorded at a weight loss of 5% ($T_{5\%}$).

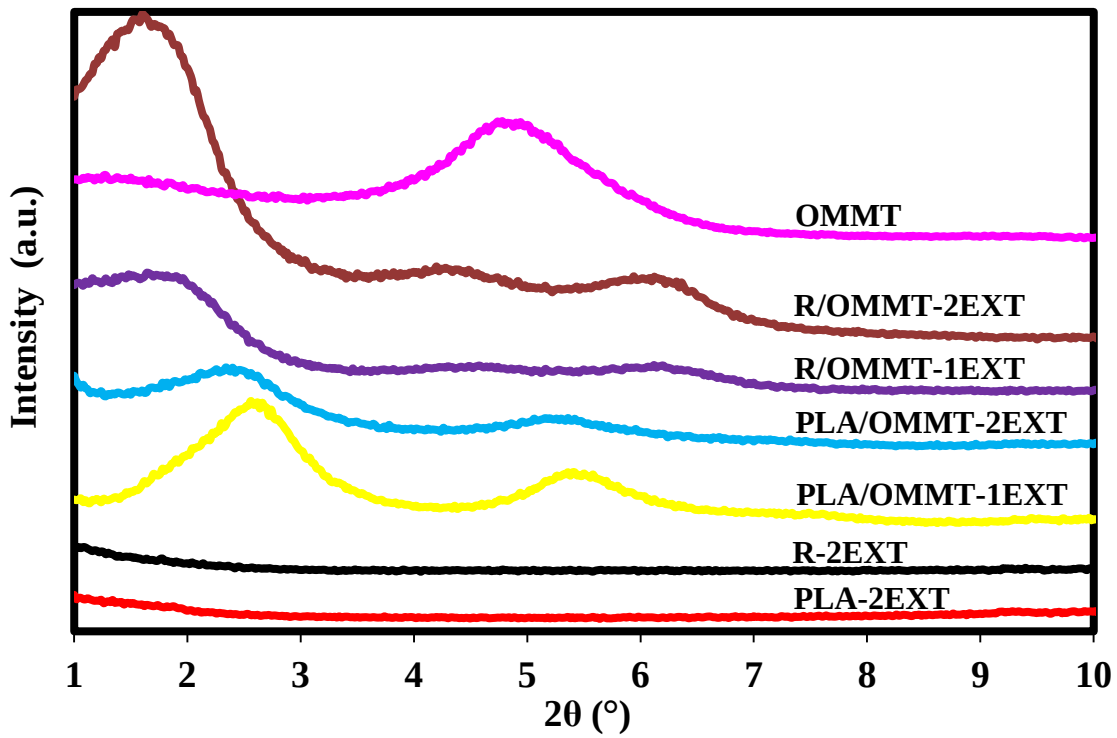

Figure VI.2 X-ray Patterns of PLA, Rubber (R), OMMT and their Corresponding Nanocomposites at 2 wt% OMMT.

When PLA/OMMT was extruded twice, the intensity of its two characteristic peaks was decreased and the peaks were shifted to lower angles 2θ=2.34° (d=3.78 nm) and 2θ=5.16° (d=1.71 nm) owing to the longer residence time of the nanocomposite in the extruder, that caused longer duration of shear applied on clay particles that is important for their delamination, and also caused longer duration of interactions between reactive groups of PLA and those of the clay surfaces and its surfactant (PLA/OMMT-2EXT in **Figure VI.2)**.

The XRD traces of the rubber-based nanocomposite extruded once (R/OMMT-1EXT) exhibited three characteristic peaks on its diffractogram recorded at 2θ=1.64° (d=5.39 nm), 2θ=4.48° (d=1.97 nm) and 2θ=6.12° (d=1.44 nm) (R/OMMT-1EXT in **Figure VI.2**). This indicates low intercalation degree of the rubber owing to its higher molecular weight (high viscosity) and lower polarity (lower affinity to clay) compared with PLA, and also to its bulky GMA groups making its intercalation into clay interlayers difficult. Subjecting this nanocomposite to a second extrusion process did not improve the dispersion of clay, because its x-ray traces revealed the same peaks at the same positions (R/OMMT-2EXT in **Figure VI.2**).

To get more insight into the intercalation process, the difference between the rubber and the PLA, the PC and CI intermediate nanocomposites were also studied (PC and CI are the intermediate nanocomposites prepared in the first extrusions steps to form PC-I and CI-P nanocomposites). The PC intermediate nanocomposites showed the two PLA/OMMT characteristic peaks of nearly the same intensities shifted to lower angles that varied from 2θ=2.50° (d=3.53 nm) to 2θ=2.12° (d=4.17 nm) and from 2θ=5.40° (d=1.64 nm) to 2θ=4.84° (d=1.83 nm) as the clay level increased suggesting improved clay dispersion (**Figure VI.3**). The CI nanocomposites exhibited three peaks as those of the R/OMMT-1EXT situated at almost the same positions 2θ=1.58° (d=5.59 nm), 2θ=4.38° (d=2.02 nm) and 2θ=6.10° (d=1.45 nm) indicating nearly identical clay dispersion for all the clay contents (**Figure VI.4**). The peak at 2θ=6.10° points out to the appreciable collapse of the clay galleries, the intensity of which decreases as the clay content decreases. These results show that PLA intercalates better than the rubber for the same reasons stated earlier.

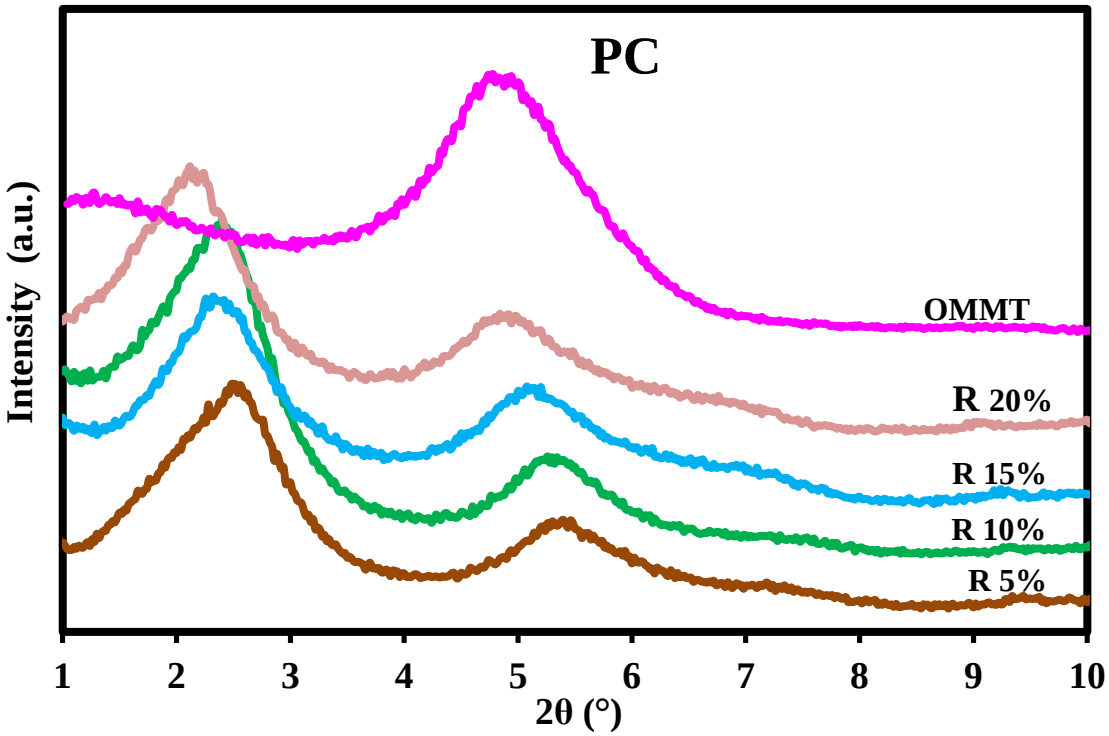

Figure VI.3 X-ray Patterns of OMMT and PC Intermediate Nanocommposites. (The R Indicates the Rubber, and the Percentages Designate its wt% in the Nanocomposites). The Curves are Shifted Vertically for Clarity.

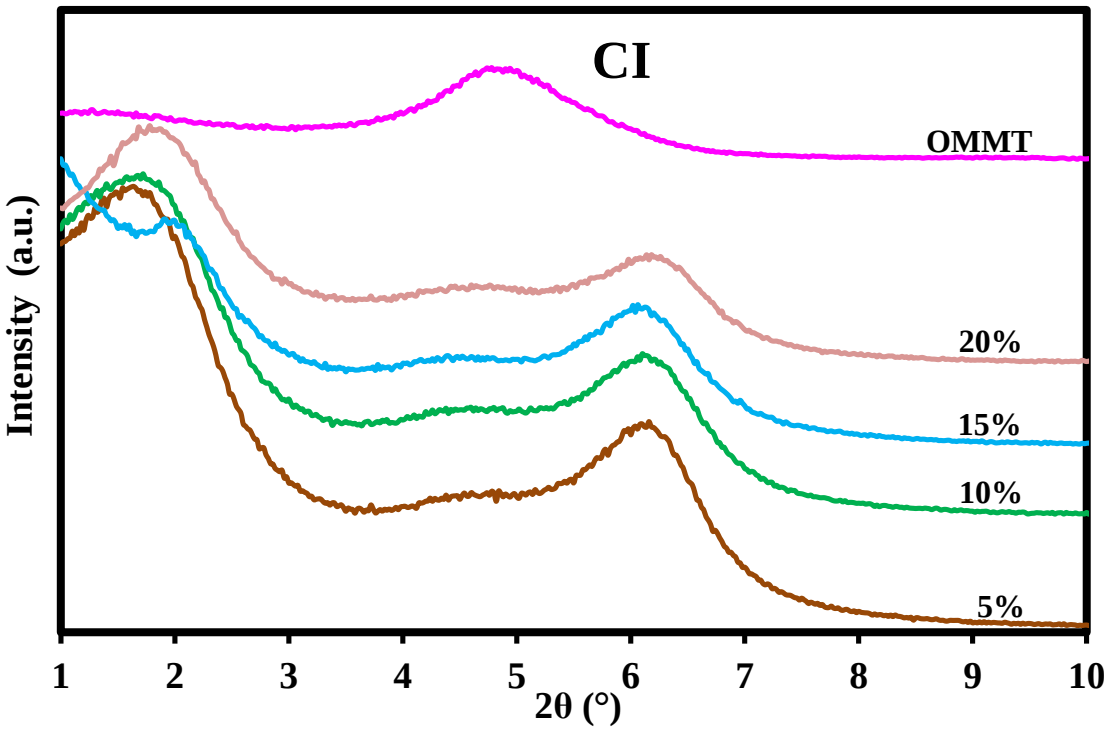

Figure VI.4 X-ray Patterns of OMMT and CI Intermediate Nanocommposites. (The R Indicates the Rubber, and the Percentages Designate its wt% in the Nanocomposites). The Curves are Shifted Vertically for Clarity.

Figures VI.5-VI.8 depict the clay dispersion in each blending mode. As it can be seen on these figures, all of the addition sequences studied led to intercalated/partially exfoliated nanostructures where the characteristic peak of the clay in the nanocomposites shifted to lower angles. Considering PC-I, the addition of 5 wt% rubber to the PC nanocomposite shown in **Figure VI.3**, shifted its two peaks from 2θ=2.50° (d=3.53 nm) and 2θ=5.40° (d=1.64 nm) to 2θ=1.98° (d=4.46 nm) and 2θ=5.16° (d=1.71 nm) (**Figure VI.5**).

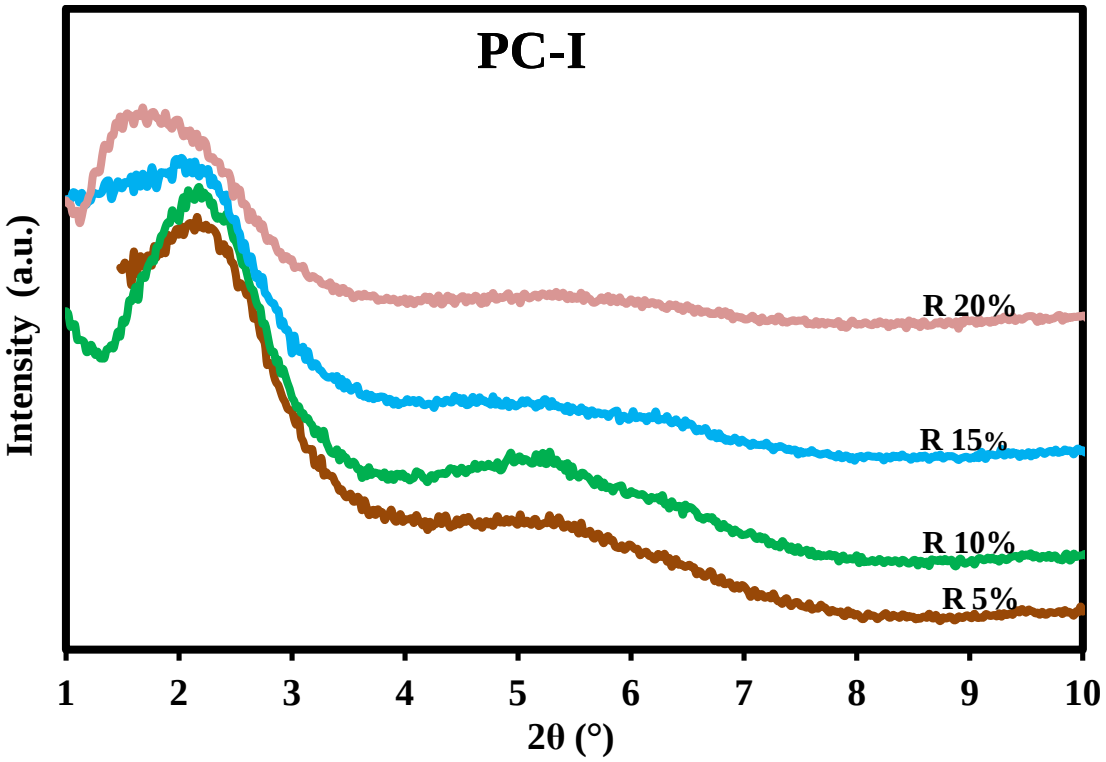

Figure VI.5 X-ray Diffractograms of PC-I Nanocomposites Prepared at Various Rubber Contents and 2 wt% OMMT. (The R Indicates the Rubber, and the Percentages Designate its wt% in the Nanocomposites). The Curves are Shifted Vertically for Clarity.

As the rubber content increased, the dispersion of clay was enhanced and better intercalated/partially exfoliated structures are observed at and above 15 wt% rubber ratio with absence of tactoids. Indeed, at 20 wt% rubber fraction, the peak at the highest diffraction angle nearly disappeared and the second one is shifted to 2θ=1.76° (d=5.02 nm). This suggests additional intercalation (co-intercalation) of the rubber into the basal spacing of the clay where PLA chains had already penetrated thus resulting in additional expansion of the interlayers of the clay sheets.**[6,14]** This occurs due to

the viscosity build up imparted by the rubber to the system that promoted high shear intensity favoring more clay nanoplatelets delamination.**[6,19-22]** Furthermore, in the PC-I sequence, both PLA and clay experienced extrusion twice contributing to improved clay dispersion by promoting more PLA molecules to diffuse into the clay spacings. In addition, this fine clay dispersion arose due to the polar interactions of the rubber and PLA ester groups, and to the chemical reaction between the rubber epoxy moieties with terminal (COOH) and (OH) groups of the PLA**[3-8]** and with the (OH) groups of the clay surfaces and those of its surfactant. The reactions of the (COOH) and (OH) groups with the epoxy groups were identified by FTIR by Yeh et al**.[3]** and Juntuek et al..**[4]** The schematic representation of these reactions was published by Sun et al.,**[5]** and their mechanism in the presence of a catalyst was discussed by Oyama et al..**[29]**

For PI-C nanocomposites, when the rubber extent was 5 wt%, the OMMT diffraction peak shifted to lower angle 2θ=2.10° (d=4.21 nm) which remained at almost the same position for all the rubber contents (**Figure VI.6**). The second peak recorded at 2θ=5.12° (d=1.73 nm) indicate that there are remaining tactoids in the 5 wt% PI-C nanocomposite. At 10 wt% rubber content, the intensities of the peaks decreased and the peak at 2θ=5.12° (d=1.73 nm) shifted to 2θ=4.90° (d=1.80 nm) pointing out to better dispersion. At 20 wt% rubber content, in addition to the two peaks detected at the same positions as in the 10 wt% nanocomposite, a third peak at 2θ=6.42° (d=1.38 nm) appeared. The third peak indicates low clay dispersion state owing to the chain extension induced by the reaction between the PLA and the rubber functional groups restricting the chain mobility of the PLA and the rubber molecules to enter into the clay galleries.**[3,5-9,11]** PI-C exhibited lower clay dispersion levels compared with PC-I, because the interactions between the PLA and the rubber were maximized during the first extrusion step (formation of PI) which reduced the total reactive groups of the polymers to interact with the clay. In addition, in the PI-C mixing order the clay was mixed only once with the polymers, whereas in PC-I it was extruded twice with the polymers.

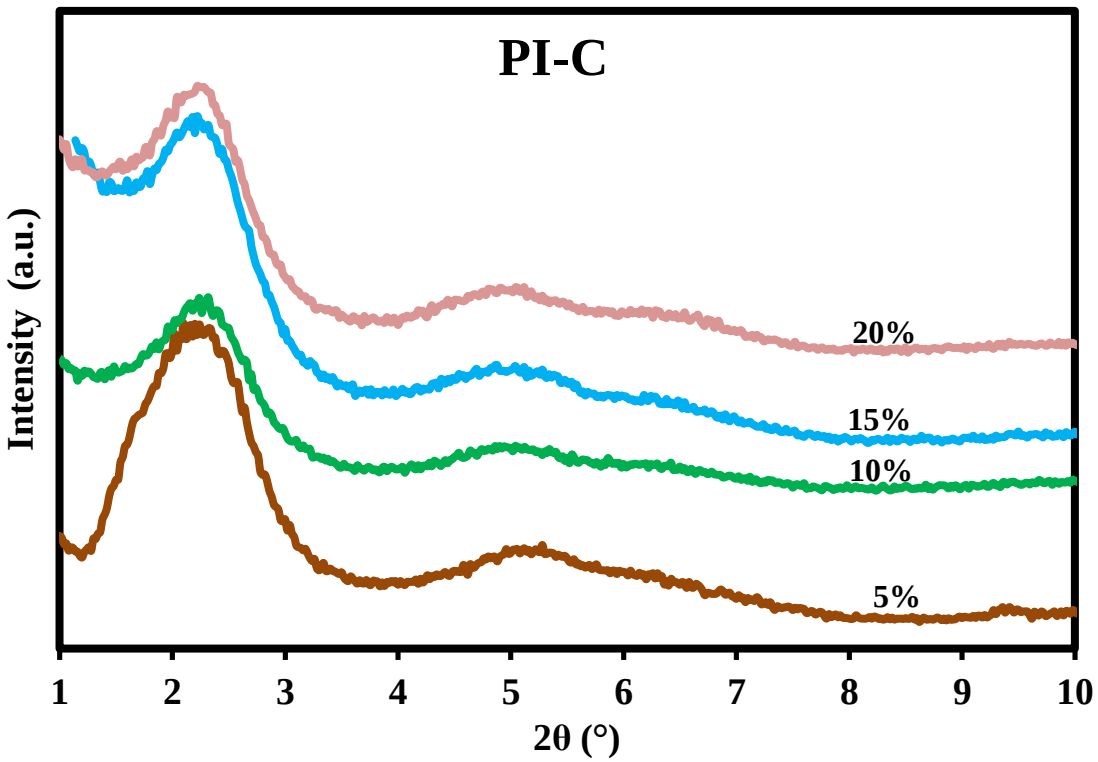

Figure VI.6 X-ray Diffractograms of PI-C Nanocomposites Prepared at Various Rubber Contents and 2 wt% OMMT. (The R Indicates the Rubber, and the Percentages Designate its wt% in the Nanocomposites). The Curves are Shifted Vertically for Clarity.

All diffractograms of CI-P nanocomposites exhibited nearly the same trend as observed in their CI intermediates with three distinct peaks positioned at the same diffraction angles regardless of the rubber ratio implying almost the same clay dispersion in these nanocomposites (**Figure VI.7**). In these mixtures, both intercalation and re-agglomeration of previously dispersed clay in the CI compounds took place. The peak at 2θ=6.10° (d=1.45 nm) was observed at the same position as in CI compounds but with lower intensities associated with reduced amount of tactoids owing to the additional intercalation by the added PLA into the clay galleries. The two peaks at 2θ=1.58° (d=5.59 nm) and 2θ=4.38° (d=2.02 nm) in CI mixtures increased in intensity and shifted to higher angles located at 2θ=2.10° (d=4.21 nm) and 2θ=4.66° (d=1.90 nm) when PLA was incorporated in the second extrusion run, suggesting the collapse of clay interlayers and/or re-agglomeration of the already expanded nanofiller in the CI compounds. Note that in this mixing mode, CI mixtures were extruded twice which was found to be deleterious on the dispersion of the clay as discussed previously

in the case of R/OMMT-2EXT (**Figure VI.2**). This fact explains the deterioration of the clay dispersion state when PLA was added in the second extrusion step to form CI-P nanocomposites.

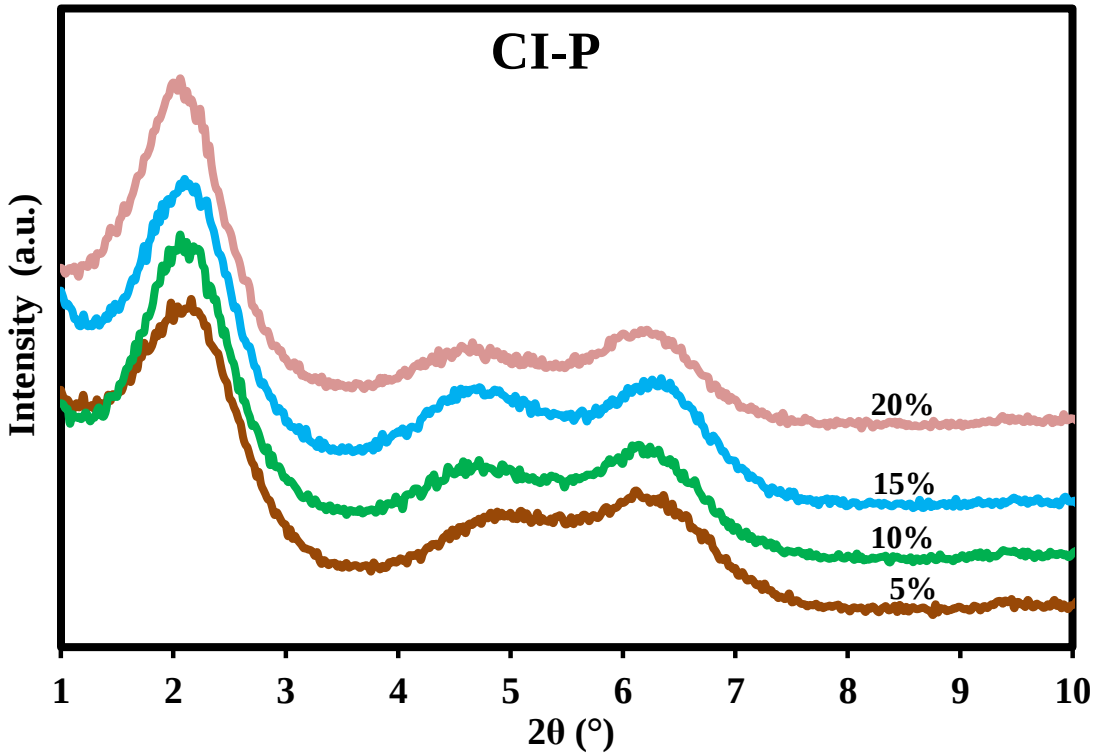

Figure VI.7 X-ray Diffractograms of CI-P Nanocomposites Prepared at Various Rubber Contents and 2 wt% OMMT. (The R Indicates the Rubber, and the Percentages Designate its wt% in the Nanocomposites). The Curves are Shifted Vertically for Clarity.

Figure VI.8 exemplifies the XRD patterns of the ALL-S extruded twice. It can be noticed that the diffractograms resemble those obtained for PI-C compounds but with diffraction angles shifted to lower angles with lower intensities designating better dispersion than that of PI-C. OMMT peak was shifted to 2θ=1.90° (d=4.65 nm) for all of the ALL-S nanocomposites, and the remaining tactoids were identified at 2θ=5.10° (d=1.73 nm) and at 2θ=4.90° (d=1.80 nm) when the rubber fraction was 5 wt% and 20 wt% respectively with the appearance of a third peak at 2θ=5.90° (d=1.50 nm) for this last composition. The highest level of dispersion is observed at 10 wt% rubber content with diffraction angles positioned at 2θ=1.90° (d=4.65 nm) and 2θ=4.78° (d=1.85 nm) which seems to be a critical concentration.

Better clay dispersion is exhibited in ALL-S nanocomposites compared with that of PI-C, because all the ingredients in ALL-S were fed at the same time into the extruder and were processed twice, consequently the interactions between the three ingredients were maximized, that is to say, the interactions between the polymers and the clay necessary for their intercalation into the clay galleries got the same chances to take place as those of these polymers between each other. However, in PI-C the interactions between polymers were favored in the first extrusion step during formation of PI, and the intercalation process was only accomplished during the second run which had affected the extent of dispersion owing to the short interaction time of the OMMT with the polymers.

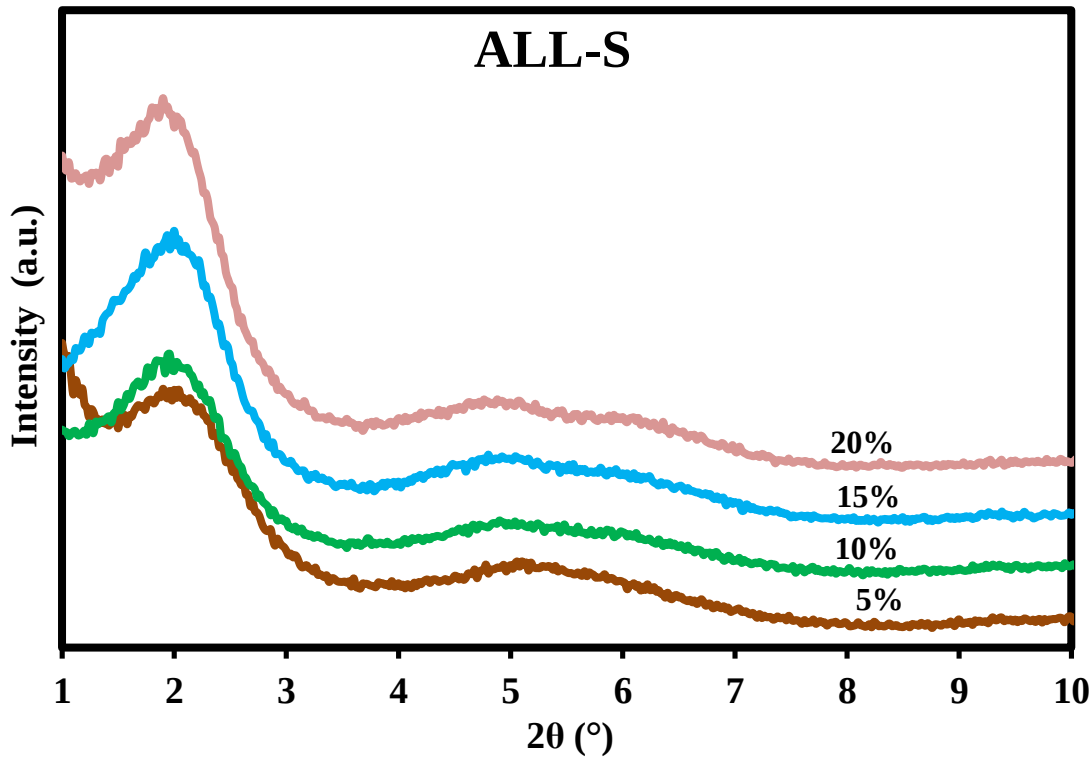

Figure VI.8 X-ray Diffractograms of ALL-S Nanocomposites Prepared at Various Rubber Contents and 2 wt% OMMT. (The R Indicates the Rubber, and the Percentages Designate its wt% in the Nanocomposites). The Curves are Shifted Vertically for Clarity.

VI-2-2 Transmission Electron Microscopy (TEM) Analyses

In complement to XRD analyses, the structure of the nanocomposites was revealed and investigated at the nanometer scale by TEM examinations of ultra-

microtomed sections. Selected TEM photomicrographs of the nanocomposites reporting typical morphologies observed at, at least, three different positions are shown in **Figures VI.9-VI.13**. All images attest to the formation of nanocomposites with structural characteristics consistent with the XRD analyses. In these micrographs, the base background represents the matrix, the dark lines and darker entities are the clay nanoplatelets and their stacks successively.

The bright field TEM photomicrograph at low magnification of PLA/OMMT nanocomposite extruded twice (PLA/OMMT-2EXT)) reveals that clay nanosheets were uniformly and randomly dispersed in the PLA (**Figure VI.9(a)**). Upon zooming to a higher magnification, the TEM image of this binary mixture displays a hybrid structure composed of intercalated/partially exfoliated clay with numerous individual isolated silicate nanoplatelets and coexistence of thin primary clay tactoids and absence of agglomerates (**Figure VI.9(b)**). Such structure originated, as aforementioned, from the strong interactions between PLA (COOH) terminal groups and hydroxyl (OH) entities of OMMT nanoplatelet surfaces and those of its ammonium surfactant. These visual observations are in close accordance with the XRD results on PLA/OMMT.

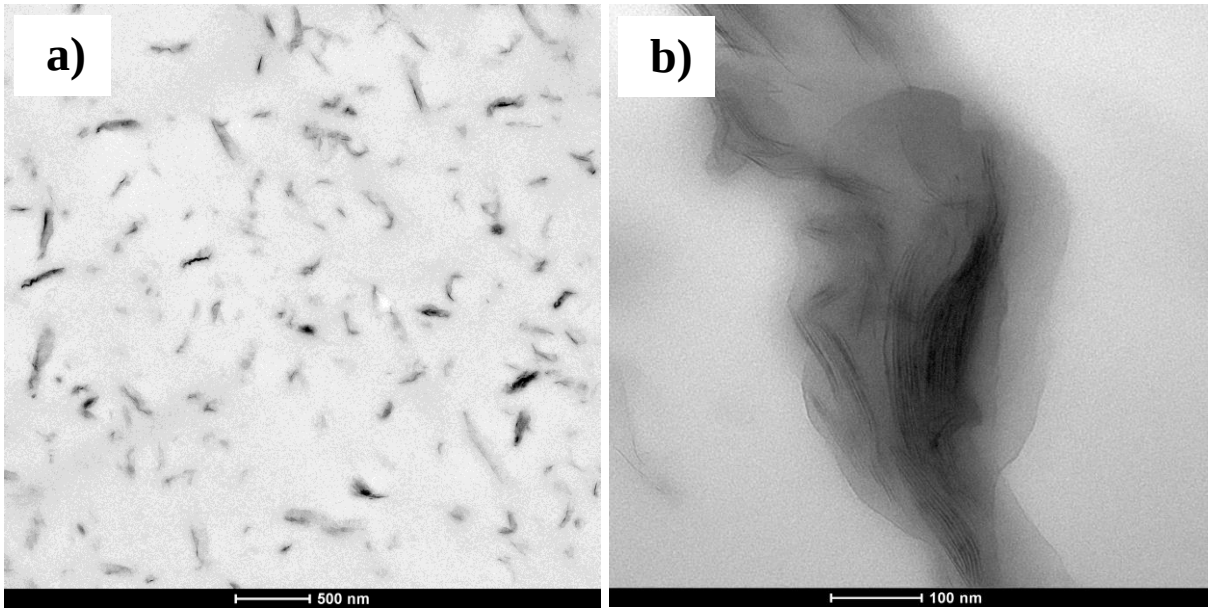

Figure VI.9 TEM Micrographs of PLA/2 wt% OMMT extruded twice (PLA/OMMT-2EXT) at: **(a)** Low Magnification and **(b)** High Magnification.

Unlike PLA/OMMT, the rubber-based nanocomposite extruded twice (R/OMMT-2EXT) and containing 2 wt% clay exhibits poor dispersion manifested by the occurrence of close clustered clay groups (**Figure VI.10(a)**). Its TEM image at high magnification clearly demonstrates intercalated/partially exfoliated clay structure with slight amount of delaminated nanosheets and thick tactoids indicative of incomplete exfoliation (**Figure VI.10(b)**).

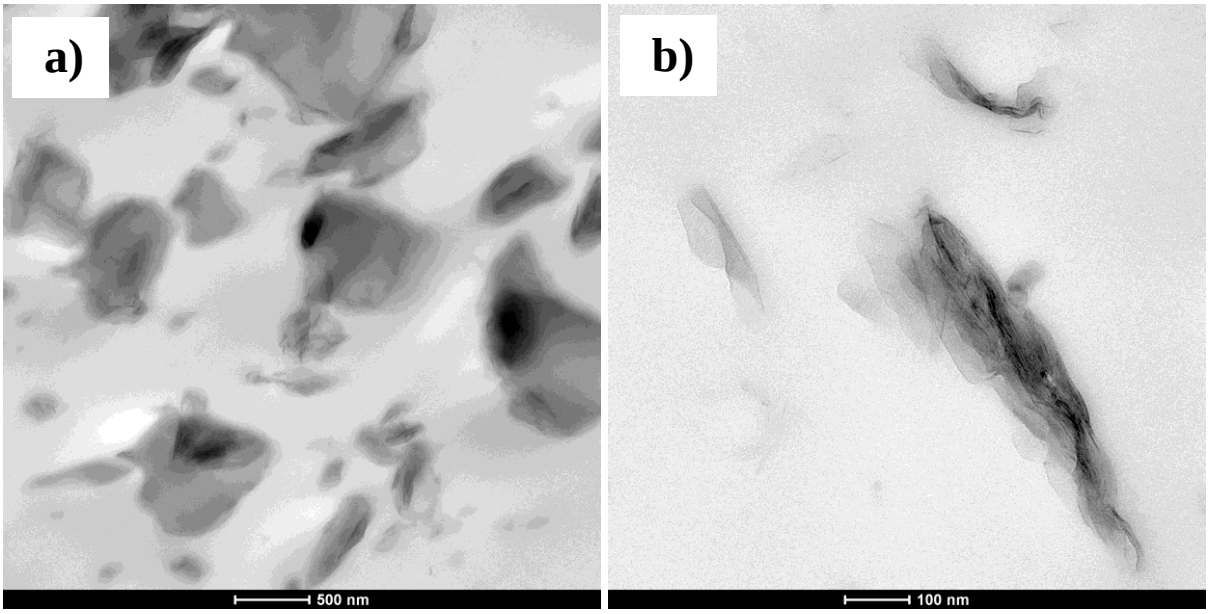

Figure VI.10 TEM Micrographs of Rubber/2 wt% OMMT extruded twice (R/OMMT-2EXT) at: **(a)** Low Magnification and **(b)** High Magnification.

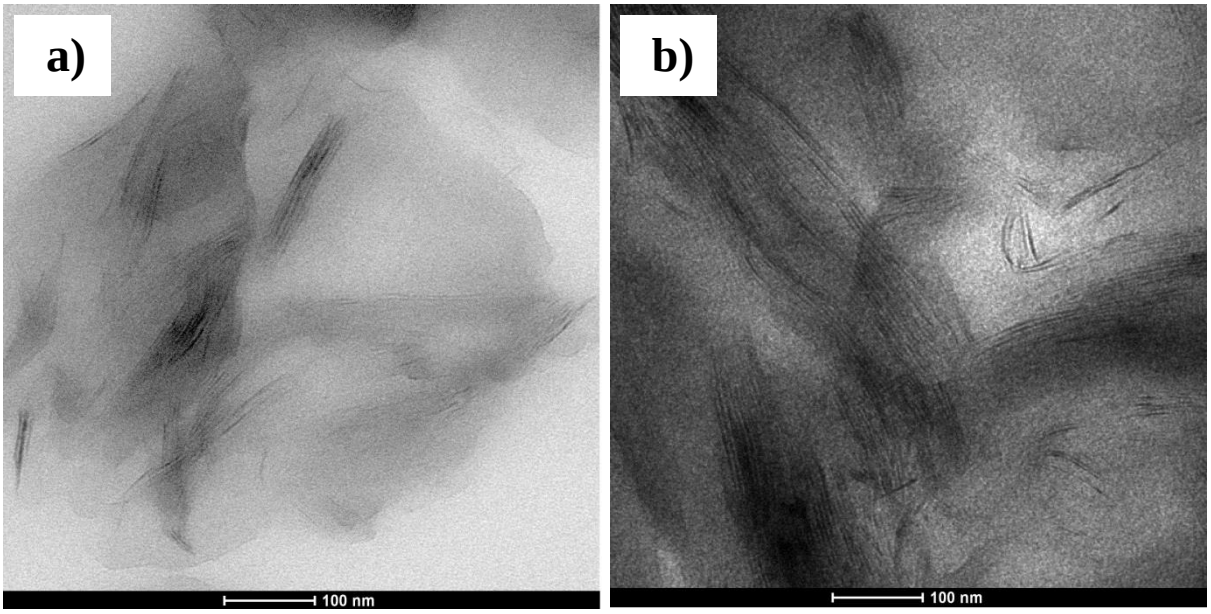

Figure VI.11 TEM Micrographs at High Magnification of **(a)** PC and **(b)** CI Intermediate Nanocomposites Prepared at 10 wt% Rubber Content and 2 wt% OMMT.

The structure of PC nanocomposite consists of abundant single exfoliated clay nanosheets and intercalated/partially exfoliated regions and thin clay stacks wherein the clay platelets kept their face-to-face structure (**Figure VI.11(a)**), whereas that of CI is mainly made of intercalated structure and very few exfoliated particles with occurrence of large number of thick clay stacks and tactoids which can be assimilated to agglomerates of different sizes (**Figure VI.11(b)**).

The TEM analyses of these four nanocomposites (PLA/OMMT, R/OMMT, PC and CI) are in good agreement with the diffraction peaks appearing in their XRD patterns confirming that clay particles are more dispersed in PLA than in the rubber as a result of the disparity in their polarities and hence their affinity to clay.

Representative high magnification TEM micrographs of the ternary nanocomposites prepared by different addition protocols are exhibited in **Figures VI.12 and VI.13**. Owing to the absence of contrast between the PLA and the rubber, it is difficult to differentiate between the two polymer phases and thus to locate the clay. Incorporation of the rubber into the nanocomposites and the preparation sequences of the nanocomposites induced evident effects on clay dispersion. Only the micrographs of the nanocomposites at the optimal 10 wt% rubber ratio are depicted, because at this composition the best stiffness-toughness balance has been acquired, especially for PC-I and PI-C mixing sequences.

The main common observation for PC-I, PI-C and ALL-S is that they all show a nanoscale dispersed morphology dependent on rubber composition identified by the presence of single clay nanosheets without appearance of any agglomeration, whereas for the CI-P nanocomposite, the rubber content did not significantly influence the nanoscale clay dispersion, and discrete agglomerates constituted most of the structure. In all preparation procedures, the OMMT particles were dispersed without any obvious orientation preference, and none of them led to completely exfoliated nanocomposite.

PC-I presented the highest level of clay dispersion (**Figure VI.12(a)**). Exfoliated clays constitute the major structure evidenced from single clay nanoplatelets surrounded by few thin stacks, and absence of tactoids indicating that the

original silicate crystalline structure of the clay was disrupted to a great extent. As can be noticed the single clay sheets are surrounded by very few fractions of intercalated clay thin stacks and no agglomeration is discernible. Such high dispersion degree was possible because the favorable reactions between the PLA reactive groups and those on the clay and its surfactant took place for a longer time (PC mixture was extruded twice). Furthermore, the shear melt viscosity became high in the second extrusion step induced by the added viscous rubber that improved delamination and breakdown of clay tactoids and helped insertion of both types of polymer molecules into the clay stacks as was confirmed by XRD.

PI-C TEM micrograph exhibits lower dispersion level than PC-I (**Figure VI.12(b)**). This image clearly shows intercalated structures, some single nanoplatelets and thin stacks, and slight amount of tactoids. This observed structure is due to the fact that in this mixing procedure most of the rubber functional groups would have reacted with those of PLA during the first extrusion run preventing thus some of the rubber molecules to intercalate into clay particles during the second mixing step. In addition, this fact would have reduced the available reactive groups of the polymers to interact with the clay in the second extrusion and also to reduced PLA chains diffusion into clay interlayers because of PLA chains extension induced by its reaction with the rubber. But most importantly is that the clay intercalation could only take place in the second extrusion run leading to shorter residence time (contact) with the polymers as compared to PI-C for which the clay was mixed twice with the polymers.

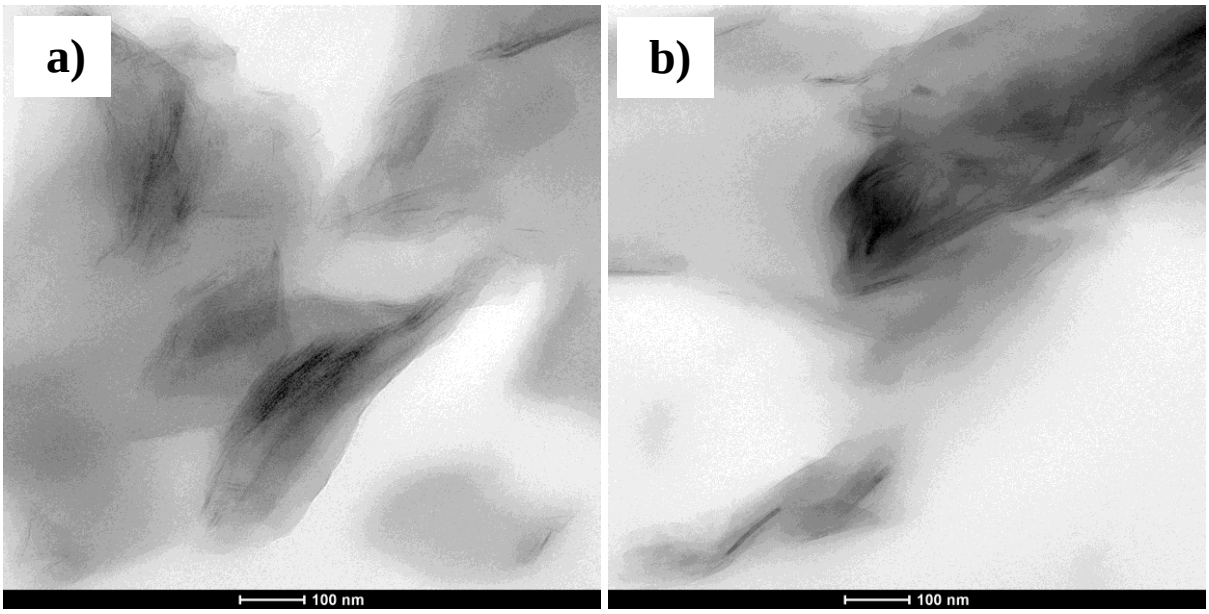

Figure VI.12 TEM Photomicrographs at High Magnification of **(a)** PC-I and **(b)** PI-C Nanocomposites Prepared at 10 wt% Rubber Content and 2 wt% OMMT.

Figure VI.13 illustrates the the TEM photomicrographs of CI-P and ALL-S nanocomposites. CI-P nanocomposite presented the worst clay dispersion state, characterized by intercalated clay particles, large amount of clay tactoids, agglomerates and almost total absence of exfoliated clay particles (**Figure VI.13(a)**). This figure also shows many tactoids of different thicknesses and agglomerated clay particles over a board region (more obvious on the right side of the micrograph) which were not broken during mixing. This structure characterized by a low degree of clay dispersion was the result of the low diffusion ability of the rubber into clay interlayers during the extrusion of CI mixture, and to its possible bonding to clay edges through interactions of its reactive groups with the hydroxyl groups of the clay surfaces that prevented the rubber and the PLA to penetrate further into clay galleries during the second extrusion step.**[6]** The deleterious effect of extruding CI intermediate nanocomposite twice on clay dispersion was discussed earlier in the XRD section. Another factor that could also be considered is the presence of clay agglomerates that constrained the motion of the polymer chains necessary for their diffusion into clay galleries.**[6,11-13,20,23]** These agglomerates stemmed from encapsulation of most of the clay by the rubber that enhanced platelet-platelet interactions, and the extensive shear forces applied by extrusion were not able to breakdown these agglomerates. In

addition, collapse of the clay galleries were triggered by the high shear intensity during CI extrusion that dissolved some of the organoclay surfactant into the PLA matrix. Dissolutions of the organoclay surfactant into the matrix during processing has been well documented in the literature.**[6,12,16]** This clay collapse induced by clay surfactant dissolution enhances filler-filler (hydroxylated egde-edge) interactions and permits rearrangements of the clay sheets to their more or less original crystal structure that reduces the peeling off of clay nanosheets from clay stacks and resulted in intercalated structure and agglomerates. These agglomerates might have acted as stress concentrators**[11,12,17,21,22]** and they likely were the main reason for the low mechanical performance in terms of impact strength and tensile properties of this nanocomposite as will be discussed in the mechanical properties section.

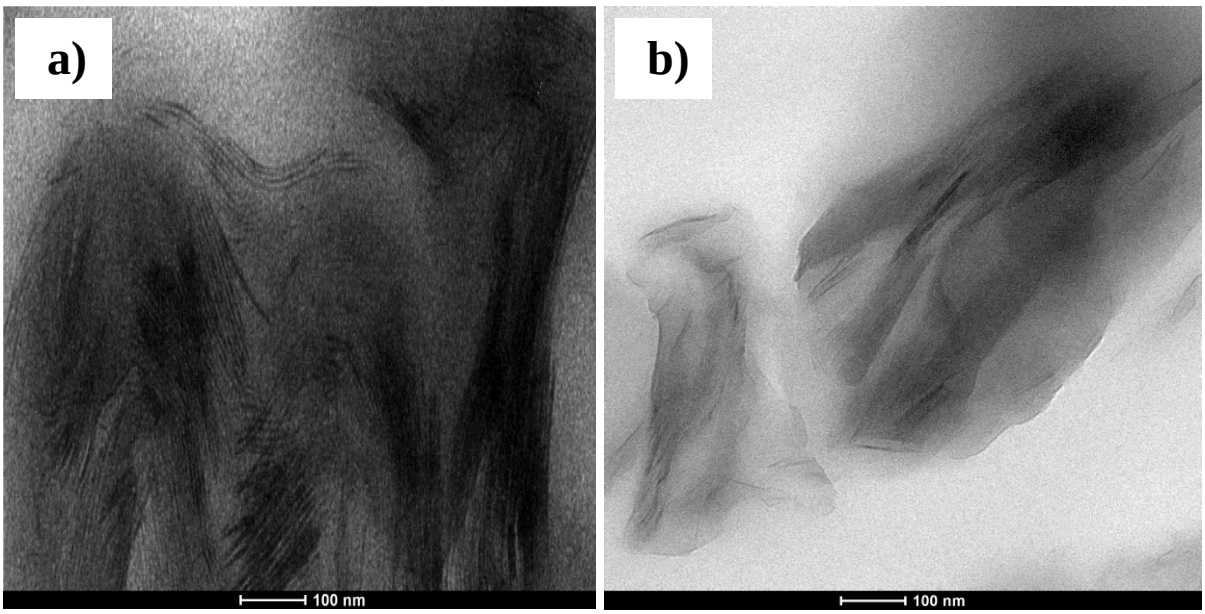

Figure VI.13 TEM Photomicrographs at High Magnification of **(a)** CI-P and **(b)** ALL-S Nanocomposites Prepared at 10 wt% Rubber Content and 2 wt% OMMT.

ALL-S presents finer clay dispersion in comparison to that of PI-C, consisting of intercalated particles and myriad single clay particles, thin clay stacks and few tactoids (**Figure VI.13(b)**). This finer dispersion compared with PI-C is the result of the competition between the rubber and the PLA to react and to simultaneously insert within the clay galleries. Moreover, in this mixing order, the ingredients were in

contact for longer time (two extrusion processes), thus giving more and equal chances for both polymers to diffuse into the clay galleries.

According to the above TEM observations, PLA was found to diffuse readily into clay spacings than the rubber does, and intercalation/partial exfoliation was the dominant structure of the clay in all prepared nanocomposites. These TEM observations corroborate well with XRD results discussed in the previous section.

VI-2-3 Scanning Electron Microscopy (SEM) Analyses

Illustrative SEM micrographs of the freeze fractured surfaces of twice extruded PLA and PLA/OMMT are shown in **Figure VI.14**. Plain PLA displays featureless morphology characterized by a typical brittle fracture surface as shown by a smooth surface and several parallel straight cracks developed throughout the surface without any discernible heterogeneities (**Figure VI.14(a)**). Upon impact, the broken specimen splitted completely into two halves and stress whitening was readily observable on the broken surfaces. Absence of crack deflections and/or bifurcations ascribed to the homogeneous structure of PLA led to rapid crack growth and abrupt breaking of PLA without any visible fragmentations and plastic strain.**[21]** These are typical features of brittle rupture with low fracture resistance that might explain the low impact-toughness of PLA.**[19]** PLA/OMMT SEM micrograph (**Figure VI.14(b)**), shows a rough surface compared with pristine PLA attributed to the effective ability of clay nanoplatelets in diverting cracks in random directions giving rise to numerous meandering short and long crack paths responsible of such feature.**[6,30]** Such mechanism responsible of the obtained morphology was possible owing to two concurrently occurring opposite energetic processes. On one hand, the clay clay-stiffening effect contributed to PLA embrittelement that should yield a smooth surface, and on the other hand the produced OMMT intercalated/partially exfoliated structure coupled with the valid interactions between functional groups of the PLA and the clay enabled improved load transfer from the matrix to the reinforcement and triggered the cracks to propagate in random directions with tortuous paths responsible of the noticed rough surface.**[6,11,12,19]** It seems that the second process prevailed over the first one

but resulted somewhat in lower impact-toughness than that of PLA which is presumably associated with the presence of some clay tactoids in PLA/OMMT nanocomposite owing to clay collapse, as was revealed by XRD and observed by TEM. These tactoids operated as stress raisers and led to early failure of PLA/OMMT nanocomposite specimens with significant visible stress whitening than observed on plain PLA.**[22,23]**

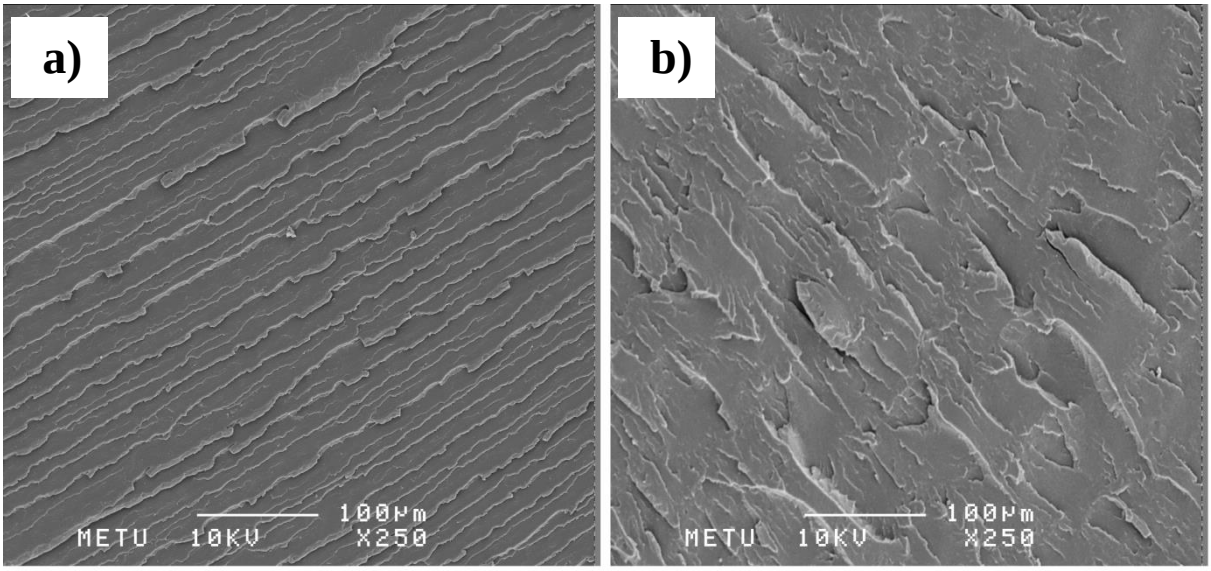

Figure VI.14 SEM Micrographs of the Cryofractured Surfaces of the Injection Molded Specimens of **(a)** PLA and **(b)** PLA/2 wt% OMMT.

Figure VI.15(a-d) exhibits representative SEM images of unetched cryofractured surfaces of PC-I, PI-C, CI-P and ALL-S ternary nanocomposites at 10 wt% rubber content. Intense macroscopic stress whitening compared with PLA and PLA/OMMT was noticed on all impacted specimen surfaces that confirm improvement of toughness. All SEM images exhibited a two-phase morphology with no obvious phase separation between the components. This sea-island morphology is typical of an immiscible polymer system, in which the rubber (high viscosity) composed the dispersed phase surrounded by the continuous PLA matrix. The interface is not clear and the fracture surfaces do not show sharp edges indicating strong adhesion between the phases derived from the in situ interfacial reaction between the functional terminal groups of the PLA and those of the elastomer giving rise to in situ formed PLA-g-rubber copolymer at the interface that simultaneously

decreased the interfacial tension and droplet coalescence rate through steric repulsion between this copolymer molecules and promoted droplet breakup rate hence resulting in fine particle size dispersion.**[4-6,24,27,29]** Furthermore, the presence of the PLA-g-rubber copolymer at the PLA/rubber boundary strengthened the interface by bridging the two phases for adequate load transfer.**[2,6,11,12,19,27,29]** This was identified by the deformation of the domains into ellipsoids and their enlargement in the stress direction demonstrating that the rubber shared the load with the matrix. These features indicate that high energy dissipation occurred in these nanocomposites which might explain the partial break of the specimens after impact test especially those of PC-I nanocomposites at high rubber content. Furthermore, these micrographs present some vacuoles corresponding to pulled-out rubber droplets during impact, whereas others were well anchored to the matrix and some were still embedded within the PLA matrix enveloped by micro-voids. These gaps might have resulted from the debonding and/or cavitation of the rubber particles at the rubber-matrix interface.**[2,7-11,15,31]** In rubber-toughened plastics both internal cavitation and debonding cavitation might coexist, however internal cavitation of the rubber domains was not observed on our SEM images probably due to the low particle size recorded for all nanocomposites.**[2]** Debonding/cavitation of rubber particles is one of the most important mechanisms of energy absorption in rubber-toughened polymers among others, such as crazing, internal rubber cavitation, shear banding, crack bridging and shear yielding, all of which are highly influenced by particle size and interface strength.**[7,31]**

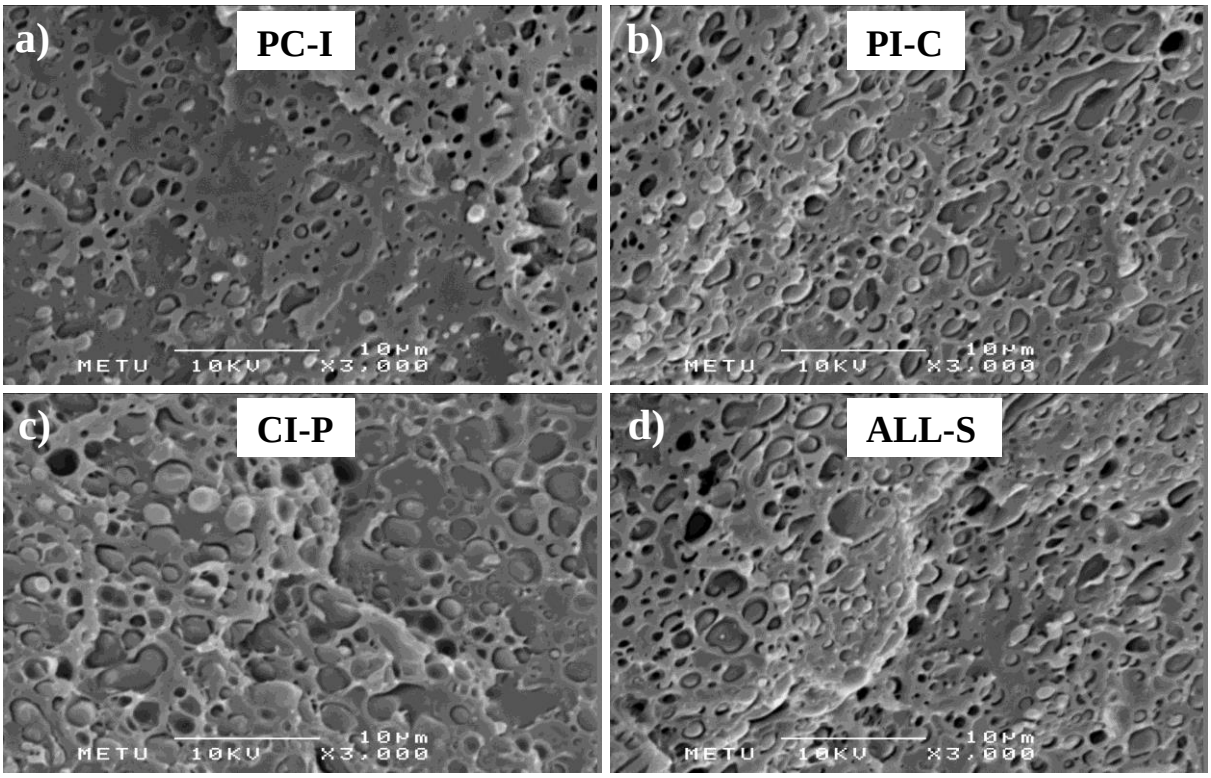

Figure VI.15 SEM Micrographs of the Fractured Injection Molded Specimens of Unetched Surfaces of the Ternary Nanocomposites all containing 10 wt% Rubber.

The morphology of etched fractured surfaces of selected ternary nanocomposites at 10 wt% rubber content is shown in **Figure VI.16(a-d)**. The craters on the photographs correspond to the location of the rubber particles selectively extracted by chemical etching from cryofractured surfaces using n-Heptane at 45°C. All of the nanocomposites present fine phase structures. The cavities are elliptical in shape with good spatial distribution testifying homogeneous and uniform dispersion of the rubber within PLA matrix. **Figure VI.6(a-d)** shows that during impact, multiple fractured surfaces were generated that are responsible of higher surface roughness than that observed in **Figure VI.14 (b)** representative of PLA/OMMT. The roughness degree increased as the rubber ratio increased indicating that much energy has been consumed to create these surfaces and testifies that the transition from brittle (crazing) to tough (shear yielding) fracture took place mainly by cavitation induced shear yielding.**[2,7-11,15,31]**

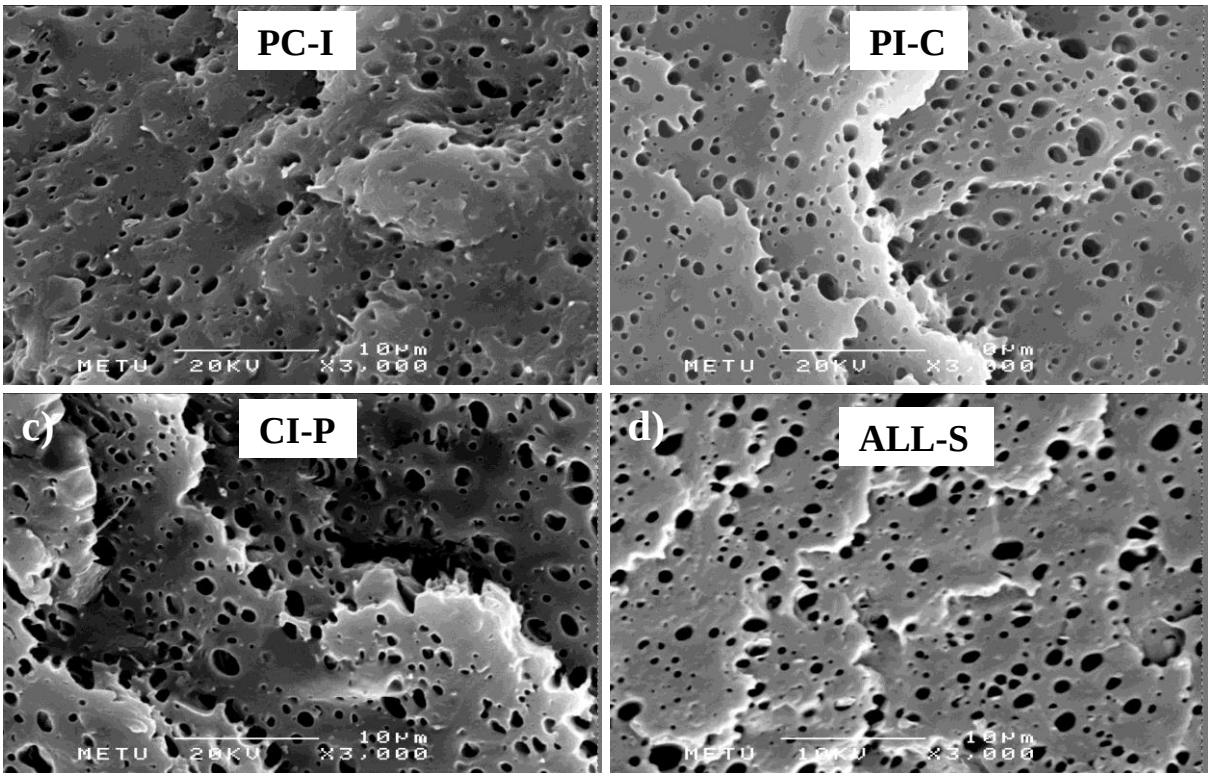

Figure VI.16 SEM Micrographs of the Fractured Injection Molded Specimens of Etched Surfaces of the Ternary Nanocomposites all containing 10 wt% Rubber.

At low rubber fraction, droplet breakup is favored against coalescence rate, owing to the low rubber concentration (low viscosity) and to decreased interfacial tension between the components imparted by the in situ formed copolymer at the interface. As a result, small particles are formed with narrow and homogeneous distribution, but at higher rubber contents, during mixing the domain size is determined by the competition between particle breakup and coalescence.**[6,29]** Moreover, the particle size could also be influenced by the presence of OMMT that generally induces a change in the phase size depending on its location.**[6,20,22-27]**

PC-I presented the lowest domain size (253-434 nm / 0.253-0.434 µm) due to the presence of most of the clay nanosheets predominately in the matrix because it was first combined with PLA before rubber was added. The clay likely maintained its location in the matrix owing to its affinity to the highly polar PLA compared to the rubber and might have acted as physical obstacles to coalescence of the rubber particles**[6,11-13,27]** (**Figure VI.16(a)**). Some of the clay may also have migrated to the interface.**[16,22-24,26,27]** Martins et al.**[22]** reported in their study of PP/PP-g-

AA/EVA/OMMT nanocomposites that the clay migrated to the EVA phase by affinity, irrespective of the blending order, even in the sequence where the clay was first mixed with polypropylene, before EVA was added. Similarly Borah et al.**[23]** observed that in LLDPE-g-MAH compatibilized LLDPE/EMA/OMMT nanocomposites, the OMMT (Cloisite®25A) was attracted to the EMA phase by affinity during the short residence time in the internal mixer even though the clay was previously mixed with the molten polyethylene and EMA was added subsequently. The presence of the clay at the PLA/rubber interface in PC-I nanocomposite might have played the role of a compatibilizer**[13,23,24,27]**, and/or might have constituted physical hindrance for coalescence of the rubbery domains, accordingly small rubber domains are generated.**[6,11-13,18,20,23,24,27]**

The rubber droplet size of PI-C (333-545 nm / 0.333-0.545 μm) (**Figure VI.16(b)**) is somewhat larger than that of PC-I. In this nanocomposite, the clay was added in the second extrusion run; consequently it should be distributed in the two phases, with preference for PLA owing to the higher polarity of PLA (higher affinity to clay) in comparison to the rubber. Dasari et al.**[25,26]**, reported that the clay was equally dispersed in PA66 and SEBS-g-MAH when they used PI-C addition mode to prepare the PA66/SEBS-g-MAH/OMMT nanocomposite. The presence of the clay in the rubber phase increased the modulus of the rubber (increased viscosity) and hence reduced its ability to breakup compared with PC-I mixing order.**[24-27]** This effect coupled with the increased viscosity of the system due to the chain extension reaction decreased droplet breakup during blending. Both of these factors might have reduced the compatibilizing effect of the clay and hampered its physical barrier behavior for coalescence, therefore in the PI-C mixing sequence larger particles were developed compared with PC-I.

For CI-P and ALL-S, most of the clay should be present in the dispersed phase. In the case of CI-P this is evident because the clay is first mixed with the rubber in the first extrusion run. For ALL-S, during blending the rubber melted earlier ($T_m \approx 53°C$) than PLA did ($T_m \approx 147°C$), therefore most of the clay should also be enclosed in the rubber. However, in both cases some of the OMMT might be present at the

PLA/rubber interface and/or in the PLA phase. This preferential location of OMMT in the elastomer phase increased the viscosity and modulus of the rubber, accordingly the droplet deformation and breakup during blending were considerably reduced leading to larger domain size in these nanocomposites in comparison to those of PC-I and PI-C.**[24,26,27]** The domain size of rubber particles in CI-P (**Figure VI.16(c)**), and ALL-S (**Figure VI.16(d)**) were (457-1524 nm/0.457-0.1524 µm), and (449-689 nm/0.449-0.689 µm) respectively. ALL-S exhibited smaller phase size than CI-P did, because all of its ingredients were extruded twice and the elastomer droplets were broken up during the early stages of their formation (efficient droplet breakup). However, CI-P was prepared from the highly viscous and rigid like CI intermediate nanocomposite that was difficult to extrude and to disperse into PLA; therefore larger particles were produced in this nanocomposite. In short, particle size of the rubber in PC-I and PI-C was influenced by rubber droplet breakup helped along with clay compatibilizing and coalescence suppression effects, whereas for CI-P and ALL-S, the final particle size resulted primarily from droplet breakup likely because of the embedment of most of the clay inside the rubber phase .

To summarize the above discussion, it can be inferred that clay platelets in PC-I and PI-C materials were able to suppress agglomeration of the dispersed rubber particles. On one hand by acting as physical restrictions for droplet coalescence due to the formed intercalated/partially exfoliated structure in these nanocomposites helped along by the adsorption of the two polymers on the solid surface of the clay as a result of the positive interactions between the filler and the polymers as aforementioned that constrained molecular mobility which in turn is responsible of coalescence retardation and prevention.**[6,11-13,27]** On the other hand, by serving as effective compatibilizer due to their interfacial active role that is a known fact reported in open literature.**[13,23,24,27]** Furthermore, extruding twice these nanocomposites (long residence time) should also be considered as an additional factor contributing to particle size reduction by droplet breakup. For CI-P and ALL-S, the selective partition of the OMMT primarily in the rubber phase might be the major factor that has

hindered its compatibilizing and coalescence suppression effects which has resulted in coarse rubber article size as compared to PC-I and PI-C.

In all the mixing methods, the domain size increased with increasing rubber content.**[3,6,10,20]** This is an expected result, as the rubber fraction increases the viscosity of the system and the tendency of particle collision and agglomeration increases, consequently the coalescence rate becomes higher than the droplet breakup rate, resulting in larger particle size.**[20]** In this study, particularly for PC-I and PI-C, at higher rubber ratio, the coalescence suppression and the compatibilizing effects of the clay were not significant probably due to its low concentration (2 wt%).

VI-3 Mechanical Properties

VI-3-1 Tensile Properties

Stress-strain curves of the studied materials were determined at room temperature (**Figure VI.17**). Upon drawing, PLA exhibited a sharp linear increase in stress with a distinct yield point accompanied thereafter by a very short necking and an abrupt rupture at very low strain (3.9%), demonstrating its brittleness and its very low tensile toughness. Addition of 2 wt% OMMT to PLA did not bring about a noticeable change to the PLA deformation behavior. However, for all the compounding modes, incorporation of the rubber to the nanocomposites transformed the fracture of PLA from brittle to ductile with almost identical stress-strain evolution dependent on rubber compositions. During stretching, these modified nanocomposites exhibited a broad yield peak and a long stable necking after which the strain increased considerably and continuously at nearly constant stress indicative of plastic flow (cold drawing), followed by a short stress softening before failure. The failure occurred at a significantly increased elongation at break signifying that high energy was dissipated.

Figures VI.18-VI.20 display the tensile properties namely tensile modulus, tensile strength and elongation at break as a function of rubber loading for each of the considered mixing protocol. For the sake of comparison, the results for PLA and its

corresponding nanocomposite (PLA/OMMT), both of them extruded twice, are written on each graph.

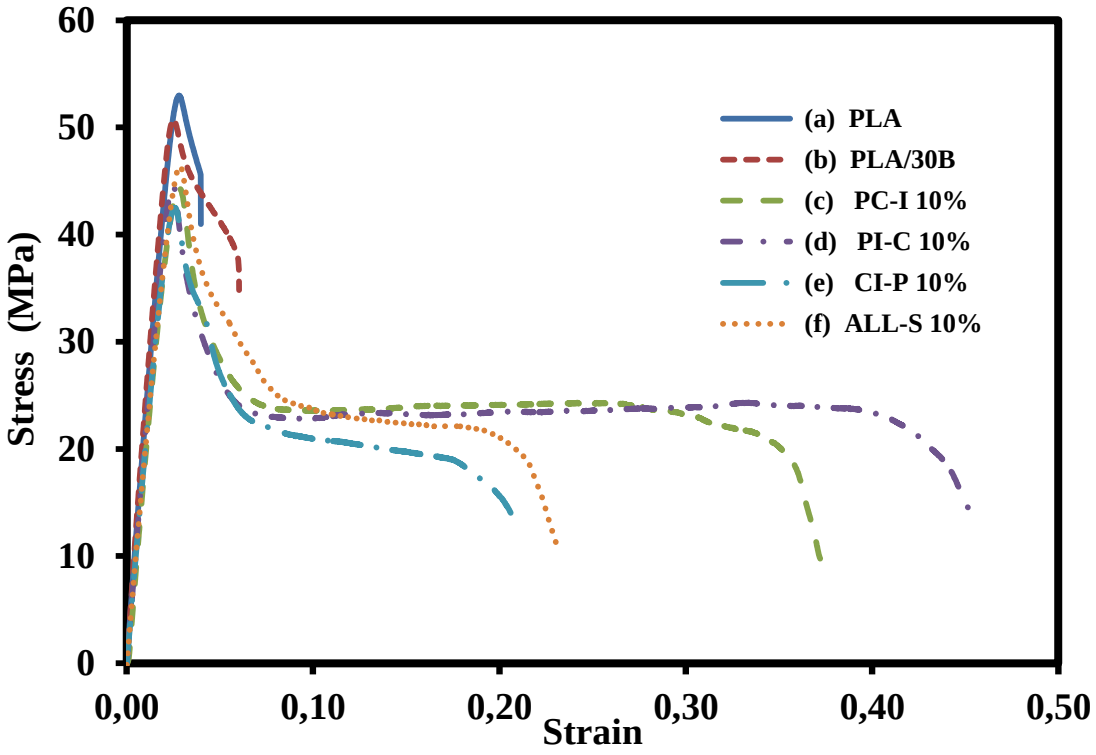

Figure VI.17 Stress-Strain Curves of Nanocomposites at 10 wt% Rubber Content.

VI-3-1-1 Tensile Modulus

The Young's modulus of neat PLA and those of the PLAs extruded once and twice were 2149.0 MPa, 2068.0 MPa and 2046.7 MPa respectively (**Figure VI.18**). There was no substantial change of PLA modulus with reprocessing, which is in line with published results in the literature.**[32,33]** Tensile modulus of PLA was found to remain constant after 7 injection cycles**[32]**, and 10 extrusion processes.**[33]**

In the presence of 2 wt% OMMT, the tensile modulus of PLA increased from 2046.7 MPa to 2373.4 MPa representing an increment of ≈16% (**Figure VI.18**). This is a common outcome attributed to the replacement of PLA molecules with OMMT that has high intrinsic stiffness and high aspect ratio.**[6,11,12,16-20,23-27]** This

increase in tensile modulus is correlated with the high level of OMMT dispersion (as was assessed by XRD and TEM) that increased the clay-polymer contact surface area and its effective volume fraction, thus imposing restrictions on chain mobility and deformation of the surrounding matrix.**[6,11-13,18,20,23-27]** In addition to these effects, the strong adhesion through interfacial interactions of PLA carboxyl end groups and the hydroxyl entities of the nanoclay contributes to efficient stress transfer from the polymer matrix to the filler giving rise to high tensile modulus of the PLA/OMMT nanocomposite.**[6,11,12,19]**

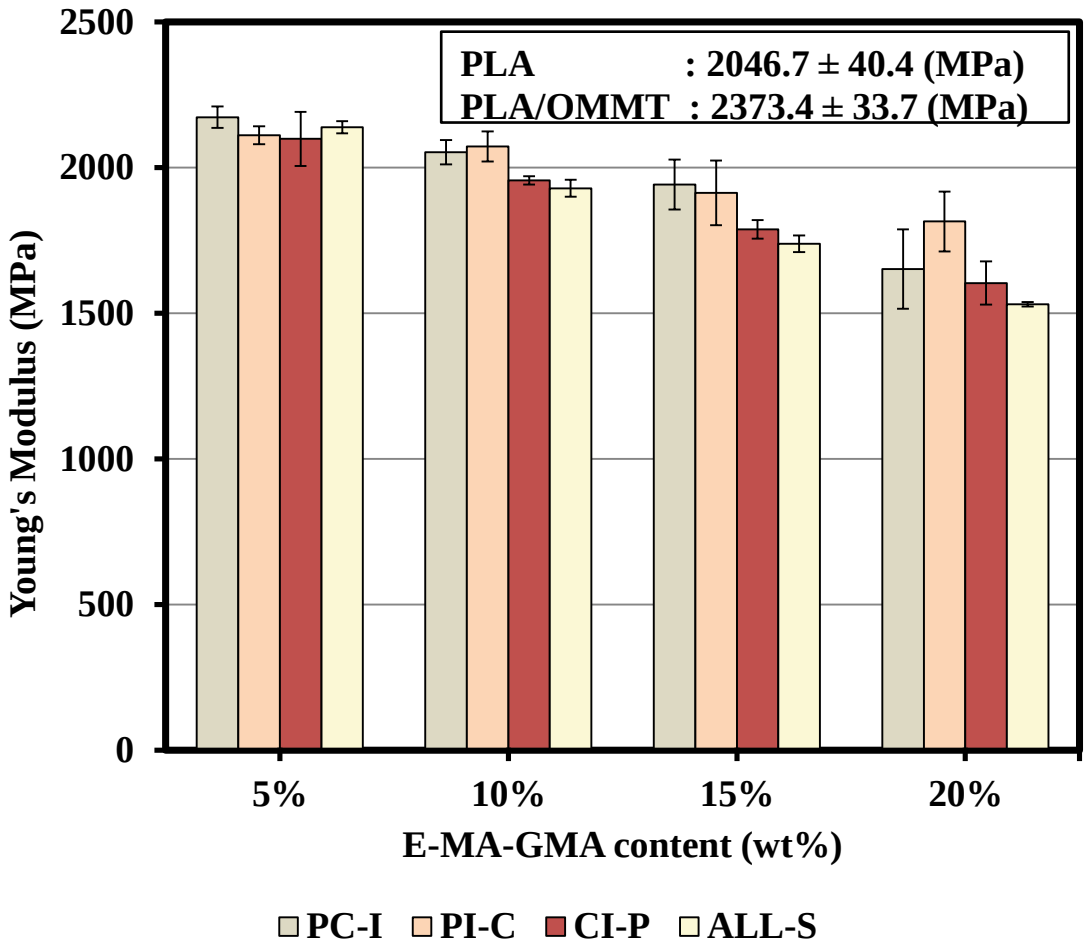

Figure VI.18 Young's Modulus of the Ternary Nanocomposites as a Function of the Rubber Content at 2 wt% clay.

The main idea behind rubber addition to the rigid PLA/OMMT was to compensate the stiffening effect of the clay and to induce some elasticity and toughness to the blend. As documented in **Figure VI.18**, for all the blending sequences

the modulus dropped steadily as the rubber quantity is increased owing to the soft nature of the rubber with low modulus. This is a typical behavior of rubber-toughened polymers for which rubber addition causes decrease in stiffness.**[1-8,10,11,13-16,18,19,21-26]** When the elastomer was added to the tune of 5 wt%, the modulus decreased from 2373.4 MPa to approximately 2100.0 MPa for all the nanocomposites corresponding to ≈13%. This expected decrease in modulus is attributed to the substitution of some of the rigid and stiff PLA by the low stiffness-low strength rubber phase which had induced some ductility. However, at 10 wt% rubber content, the Young's modulus was more or less retained, especially for PC-I and PI-C mixing orders. Above this rubber content, PC-I and PI-C still displayed the highest modulus that might be due to the fine dispersion of the OMMT in the PC-I mixing order that contributed to chain immobilization, responsible of increased chain stiffening. For the PI-C mixing order, the increase might be ascribable not only to the fine clay dispersion, but also to promoted chain extension associated with significant reaction extent between the functional groups of PLA and those of the impact modifier that increased the molecular weight, and resulted in more stabilized and strengthened interface. Both of these phenomena, increased chain stiffening and increased molecular weight, have been instrumental in dissipating high energy, consequently high moduli ensued.

CI-P and ALL-S nanocomposites exhibit lower tensile modulus than that of PC-I and PI-C (**Figure VI.18**). For the CI-P and ALL-S mixing orders, the OMMT was mostly present in the elastomer phase as discussed in TEM section. This not only hindered its stiffening effect, but also decreased the elasticity of the rubber that reduced its toughening/cavitation ability.**[24-26]** These two effects hence were the main reasons for the lower moduli noticed for these nanocomposites. It is interesting to note that comparable moduli were obtained for CI-P and ALL-S even though better clay dispersion was revealed in All-S as compared with CI-P which presented clay agglomerations in its nanostructure. This points out that irrespective of the clay dispersion state; the encapsulation of the clay layers by the rubber phase has an adverse effect on their stiffening effectiveness.

VI-3-1-2 Tensile Strength

PLA is a very rigid polymer, thus it showed a high tensile strength of 56.5 MPa (**Figure VI.19**). No significant change of this property was distinguished after addition of 2 wt% OMMT to PLA. This is associated with the intercalated/partially exfoliated nanostructure of OMMT in this nanocomposite, to its homogeneous distribution as well as to the adequate interfacial adhesion between the nanofiller and the PLA which should have facilitated the stress transfer between the phases that helped to retain constant the tensile strength.**[6,11,12,19]** However, the tensile strength of the material is strongly dependent on the orientation of the clay layers, and if the clay layers in the tensile bar are not preferentially oriented in the testing direction the increase in the tensile strength would be minimal.

The tensile strength as a function of the rubber ratio followed the same trend as that of the tensile modulus (**Figure VI.19**). It decreased as the elastomer fraction was increased, regardless of the compounding protocol which is again assigned to the elastomeric nature of the rubber. This reduction in the tensile strength is consistent with previous research studies which reported reduced tensile strength in rubber-toughened PLA blends**[1-4,6,10,11,13,15-17]** and in other toughened polymer blends.**[18-20,23]**

At 5 wt% rubber content, the tensile strength was almost retained at 49.0 MPa independent of the compounding order, as a result of the somewhat similar OMMT dispersion level developed at this rubber ratio in all the compounding sequences. This indicates that at this low rubber content, the location of the clay in the nanocomposites did not significantly affect the tensile strength, and the presence of clay agglomerates in the CI-P nanocomposite was not so detrimental. At 10 wt% rubber concentration, the tensile strength of all nanocomposites underwent approximately the same decrease. At this composition, the tensile strength for PC-I and PI-C was approximately 45.6 MPa corresponding to nearly 19% decrement. While for CI-P and ALL-S the reduction in tensile strength was more pronounced approaching 43.0 MPa which is close to a drop of 24%. This clearly demonstrates that, even though the clay dispersion was better than that at 5 wt% rubber ratio, especially in PC-I, PI-C and ALL-S, the

clay was not able to significantly counteract the negative influence of the soft elastomer on the tensile strength likely in consequence of its low loading (2 wt%) compared with that of the rubber (10 wt%). Furthermore, although the tensile strength of these nanocomposites is lower than that of pristine PLA and PLA/OMMT nanocomposites, it is still larger than those of known high tonnage commodity plastics such as PE and PP.**[8,10]** In short, at 10 wt% rubber concentration, the tensile strength of all the nanocomposites underwent approximately the same decrease.

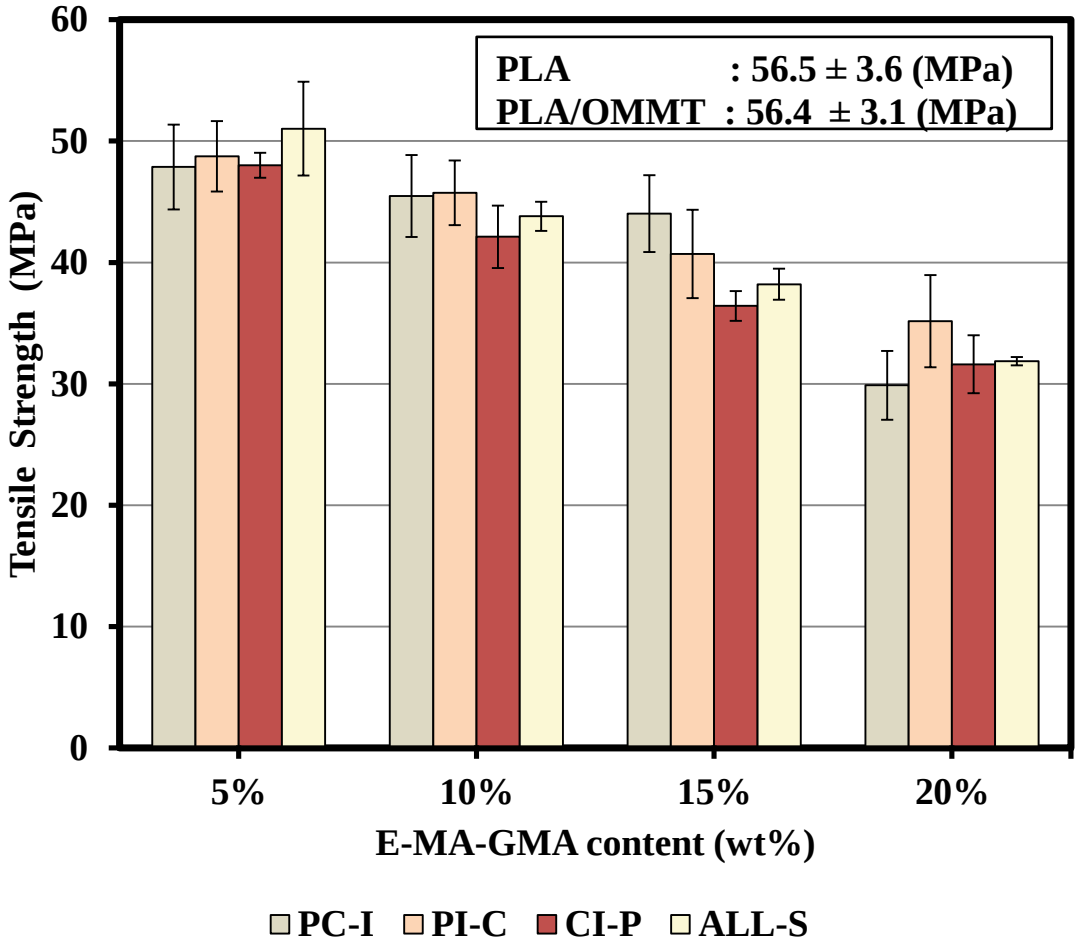

Figure VI.19 Tensile Strength of the Ternary Nanocomposites as a Function of the Rubber Content at 2 wt% Clay.

When the rubber was added to the tune of 15 wt%, higher tensile strengths, above 40 MPa, were recorded for PC-I and PI-C, while those of CI-P and ALL-S declined well below this value and were roughly around 37 MPa. The high tensile strength for PC-I and PI-C compared to those of CI-P and ALL-S can be assigned to the presence of most of the clay in the PLA matrix in PC-I,**[25,26]** and to extensive

reaction between the functional groups of the PLA and those of the rubber in PI-C, and to the enhanced clay dispersion in both of these nanocomposites as evaluated by XRD and TEM. However, the low tensile strengths of CI-P and ALL-S are due to the encapsulation of most of the clay inside the rubber which had rigidified the elastomeric phase and might have thus reduced its toughening efficiency in these nanocomposites. Moreover, the presence of agglomerates in CI-P nanocomposite, especially at 15 wt% rubber content, might have acted as flaws and/or as stress concentrators facilitating easy initiation and propagation of microcracks and leading to premature failure responsible of low tensile strength.**[11,12,17,22]**

When the rubber content reached 20 wt%, the tensile strength underwent a drastic drop in all the mixing protocols that could be due to the considerable softening effect induced by the rubber that hindered the benefits of the OMMT addition.**[6,8]**

VI-3-1-3 Elongation at Break

Figure VI.20 illustrates the effect of rubber and clay addition on the elongation at break (ε_b) of the prepared nanocomposites. PLA is a stiff and brittle material, therefore as expected, it displayed very low extensibility of 3.9% with slight stress whitening around the broken surfaces indicating that PLA deformed primarily by crazing mechanism**[6,9,10]**, and because of the absence of craze stoppers and/or craze diverting processes, the crazes that formed during extension grew and coalesced rapidly to form catastrophic cracks that resulted in premature breakup with low energy consumption and limited deformation, thus demonstrating the brittle failure nature of PLA.

Upon inclusion of 2 wt% OMMT into PLA, the tensile strain at break increased to 5.1% with substantial stress whitening on the specimen surfaces exhibiting higher degree of crazing and toughness enhancement. This result is in line with nanofiller reinforced PLA.**[11,15]** This slight increase in PLA drawability is ascribed to intercalated/partially exfoliated dispersion of clay that promotes effective crack deflection that lengthens crack propagation paths and retards crack growth to fatal cracks.**[6,30]** Furthermore, the strong interfacial adhesion that results from interactions

between the functional groups of PLA and those of the OMMT enables efficient load transfer between the phases. These two effects are believed to be the main factors contributing to higher energy dissipation reflected by a somewhat improved drawability compared to neat PLA. However, this improvement in ε_b of PLA/OMMT was low due to the presence of tactoids as detected by XRD and TEM, and likely to the low OMMT content (2 wt%).

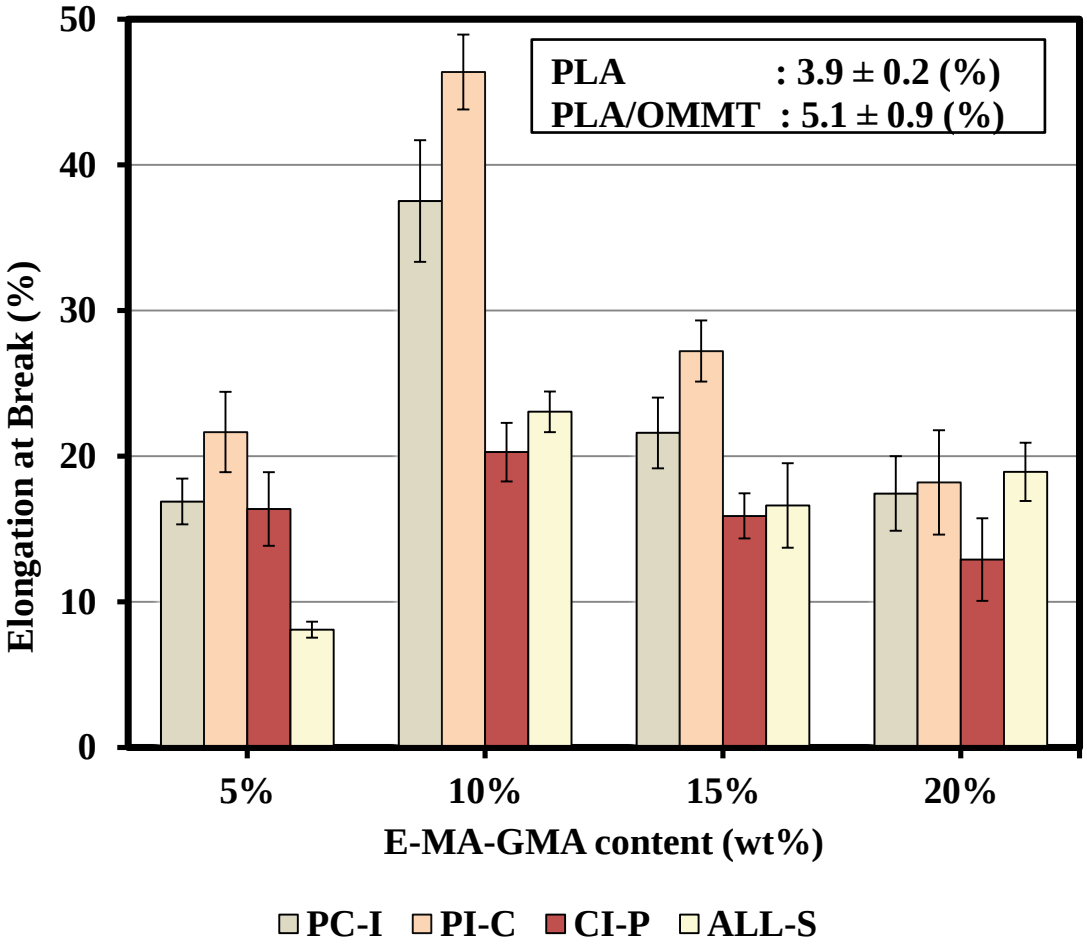

Figure VI.20 Elongation at Break of the Ternary Nanocomposites as a Function of the Rubber Content at 2 wt% Clay.

For all the mixing methods, when the rubber was incorporated to PLA/OMMT, all of the formulations displayed higher ε_b than pristine PLA with extensive stress whitening throughout the specimens induced by large amount of crazes giving rise to ductile deformation. The increase in tensile strain at break can be attributed to the high flexibility of the elastomer and to the effective stress transfer between the PLA and the

rubber owing to the strengthened interface by the in situ formed PLA-g-rubber copolymer at the interface via the chemical reaction between the PLA and the rubber functional groups. This copolymer acted as stress concentration around the rubber particles promoting thus strain energy consumption by plastic deformation. This energy dissipation and high extension stemmed from a combination of massive crazes observed on the specimens and debonding/cavitation of the rubber particles as observed by SEM. Cavitation occurs during debonding and results in matrix drawing or matrix shear yielding responsible of energy dissipation that improves tensile toughness.**[2,7-11,15,31]** This increase in elongation at break due to rubber addition is consistent with results published on rubber-toughened PLA.**[1-8,10,11,13,15]**

At 5 wt% rubber loading, an appreciable improvement in ε_b (ductility) was discerned especially for PC-I, PI-C and CI-P for which the value was in the range 16-21% while that of ALL-S was only 8.10% but still almost two folds higher than that of pristine PLA (3.9%). At this low elastomer extent, the materials still broke in brittle fashion which might indicate that most of the applied deformation stress was carried by PLA. At 10 wt% rubber ratio, The ε_b attained a maximum beyond which it declined steadily.

The ε_b attained a maximum at 10 wt% rubber fraction for all the preparation protocols without significant sacrifice of strength and toughness. At this rubber concentration the ε_b results were 37.50%, 46.40%, 23.10% and 20.30% for PC-I, PI-C, ALL-S and CI-P respectively. However beyond this rubber content the elongation at break declined steadily. The highest ε_b observed for PI-C and PC-I at this rubber loading is attributed to enhanced clay dispersion and to small rubber phase size in these mixing orders as observed by SEM. This high elongation at break reflects high tensile energy dissipation stemmed from a combination of various mechanisms such as massive crazes visually detected on the specimens and debonding/cavitation of the rubber particles as evidenced by SEM which helped plastic deformation of the matrix to occur in the form of matrix drawing. PI-C showed higher ε_b than PC-I did, due to the higher intermolecular reaction between the end groups of PLA and rubber in this

mixing order compared with PC-I. The low ε_b for ALL-S and CI-P mixing orders might be due to the location of the clay in the dispersed phase in these nanocomposites that reduced rubber toughening efficiency by hindering its cavitation ability, and to the large rubber particle size as determined by SEM.

Beyond 10 wt% rubber content, the ε_b decreased considerably in all the preparation sequences owing to the presence of clay tactoids for PI-C and ALL-S and even agglomerates for CI-P that might have acted as flaws and defects, and also to increased rubber domain size as observed by SEM. Because of the high difference in modulus between the rubber and the matrix, these large rubber domains might have acted as stress concentration points causing microdamages to develop readily to fatal cracks that lead to low ε_b.**[3,4,8,11,15]** When the rubber quantity reached 20 wt%, the elongation at break dropped below 20% for all the nanocomposites that could be due to the considerable softening effect induced by the rubber that hindered the benefits of the OMMT.**[6,8]** PC-I, PI-C and ALL-S exhibit the same ε_b of about 18% but CI-P showed a pronounced reduction ($\varepsilon_b \approx 12\%$) connected with its coarse phase size and with the excessive rigidifying effect of the rubber by the enclosed nanofiller that excessively limited its deformation ability.

VI-3-2 Impact Strength

Toughness of polymers is usually investigated using impact test because of its availability, simplicity and low cost. **[11,15] Figure VI.21** exhibits the effect of mixing sequences on unnotched Charpy impact strength (IS) as a function of rubber loading.

As expected, neat PLA failed in a brittle manner with a recorded IS of only 18.4 J/m^2. Addition of 2 wt% OMMT to PLA reduced its IS to 17.0 J/m^2 corresponding to a decrement of nearly 8%. This is a well-known fact, that is, the stiffness and strength improvement in nanocomposites is generally accompanied with a concomitant reduction in fracture-toughness.**[11,12,18,24,26]** This slight reduction in impact toughness is due to the constraining effect of the OMMT on molecular mobility

making the material more brittle,**[6,11-14,18,20,23-26]** and to the absence of efficient toughening mechanisms such as crack-tip blunting and crack bridging encountered in fracture processes of traditional polymer micro-composites, because the intercalated/partially exfoliated nanosheets are unable of producing such energy dissipating mechanisms.**[31]** Another reason for the decline in IS can also be assigned to the presence of tactoids in the PLA/OMMT nanocomposite as revealed by XRD and TEM analyses. These tactoids act as stress raisers and lead to early failure with significant visually observable stress whitening than observed on neat PLA samples.**[22,23]** However, the decrease in IS was not high, because the effects of the negative factors are counteracted by the effective interactions between the clay nanoplatelets and PLA contributing to enhanced load transfer between the matrix and the nanoreinforcement.

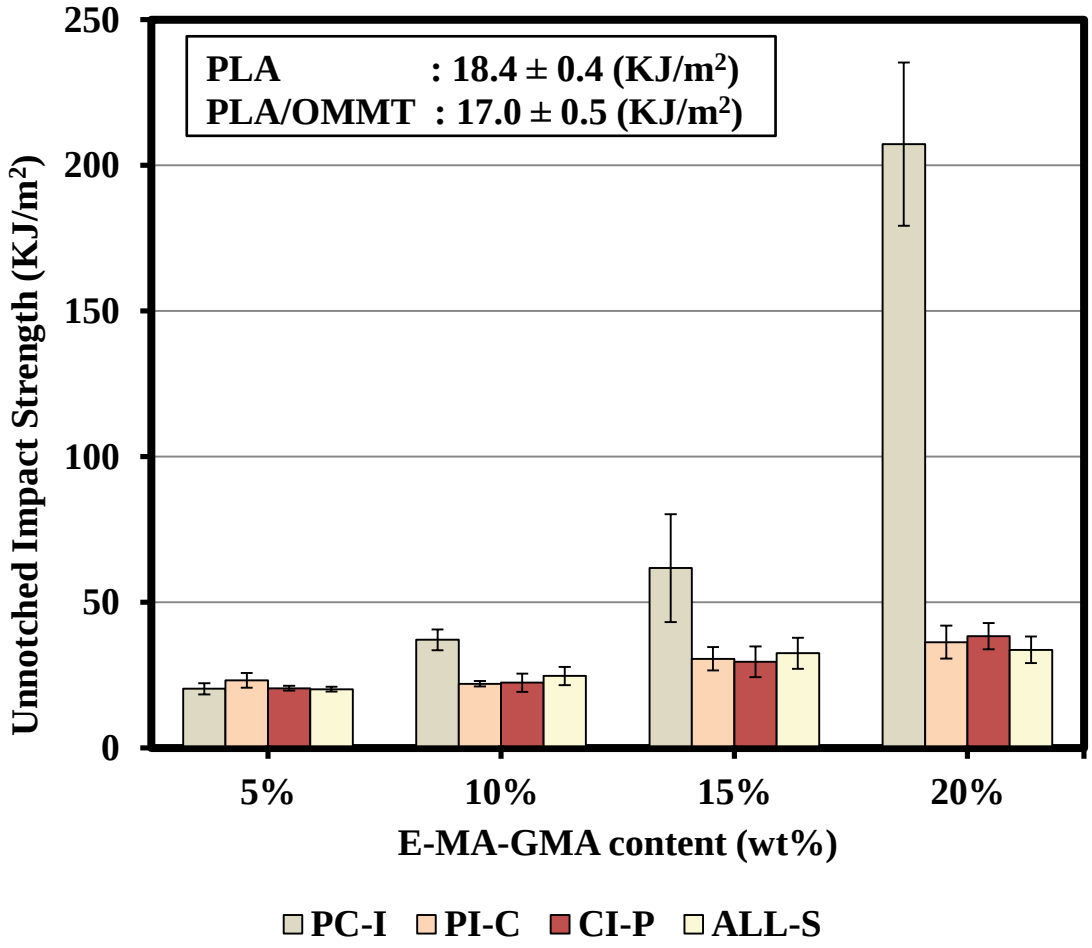

Figure VI.21 Unnotched Charpy Impact Strength of the Ternary Nanocomposites as a Function of Rubber Content at 2 wt% Clay.

The effects of the rubber and mixing sequences on IS were totally different from that on tensile properties (**Figure VI.21**). It was, interesting to note that the presence of E-MA-GMA rubber reduced the negative influence of the organoclay on the impact strength of the nanocomposites. For all the preparation procedures, the IS was gradually improved as the rubber fraction increased from 5 wt% to 20 wt% (**Figure VI.21**). This correlates with the elastomeric nature of the rubber and with the in situ formation of graft copolymer (PLA-g-rubber) at the interface. This copolymer situated at the interface promotes load transfer, consequently improving the IS. In addition, the homogeneous dispersion of the rubber domains initiates multiple crazes (as observed by the intense stress whitening on fractured specimens) and stops and/or deflects the crazes and cracks giving rise to efficient strain energy dissipation responsible of enhanced IS. This improvement of IS owing to addition of the low stiffness-low strength E-MA-GMA rubber to PLA corroborates with the results of different research studies.**[1,2,4-8,11,15,17,18,20,22-26]**

At 5 wt% rubber concentration, all of the nanocomposites displayed similar IS of nearly 20.0 J/m^2. However, at 10 wt% and higher rubber content, the PC-I nanocomposites exhibited the highest IS owing to their small rubber domain size and to superior clay dispersion, as detected by XRD and TEM techniques. Especially, above 10 wt% rubber content high degree of clay dispersion was achieved resulting in favorable impact resistance enhancement. Furthermore, the likely presence of most of the clay in the PLA continuous phase, as discussed earlier, should be another important factor for the high IS recorded for PC-I nanocomposites.**[25,26]**

A super-tough PC-I nanocomposite was obtained at 20 wt% rubber content with an IS above 207.3 J/m^2 representing 11-fold increase compared with that of neat PLA. The PC-I specimens with 10 wt% and 15 wt% rubber content were partially broken, whereas some of the specimens with 20 wt% rubber did not break, but only bended indicating that the actual IS would be greater than 207.3 J/m^2 (**Figure VI.22**).

PI-C, CI-P and ALL-S nanocomposites displayed almost similar IS at all rubber contents, and this value was lower than that of the IS of PC-I owing to their larger

rubber particle size compared with PC-I. Large rubbery domain size increase stress concentration effects, thus reducing the beneficial effect of the rubber. The results of IS demonstrate that, especially for PI-C and PC-I, at 10 wt% better stiffness-toughness balance was accomplished.

Figure VI.22 Representative Broken Samples of the PC-I Ternary Nanocomposites at 20 wt% Rubber Ratio.

These above results of mechanical properties first demonstrate the effectiveness of the rubber incorporation to change the fracture behavior of the PLA nanocomposite from brittle to ductile as a result of its ability to absorb and dissipate energy upon applied external deformation stresses, and second that the optimum rubber content for improved tensile and impact toughness was 10 wt% identified especially for PI-C and PC-I for which a stiffness-toughness balance was accomplished. Finally it can be stated that the interfacial strength associated with the effective physical and chemical interactions between the phases were the key factors for tensile and impact properties enhancement that were highly affected by the compounding protocol, clay dispersion and the size of the rubber domains, but not by the degree of crystallinity since, as was estimated by DSC in next section, all of the nanocomposites had nearly comparable low crystallinity levels in the range 4-8% irrespective of the preparation sequence.

VI-4 Thermal Characterization: Differential Scanning Calorimetry (DSC)

Differential scanning calorimetry (DSC) was performed on samples from injected dog-bone tensile specimens to investigate the thermal behavior of PLA and its nanocomposites. In order to clarify whether PLA crystallization had any influence on toughening of the nanocomposites, the crystallization and melting behaviors of PLA in the nanocomposites were studied. Consequently, the DSC data were determined from only one heating scan (0°C to 220°C), because it is the crystallinity of PLA in the as molded specimens that might affect the mechanical performance of the nanocomposites, the goal was thus to find this crystallinity from the tensile test samples. PLA and the nanocomposites exhibited similar thermograms (**Figure VI.23**) characterized by three prominent transitions namely: a glass transition temperature (T_g), a crystallization exotherm (T_c and ΔH_c), and a melting endotherm (T_m and ΔH_m). Values of these relevant thermal properties derived from the thermograms are shown in **Table VI.1** including the estimates of the degree of crystallinity (χ_c) of PLA computed using equation 3.8 of chapter 3 and a value of 93 J/g for the heat of fusion of 100% crystalline PLA.**[3,8]**

The T_g of PLA was clearly observed on all the DSC traces and that of the rubber which is below room temperature was not detected by this DSC analysis, consequently it was not studied here. The pure rubber shows only a melting temperature (T_m) recorded at 53.10°C.

Neat PLA had a T_g centered at 56.13°C, a crystallization peak T_c at 115.79°C and a subsequent melting peak T_m at 147.07°C. The areas of the crystallization and melting peaks on its thermogram were almost the same indicating that PLA was primarily in the amorphous state after the injection process. This was also confirmed through its computed degree of crystallization using equation 3.8 of chapter 3 ($\chi_c \approx 5.94\%$).

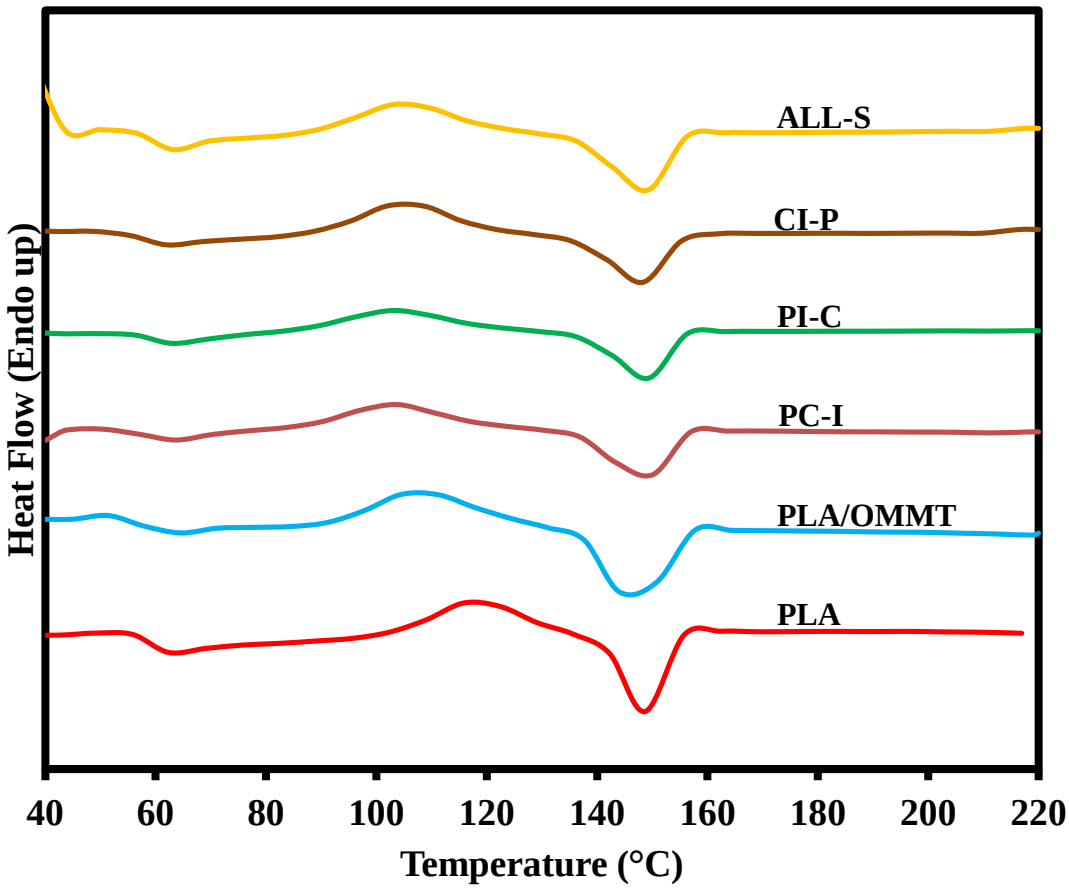

Figure VI.23 DSC Thermogram of PLA, PLA/OMMT and PC-I, PI-C, CI-P and ALL-S Nanocomposites Prepared with 10 wt% E-MA-GMA Rubber.

As can be noticed from **Table VI.1**, neither clay and rubber addition nor the blending protocols and rubber fraction significantly affected the T_g of PLA in the nanocomposites suggesting that after blending the macromolecular chains conserved their mobility and that the PLA and the rubber were immiscible.**[8,16]** Interestingly, T_m of all the nanocomposites also remained relatively unchanged with variations of about only 1-3°C implying that the rubber and the clay did not significantly modify the PLA crystal structure and did not affect the integrity of its crystals.**[1]** Unaltered T_g after OMMT and rubber addition to PLA was observed in various studies**[6,11,14]** and similar results were also found by Chow et al.**[15]** for PLA/SEBS-g-MAH/nanoprecipitated $CaCO_3$ (NPCC), and by Alyamac and Yilmazer**[21]** for PET/E-MA-GMA/OMMT nanocomposites.

TABLE VI.1
Calorimetric Characteristics of PLA and its Ternary Nanocomposites

	T_g (°C)	T_c (°C)	T_m (°C)	χ_c (%)
PLA	56.13	115.79	147.07	5.94
PLA/OMMT, Clay (2wt%)	57.20	109.40	150.74	3.70
PC-I, Rubber (wt%)				
5	58.55	102.76	149.30	4.42
10	57.44	102.93	148.25	5.78
15	58.28	104.52	147.51	7.20
20	57.58	108.58	148.11	7.82
PI-C, Rubber (wt%)				
5	58.89	104.12	149.08	4.39
10	58.96	103.38	148.09	4.88
15	57.45	103.78	147.58	5.08
20	57.70	103.90	145.07	6.26
CI-P, Rubber (wt%)				
5	57.39	105.79	146.44	3.92
10	57.08	105.38	145.92	6.10
15	55.98	107.48	146.20	7.05
20	57.55	110.51	150.58	7.62
ALL-S, Rubber (wt%)				
5	58.70	104.26	146.13	4.07
10	59.16	105.28	145.91	5.51
15	58.91	105.01	146.34	5.99
20	58.77	105.78	146.66	7.62

There was a substantial shift to lower temperature of the PLA crystallization transition peaks (**Table VI.1**). The T_c of PLA decreased from 115.79°C to 109.40°C after addition of 2 wt% OMMT showing that clay served as a heterogeneous nucleating agent enhancing thus PLA ability to crystallize fast owing to OMMT low aspect ratio (large surface area). **[6,11-14,16,17]** The nucleating effect of OMMT was more significant in the case of PC-I, PI-C and ALL-S nanocomposites owing to their high clay dispersion level (high aspect ratio) and high contact area that are favorable for crystal nucleation. In a previous work on PET/E-MA-GMA/OMMT, a decrease of T_c from 138°C to 128°C was detected at 1 wt% OMMT. The decrease in T_c was more significant at higher clay contents, and this decrease in T_c was found to be independent

of the compounding sequence of the nanocomposites and it was ascribed to the nucleating effect of OMMT.**[21]**

Regardless of the mixing order, addition of the rubber in all the nanocomposites induced a further decrease in T_c (**Table VI.1**) pointing out to the nucleating activity of the rubber.**[6,16]** The T_c of PLA decreased after being toughened by an ethylene copolymer (Biostrong from DuPont), and then underwent a progressive decrease as the clay content increased. This effect was attributed to the nucleating behavior of both clay and Biostrong.**[17]** Dasari et al.**[25]** also reported the nucleating effect of SEBS-g-MAH in binary PA66/SEBS-g-MAH blend, before incorporation of OMMT. The thermal results reported here (T_g, T_m, T_c) are also in line with those obtained by Balakrishnan et al..**[17]** It was reported that T_g and T_m were unchanged after Biostrong and clay addition; whereas both of these additives were found to exert strong nucleating effect on PLA and reduced its T_c.

According to **Table VI.1**, significant decrease in T_c is observed for PC-I, because it was in this compounding order that the clay was the best dispersed and the clay mostly resided in PLA phase permitting the clay to serve as effective heterogeneous nucleating agent for PLA. The lowest drop in T_c was recorded for CI-P probably due to confinement of most of the clay particles inside the rubber phase which therefore blocked its ability to act as nucleating species.**[11,14]** In the study of PLA/SEBS-g-MAH/NPCC, Chow et al.**[15]** found that the nucleating effect of the NPCC was inhibited owing to its embedment in the rubber.

As the rubber content was increased, the value of T_c stabilized for PI-C and ALL-S and increased for PC-I and CI-P. For the two former nanocomposites this is attributed to the maximized interactions of the rubber with PLA in these nanocomposites which might have hindered clay heterogeneous nucleating activity. For the two later, this is ascribed to the intercalation of most of the rubber into the clay galleries in PC-I which hampered its additional nucleating behavior besides that of the clay, and to the encapsulation of most of the clay in the rubber phase in the case of CI-P that inhibited clay nucleating role.

The degree of crystallinity (χ_c) of PLA decreased slightly from 5.94% to 3.70% after incorporation of OMMT to PLA, because the clay imposed restrictions to chain motion necessary for crystallization.**[6,11,13,18,23]** For all mixing sequences, when the rubber was added to the tune of 5 wt% there was a marginal increase in χ_c. As the rubber loading increased, the χ_c did not undergo noticeable change, and its values for the different nanocomposites were nearly around that of the control PLA (6-8%). This is associated with the low clay loading and with clay intercalated/partially exfoliated structure in PC-I, PI-C and ALL-S, and with the presence of large agglomerates in CI-P which allowed clay particles to serve as physical obstacles impeding thus PLA molecules to rearrange and crystallize **[6,11-13,20,23]**. In addition, the reaction of PLA with clay decreased the amount of PLA crystallizing molecules, whereas that with the rubber not only imparted the same effect, but also diminished molecular mobility necessary for chain packing first due to viscosity buildup by PLA chain extension, and second due to these formed PLA extended chains which constrained and prevented PLA molecules to take part in the crystallization process.**[3,5-9,11]** In short it can be stated that for all the mixing sequences there was a slight increase in χ_c as the rubber loading increased, but the level of crystallinity was less than 8%.

VI-5 CONCLUSIONS

PLA was reactively melt blended with an E-MA-GMA rubber in the presence of 2 wt% of an organo-modified montmorillonite (OMMT). The rubber content was varied from 5 to 20 wt% and four components addition protocols were used to prepare the nanocomposites in a co-rotating twin screw extruder.

XRD results, which were confirmed by TEM, revealed that PC-I resulted in the best clay dispersion and CI-P resulted in the worst one. Complete exfoliation of OMMT was not achieved, and all of the nanocomposites exhibited intercalated/partially exfoliated structures.

SEM observations revealed that PLA and the rubber were immiscible, but compatible attributed to the effective chemical reaction between the functional groups

of the polymers. The rubber formed sub-micron dispersed phase, the size of which was influenced by the preparation procedure. PC-I and PI-C nanocomposites exhibited the smallest rubber particle size associated with their superior clay dispersion and with the active role of clay that acted as a barrier for coalescence, whereas ALL-S and CI-P nanocomposites showed larger phase size as a result of the encapsulation of most of the clay in the rubber which hindered the barrier effect of clay for coalescence and reduced droplet breakup by stiffening the rubber. Incorporation of the rubber into the nanocomposites resulted in debonding/cavitation, crazing and shear yielding energy dissipating mechanisms in all of the nanocomposites and changed PLA deformation behavior from brittle to ductile.

Mechanical performance of the nanocomposites was influenced by the mixing sequence. The rubber and OMMT addition improved ductility and toughness of PLA without significantly sacrificing the strength, and optimum stiffness-fracture toughness was achieved at 10 wt% rubber content. PC-I nanocomposites showed the highest impact toughness and PI-C nanocomposites exhibited the highest elongation at break in tensile tests, owing to their better clay dispersion and their small rubber particle size. ALL-S and CI-P displayed lower mechanical performance than the PC-I and PI-C, because of their large particle size and reduced rubber cavitation ability due to the encapsulation of most of the clay in the rubber in these nanocomposites.

DSC analyses confirmed the immiscibility of the blended polymers. After addition of rubber and OMMT to PLA, T_g and T_m of the matrix remained relatively unaltered, but T_c underwent a substantial decrease demonstrating the heterogeneous nucleating role of the elastomer and the clay. These thermal characteristics and the degree of crystallinity were found to be independent of the preparation procedure.

REFERENCES

[1] Zeng, J.; Li, Y.; He, Y. ; Li, S.; Wang, Y. Ind. Eng. Chem. Res., Vol. 50, pp 6124 **(2011)**.

[2] Zhao, Q.; Ding, Y.; Yang, B.; Ning, N.; Fu, Q. Polymer Testing, Vol. 32, pp 299 **(2013)**.

[3] Yeh, J.; Tsou, C.; Li, Y.; Xiao, H.; Wu, C.; Chai, W.; Lai, Y.; Wang, C. J. Polym. Res., Vol. 19, pp 9766 **(2012)**.

[4] Juntuek, P.; Ruksakulpiwat, C.; Chumsamrong, P.; Ruksakulpiwat, Y. J. Appl. Polym. Sci., Vol. 125, pp 745 **(2012)**.

[5] Sun, S.; Zhang, M.; Zhang, H.; Zhang, X. J. Appl. Polym. Sci., Vol. 122, pp 2992 **(2011)**.

[6] Baouz, T.; Rezgui, F.; Yilmazer, U. J. Appl. Polym. Sci., Vol. 128, pp 3193 **(2013)**.

[7] Zhang, N.; J. Wang, Q.; Ren, J.; Wang, L. J. Mater. Sci., Vol. 44, pp 250 **(2009)**.

[8] Taib, R. M.; Ghaleb, Z. A.; Mohd Ishak, Z. A. J. Appl. Polym. Sci., Vol. 123, pp 2715 **(2012)**.

[9] Bhardwaj, R.; Mohanty A. K. Biomacromolecules, Vol. 8, pp 2476 **(2007)**.

[10] Meng, B.; Deng, J.; Liu, Q.; Wu, Z.; Yang, W. Eur. Polym. J., Vol. 48, pp 127 **(2012)**.

[11] Leu, Y. Y. ; Mohd Ishak, Z. A.; Chow, W. S. J. Appl. Polym. Sci., Vol. 124, pp 1200 **(2012)**.

[12] Balakrishnan, H.; Hassan, A.; Wahit, M. U.; Yussuf, A. A.; Abdul Razak S. B. Materials and Design, Vol. 31, pp 3289 **(2010)**.

[13] Yu, Z.; Yin, J.; Yan, S.; Xie, Y. ; Ma, J. ; Chen, X. Polymer, Vol. 48, pp 6439 **(2007)**.

[14] Chow, W. S.; Lok, S. K. J. Therm. Analys. Calorim., Vol. 95, pp 627 **(2009)**.

[15] Chow, W. S.; Leu, Y. Y. ; Mohd Ishak, Z. A. eXPRESS Polym. Lett., Vol. 6, pp 503 **(2012)**.

[16] Lewitus, D.; McCarthy, S.; Ophir, A.; Kenig, S. J. Polym. Environ., Vol. 14, pp 171 **(2006)**.

[17] Balakrishnan H.; Masoumi, I.; Yussuf, A. A.; Imran, M.; Hassan, A.; Wahit, M. U. Polym-Plast. Technol. Eng., Vol. 51, pp 19 **(2012)**.

[18] Ahn, Y.; Paul, D. R.; Polymer, Vol. 47, pp 2830 **(2006)**.

[19] Coskunses, F. I.; Yilmazer, U. J. Appl. Polym. Sci., Vol. 120, pp 3087 **(2011)**.

[20] Yeniova, C. E.; Yilmazer, U. Polym. Comp., Vol. 31, pp 1853 **(2010)**.

[21] Alyamac, E.; Yilmazer, U. Polym. Comp., Vol. 28, pp 251 **(2007)**.

[22] Martins, C. G.; Larocca, N. M. ; Paul, D. R.; Pessan L. A. Polymer, Vol. 50, pp 1743 **(2009)**.

[23] Borah, J. S., Karak, N.; Chaki, T. K. Mat. Sci. Eng. Part: A, Vol. 528, pp 2820 **(2011)**.

[24] Oliveira, A. D.; Larocca, N. M.; Paul, D. R.; Pessan, L. A. Polym. Eng. Sci., Vol. 52, pp 1909 **(2012)**.

[25] Dasari A.; Yu, Z.; Yang, M.; Zhang, Q.; Xie, X. ; Mai, Y. Comp. Sci. Tech., Vol. 66, pp 3097 **(2006)**.

[26] Dasari, A.; Yu, Z.; Mai, Y. Polymer, Vol. 46, pp 5986 **(2005)**.

[27] Hong, J. S.; Namkung, H.; Ahn, K. H.; Lee, S. J.; Kim C. Polymer, Vol. 47, pp 3967 **(2006)**.

[28] Ghasemi, H.; Carreau, P.J.; Kamal, M.R.; Uribe-Calderon J., Vol. 51, pp 1178 **(2011)**.

[29] Oyama, H. T.; Kitagawa T.; Ougizawa, T.; Inoue,T.; Weber M. Polymer, Vol. 45, pp 1033 **(2004)**.

[30] Balakrishnan S.; Start P. R.;Raghavan D.; Hudson, S. D. Polymer, Vol. 46, pp 11255 **(2005)**.

[31] Lim, S.; Dasari, A.; Yu, Z.; Mai, Y.; Liu, S.; Yong, M. S. Comp. Sci. Tech., Vol. 67, pp 2914 **(2007)**.

[32] Pillin I.; Montrelay N.; Bourmaud A.; Grohens Y. Polym. Degrad. Stab., Vol. 93, pp 321 **(2008)**.

[33] Zenkiewicz, M.; Richert, J.; Rytlewski, P.; Moraczewski, K.; Stepczynska, M.; Karasiewicz T. Polymer Testing, Vol. 28, pp 412 **(2009)**.

Chapter VII

GENERAL CONCLUSIONS AND RECOMMENDATIONS

Chapter VII - General Conclusions and Recommendations

VII-1 General Conclusions

The low toughness of PLA characterized by low impact strength (as low as 2.5-3 kJ/m^2), and its low tensile elongation (less than 4%) have been the major bottle necks for its widespread utilization. Undoubtedly, the improvements of these PLA characteristics will enlarge its application window were these properties are required. Our literature survey showed that most of PLA modification attempts for toughness enhancement were performed by melt blending with either flexible polymers or rubbers. Our present research is a contribution in this research area that is still attracting great interest of researchers from both academia and industry

In the first part of our research study, PLA was reactively melt blended with an ethylene-methyl acrylate-glycidyl methacrylate rubber (E-MA-GMA) in the range 5-30 wt% using a twin screw extruder. Addition of 2 wt% of an organo-montmorillonite (OMMT) was necessary to compensate the negative effect of the rubber on strength. In the second part of this study, and with the same aim of increasing further PLA toughness, the effects of four addition sequences of the components of the ternary nanocomposites (PLA/OMMT/E-MA-GMA) was also carried out. The main findings and conclusions from both studies can be outlined as follows:

PLA/E-MA-GMA blend forms an immiscible but compatible polymer mixture characterized by finer sub-micron dispersion of the rubber particles in the binary blends than in the nanocomposites. Rubber particle size increases with increasing rubber content, and the OMMT did not play the role of a barrier for the coalescence in the nanocomposites, especially for ALL-S and CI-P owing probably to its encapsulation in the rubber. Furthermore, particle size was significantly influenced by the nanocomposites preparation procedure, which in turn has influenced the performance of the mixtures.

OMMT disperses better in PLA than in the rubber, and all nanocomposites showed intercalated/exfoliated structures. Complete clay exfoliation was not attained for all nanocomposites,except at the critical rubber concentration of 10wt% for ALL-S

extruded once as discussed in chapter 4. Dispersion of OMMT was enhanced in the nanocomposites as the rubber ratio increased in nanocomposites especially for PC-I due to co-intercalation of the rubber with PLA into clay galleries, a fact not at all observed for CI-P.

E-MA-GMA is an effective toughener for PLA, it changed the deformation behavior of PLA from brittle to ductile. All nanocomposites exhibited balanced stiffness-toughness at 10 wt% rubber content. High impact toughness was attained when PLA was first mixed with the clay before the rubber was added (PC-I), and the highest tensile toughness was obtained when PLA was first compounded with the rubber, and then clay was incorporated into the mixture (PI-C).

The viscosity of the mixtures as measured by melt flow index was highly influenced by the rubber and the OMMT, and a plasticizing phenomenon was observed above 20 wt% rubber ratio.

Both OMMT and the rubber acted as nucleating agents for PLA and reduced its crystallization temperature, but both did not affect much the T_g confirming thus the immiscibility of the blends. In addition, the degree of crystallinity and the other thermal properties of PLA were not affected neither by these additives nor by the preparation sequence.

VII-2 Recommendations for Future Research Work

Being the first in its kind, we hope this work will open new windows in building structure-processing relationships of PLA/rubber nanocomposites. This research study is far from being complete and several research aspects that needed deep investigations and other new questions that arose from this work present some opportunities for future research work. In this regard, the recommendations to continue this work are as follows:

- The promising results of this study encourage carrying out simultaneous rubber-toughening and plasticization using preferentially a reactive plasticizer for further improvements of PLA toughness and extensibility.
- Even though the reaction between PLA functional groups and those of the rubber have been evidenced in literature, it would be informative to study a possible enhancement of this reaction through the use of a catalyst and conduct an FTIR investigation.
- In this study it was observed that one of the processing parameters played an important role on the performance of the designed materials. In this regard processing optimization can be extended to include other parameters such as processing temperature, screw speed and configuration, in addition to the use of the masterbatch technique as a complementary mixing method to the already investigated four addition modes of the nanocomposites components.
- Because PLA is shear sensitive, it is also interesting to investigate the effect of reprocessing PLA in some of the used protocols. In this direction, the determination of Mw, for example by gel permeation chromatography, may give valuable information. This also can be complemented by a study of the effects of the rubber and the clay on the thermal stability of the mixtures.
- Since the MFI was found to be highly influenced by the rubber and nanofiller addition, the rheology of the blends and nanocomposites deserves a deep investigation.
- Because the study was aimed to prepare a new material for packaging applications, it is recommended that the barrier properties of the new ternary nanocomposites to be thoroughly studied.
- Finally, it is recommended to explore the effects of the rubber and the clay on the biodegradability of PLA.

Published Peer-Reviewed Manuscript 1

Journal of Applied Polymer Science

Ethylene-Methyl Acrylate-Glycidyl Methacrylate Toughened Poly(lactic acid) Nanocomposites

Touffik Baouz,[1] Farouk Rezgui,[1] Ulku Yilmazer[2]

[1]Laboratoire des Matériaux Organiques, Faculté de Technologie, Département de Génie des Procédés, Université Abderrahmane Mira, Béjaia 06000, Algeria

[2]Chemical Engineering Department, Middle East Technical University, 06800, Ankara, Turkey

Correspondence to: T. Baouz (E-mail: baouztoufik@yahoo.fr)

ABSTRACT: Poly (lactic acid) (PLA) was melt blended in a twin screw extruder using an ethylene-methyl acrylate-glycidyl methacrylate rubber as a toughener. PLA/rubber blends were immiscible as observed by scanning electron microscopy. Impact strength and ductility of PLA were improved by the addition of the rubber at the expense of strength and stiffness. An organo-montmorillonite (OMMT) was used at 2 wt % to counteract the negative effect of the rubber on modulus, and balanced properties were observed at 10 wt % rubber content. X-ray diffraction and transmission electron microscopy revealed the formation of intercalated/exfoliated structure in the ternary nanocomposites. Thermal behavior analysis indicated that the degree of crystallinity is slightly affected by the clay and the rubber. Both the clay and the rubber decreased the crystallization temperature of PLA and acted as nucleating agents for PLA. The viscosity of the mixtures as measured by melt flow index was highly influenced by the rubber and the OMMT. © 2012 Wiley Periodicals, Inc. J. Appl. Polym. Sci. 128: 3193–3204, 2013

KEYWORDS: Poly(lactic acid); nanocomposite; organoclay; rubber toughening; glycidyl methacrylate

Received 19 April 2012; accepted 19 August 2012; published online 20 September 2012
DOI: 10.1002/app.38529

INTRODUCTION

Biodegradable polymers play a major role in the protection of the environment by reducing the amount of wastes derived from petroleum based polymers, and they limit the depletion of natural resources that are finite. Among a number of bio-based polymers, poly (lactic acid) produced from renewable resources is a linear aliphatic thermoplastic polyester with promising potential to substitute for conventional polymers owing to its biodegradability, renewability, processability, and climate-naturality.[1,2]

PLA found use in diverse applications such as in biomedical and packaging fields.[2,3] Although PLA has comparable properties to many conventional polymers, its brittleness and low glass transition temperature hindered its applications where toughness is desired. To overcome this limitation various strategies have been adopted such as copolymerization, plasticization, addition of organic/inorganic fillers, and melt-blending with either biodegradable or nonbiodegradable polymers.[2–4]

It is proposed that improvement of several mechanical properties are possible by copolymerization; however, up to now none of the PLA copolymers are reported to be economically feasible or commercially available.[5,6] Plasticizers are used to enhance ductility and flexibility, but researchers are faced with two major issues: evaporation of small-sized plasticizers during processing at elevated temperatures and migration of the plasticizers to the surface of the polymer matrix.[7,8] As rigid fillers, metal oxides,[9] calcium carbonate,[10] hydroxyapetite,[11] and organically modified clays were investigated.[12,13] Organically modified layered silicates are favored since their high aspect ratio was shown to bring superior mechanical, rheological, fire retardancy, and gas barrier properties.[14–16] In most cases, addition of layered silicates is known to increase rigidity, but decrease toughness. Chang et al.[17] prepared nanocomposites using a montmorillonite modified with hexadecylamine (C_{16}-MMT) and a fluorinated-mica modified with hexadecylamine (C_{16}-Mica) via solution intercalation. The maximum ultimate tensile strength was observed at a certain clay concentration (4 wt %) for both types of fillers. Furthermore, in C_{16}-MMT, the initial modulus increased with increasing organoclay content up to the same critical clay concentration.

Melt blending with various polymers is the mostly preferred strategy in toughening PLA. Numerous biodegradable polymers were reported to have been melt blended with PLA to enhance toughness.[2,18] Among the biodegradable ones, polycaprolactone (PCL) is one of the most extensively investigated polymers.

However, it is immiscible with PLA, hence it requires compatibilizers. Broz et al.[19] produced binary blends of PLA/PCL and obtained an increase in strain at break above a PCL content of 60 wt %, accompanied by reduction in tensile modulus and strength. On the other hand, addition of a small amount of PLA–PCL–PLA triblock copolymer (4 wt %) to PLA/PCL binary blends improved the dispersion of PCL in PLA and enhanced the ductility. PLA was also toughened with miscellaneous nonbiodegradable polymers such as Linear Low Density Polyethylene[20] Polycarbonate[21] and Poly(Ethylene Oxide).[22]

Addition of suitable rubbery polymer is an effective way to enhance toughness, since the rubber blended with the brittle polymer dissipates the stress so that the material shows ductility and plastic deformation. Among the factors governing the performance of rubber toughened polymers the rubber content, rubber domain size and distribution, interfacial tension and viscosity ratio between the polymer matrix and the rubber can be cited.[23,24] The main toughening mechanisms responsible for energy dissipation resulting in enhanced properties include crazing and shear yielding of the polymer matrix and cavitation of the rubber inclusions.[2,25]

Numerous research studies have been published where biodegradable[3,26] and nonbiodegradable rubbers[27–30] were used to toughen PLA. Sun et al.[4] synthesized glycidyl methacrylate (GMA) functionalized acrylonitrile-butadiene-styrene (ABS-*g*-GMA) by emulsion polymerization at different concentrations of GMA and used them to improve the toughness of PLA. The reaction of the epoxy groups of ABS-*g*-GMA and carboxyl and hydroxyl terminal groups of PLA was observed by torque measurements. These reactions are schematically shown in Reference 4. Hashima et al.[31] improved the impact strength and elongation at break of PLA by the addition of hydrogenated styrene-butadiene-styrene block copolymer (SEBS) rubber to PLA, and further enhancement was observed by using poly (ethylene-glycidyl-methacrylate) EGMA as a compatibilizer. Oyama[28] studied a reactive blend of PLA with EGMA rubber. The reported Charpy impact strength (72 KJ/m^2) for the blend (80/20, w/w) was 50 times higher than that of the pristine PLA after annealing the samples at 90°C for 2.5 h.

Production of ternary nanocomposites for combining the advantages of layered silicates and rubbers is another alternative to improve the properties of PLA. Recently PLA/organo-montmorillonite (PLA/OMMT) toughened with maleated styrene-ethylene-butylene-styrene (SEBS-*g*-MAH) was studied by Leu et al.[29] It was reported that some of the clay was encapsulated into the rubber phase owing to its affinity to the maleic anhydride groups of the rubber. It was also observed that the degree of crystallinity decreased with increasing rubber content and both elongation and tensile impact strength were improved at the expense of modulus and strength. Bitinis et al.[32] toughened PLA with natural rubber (NR) using three different nanoclays. The two organo-montmorillonites were observed to be located at the interface and they acted as compatibilizer and barrier for coalescence of the rubbery phase, resulting in finer particle dispersion of the rubber. However, the unmodified clay resided in the PLA matrix and did not affect the NR droplet morphology. PLA rubber toughened blends are rather well documented, but the literature on their ternary nanocomposites is scarce.

The objective of this work was an attempt to toughen PLA with an ethylene-methyl acrylate-glycidyl methacrylate (E-MA-GMA) rubber by reactive blending in a twin screw extruder. To counterbalance the loss in modulus of these blends, an organo-montmorillonite clay was used to prepare ternary nanocomposites. The structure of the materials was investigated by XRD, TEM, and SEM. Thermal properties of the materials were studied by DSC, and their mechanical performance was evaluated by impact and tensile testing. Melt Flow Index (MFI) measurements were carried out to determine the rheological properties of the mixtures.

EXPERIMENTAL

Materials

PLA (PLI 005) of commercial injection grade was obtained from NaturePlast (Caen, France). According to the manufacturer, it has a density of 1.25 g/cm^3 (ISO 1183), and a melting temperature in the range of 145–155°C. The rubber, Lotader® AX8900 was obtained from ARKEMA (Puteaux, France). It is a terpolymer of ethylene-methyl acrylate and glycidyl-methacrylate (E-MA-GMA). According to the data sheet of the material, methyl acrylate and GMA contents are 24 and 8 wt % respectively. The nanoscale filler was an organo-modified montmorillonite clay, Closite® 30B, provided by Southern Clay Products (Gonzales, Texas, USA). The cation of the organic modifier of the clay is methyl, tallow, bis-2-hydroxyethyl, quaternary ammonium (MT2EtOH) used at a concentration of 90 mEq/100 g clay, and the anion is chloride.

Preparation of the Samples

Before the extrusion step, PLA and organoclay were dried overnight at 80°C in a vacuum oven and the rubber was dried overnight at 45°C in a conventional oven. In the binary and ternary nanocomposites, the weight percent of the rubber was varied in the range of 5–30 wt %, and the amount of clay in the nanocomposites was kept constant at 2 wt %. All the mixtures were prepared using a Thermoprism TSE 16 TC fully intermeshing, co-rotating twin screw extruder (L/D = 24) with processing zone temperatures of 150–170–170–170–170°C from the hopper to the die. The dry mixtures were tumbled in a plastic bag and fed directly into the hopper equipped with a mixer. The screw speed was 250 rpm and the feed rate was 25 g/min.

The extruded rods were collected on aluminum plates and cooled at ambient temperature to avoid hydrolysis of PLA by water cooling. Thereafter, a pelletizer was used to grind the extrudates. For comparison, PLA was extruded at the same conditions as for the blends and nanocomposites to serve as reference.

Specimens for characterization tests were prepared using a DSM Xplore mini injection molding equipment at cylinder and mold temperatures of 170 and 60°C, respectively. Prior to injection molding, all materials were dried overnight in a vacuum oven at 80°C.

CHARACTERIZATION

X-Ray Diffraction (XRD) and Transmission Electron Microscopy (TEM)

The nanocomposite samples for XRD tests were cut from dog-bone tensile bars. X-ray diffraction (XRD) measurements were performed at room temperature in the reflection mode for the organoclay pristine powder and the molded nanocomposites using a Rigaku D/MAX 2200/PC X-ray diffractometer. A monochromatic CuKα radiation ($\lambda = 1.5418$ Å), that generated a voltage of 40 kV and current of 40 mA, was used as a source. X-ray patterns were recorded with a step size of 0.02° from $2\theta = 1°$ to 10° at 1°/min scan rate. The basal spacing or (d_{001}) reflection of the samples was calculated from the peak positions using Bragg's law.

The microstructure of the nanocomposites was observed using a FEI Spirit G^2 Biotwin transmission electron microscope under an accelerating voltage of 80 kV in bright field mode. Ultrathin sections (70–80 nm) of the nanocomposites were obtained from impact test bars with Leica Ultracut UCT Ultramicrotome and deposited onto copper grids.

Scanning Electron Microscopy

Scanning electron microscopy (SEM) observations were made on cryofractured specimens. Injection molded impact test bars were immersed and kept in liquid nitrogen for 5 min and then broken. Etching of the rubber phase was carried out in a sonication bath at 45°C with liquid n-heptane until the surface of the specimen was whitened. The etched cryofractured surfaces were coated with thin gold film and analyzed with a Jeol JSM-6400 low voltage microscope. Domain size of the dispersed rubber phase in the prepared materials was determined by using ImageJ software program.[33]

Mechanical Properties

The mechanical tests were performed at room temperature. The tensile modulus, tensile strength, and elongation at break were obtained through tensile tests carried out according to ISO 527 using a Shimadzu Autograph AG-IS 100 KN dynamometer at a crosshead speed of 3 mm/min. Notched Charpy impact strength measurements were done by using a Ceast Resil Impactor pendulum according to ISO 179. The notch had a radius of 0.1°, an angle of 45°, and a depth of 2 mm. In both tests, at least five specimens were tested for each set of samples, and the mean value and the standard deviations are reported.

Melt Flow Index Measurements

Melt flow index (MFI) of the neat components and the mixtures was measured according to ISO 1133 using Omega Melt Flow Indexer at a temperature of 190°C under a load of 2.16 kg. At least five measurements were taken for each sample and the results were averaged to obtain a mean value.

Thermal Properties

Thermal behavior of the materials was studied using DSC-60 Shimadzu Differential Scanning Calorimetry (DSC). Samples of 9–10 mg were cut from injection molded tensile bars, sealed in aluminum pans and heated from room temperature to 220°C at a heating rate of 10°C/min under nitrogen purge to avoid moisture and oxidative degradation. The glass transition temperature (T_g), crystallization temperature (T_c), melting temperature (T_m), crystallization enthalpy (ΔH_c), and melting enthalpy (ΔH_m) were determined from this scan. The degree of crystallinity of PLA in the compounds was estimated using the following equation:

$$W_c(\%) = \left(\frac{\Delta H_m - \Delta H_c}{\Delta H_f \times \emptyset_{PLA}}\right) \times 100 \quad (1)$$

where $W_c(\%)$ is the degree of crystallinity, ΔH_m and ΔH_c are the heats of fusion and crystallization of the sample respectively, ΔH_f is the heat of fusion of 100% crystalline PLA, and $\emptyset_{PLA}$ is the weight fraction of the PLA in the sample.

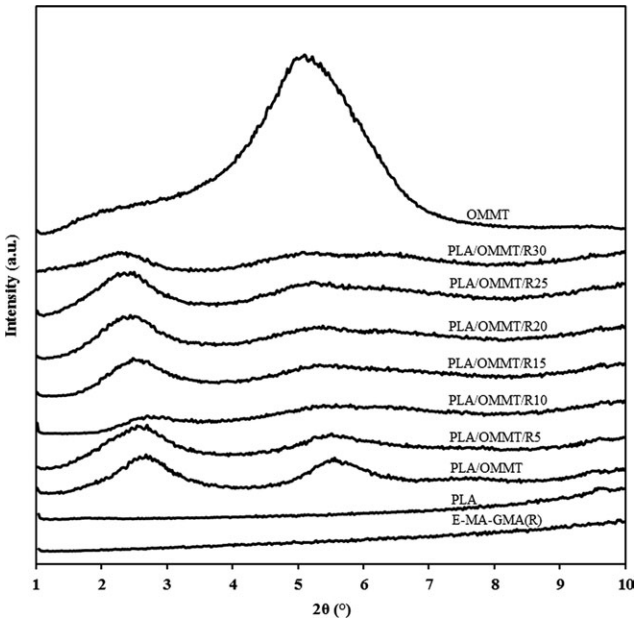

Figure 1. X-Ray patterns of PLA, rubber and the nanocomposites at 2 wt % OMMT. (The R indicates the rubber, and the number following R indicates the wt % of the rubber). The curves are shifted vertically for clarity.

RESULTS AND DISCUSSION

XRD Analyses

The structure of a nanocomposite, i.e. the extent of intercalation and exfoliation govern its properties. Thus, it is of paramount importance to determine the degree to which polymers intercalate the silicate sheets of the clay. TEM and XRD techniques have been widely used to evaluate the dispersion state of the clay platelets in polymer/clay nanocomposites.[2,12,15] The structure of a nanocomposite is usually established using XRD analysis at low angles ($2\theta < 10°$).[2,14,15] The interlayer spacing, called also "*d*-spacing", of the clay platelets can be evaluated from the primary diffraction peak position of the organoclay in the XRD diffractogram and Bragg's law ($n\lambda = 2\ d\ \sin\theta$). The disappearance of the characteristic peak, its shift to lower diffraction angle and the broadening of the peak suggest exfoliation, intercalation, and partial exfoliation respectively.[34]

Figure 1 shows the XRD traces recorded for PLA/OMMT and PLA/OMMT/rubber nanocomposites. XRD diffractograms of

OMMT, PLA, and rubber are also presented for comparison. The OMMT weight fraction in the nanocomposites was maintained constant at 2 wt %. PLA and the rubber displayed no characteristic peak in the range of observation, while the reference diffractogram of OMMT clay in pure powder form exhibited a strong peak at a diffraction angle of ($2\theta = 5.1°$), which corresponds to an interlayer spacing of 1.73 nm. This value corroborates with that reported in the manufacturer's data sheet.

When compounded with PLA, the characteristic diffraction peak of the organoclay shifted to lower diffraction angle ($2\theta = 2.58°$) and the intensity decreased suggesting that the *d*-spacing (d_{001}) increased to 3.42 nm. The distance between the clay platelets in the binary PLA/OMMT nanocomposite is larger than that in the neat clay indicating intercalation. The intercalated structure might be attributed to the affinity of PLA to the organoclay through hydrogen bonding between the carboxyl and hydroxyl end groups of PLA with the surface of OMMT and to possible interactions that might have also occurred between the terminal carboxyl groups of PLA with the hydroxyl groups of the surfactant present in the OMMT.[20] The original peak of the clay still appears in the diffractogram of this nanocomposite with lower intensity suggesting that some of the clay layers were not intercalated.

Addition of 5 wt % rubber to PLA/OMMT did not significantly affect the structure of the nanocomposite (Figure 1). As it can be observed, the original peak of the organoclay at ($2\theta = 5.1°$) still exists, but is smaller and broader implying intercalation and partial exfoliation due to additional intercalation of the rubber between the galleries of the clay. When the rubber content was increased to 10 wt %, both peaks disappeared from the diffractogram indicating complete exfoliation of the organoclay. This may be attributed to the affinity of the reactive rubber to the modifier of the clay. The rubber contains glycidyl reactive groups and ester moieties that might have interacted with both the clay modifier and PLA. In this sense, the rubber modifier also played the role of a compatibilizer and promoted dispersion of the OMMT.[15,34] Similar results were obtained by Chow et al.[14] In their study, they reported an incremental increase in the d-spacing when EPM-g-MAH was added to the PLA/OMMT system that was attributed to the diffusion of the rubber into the galleries of clay. Furthermore, addition of the rubber increased the shear intensity applied on the clay during processing owing to its high viscosity. Hence, more clay platelets were delaminated and dispersion and intercalation were improved.[34]

Except for the 10 wt % rubber content, it can be seen that the original peak of the clay still existed with a slight shift to lower angle, but it became broader and decreased in intensity, implying the presence of ordered tactoids.[34] It should be noted that at 10 wt % rubber content, an optimum balance of the mechanical properties was obtained. Beyond 10 wt % rubber content, the two peaks reappeared at approximately the same diffraction angles ($2\theta = 2.44°$) and ($2\theta = 5.08°$) corresponding to basal spacings of 3.62 nm and 1.74 nm, respectively, and no further enhancement was observed in the intercalation/exfoliation process. This might be explained by the competitive interaction between the PLA and the rubber, in comparison to that between the polymers and the clay. Another possibility is that the rubber might have bonded to the edges of the clays through interactions of the hydroxyl groups of the clay and no further penetration into the clay galleries took place.

TEM Analyses

XRD results do not give complete information about the spatial distribution of the clay. Thus, TEM is generally used as a complementary technique to get a direct visualization of the dispersion state in the nanocomposites.[2,15,34] Typical TEM micrographs of the nanocomposites are shown in Figure 2. The TEM micrographs reveal the formation of nanocomposites that corroborate with the XRD results discussed earlier. The dark bundles and ribbons represent the clay particles and the light grey areas show the polymer matrix.

Figure 2(a) is a TEM micrograph of binary PLA/OMMT at low magnification illustrating that the clay nanoplatelets were dispersed quite homogeneously. Figure 2(b) exhibits the formation of intercalated/exfoliated structure in the binary PLA/OMMT nanocomposite, and Figure 2(c) displays the TEM image of the ternary nanocomposite with 10 wt % rubber content. Isolated exfoliated platelets, intercalated clay and small tactoids can be clearly observed in Figures 2(b, c). All of the ternary nanocomposites exhibited partial exfoliation, intercalation and small tactoids. It is also clearly observed from Figure 2(d–f) that addition of more rubber did not further improve exfoliation. These observations are consistent with the results of XRD analysis.

It is reported that the location of the clay in a rubber toughened nanocomposite affects the particle size of the dispersed phase and thus the performance of the mixture. There are controversial reports on the effects of organoclay location on toughness in rubber toughened nanocomposites. Some reports point out that the highest toughness was achieved when the clay was dispersed in the continuous phase, whereas others claim that the highest improvement in toughness was obtained when the clay was at the interface or dispersed inside the minor phase.[35]

It was not possible to determine the position of the clay particles in the mixtures by the TEM micrographs owing to the low contrast difference between the PLA and the rubber. Clay particles are more likely to be located in the PLA matrix, since it is more polar than the rubber, and it has lower viscosity than the rubber. However, scanning electron microscopy and mechanical properties analyses that are discussed later suggest that most of the clay particles might be embedded in the rubber phase and some were located at the interface of the rubber and PLA as well as in the PLA matrix. This could be due to the fact that during melt compounding, the rubber melted first ($T_m \approx 53°C$) and encapsulated most of the clay before PLA started melting at ~152°C.

SEM Analyses

SEM micrographs of the unetched surfaces of PLA and PLA/OMMT are displayed in Figures 3(a, b), respectively. As can be observed from Figure 3(a), PLA exhibits a typical fractured surface of a brittle material with rather a smooth surface with no plastic deformation. Few straight parallel lines of crack

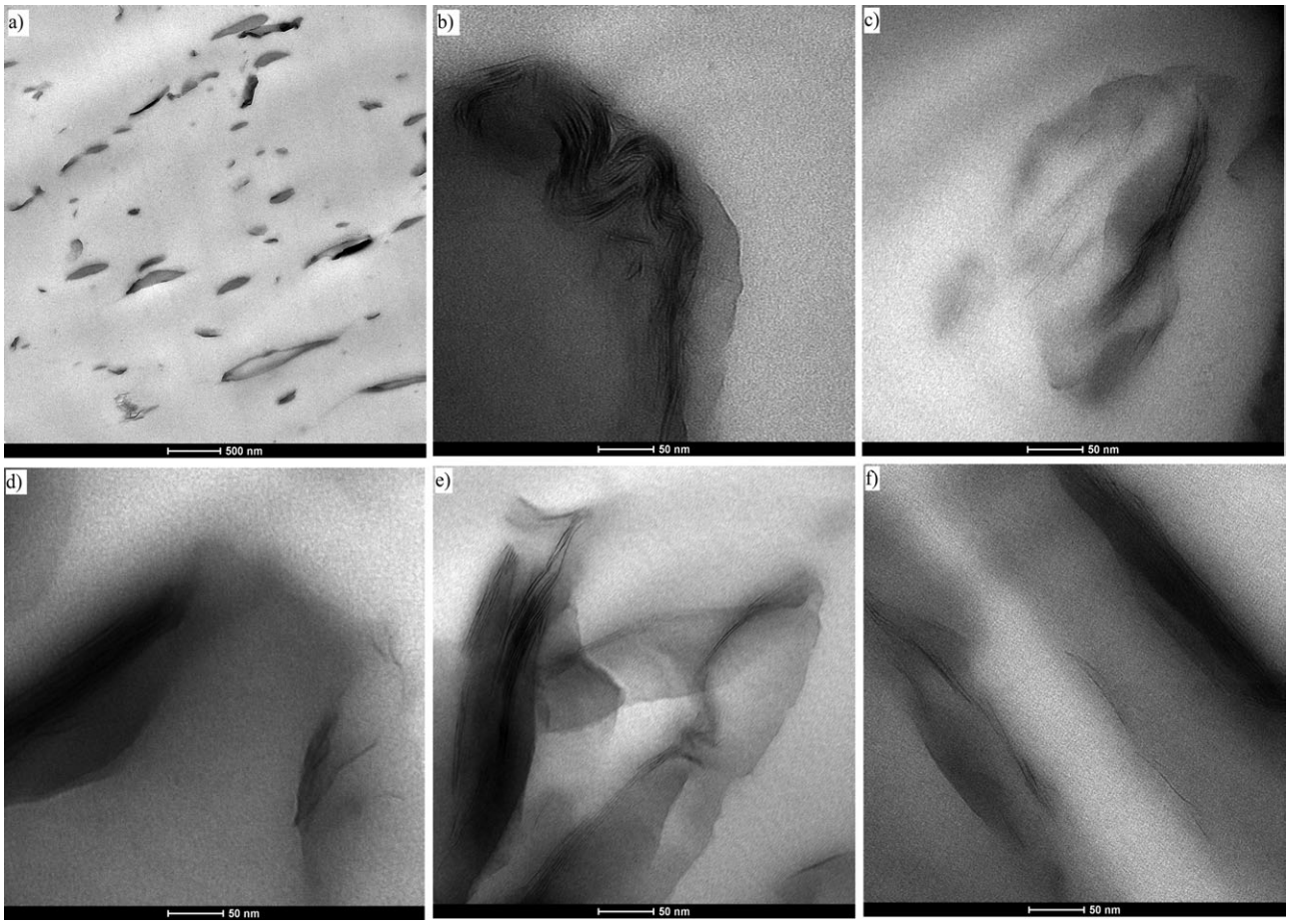

Figure 2. TEM micrographs of the nanocomposites containing 2 wt % clay: (a) PLA/OMMT (500 nm), (b) PLA/OMMT (50 nm), (c) PLA/OMMT/R10 (50 nm), (d) PLA/OMMT/R15 (50 nm), (e) PLA/OMMT/R20 (50 nm), (f) PLA/OMMT/R30 (50 nm). (The R indicates the rubber, and the number following *R* indicates the wt % of the rubber).

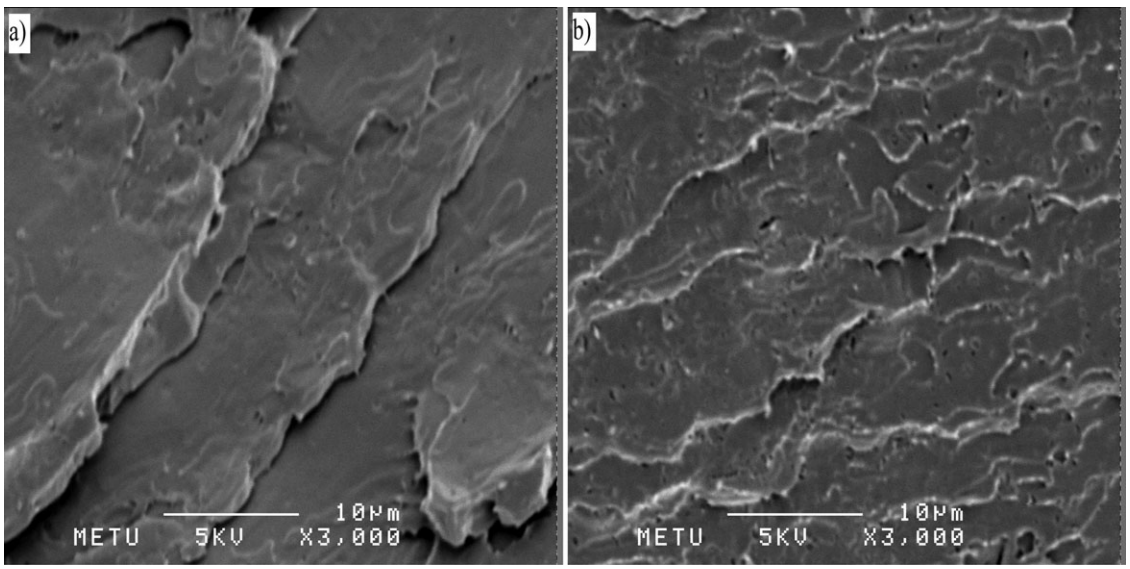

Figure 3. SEM micrographs of the fractured surfaces of the unetched injection molded specimens of (a) PLA and (b) PLA/2 wt % OMMT.

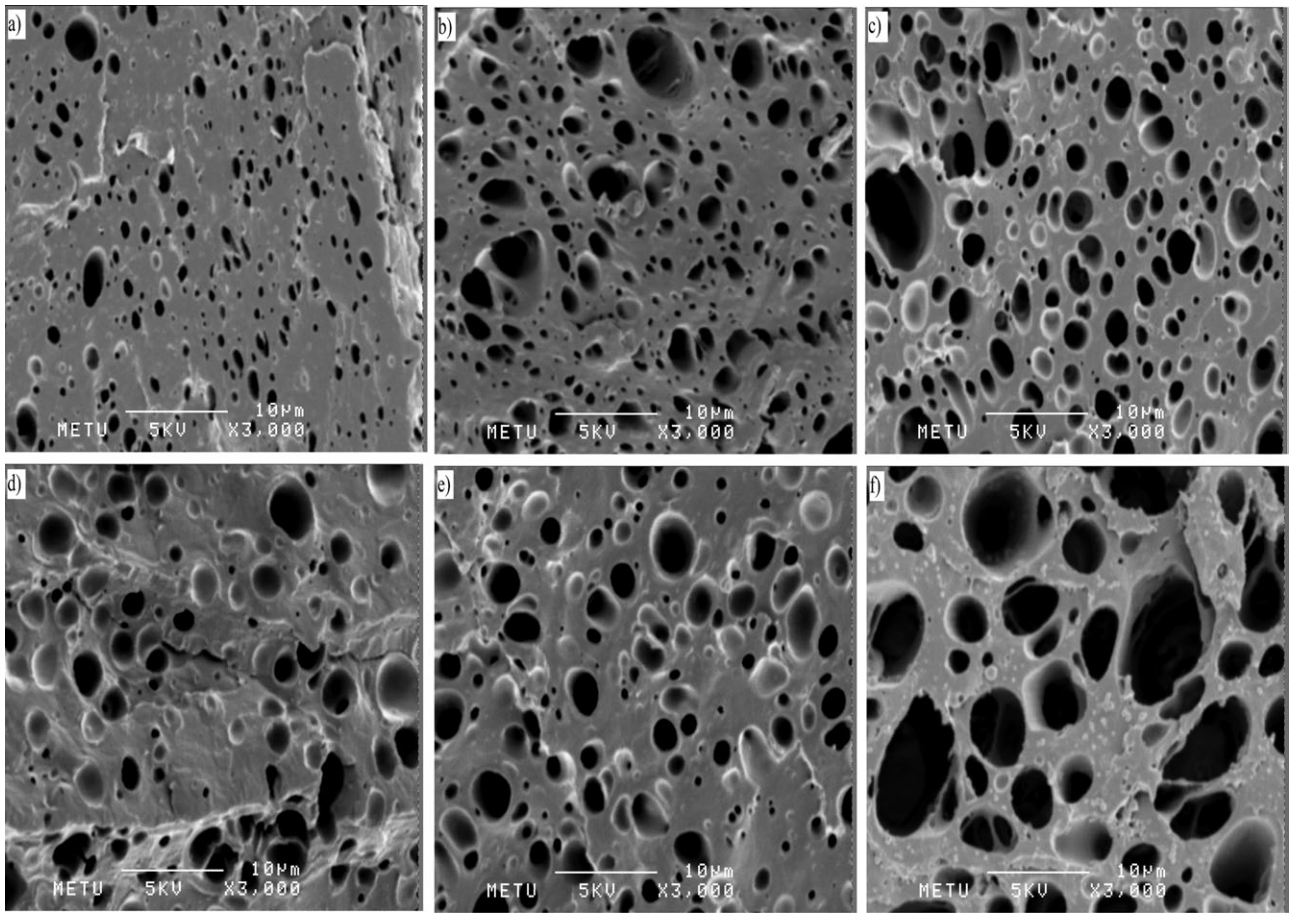

Figure 4. SEM micrographs of the fractured etched surfaces of the injection molded specimens of the binary blends (a–c) and the ternary nanocomposites (d–f) at 10, 20, and 30 wt % rubber content.

propagation are clearly noticeable with no deviations of the cracks implying easy crack initiation and propagation and rapid progress of catastrophic cracks responsible for premature fracture with low energy dissipation.[15,24] PLA/OMMT micrograph shows a rougher fractured surface with multiple small and long crack lines developed in different directions due to the presence of the clay [Figure 3(b)]. This suggests that clay particles deflected the cracks and increased their path. This mechanism that is responsible for roughness and low energy absorption before failure was also observed in Reference12 for PLA/OMMT. The SEM observations of these materials are consistent with the low impact strength and toughness results obtained in mechanical characterization.

Figure 4(a–c) shows typical SEM images of the etched surfaces of the binary blends of PLA/rubber. The vacuoles left after etching reflect the morphology of the dispersed phase. The morphology of the mixtures is that of a two-phase binary blend where PLA formed the continuous phase and the rubber was segregated as spherical domains typical of an immiscible blend, supporting the DSC results discussed later. The rubber particles are evenly dispersed at all concentrations used with narrow size distribution. Their sub-micron mean size (0.4 μm-0.8 μm) suggests low interfacial tension owing to the efficient reaction during compounding between the epoxy groups of the rubber and the hydroxyl and carboxyl terminal groups of the PLA,[1,4,28,31] as well as other possible polar interactions between the ester groups of PLA and those of rubber. Such reaction was proved by Fourier transform infrared spectroscopy by Su et al.[1] in their study of blends of PLA and glycidyl methacrylate grafted poly(ethylene octane) (PLA/mPOE). As also observed in Figure 4(a–c) the domain size increased with increasing rubber content. The viscosity of the dispersed phase increased with increasing rubber content, consequently the droplet coalescence rate increased at the expense of the droplet break up rate, thus large particles were formed.[4] The craters observed are deformed and shaped like ellipsoids with irregular surfaces indicating that the rubber phase shared the impact load with the matrix and was tightly bonded to the PLA. This might also be ascribed to the reaction between the PLA functional groups and the reactive groups of the rubber as mentioned earlier. The copolymer formed at the interface leads to better spatial distribution of the dispersed phase and plays the role of an emulsifier by reducing interfacial tension. Thus, the droplet breakup rate is increased and phase coalescence rate is retarded during melt compounding, consequently small particle size is generated.[4] This copolymer is also efficient in bridging the two components of the blend for efficient load transfer responsible for toughness improvement that is consistent with the results of the mechanical properties.[34] The function of the rubber domains is not only

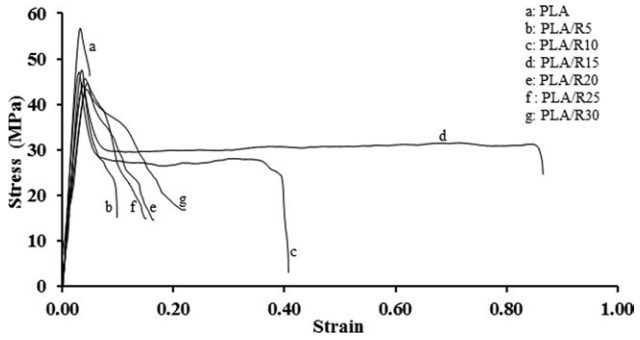

Figure 5. Typical stress–strain curves of the binary blends.

to share the load with the matrix, but to contribute to energy dissipation by initiating multiple crazing in the matrix and to stop and/or divert cracks to prevent their development to rapid catastrophic cracks.[27] Few cracks are also visible in Figure 4(a) with tortuous path due to the presence of the rubber. This indicates that the rubber domains were able to deflect the propagation of the cracks, and the long crack propagation paths absorbed considerable energy contributing to energy dissipation that is responsible for toughness improvement.

Figure 4(d–f) displays the morphology of the ternary nanocomposites. The observed craters had the same morphological features as those of the binary compounds suggesting that the clay did not interfere with the reaction between the rubber and the PLA, but influenced the size of the rubber domains. As observed in these figures, the mean domain size of the nanocomposites increased with increasing rubber content (0.4–1.5 μm) and was mostly larger than that of the binary blends (0.4–0.8 μm). The higher domain size in the nanocomposites suggests that the clay particles did not act as barriers for coalescence, but enlarged the rubber phase domains by affecting the viscosity ratio between the rubber and PLA matrix.[32,34,35]

Mechanical Properties

In general, rubber toughening of polymers leads to reduced strength and stiffness and enhanced toughness provided that a strong interface exists between the phases. However, addition of rigid nanofillers into polymers to form nanocomposites increases strength and stiffness, but may decrease toughness.

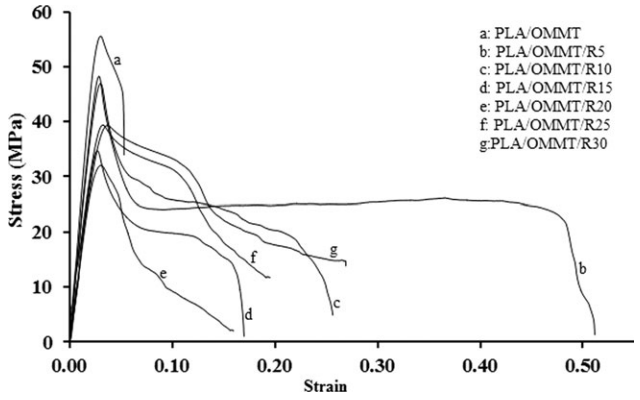

Figure 6. Typical stress–strain curves of the nanocomposites.

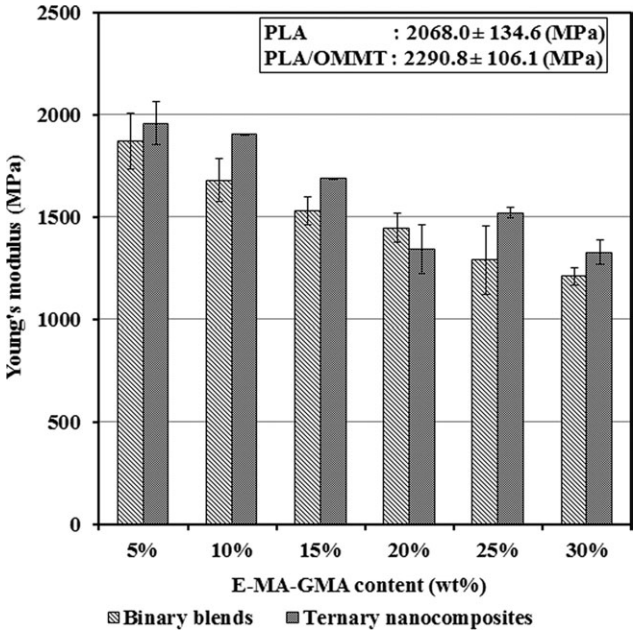

Figure 7. Effect of the rubber content on the Young's modulus of the binary blends and ternary nanocomposites at 2 wt % clay.

Combining the two techniques may lead to balanced properties or even to simultaneous improvement in all the three properties.[35,36] It is reported that in both polymer blends and nanocomposites, the interfacial interactions and the level of dispersion of the components are the key factors that govern the final properties.[34]

Figures 5 and 6 display typical stress–strain curves of pristine PLA, and its binary blends and ternary nanocomposites, and Figures 7–9 show the effect of the rubber and the OMMT on

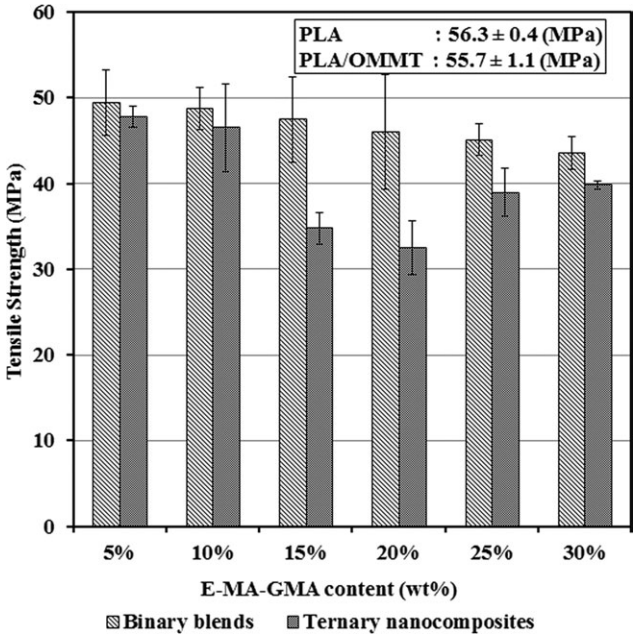

Figure 8. Effect of the rubber content on the tensile strength of the binary blends and ternary nanocomposites at 2 wt % clay.

Applied Polymer SCIENCE

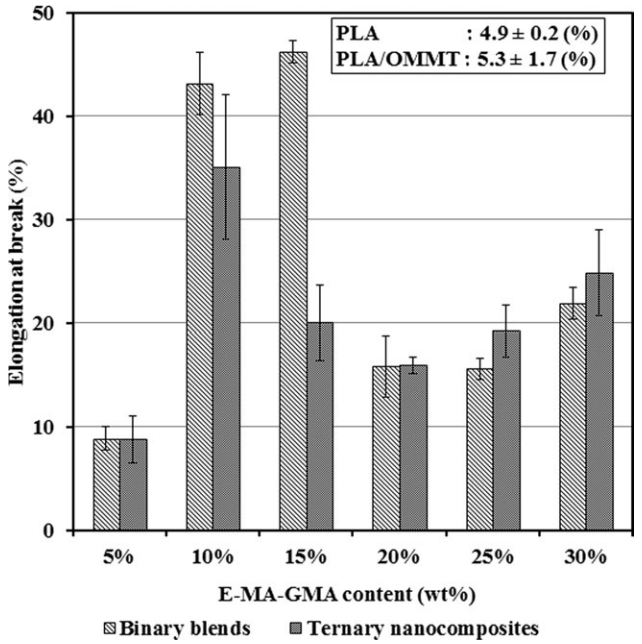

Figure 9. Effect of the rubber content on the elongation at break of the binary blends and ternary nanocomposites at 2 wt % clay.

Young's modulus, tensile strength and elongation at break of these materials respectively.

As can be observed in Figure 5, PLA shows the behavior of a typical rigid and brittle material. During stretching, PLA deformed with a steep linear increase in stress, followed by a yield point and a very short necking. Finally, it fractured catastrophically at very low elongation (ca. 5%) due to lack of crack deviation and cavitation mechanisms as reported by He et al.[37] Slight stress-whitening were visible on specimens indicating that PLA deformed by crazing mechanism.[25] PLA deformation behavior was not significantly affected by the addition of 2 wt % OMMT, and the same mode of deformation was observed. However, more stress-whitening was noticed after the failure of PLA/OMMT. Addition of the rubber induced a substantial change in the tensile behavior of PLA (Figure 5). The failure mode changed from brittle to ductile with a noticeable yield point, longer necking and increased plastic deformation followed by stress softening before failure. All of the stress–strain curves of the binary blends (Figure 5) and nanocomposites (Figure 6) exhibited the same pattern.

Young's Modulus

Addition of 2 wt % organoclay resulted in increase of the tensile modulus of PLA from 2068.0 MPa to 2290.8 MPa (Figure 7). The enhancement in modulus with the addition of OMMT corroborates with the results of other research studies.[2,15,20,29,32] The increase in tensile modulus may be ascribed to the stiffening effect of the dispersed rigid clay layers, as well as the reduced chain mobility of PLA by the surface of the clay.[2,15,20,29] The intercalated/exfoliated structure of the OMMT results in high contact surface area favorable for enhanced interfacial interactions between the carboxyl end groups of PLA and the hydroxyl groups on the organoclay and contributes to chain immobilization.[15,20,29] These interactions are responsible for enhanced adhesion between the PLA matrix and the filler. As a result, an effective stress transfer from the matrix to the filler is established leading to increased elastic modulus.[20]

In the binary blends the modulus dropped steadily as the rubber content is increased (Figure 7) owing to the elastomeric nature of the rubber with low modulus.[2,32,37] The decrease in the modulus was in the range of 10–40% in the composition interval studied. For example, at 20 wt % rubber content, the decrease is around 26% which is lower than the 31% reduction reported for the PLA/poly(ethylene-glycidyl-methacrylate) (PLA/EGMA) blend.[28] This might be ascribed to the presence of methyl acrylate groups in the rubber of the present study. Compared to other findings, the reduction in modulus is similar to the 25% decrease obtained in PLA/NR-*g*-PBA blend,[27] but far less than the 50% decrease in PLA/TPO blend containing 5 phr TPO-PLA as compatibilizer.[30]

In Figure 7 it can be observed that incorporation of 2 wt % OMMT induced a substantial increase in the modulus for all the nanocomposites owing to the stiffening effect of the OMMT that induced chain immobilization as discussed for the PLA/OMMT nanocomposite.[2,15,20,29,32]

Tensile Strength

Figure 8 shows the tensile strength of the blends and nanocomposites. A slight decrease in the tensile strength from 56.3 to 55.7 MPa was observed after addition of 2 wt % OMMT to PLA. In the binary blends, the tensile strength decreased from 49.4 to 43.5 MPa as the rubber content increased from 5 to 30 wt % owing to the elastomeric nature of the rubber.[1,15,29] It should be noted that the tensile strength was affected less by the rubber than the elastic modulus was. The addition of the OMMT to the binary blends also decreased the tensile strength of the binary blends. Similar decrease in tensile strength was observed in a recent study of PLA/SEBS-g-MAH/OMMT nanocomposites.[29] The OMMT counteracted the negative effect of the rubber on the tensile strength only when the rubber content was less than 15 wt % owing to its low content (2 wt %).

Elongation at Break

PLA is a hard and brittle material reported to elongate not more than 10%.[3] Figure 9 shows the effect of the rubber on PLA and its binary blends and ternary nanocomposites. As expected, the elongation at break of pure PLA was very low (≈5%) owing to its rigid nature.

Addition of 2 wt % OMMT did not significantly affect the elongation at break of the PLA, but induced stress whitening upon extension.

Addition of the rubber up to 15 wt% increased the elongation at break of the blends to reach a maximum value of 46% representing 9-fold increase in comparison to that of pristine PLA. Thus, the rubber changed the deformation of PLA from brittle to ductile. This implies that high energy was dissipated during crack propagation before failure owing to the elastic nature of the rubber and to the strong interface developed through the interactions of the ester groups of the rubber and PLA, and the reaction of the epoxy groups of the dispersed rubber phase and

hydroxyl and carboxyl end groups of the PLA matrix leading to the formation of PLA-*g*-rubber at the interface.[2] In addition, this copolymer might have reduced the stress concentration around the dispersed rubber particles by local plastic deformation favorable for increased elongation at break.[15] Beyond 15 wt % rubber content, the elongation at break underwent a drastic reduction and attained a value of ~16% in the range of 20–25 wt % rubber loading. This may be attributed to chain entanglements formed at the interface that might have reduced the chain mobility.[38] Beyond 25 wt % rubber, the elongation at break increased due to high rubber fraction.

The elongation at break of the ternary nanocomposites exhibited the same trend as that of the binary blends. Up to 20 wt % rubber loading, the values of elongation at break of the ternary nanocomposites were lower than those of the binary compositions, due to the constraining effect of OMMT on the molecular mobility.[20,29] Beyond this rubber content, the elongation at break increased owing to higher rubber content.

Impact Strength

Notched impact strength is a measure of the energy necessary to propagate an existing notch (resistance to crack propagation), while unnotched impact strength is a measure of the energy to initiate and propagate a crack (resistance to crack initiation and propagation).[39]

Rubbers containing glycidyl moieties were generally used as impact modifiers and/or as compatibilizers with different success.[2,4,28,40] In rubber toughened polymer blends numerous factors such as the extent of mixing, rubber content, viscosity ratio, interfacial adhesion, and rubber particle size affect the final morphology and hence the final properties.[23,24]

The effects of the OMMT and the rubber on notched Charpy impact strength (IS) of neat PLA are reported in Figure 10. PLA subjected to impact load failed in a brittle manner typical of a glassy polymer and the low impact strength recorded was only 3.2 KJ/m^2. Broken specimens showed intense stress whitening especially near the notch tip characteristic of local crazing. The incorporation of the clay imparted a negligible decrease (≈3%) in the IS of plain PLA which is within the experimental error. Similar results were obtained for nylon-clay nanocomposites.[41] The IS was maintained relatively constant owing to the efficient interactions between PLA and the OMMT and to the intercalation/exfoliation as revealed by XRD and TEM. However, no improvement could be obtained owing to the absence of deformation mechanisms to absorb and dissipate energy such as crazing, cavitation and shear yielding.[15]

The addition of the rubber significantly enhanced the impact strength of the PLA. The IS increased steadily from 4 KJ/m^2 at 5 wt % rubber content to reach a maximum of 9.5 KJ/m^2 at 30 wt % rubber content. This is attributed to the elastomeric nature of the rubber and its fine and homogeneous dispersion, as well as to the strong interface developed during compounding as discussed earlier.[4,15] The reactions led to the formation of a grafted copolymer (PLA-*g*-rubber) located at the interface that acted as an emulsifier and reduced the interfacial tension between the two phases resulting in high level of dispersion,

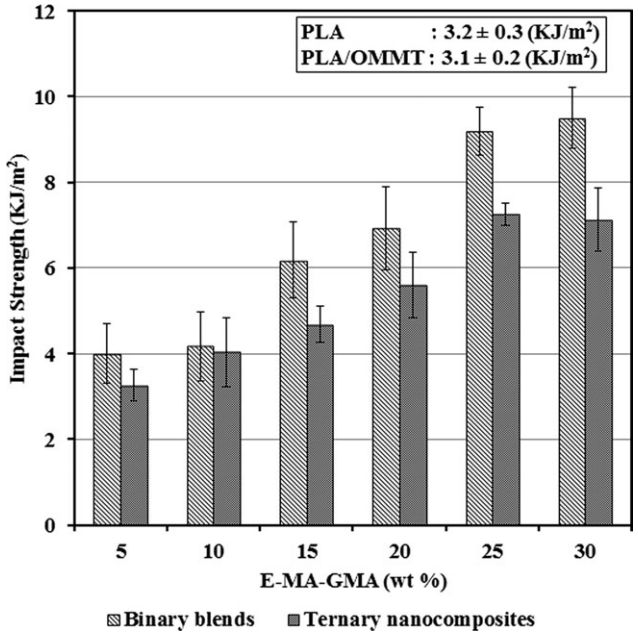

Figure 10. Effect of the rubber content on the notched Charpy impact strength of the binary blends and ternary nanocomposites at 2 wt % clay.

fine particle size, and low polydispersity as observed by SEM. The rubber inclusions acted as stress concentrators during impact deformation and transformed the behavior of the PLA from brittle to ductile by changing the mechanism of deformation. Such mechanisms of deformation might include crazing, cavitation, shear bending, crack bridging and shear yielding that are well known in toughened polymer blends.[2]

At 10 wt % rubber content, the binary blend and the ternary nanocomposite exhibited nearly the same IS value, probably due to the highest exfoliation state observed in this nanocomposite. At other rubber contents, the IS values of the ternary nanocomposites were lower than those of the corresponding binary blends. This could be attributed to their larger particle size (0.4–1.5 μm). It was reported that well dispersion of clay into a blend might suppress coalescence.[32] However, the opposite result was obtained in the present study that might indicate that most of the clay was encapsulated in the rubber phase with some clay residing at the interface between the PLA and the rubber and in the PLA matrix as discussed earlier in the XRD and TEM sections. Yu et al.[42] reported that high toughness is obtained when maximum quantity of exfoliated clay is dispersed in the continuous phase of a functionalized rubber toughened blend. In conclusion, in this study, the organoclay was more effective for improvement of modulus than for improvement of impact toughness. At 2 wt % OMMT, balanced stiffness-toughness was observed at 10 wt % rubber content that exhibited the highest level of exfoliation.

Melt Flow Index Measurements

Rheological measurements are widely used as a mean to determine the extent of interactions in reactive polyblends.[15,37] The rheological properties of the pristine materials, the blends and the nanocomposites were determined using melt flow index measurements (MFI).

Applied Polymer SCIENCE

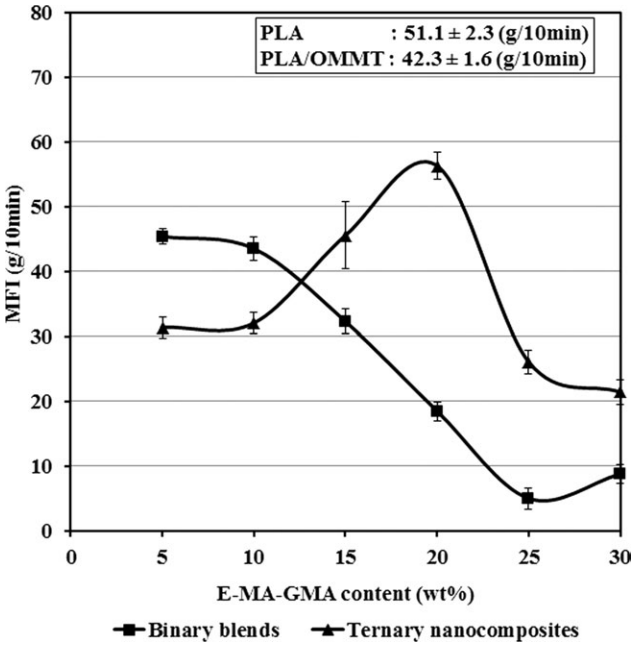

Figure 11. Effect of the rubber content on the MFI of the binary blends and ternary nanocomposites at 2 wt % clay.

Figure 11 shows the MFI of the starting materials and the compounds. The MFI of the injection grade PLA increased from 47.2 to 51.1 g/10 min after extrusion indicating that its molecular weight has been decreased as expected, since PLA is known to be a shear sensitive material.[13]

Addition of 2 wt % clay to PLA decreased the MFI to 42.3 g/10 min. The decrease in the MFI (increase in viscosity) is attributed to the "filler effect," as well as to the enhanced interactions of the modified clay and the PLA through possible interactions of the carboxyl and hydroxyl terminal groups of the PLA with the hydroxyl groups of the surfactant of the clay that constrain chain mobility.[15,20] Also, the aspect ratio of clay increases through delamination of the clay agglomerates and exfoliation as observed by XRD and TEM giving rise to larger surface area for interactions that restrict the flowability of the material.[20]

In the binary blends of PLA/rubber, addition of the rubber up to 25 wt % to PLA decreased the MFI. The decrease in MFI is attributed to the high viscosity of the rubber and to the reaction of the epoxy groups of the rubber with the hydroxyl and carboxyl end groups of the PLA and the likely polar interactions of their ester groups. The reaction might lead to formation of a graft copolymer at the PLA and the rubber interface that would strengthen the interfacial adhesion, restrict chain mobility, and reduce slippage of the chains at the interface.[15,20] In the literature, interfacial interactions are reported to result in increase in viscosity (decrease in MFI) in several polymer systems.[1,29,30] For example, Kusmono et al.[15] reported a decrease in MFI after addition of SEBS-*g*-MAH to compatibilize a PA6/PP blend. They attributed such a decrease to the formation of SEBS-*g*-PA6 copolymer at the interface due to reaction of PA6 amine groups with maleic anhydride groups of SEBS-MAH. At 30 wt % rubber content, the MFI of the blend increased to reach approximately the MFI of the neat rubber measured as 8.3 g/10 min.

In the ternary nanocomposites, the MFI increased up to the composition containing 20 wt % of rubber. This increase might be due to plasticizing effect of the dissolved clay surfactant. As the viscous rubber content is increased, more of the clay platelets are delaminated and some of the surfactant of the clay dissolves in the matrix inducing plasticization and increasing the MFI.[13,20] At even higher rubber contents, the plasticization effect of the clay surfactant was hindered by the high content of the highly viscous rubber, consequently the MFI decreased.

Thermal Properties

Differential Scanning Calorimetry was performed from room temperature to 220°C using samples from tensile injected dogbones to evaluate the effects of the organoclay and the rubber on the phase transition behavior of the PLA and the mixtures. Thermograms of PLA and its binary blends and ternary nanocomposites exhibited three main transitions namely: a glass transition temperature (T_g), a crystallization exotherm (characterized by T_c and ΔH_c), and a melting endotherm (characterized by T_m and ΔH_m). Table I summarizes the values of these calorimetric parameters and the degree of crystallization of PLA calculated from eq. (1) using a value of 93 J/g for the heat of fusion of 100% crystalline PLA.[24,27,28]

The melting temperature of the rubber was recorded as 53.1°C, and its glass transition temperature that is below room temperature was not studied here. The thermogram of pure PLA is characterized by a glass transition temperature at 58.9°C, a crystallization exotherm at $T_c = 118.2$°C, and a melting endotherm at $T_m = 152.7$°C (Table I). As shown in this table, and considering the experimental error of the measurements, PLA in the binary blends and ternary nanocomposites exhibited the same glass transition temperature as the pure PLA, suggesting that PLA and the rubber were immiscible in the composition range studied. Similarly, Ishida et al. studied toughening of PLA with different types of rubbers, and the DSC thermograms of all the blends exhibited a single glass transition temperature, thus it was concluded that the compounds were immiscible.[23]

In the binary blends, the addition of the rubber had no significant effect on the melting temperature of the PLA. This suggests that the incorporation of the rubber did not change the crystal structure of PLA as also observed by Zeng et al.[3] On the other hand, the crystallization temperature decreased substantially, after addition of only 5 wt % of rubber, and it dropped from 118.2 to 109.5°C due to the nucleating effect of the rubber that favors initiation and crystal growth at many sites. In a recent study, Petchwattana et al.[24] reported that addition of only 0.5 wt % ultrafine acrylate rubber did not affect the melting temperature of PLA, but it decreased the crystallization temperature. This result was attributed to the rubber particles that might have acted as nucleating sites for crystallization. It was also found that further increase of the rubber content inhibited crystallization. Oyama[28] reported that the dispersed poly(ethylene-glycidyl-methacrylate) rubber (EGMA) in PLA played the role of nucleating agent and promoted the crystallization of PLA, and further annealing of the blends for 2.5 h at 90°C

Table I. Thermal Parameters of PLA, the Binary Blends and the Nanocomposites

Sample	T_g (°C)	T_c (°C)	$\triangle H_c$ (J/g)	T_m (°C)	$\triangle H_m$ (J/g)	W_c (%)
Thermal parameters of PLA and the binary blends						
PLA	58.9	118.2	20.2	152.7	25.6	5.8
PLA/R5	57.3	109.5	23.3	152.4	27.7	5.0
PLA/R10	57.4	108.4	19.8	152.8	24.4	5.5
PLA/R15	57.6	107.8	19.4	152.6	24.9	6.9
PLA/R20	57.5	106.5	15.9	152.1	23.9	10.8
PLA/R25	57.9	108.2	13.8	152.2	22.4	12.3
PLA/R30	58.1	109.3	13.6	151.9	21.3	11.8
Thermal parameters of PLA and the nanocomposites						
PLA	58.9	118.2	20.2	152.7	25.6	5.8
PLA/OMMT	57.5	107.6	23.2	151.7	26.2	3.3
PLA/OMMT/R5	57.0	109.7	21.3	151.9	26.6	6.1
PLA/OMMT/R10	57.7	105.2	17.1	151.8	25.6	10.4
PLA/OMMT/R15	57.8	103.2	16.5	151.1	23.1	8.6
PLA/OMMT/R20	58.5	104.9	15.9	151.3	20.4	6.3
PLA/OMMT/R25	58.5	105.5	14.4	151.4	19.8	8.0
PLA/OMMT/R30	58.1	108.8	14.4	151.2	19.2	7.6

resulted in super-tough PLA blends. Table I shows that in general the degree of crystallization of the binary blends increased with higher rubber loading, possibly due to the chemical reaction between the epoxy groups of the rubber and the carboxyl and hydroxyl terminal groups of PLA and the likely polar interactions of their ester groups that increased the viscosity of the system. According to Oyama,[28] the high viscosity causes a high shear force during mixing and pulls out the copolymer formed by the reaction of PLA and EGMA at the interface, to the PLA matrix. In the present study, it is thought that this phenomenon has also occurred in our PLA based blends and the pull out of the copolymer from the interface to the bulk of the matrix induced the chain mobility necessary for crystallization, thus the degree of crystallization increased.

Table I indicates that the incorporation of 2 wt % OMMT into PLA did not significantly affect the melting temperature and glass transition temperature of PLA as also found by Chow et al.[16] On the other hand, the crystallization temperature was drastically decreased from 118.2 to 107.6°C. This is ascribed to the nucleation effect of the clay owing to its large surface area.[20,29] The intercalated/exfoliated structure as observed by XRD and TEM could also have contributed to the increase in the nucleating sites as reported by Balakrishnan et al.[20] Similar results were also reported by other research groups.[12,16] The degree of crystallinity of PLA/OMMT was lower than that of the neat PLA. This might be due to the hindrance caused by exfoliated/intercalated structure of the organoclay that reduced the mobility of polymer chains.[15,29]

The crystallization temperatures of the ternary nanocomposites are generally lower in comparison to the crystallization temperatures of the binary blends that have the same quantity of rubber (Table I). This is also attributed to the nucleating effect of the nanofiller.[20,29] In the ternary nanocomposites with 5–10 wt % rubber, the viscosity increased (MFI decreased) in comparison to that of PLA/OMMT as shown in Figure 11. The degree of crystallization increased owing to the effect described by Oyama[28] overcoming the hindrance effect of the clay. In the ternary nanocomposites with 15–20 wt % rubber, the viscosity decreased (Figure 11), thus the chain mobility is expected to be enhanced. However, in this range, the degree of crystallization decreased that might be attributed to immobilization of the polymer molecules by clay. In the ternary nanocomposites with 20–30 wt % of rubber, the degree of crystallization levels up owing to high viscosity and the constraining effect of the clay. Both of these factors reduce chain mobility needed for crystallization. The effect described by Oyama[28] did not take place at this high level of rubber content possibly due to saturation of the interface corresponding to maximum interactions.[39]

CONCLUSIONS

PLA was successfully toughened by melt blending with E-MA-GMA rubber in the range of 5 to 30 wt % using a twin screw extruder. Organoclay was added at 2 wt % to compensate the decrease in other mechanical properties. XRD and TEM showed that PLA/OMMT binary nanocomposite exhibited intercalated/exfoliated structure with some remaining tactoids. Addition of the rubber promoted dispersion of the OMMT by intercalating with PLA molecules into the clay galleries. At 10 wt % rubber content exfoliation was observed. Beyond this rubber content, intercalated/exfoliated structure reappeared and no further enhancement in dispersion was observed.

The morphology revealed by SEM showed that PLA and E-MA-GMA were immiscible in the range of rubber content studied, and the rubber formed the dispersed phase. The addition of rubber changed the brittle behavior of PLA to ductile by inducing debonding and/or cavitation. The rubber domain size increased with increasing rubber content in both the blends and

nanocomposites. The nanocomposites exhibited coarser morphology suggesting that the clay did not act as a barrier for the coalescence owing to its likely preferential location in the rubber.

The impact strength and the elongation at break were improved in the binary blends and ternary nanocomposites at the expense of stiffness and strength. In the ternary nanocomposites, the best balance of these properties was observed at 10 wt % rubber content.

The viscosity of the blends and nanocomposites, evaluated by MFI measurements, was highly influenced by the rubber and the clay. The MFI of the binary blends decreased with increasing rubber content up to 25 wt % rubber. In the ternary nanocomposites, an increase of the MFI was observed up to 20 wt % rubber content owing to the plasticization effect of the dissolved organoclay surfactant, and beyond this rubber content, the MFI decreased owing to the highly viscous rubber content.

DSC analysis showed that the T_g of PLA in the blends and nanocomposites was not significantly influenced by the presence of the rubber confirming the immiscibility of the mixtures. Both the clay and the rubber decreased the crystallization temperature of PLA and acted as nucleating agents for PLA and affected its crystallization.

REFERENCES

1. Su, Z.; Li, Q.; Liu, Y.; Hu, G.; Wu, C. *Eur. Polym. J.* **2009,** *45*, 2428.
2. Kumar, M.; Mohanty, S.; Nayak, S. K.; Parvaiz, M. R. *Biores. Techn.* **2010,** *101*, 8406.
3. Zeng, J.; Li, Y.; He, Y.; Li, S.; Wang, Y. *Ind. Eng. Chem. Res.* **2011,** *50*, 6124.
4. Sun, S.; Zhang, M.; Zhang, H.; Zhang, X. *J. Appl. Polym. Sci.* **2011,** *122*, 2992.
5. Liu, H.; Zhang, Z. *J. Polym. Sci. Part B: Polym. Phys.* **2011,** *49*, 1051.
6. Meng, B.; Tao, J.; Deng, J.; Wu, Z.; Yang, M. *Mater. Lett.* **2011,** *65*, 729.
7. Ljungberg, N.; Andersson, T.; Wesslén, B. *J. Appl. Polym. Sci.* **2003,** *88*, 3239.
8. Martino, V. P.; Jiménez, A.; Ruseckaite, R. A. *J. Appl. Polym. Sci.* **2009,** *112*, 2010.
9. McManus, A. J.; Doremus, R.; Siegel, R.; Bizios, R. *J. Biomed. Mater. Res. A* **2005,** *72*, 98.
10. Kasuga, T.; Maeda, H.; Kato, K.; Nogami, M.; Hata, I.; Ueda M. *Biomaterials* **2003,** *24*, 3247.
11. Kasuga, T.; Ota, Y.; Nogami, M.; Abe, Y. *Biomaterials* **2001,** *22*, 19.
12. Marras, S. I.; Zuburtikudis, I.; Panayiotou, C. *Eur. Polym. J.* **2007,** *43*, 2191.
13. Carrascoa, F.; Gamez-Perez, J.; Santanac, O. O.; Maspoch, M. L. L. *Chem. Eng. J.* **2011,** *178*, 451.
14. Chow, W. S.; Lok, S. K. *J. Thermo. Comp. Mater.* **2008,** *21*, 265.
15. Kusmono; Ishak, Z.; Chow, W. S.; Takeichi, T.; *Rochmadi. Euro. Polym. J.***2008,** *44*, 1023.
16. Chow, W. S.; Lok, S. K. *J. Therm. Calorim.* **2009,** *95*, 627.
17. Chang, J. H.; An, Y. U.; Cho, D.; Giannelis, E. P. *Polymer* **2003,** *44*, 3715.
18. Yokohara, T.; Yamaguchi, M. *Eur. Polym. J.* **2008,** *44*, 677.
19. Broz, M. E.; VanderHart, D. L.; Washburn, N. R. *Biomaterials* **2003,** *24*, 4181.
20. Balakrishnan, H.; Hassan, A.; Wahit, M. U.; Yussuf, A. A.; Abdul Razak, S. B. *Mater. Des.* **2010,** *31*, 3289.
21. Lee, J. B.; Lee, Y. K.; Choi, G. D.; Na, S. W.; Park, T. S.; Kim, W. N. *Polym. Degrad. Stab.* **2011,** *96*, 553.
22. Nijenhuis, A. J.; Colstee, E.; Grijpma, D. W.; Pennings, A. *J. Polymer* **1996,** *37*, 5849.
23. Ishida, S.; Nagasaki, R.; Chino, K.; Dong, T.; Inoue, T. *J. Appl. Polym. Sci.* **2009,** *113*, 558.
24. Petchwattana, N.; Covavisaruch, S.; Euapanthasate, N. *Mater Sci. Eng. A* **2012,** *532*, 64.
25. Theryo, G.; Jing, F.; Pitet, L. M.; Hillmyer, M. A. *Macromolecules* **2010,** *43*, 7394.
26. Li, Y.; Shimizu, H. *Macromol. Biosci.* **2007,** *7*, 921.
27. Zhang, C.; Man, C.; Pan, Y.; Wang, W.; Jiang, L.; Dan, Y. *Polym. Int.* **2011,** *60*, 1548.
28. Oyama, H. T. *Polymer* **2009,** *50*, 747.
29. Leu, Y. Y.; Mohd Ishak, Z. A.; Chow, W. S. *J. Appl. Polym. Sci.* **2012,** *124*, 1200.
30. Ho, C.; Wang, C.; Lin, C.; Lee, Y. *Polymer* **2008,** *49*, 3902.
31. Hashima, K.; Nishitsuji, S.; Inoue, T. *Polymer* **2010,** *51*, 3934.
32. Bitinis, N.; Verdejo, R.; Maya, E. M.; Espuche, E.; Cassagnau, P.; Lopez-Manchado, M. A. *Comp. Sci. Tech.* **2012,** *72*, 305.
33. Abramoff, M. D.; Magalhaes, P. J.; Ram, S. *J. Biophotonics Int.* **2004,** *11*, 36.
34. Yeniova, C.; Yilmazer, U. *Polym. Comp.* **2010,** *31*, 1853.
35. Martins, C. G.; Larocca, N. M.; Paul, D. R.; Pessan, L. A. *Polymer* **2009,** *50*, 1743.
36. Alyamac, E.; Yilmazer, U. *Polym. Comp.* **2007,** *28*, 251.
37. He, S.; Wu, W.; Wang, R.; Pu, W.; Chen, Y. *Polym.-Plast. Technol. Eng.* **2011,** *50*, 719.
38. Chow, W. S.; Neoh, S. S. *Polym.-Plast. Technol. Eng.* **2010,** *49*, 62.
39. Baouz, T.; Fellahi, S. *J. Appl. Polym. Sci.* **2005,** *98*, 1748.
40. Coskunses, F. I.; Yilmazer, U. *J. Appl. Polym. Sci.* **2011,** *120*, 3087.
41. Okada, A. *Mater. Sci. Eng. C* **1995,** *3*, 109.
42. Yu, Z. Z.; Hu, G. H.; Varlet, J.; Dasari, A.; Mai, Y. W. *J. Polym. Sci. Part. B: Polym. Phys.* **2005,** *43*, 1100.

Published Peer-Reviewed Manuscript 2

Journal of Applied Polymer Science

Effects of Mixing Protocols on Impact Modified Poly(lactic acid) Layered Silicate Nanocomposites

Touffik Baouz,[1] Eda Acik,[2] Farouk Rezgui,[1] Ulku Yilmazer[2]

[1]Laboratoire des Matériaux Organiques, Faculté de Technologie, Département de Génie des Procédés, Université Abderrahmane Mira, Béjaia 06000, Algeria

[2]Chemical Engineering Department, Middle East Technical University, 06800, Ankara, Turkey

Correspondence to: U. Yilmazer (E-mail: yilmazer@metu.edu.tr)

ABSTRACT: Poly(lactic acid)/2 wt % organomodified montmorillonite (PLA/OMMT) was toughened by an ethylene-methyl acrylate-glycidyl methacrylate (E-MA-GMA) rubber. The ternary nanocomposites were prepared by melt compounding in a twin screw extruder using four different addition protocols of the components of the nanocomposite and varying the rubber content in the range of 5–20 wt %. It was found that both clay dispersion and morphology were influenced by the blending method as detected by X-ray diffraction (XRD) and observed by TEM and scanning electron microscopy (SEM). The XRD results, which were also confirmed by TEM observations, demonstrated that the OMMT dispersed better in PLA than in E-MA-GMA. All formulations exhibited intercalated/partially exfoliated structure with the best clay dispersion achieved when the clay was first mixed with PLA before the rubber was added. According to SEM, the blends were immiscible and exhibited fine dispersion of the rubber in the PLA with differences in the mean particle sizes that depended on the addition order. Balanced stiffness-toughness was observed at 10 wt % rubber content in the compounds without significant sacrifice of the strength. High impact toughness was attained when PLA was first mixed with the clay before the rubber was added, and the highest tensile toughness was obtained when PLA was first compounded with the rubber, and then clay was incorporated into the mixture. Thermal characterization by DSC confirmed the immiscibility of the blends, but in general, the thermal parameters and the degree of crystallinity of the PLA were not affected by the preparation procedure. Both the clay and the rubber decreased the crystallization temperature of the PLA by acting as nucleating agents. © 2014 Wiley Periodicals, Inc. J. Appl. Polym. Sci. **2015**, *132*, 41518.

KEYWORDS: mixing protocol; nanocomposite; organoclay; poly(lactic acid); rubber-toughening

Received 14 July 2014; accepted 14 September 2014

DOI: 10.1002/app.41518

INTRODUCTION

Biodegradable polymers have attracted much attention from both academic and industrial points of view owing to the growing environmental and social concerns brought about by the environmental impact of plastics wastes stemming from conventional petrochemical polymers.[1,2] Polylactic acid (PLA) as one of this class of polymers derived from renewable resources, competes well with many available synthetic polymers owing to its good mechanical and physical properties, biocompatibility, and ease of processability.[1,2] These attributes make it an outstanding candidate with high potential to substitute for petroleum-based polymers in various applications such as biomedical, packaging, automotive, and others.[1,3] However, because of its inherent brittleness and low toughness, this linear thermoplastic polyester needs some modifications to tackle these drawbacks and enlarge its application window. In this sense, various approaches were investigated for this goal such as copolymerization, plasticization, addition of organic/inorganic fillers, and melt-blending with either biodegradable or nonbiodegradable polymers.[1–10]

Toughening of PLA by flexible polymers has gained much attention.[1–10] To compensate the softening effect of the toughener, addition of nanofillers, mostly organomodified montmorillonite (OMMT), was considered to form nanocomposites.[11–17] It is generally known that the performance of toughened blends depends on various parameters such as components ratios and their properties, interfacial adhesion between the components, rubber particle size and shape, processing conditions and preparation methods, etc.[6,8] In this context, the effect of addition procedure on the performance and properties of ternary nanocomposites has been examined for many systems, including PA6/EPR-g-MA/OMMT,[18] LDPE/E-MA-GMA/OMMT,[19] PS/SEBS-g-MA/OMMT,[20] PET/E-MA-GMA/OMMT,[21] PP/PP-g-AA/EVA/OMMT,[22] and others.[23–26] Borah et al.[23] studied LLDPE/EMA/OMMT using three different compounding protocols and two types of OMMT. It was found that the morphology and the properties of

the nanocomposites were dependent on the blending sequence and on the type of the clay used. The Cloisite®25A clay migrated from the LLDPE phase to the EMA phase at a surprisingly high rate and the corresponding nanocomposites exhibited high impact strength as compared with the neat blend. However, Cloisite®30B clay was mainly located at the interface of LLDPE and EMA, and the compound exhibited low impact strength. In PA6/ABS/OMMT using SMA as a compatibilizer, the OMMT was preferentially located in the PA6 matrix in exfoliated state irrespective of the compounding mode, and the morphology of ABS dispersed phase was reported to be highly altered by the mixing sequence, which in turn affected the mechanical properties.[24] The X-ray diffraction (XRD) results of PA66/SEBS-g-MA/OMMT showed exfoliated structure regardless of the preparation order, whereas TEM observations indicated that OMMT location was affected by the mixing procedure.[25] Moreover, the OMMT in the matrix or at the interface was found in the exfoliated state, but the clay that was enclosed in the rubber was only intercalated as a result of the high affinity of clay to PA66, suggesting that clay dispersion cannot be determined solely on the basis of XRD, but needs to be complemented by visual tools such as TEM. Dasari et al.[26] concluded that for PA66/SEBS-g-MA/OMMT, it is beneficial in terms of impact strength to have the maximum amount of the exfoliated organoclay in the PA66 matrix, because the presence of OMMT in the rubber phase decreases its cavitation ability because of the stiffening effect of OMMT and accordingly it reduces the toughening efficiency.

To the best of the authors' knowledge, the effects of blending order of the components of rubber-toughened PLA nanocomposites have not been studied yet. The objective of this work is to investigate the effects of four different melt compounding protocols on the performance of rubber-toughened PLA nanocomposites. The structure and the morphology of the nanocomposites were observed by XRD, TEM and scanning electron microscopy (SEM), their mechanical performance was evaluated by tensile and impact tests, and their thermal characteristics were measured by differential scanning calorimetry (DSC).

EXPERIMENTAL

Materials

An injection grade PLA (PLI 005) resin, with a density of 1.25 g/cm^3 (ISO 1183) and a melting temperature in the range of 145–155°C was purchased from NaturePlast (Caen, France). The rubber modifier, Lotader® AX8900, an ethylene-methyl acrylate-glycidyl methacrylate terpolymer (E-MA-GMA) with an EMA and GMA contents of 24 and 8 wt %, respectively, was supplied by Arkema (Puteaux, France). The clay nanofiller was an OMMT, (Cloisite®30B), from Southern Clay Products (Gonzales, TX, USA). It is a natural montmorillonite modified with a quaternary ammonium salt. The cation of the organic modifier is methyl, tallow, bis-2-hydroxyethyl, quaternary ammonium (MT2EtOH) at a concentration of 90 mEq/100 g clay, and the anion is chloride. Hydrophilic Cloisite®30B was chosen as the organoclay, because it is more compatible with hydrophilic PLA in comparison to hydrophobic Cloisite®20A, Cloisite®25A, and Cloisite® 15A. It contains two hydroxyl groups that can react both with the carboxyl groups of PLA and epoxy groups of the impact modifier.

Compounding and Sample Preparation

In the nanocomposites, the weight percent of the rubber was varied in the range of 5–20 wt %, and the amount of clay was kept constant at 2 wt %. The nanocomposites were compounded using a fully intermeshing co-rotating twin screw extruder ($L/D = 24$) (Thermo Prism TSE 16 TC). The processing conditions were: screw speed = 250 rpm, feed rate = 25 g/min, and extruder zone temperatures of 150–170–170–170–170°C from the hopper to the die. The extruded rods were collected using a belt conveyor and air cooled at room temperature. Thereafter, the rods were pelletized and stored in sealed plastic bags and kept in desiccators. Specimens for different characterizations were prepared using a mini-injection molding equipment (DSM Xplore®) at cylinder and mold temperatures of 170 and 60°C, respectively. Before extrusion and injection processes, PLA, OMMT, and the prepared formulations were vacuum dried over night at 80°C and the rubber was dried at 45°C.

Four addition modes (PC-I, PI-C, CI-P, and ALL-S) were considered to investigate the effects of addition method of the components on the final structure and properties of the nanocomposites. In the first three modes: P, C, and I stand for PLA, clay, and the impact modifier, respectively. For instance, in the PC-I sequence, the PLA and the clay were compounded in the first extrusion process, and the rubber modifier was added to the obtained mixture in the subsequent second run. In the ALL-S, all of the ingredients of the nanocomposite were fed simultaneously into the hopper. Because in the first three modes of addition, at least two of the ingredients experienced extrusion twice; the All-S mixture was also extruded twice so that its components experience more or less the same thermal and mechanical history as for the other mixtures. Neat PLA was also extruded twice under the same conditions to serve as a control material. Hereafter, the materials are referred to according to their sample codes.

CHARACTERIZATION

XRD and Transmission Electron Microscopy (TEM)

A Rigaku D/MAX 2200/PC X-ray diffractometer operating in reflection mode was used to record the XRD patterns of the pristine OMMT powder and the nanocomposites. Diffractograms were acquired at room temperature with a step size of 0.02° from $2\theta = 1°$ to 10° and 1°/min scan rate using a CuKα X-ray radiation ($\lambda = 1.5418$ Å) generated at 40 kV and 40 mA. The interlayer spacing (d_{001}-reflection) of the OMMT nanosheets in the samples was derived from the peak position in the XRD diffractograms according to Bragg's law ($n\lambda = 2\ d\ \sin\theta$).

The dispersion state of the filler in the nanocomposites was assessed by TEM imaging using a FEI Tecnai® Spirit G^2 Biotwin transmission electron microscope operating at 80 kV in bright field mode (FEI Company, OR, USA). Ultrathin sections (70–80 nm) of the nanocomposites were produced from freeze-fractured impact test bars. Sections were cut at cryogenic temperature using Leica® EM UC6 ultra-microtome (Leica Microsystems, Wetzlar, Germany) equipped with a diamond knife.

SEM

A Jeol JSM-6400 (Jeol, Tokyo, Japan) low-voltage scanning electron microscope was used to examine the morphology of the prepared materials. The samples were obtained from

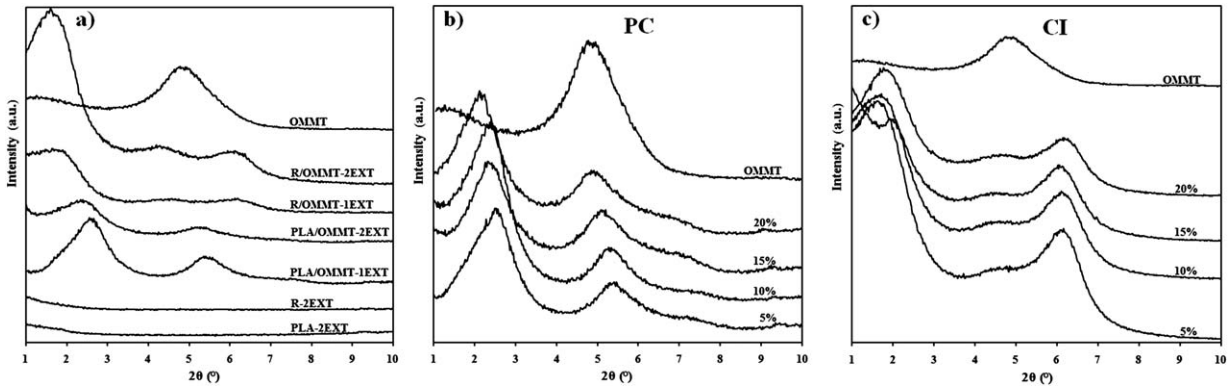

Figure 1. X-ray patterns of: (a) PLA, rubber, OMMT and their corresponding nanocomposites at 2 wt % OMMT, and (b) and (c) the PC and CI intermediate nanocomposites at different rubber contents, respectively. (The R indicates the rubber, and the percentages designate its wt %). The curves are shifted vertically for clarity.

cryofractured impact test bars. The etched surfaces, from which the rubber was selectively removed at 45°C using *n*-Heptane, were prepared with the aid of a sonicator. The surfaces were coated with a thin layer of gold to avoid electrostatic charging during observation. The impact modifier droplet size in all of the formulations was evaluated by the image processing software "ImageJ" (Rasband, W.S., ImageJ, U. S. National Institutes of Health (NIH), Bethesda, Maryland, USA, http://imagej.nih.gov/ij/, 1997–2011). Typically, a number of particles (approximately 250–300) from three to four independent SEM micrographs were analyzed by the program to estimate first the average area (A_i) of each individual particle (i). This obtained cross-sectional area (A_i) was then converted into equivalent diameter (d_i) of a sphere using eq. (1), and the number-average particle diameter (D_n) was computed by using eq. (2).

$$d_i = 2\sqrt{(A_i/\pi)} \tag{1}$$

$$D_n = \frac{\sum n_i d_i}{\sum n_i} \tag{2}$$

where n_i is the number of the dispersed domains having the apparent particle diameter d_i counted from the SEM images.

Thermal Characterization (DSC)

Thermal properties of the materials were investigated with the aid of a Shimadzu DSC-60 differential scanning calorimeter (DSC) (Shimadzu, Tokyo, Japan). The samples (9–10 mg) were heated from room temperature to 200°C at a heating rate of 10°C/min under constant nitrogen flow of 50 mL/min. The following events were determined from this scan: the glass transition temperature (T_g), crystallization temperature (T_c), melting temperature (T_m), crystallization enthalpy (ΔH_c), and melting enthalpy (ΔH_m).

The degree of crystallinity (χ_c) of PLA in the compounds was estimated using the following equation:

$$\chi_c\% = \left(\frac{\Delta H_m - \Delta H_c}{\Delta H_f \times \varphi_{\mathrm{PLA}}}\right) \times 100 \tag{3}$$

Where χ_c (%) is the degree of crystallinity, ΔH_m and ΔH_c are the heats of fusion and crystallization of the sample, respectively. ΔH_f is the heat of fusion of 100% crystalline PLA, and φ_{PLA} is the weight fraction of the PLA in the sample.

Mechanical Properties

Mechanical performance of the materials was investigated at room temperature. Tensile properties (Tensile modulus, tensile strength, and elongation at break) were determined according to ISO 527 at strain rate of 0.1 min^{-1} using a Shimadzu Autograph AG-IS 100 KN universal testing machine (Shimadzu, Tokyo, Japan). Unnotched Charpy impact strength (IS) measurements were assessed by using a Ceast Resil Impactor pendulum following the ISO 179 standard. At least five samples were tested for each property, and the values were averaged and reported together with their respective standard deviations.

RESULTS AND DISCUSSION

XRD Analyses

XRD patterns of the PLA and the rubber did not show any characteristic basal diffraction peak in the studied range of $2\theta = 1$–$10°$. However, the pure OMMT powder displayed a single strong characteristic peak at $2\theta = 4.78°$ ($d = 18.49$ Å) [OMMT in Figure 1(a)].

The characteristic peak of the OMMT in the binary PLA/OMMT nanocomposite extruded once was shifted to a lower angle $2\theta = 2.56°$ ($d = 34.51$ Å) [PLA/OMMT-1EXT in Figure 1(a)]. This indicates intercalation of the PLA molecules between the clay galleries, attributed to the favorable interactions of the PLA carboxyl (COOH) end groups with the hydroxyl entities of the clay surfaces and those of its surfactant.[6,12,19] Another OMMT peak with low intensity was observed at a higher angle $2\theta = 5.36°$ ($d = 16.49$ Å) than that of pure clay, because of the presence of tactoids [PLA/OMMT-1EXT in Figure 1(a)]. Clays are generally modified with an excess of surfactants,[27] thus the decrease in the original interlayer spacing of the OMMT is believed to be due to the collapse of the clay galleries resulting from the dissolution of some surfactant parts from clay galleries into polymer matrix[22,23] and/or to rearrangement of the alkyl ammonium chains of the OMMT.[19] When PLA/OMMT was extruded twice, the intensity of its two characteristic peaks was decreased and the peaks were shifted to lower angles $2\theta = 2.34°$ ($d = 37.75$ Å) and $2\theta = 5.16°$ ($d = 17.13$ Å) owing to the longer

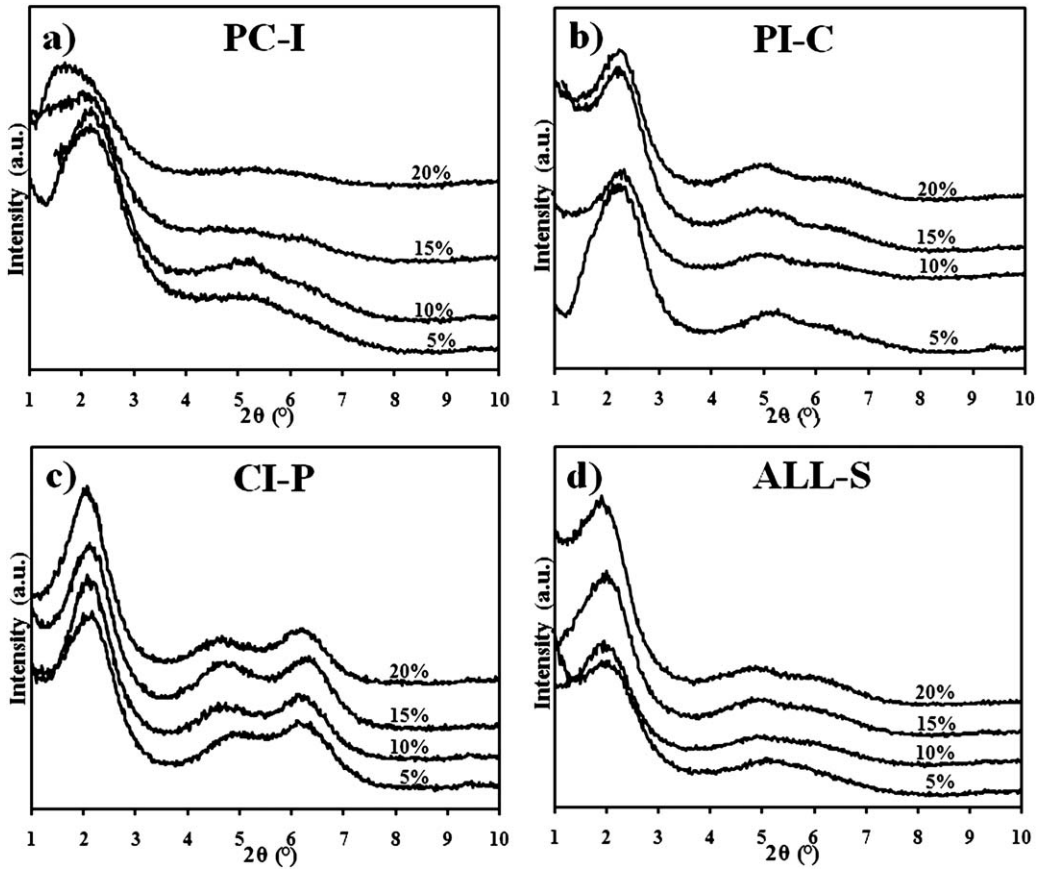

Figure 2. X-ray diffractograms of: (a) PC-I, (b) PI-C, (c) CI-P, and (d) ALL-S nanocomposites prepared at various rubber contents. The curves are shifted vertically for clarity.

residence time of the nanocomposite in the extruder, that caused longer duration of shear and interactions between reactive groups of PLA and those of the clay surfaces and its surfactant [PLA/OMMT-2EXT in Figure 1(a)].

The rubber-based nanocomposite extruded once (R/OMMT-1EXT) exhibited three characteristic peaks on its diffractogram recorded at $2\theta = 1.64°$ ($d = 53.87$ Å), $2\theta = 4.48°$ ($d = 19.72$ Å) and $2\theta = 6.12°$ ($d = 14.44$ Å) [R/OMMT-1EXT in Figure 1(a)]. This indicates low intercalation degree of the rubber owing to its higher molecular weight (high viscosity) and lower polarity (lower affinity to clay) compared with PLA, and to its bulky GMA groups making its intercalation into clay interlayers difficult. Subjecting this nanocomposite to a second extrusion process did not improve the dispersion of clay, because its X-ray traces revealed the same peaks at the same positions [R/OMMT-2EXT in Figure 1(a)].

To get more insight into the intercalation process, the difference between the rubber and the PLA, the PC and CI intermediate nanocomposites were also studied. The PC nanocomposites showed the two PLA/OMMT characteristic peaks of nearly the same intensities shifted to lower angles that varied from $2\theta = 2.50°$ ($d = 35.34$ Å) to $2\theta = 2.12°$ ($d = 41.67$ Å) and from $2\theta = 5.40°$ ($d = 16.37$ Å) to $2\theta = 4.84°$ ($d = 18.26$ Å) as the clay level increased suggesting improved clay dispersion [Figure 1(b)]. The CI nanocomposites exhibited three peaks as those of the R/OMMT-1EXT situated at almost the same positions $2\theta = 1.58°$ ($d = 55.91$ Å), $2\theta = 4.38°$ ($d = 20.17$ Å) and $2\theta = 6.10°$ ($d = 14.49$ Å) indicating nearly identical clay dispersion for all the clay contents [Figure 1(c)]. The peak at $2\theta = 6.10°$ points out to the appreciable collapse of the clay galleries, the intensity of which decreases as the clay content decreases. These results show that PLA intercalates better than the rubber for the same reasons stated earlier.

Figure 2(a–d) depicts the clay dispersion in each blending mode. As it can be seen on this figure, all of the addition sequences studied led to intercalated/partially exfoliated nanostructures. Considering PC-I, the addition of 5 wt % rubber to the PC nanocomposite shown in Figure 1(b), shifted its two peaks from $2\theta = 2.50°$ ($d = 35.34$ Å) and $2\theta = 5.40°$ ($d = 16.37$ Å) to $2\theta = 1.98°$ ($d = 44.62$ Å) and $2\theta = 5.16°$ ($d = 17.13$ Å) [Figure 2(a)]. As the rubber content increased, the dispersion of clay was enhanced and better intercalated/partially exfoliated structures are observed at and above 15 wt % rubber ratio with absence of tactoids. Indeed, at 20 wt % rubber fraction, the peak at the highest diffraction angle nearly disappeared and the second one is shifted to $2\theta = 1.76°$ ($d = 50.19$ Å). This suggests additional intercalation of the rubber into the basal spacing of the clay where PLA chains had already penetrated.[6,14] This occurs due to

the viscosity build up imparted by the rubber to the system that promoted high shear intensity favoring more clay nanoplatelet delamination.[6,19–22] In addition, in the PC-I sequence, both PLA and clay experienced extrusion twice contributing to improved clay dispersion by promoting more PLA molecules to diffuse into the clay spacings. In addition, this fine clay dispersion arose due to the polar interactions of the rubber and PLA ester groups, and to the chemical reaction between the rubber epoxy moieties with terminal (COOH) and (OH) groups of the PLA[3–8] and with the (OH) groups of the clay surfaces and those of its surfactant. The reactions of the (COOH) and (OH) groups with the epoxy groups were identified by FTIR by Yeh et al.[3] and Juntuek et al.[4] The schematic representation of these reactions was published by Sun et al.,[5] and their mechanism in the presence of a catalyst was discussed by Oyama et al.[28]

For PI-C nanocomposites, when the rubber extent was 5 wt %, the OMMT diffraction peak shifted to lower angle $2\theta = 2.10°$ ($d = 42.07$ Å), which remained at almost the same position for all the rubber contents [Figure 2(b)]. The second peak recorded at $2\theta = 5.12°$ ($d = 17.26$ Å) indicate that there are remaining tactoids in 5 wt % PI-C nanocomposite. At 10 wt % rubber content, the intensities of the peaks decreased and the peak at $2\theta = 5.12°$ ($d = 17.26$ Å) shifted to $2\theta = 4.90°$ ($d = 18.03$ Å) pointing out to better dispersion. At 20 wt % rubber content, in addition to the two peaks detected at the same positions as in the 10 wt % nanocomposite, a third peak at $2\theta = 6.42°$ ($d = 13.77$ Å) appeared. The third peak indicates low clay dispersion state owing to the chain extension induced by the reaction between the PLA and the rubber functional groups restricting the chain mobility of the PLA and the rubber molecules to enter into the clay galleries.[3,5–9,11] PI-C exhibited lower clay dispersion levels compared with PC-I, because the interactions between the PLA and the rubber were maximized during the first extrusion step (formation of PI) which reduced the total reactive groups of the polymers to interact with the clay. In addition, in the PI-C mixing order the clay was mixed only once with the polymers.

All diffractograms of CI-P nanocomposites exhibited nearly the same trend with three distinct peaks positioned at the same diffraction angles regardless of the rubber ratio implying almost the same clay dispersion in these nanocomposites [Figure 2(c)]. In these mixtures, both intercalation and re-agglomeration of previously dispersed clay in the CI compounds took place. The peak at $2\theta = 6.10°$ ($d = 14.49$ Å) was observed at the same position as in CI compounds but with lower intensities associated with reduced amount of tactoids owing to the additional intercalation by the added PLA into the clay galleries. The two peaks at $2\theta = 1.58°$ ($d = 55.91$ Å) and $2\theta = 4.38°$ ($d = 20.17$ Å) in CI mixtures increased in intensity and shifted to higher angles located at $2\theta = 2.10°$ ($d = 42.07$ Å) and $2\theta = 4.66°$ ($d = 18.96$ Å) when PLA was incorporated, suggesting the collapse of clay interlayers and/or re-agglomeration of the already expanded nanofiller in the CI compounds. Note that in this mixing mode, CI mixtures were extruded twice which was found to be deleterious on the dispersion of the clay as discussed previously in the case of R/OMMT-2EXT [Figure 1(a)]. This fact explains the deterioration of the clay dispersion state when PLA was added in the second extrusion step to form CI-P nanocomposites.

Figure 2(d) shows the XRD patterns of the ALL-S extruded twice. It can be noticed that the diffractograms resemble those obtained for PI-C compounds but with diffraction angles shifted to lower angles with lower intensities designating better dispersion than that of PI-C. OMMT peak was shifted to $2\theta = 1.90°$ ($d = 46.50$ Å) for all of the ALL-S nanocomposites, and the remaining tactoids were identified at $2\theta = 5.10°$ ($d = 17.33$ Å) and at $2\theta = 4.90°$ ($d = 18.03$ Å) when the rubber fraction was 5 and 20 wt % respectively with the appearance of a third peak at $2\theta = 5.90°$ ($d = 14.98$ Å) for this last composition. The highest level of dispersion is observed at 10 wt % rubber content with diffraction angles positioned at $2\theta = 1.90°$ ($d = 46.50$ Å) and $2\theta = 4.78°$ ($d = 18.49$ Å).

Better clay dispersion is exhibited in ALL-S nanocomposites compared with that of PI-C, because all the ingredients in ALL-S were fed at the same time into the extruder and were processed twice, consequently the interactions between the three ingredients were maximized. However, in PI-C the interactions between polymers were favored in the first extrusion step (PI), and the intercalation process was only accomplished during the second run which had affected the extent of dispersion owing to the short interaction time of the OMMT with the polymers.

TEM Analyses

Selected TEM photomicrographs of the nanocomposites are shown in Figures 3 and 4. All images attest to the formation of nanocomposites with structural characteristics consistent with the XRD analyses. In these micrographs, the base background represents the matrix, the dark lines and darker entities are the clay nanoplatelets and their stacks successively.

TEM photomicrograph at low magnification of PLA/OMMT nanocomposite reveals that clay nanosheets were uniformly and randomly dispersed in the PLA [Figure 3(a)]. Upon zooming to a higher magnification, the TEM image of this binary mixture displays a hybrid structure composed of intercalated/partially exfoliated clay with numerous individual isolated silicate nanoplatelets and coexistence of thin primary clay tactoids [Figure 3(b)]. Such structure originated, as aforementioned, from the strong interactions between PLA terminal groups and hydroxyl entities of OMMT nanoplatelet surfaces and of its ammonium surfactant. These visual observations are in close accordance with the XRD results on PLA/OMMT.

Unlike PLA/OMMT, the R/OMMT extruded twice (R/OMMT-2EXT) exhibits poor dispersion manifested by the occurrence of close clustered clay groups [Figure 3(c)]. Its TEM image at high magnification clearly demonstrates intercalated/partially exfoliated clay structure with slight amount of delaminated nanosheets and thick tactoids indicative of incomplete exfoliation [Figure 3(d)].

The structure of PC nanocomposite consists of abundant single exfoliated clay nanosheets and intercalated/partially exfoliated regions and thin clay stacks [Figure 3(e)], whereas that of CI is

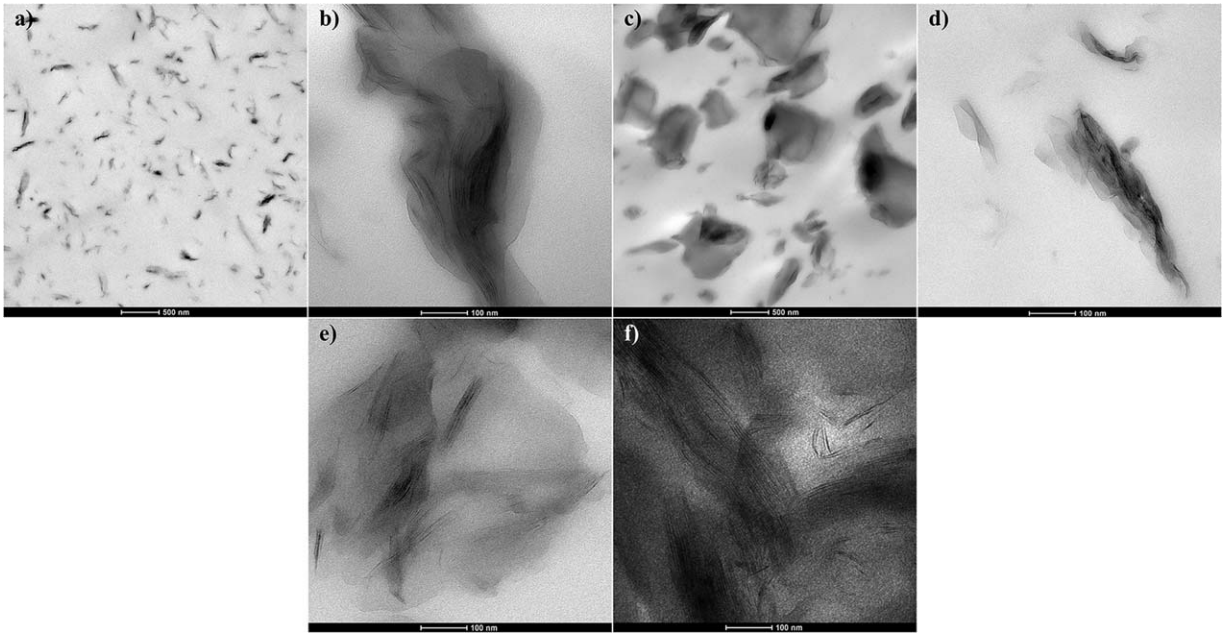

Figure 3. TEM micrographs at low and high magnification of (a, b) PLA/2 wt % OMMT and (c, d) R/2 wt % OMMT, respectively, and TEM micrographs at high magnification of (e) PC and (f) CI intermediate nanocomposites.

mainly made of intercalated structure and few exfoliated particles with occurrence of large number of thick clay stacks and tactoids which can be assimilated to agglomerates of different sizes [Figure 3(f)].

The TEM analyses of these four nanocomposites (PLA/OMMT, R/OMMT, PC, and CI) are in good agreement with the diffraction peaks appearing in their XRD patterns confirming that clay particles are more dispersed in PLA than in the rubber as a result of the disparity in their polarities and hence their affinity to clay.

Representative high magnification TEM micrographs of the ternary nanocomposites prepared by different addition protocols are exhibited in Figure 4. Owing to the absence of contrast between the PLA and the rubber, it is difficult to differentiate between the two polymer phases and thus to locate the clay. For the sake of brevity only the micrographs of the nanocomposites at the optimal 10 wt % rubber ratio are shown, because at this composition the best stiffness-toughness balance has been acquired, especially for PC-I and PI-C mixing sequences.

The main common observation for PC-I, PI-C and ALL-S is that they all show a nanoscale dispersed morphology dependent on rubber composition identified by the presence of single clay nanosheets without appearance of any agglomeration, whereas for the CI-P nanocomposite, the rubber content did not significantly influence the nanoscale clay dispersion, and discrete agglomerates constituted most of the structure. In all preparation procedures, the OMMT particles were dispersed without any obvious orientation preference, and none of them led to completely exfoliated nanocomposite.

PC-I presented the highest level of clay dispersion [Figure 4(a)]. Exfoliated clays constitute the major structure evidenced from single clay nanoplatelets, thin stacks and absence of tactoids. Such high dispersion degree was possible because the favorable reactions between the PLA reactive groups and those on the clay took place for a longer time (PC mixture was extruded

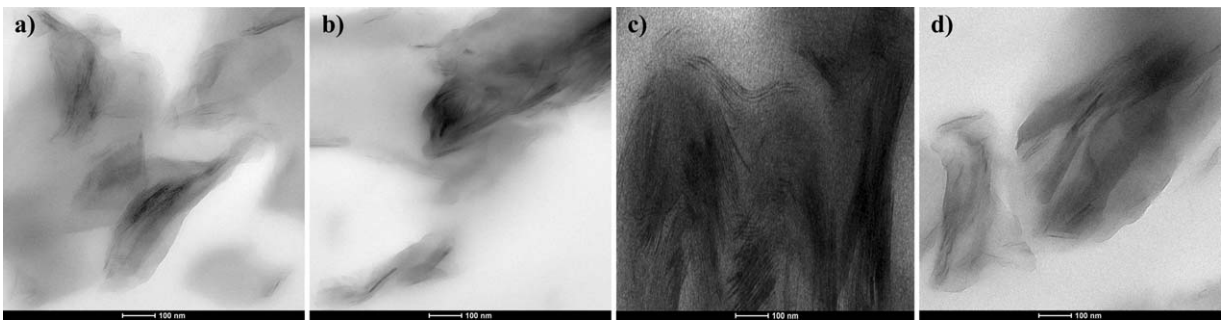

Figure 4. TEM photomicrographs of: (a) PC-I, (b) PI-C, (c) CI-P, and (d) ALL-S nanocomposites prepared at 10 wt % rubber content.

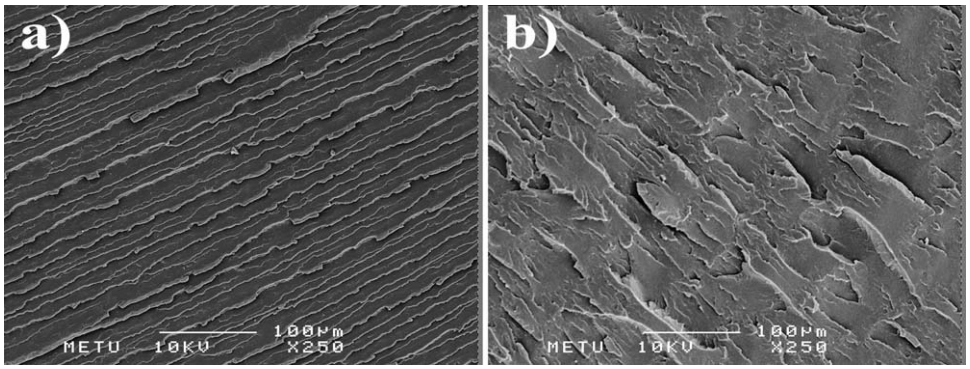

Figure 5. SEM micrographs of the cryofractured surfaces of the injection molded specimens of (a) PLA and (b) PLA/2 wt % OMMT.

twice). Furthermore, the shear melt viscosity became high in the second extrusion step induced by the added viscous rubber that improved delamination and breakdown of clay tactoids and helped insertion of both types of polymer molecules into the clay stacks as was confirmed by XRD.

PI-C TEM micrograph exhibits lower dispersion level than PC-I [Figure 4(b)]. This image shows intercalated structures, some single nanoplatelets and thin stacks, and slight amount of tactoids. This is the result of the interactions between the polymers in the first extrusion run that reduced the available reactive groups of the polymers to interact with the clay, and also the intercalation could only take place in the second extrusion run (short residence time).

CI-P nanocomposite presented the worst clay dispersion state, characterized by intercalated clay particles, large amount of clay tactoids, agglomerates and almost total absence of exfoliated clay particles Figure 4(c). This structure was the result of the low diffusion ability of the rubber into clay interlayers during the extrusion of CI mixture, and to its possible bonding to clay edges through interactions of its reactive groups with the hydroxyl groups of the clay surfaces that prevented the rubber and the PLA to intrude further into clay galleries during the second extrusion step.[6] The deleterious effect of extruding CI intermediate nanocomposite twice on clay dispersion was discussed earlier in the XRD section. Another factor that could also be considered is the presence of clay agglomerates that constrained the motion of the polymer chains necessary for their diffusion into clay galleries.[6,11–13,20,23] These agglomerates stemmed from encapsulation of most of the clay by the rubber that enhanced platelet-platelet interactions, and the extensive shear forces applied by extrusion were not able to breakdown these agglomerates. In addition, collapse of the clay galleries were triggered by the high shear intensity during CI extrusion. Dissolutions of the organoclay surfactant into the matrix during processing has been well documented in the literature.[6,12,16]

ALL-S presents finer clay dispersion in comparison to that of PI-C, consisting of intercalated particles and myriad single clay particles, thin clay stacks and few tactoids [Figure 4(d)]. This finer dispersion compared with PI-C is the result of the competition between the rubber and the PLA to react and to simultaneously enter within the clay galleries. Moreover, in this mixing order, the ingredients were in contact for longer time (two extrusion processes), thus giving more and equal chances for both polymers to diffuse into the clay galleries.

Morphology (SEM) Analyses

Illustrative SEM micrographs of the freeze fractured surfaces of twice extruded PLA and PLA/OMMT are shown in Figure 5. PLA displays a typical brittle fracture surface as shown by a smooth surface and several parallel straight cracks developed throughout the surface [Figure 5(a)]. Absence of crack deflections ascribed to the homogeneous structure of PLA led to rapid crack growth and abrupt breaking of PLA with low fracture resistance and observable stress whitening on the specimens that might explain the low impact toughness of PLA.[19] PLA/OMMT SEM micrograph [Figure 5(b)], shows a rough surface compared with PLA attributed to the effective ability of clay nanoplatelets in diverting cracks in random directions giving rise to numerous short and long crack paths responsible of such feature.[6,29] Such mechanism was possible owing to the produced OMMT intercalated/partially exfoliated structure coupled with the valid interactions between the functional groups of the PLA and the clay that enabled improved load transfer from the matrix to the reinforcement.[6,11,12,19]

Figure 6(a–d) exhibits representative SEM images of unetched cryofractured surfaces of the ternary nanocomposites at 10 wt % rubber content. Intense macroscopic stress whitening compared with PLA and PLA/OMMT was noticed on all impacted specimen surfaces that confirm improvement of toughness. All SEM images exhibited a two-phase morphology. This morphology is typical of an immiscible polymer system, in which the rubber composed the dispersed phase surrounded by the continuous PLA matrix. The interface is not clear indicating strong adhesion between the phases derived from the *in situ* interfacial reaction between the functional terminal groups of the PLA and those of the elastomer giving rise to *in situ* formed PLA-g-rubber copolymer that strengthened the interface by bridging the two phases for adequate load transfer.[2,6,11,12,19,27,28] This was identified by the deformation of the domains into ellipsoids and their enlargement in the stress direction demonstrating that the rubber shared the load with the matrix. The presence of this copolymer at the interface simultaneously decreased the interfacial tension and droplet coalescence rate through steric repulsion between the copolymer

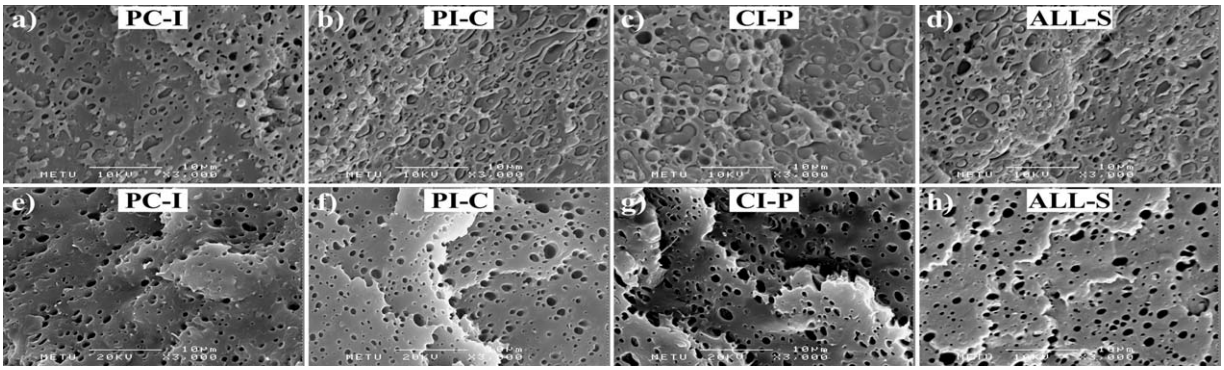

Figure 6. SEM micrographs of the fractured injection molded specimens of (a–d) unetched surfaces, and (e–h) etched surfaces of the ternary nanocomposites all with 10 wt % rubber content.

molecules and promoted droplet breakup rate hence resulting in fine particle size dispersion.[4–6,24,27,28] Furthermore, these micrographs present some vacuoles corresponding to pulled-out rubber droplets during impact, whereas others were well anchored to the matrix and some were still embedded within the PLA matrix enveloped by micro-voids. These gaps might have resulted from the debonding and/or cavitation of the rubber particles at the interface.[2,7–11,15,30] Debonding/cavitation of rubber particles is one of the most important mechanisms of energy absorption in rubber-toughened polymers among others, such as crazing, internal rubber cavitation, shear banding, crack bridging and shear yielding, all of which are highly influenced by particle size and interface strength.[7,30]

The morphology of etched fractured surfaces of selected ternary nanocomposites at 10 wt % rubber content is shown in Figure 6(e–h). The craters on the photographs correspond to the location of the rubber particles extracted by chemical etching. All of the nanocomposites present fine phase structures. Figure 6(e–h) shows that during impact, fracture surfaces with higher surface roughness than that of PLA/OMMT [Figure 5] were generated. This indicates that much energy has been consumed to create these surfaces and shows that the transition from brittle (crazing) to tough (shear yielding) fracture took place mainly by cavitation induced shear yielding.[2,7–11,15,30]

At low rubber fraction, droplet breakup is favored against coalescence, owing to the low rubber concentration (low viscosity) and to decreased interfacial tension between the components imparted by the *in situ* formed copolymer at the interface. As a result, small particles are formed with narrow and homogeneous distribution, but at higher rubber contents, during mixing the domain size is determined by the competition between particle breakup and coalescence.[6,28] Moreover, the particle size could also be influenced by the presence of OMMT that generally induces a change in the phase size depending on its location.[6,20,22–27]

PC-I presented the lowest domain size (253–434 nm) because of the presence of most of the clay nanosheets predominately in the matrix that might have acted as physical obstacles to coalescence of the rubber particles[6,11–13,27] [Figure 6(e)]. Some of the clay may also have migrated to the interface.[16,22–24,26,27] Martins et al.[22] reported in their study of PP/PP-g-AA/EVA/OMMT nanocomposites that the clay migrated to the EVA phase by affinity, irrespective of the blending order, even in the sequence where the clay was first mixed with polypropylene, before EVA was added. Similarly, Borah et al.[23] observed that in LLDPE-g-MA compatibilized LLDPE/EMA/OMMT nanocomposites, the OMMT (Cloisite®25A) was attracted to the EMA phase by affinity during the short residence time in the internal mixer even though the clay was previously mixed with the molten polyethylene and EMA was added subsequently. The presence of the clay at the PLA/rubber interface in PC-I nanocomposite might have constituted physical hindrance for coalescence of the rubbery domains, accordingly small rubber domains are generated.[6,11–13,18,20,23,24,27]

The rubber droplet size of PI-C (333–545 nm) [Figure 6(f)] is somewhat larger than that of PC-I. In this nanocomposite, the clay was added in the second extrusion run, consequently it should be distributed in the two phases, with preference for PLA owing to the higher polarity of PLA in comparison to the rubber. Dasari et al.,[25,26] reported that the clay was equally dispersed in PA66 and SEBS-g-MA when they used PI-C addition mode to prepare the PA66/SEBS-g-MA/OMMT nanocomposite. The presence of the clay in the rubber phase increased the modulus of the rubber and hence reduced its ability to breakup compared with PC-I mixing order.[24–27] This effect coupled with the increased viscosity of the system due to the chain extension reaction decreased droplet breakup during blending. Both of these factors might have reduced the compatibilizing effect of the clay and hampered its physical barrier behavior for coalescence, therefore in the PI-C mixing sequence larger particles were developed compared with PC-I.

For CI-P and ALL-S, most of the clay should be present in the dispersed phase. In the case of CI-P this is evident because the clay is first mixed with the rubber. For ALL-S, during blending the rubber melted earlier (T_m ≈53°C) than PLA did (T_m ≈147°C), therefore most of the clay should also be enclosed in the rubber. However, in both cases, some of the OMMT might be present at the PLA/rubber interface and/or in the PLA phase. This preferential location of OMMT in the elastomer phase increased the viscosity and modulus of the rubber, accordingly the droplet deformation and breakup during blending were considerably reduced leading to larger domain size in these

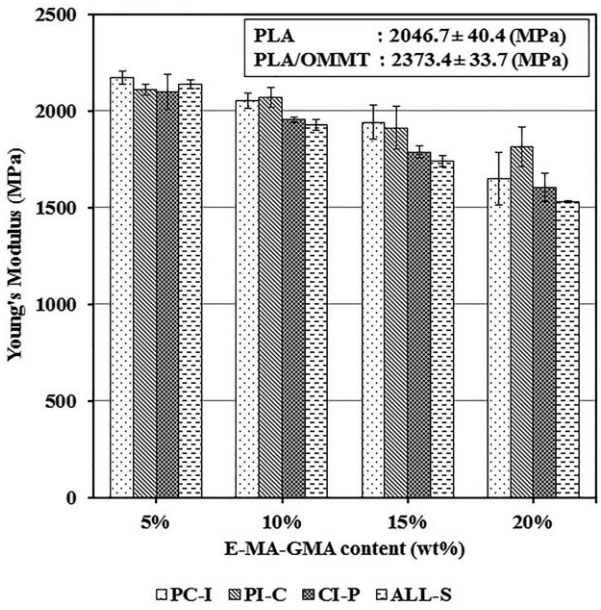

Figure 7. Young's modulus of the ternary nanocomposites as a function of the rubber content at 2 wt % clay.

nanocomposites in comparison to those of PC-I and PI-C. The domain size of ALL-S [Figure 6(g)], and CI-P [Figure 6(h)] were (449–689 nm) and (457–1524 nm) respectively. ALL-S exhibited smaller phase size than CI-P did, because all of its ingredients were extruded twice and the elastomer droplets were broken up during the early stages of their formation. However, CI-P was prepared from the highly viscous CI intermediate compound that was difficult to extrude and to disperse into PLA; therefore, larger particles were produced in this nanocomposite.

In all the mixing methods, the domain size increased with increasing rubber content (not shown here).[3,6,10,20] This is an expected result, as the rubber fraction increases the viscosity of the system and the tendency of particle collision and agglomeration increases, consequently the coalescence rate becomes higher than the droplet breakup rate, resulting in larger particle size.[20] In this study, particularly for PC-I and PI-C, at higher rubber ratio, the coalescence suppression and the compatibilizing effects of the clay were not significant probably due to its low concentration (2 wt %).

Mechanical Properties

Stress–strain curves of the studied materials (not shown here) were determined at room temperature. Upon drawing, PLA exhibited a sharp linear increase in stress with a distinct yield point accompanied thereafter by a short necking and an abrupt rupture at low strain (3.9%), demonstrating its brittleness and its low tensile toughness. Addition of 2 wt % OMMT to PLA did not bring about a noticeable change to the PLA deformation behavior. However, for all the compounding modes, incorporation of the rubber to the nanocomposites transformed the fracture of PLA from brittle to ductile. During stretching, these modified nanocomposites exhibited a broad yield peak and a long stable necking after which the strain increased considerably and continuously at nearly constant stress indicative of plastic flow (cold drawing), followed by a short stress softening before failure. The failure occurred at a significantly increased elongation at break signifying that high energy was dissipated.

Figures 7–9 display the tensile properties namely tensile modulus, tensile strength and elongation at break as a function of rubber loading for each of the considered mixing protocol. For the sake of comparison, the results for PLA and its corresponding nanocomposite (PLA/OMMT), both of them extruded twice, are written on each graph.

Tensile Modulus

The Young's modulus of neat PLA and those of the PLAs extruded once and twice were 2149.0, 2068.0, and 2046.7 MPa, respectively. There was no substantial change of PLA modulus with reprocessing, which is in line with published results in the literature.[31,32] Tensile modulus of PLA was found to remain constant after seven injection cycles,[31] and 10 extrusion processes.[32]

In the presence of 2 wt % OMMT, the tensile modulus of PLA increased from 2046.7 to 2373.4 MPa [Figure 7]. This is a common outcome attributed to the replacement of PLA molecules with OMMT that has high intrinsic stiffness and high aspect ratio.[6,11,12,16–20,23–27] This increase is correlated with the high level of OMMT dispersion (as was assessed by XRD and TEM) that increased the clay-polymer contact surface area and its effective volume fraction, thus imposing restrictions on chain mobility and deformation of the surrounding matrix.[6,11–13,18,20,23–27] In addition to these effects, the strong adhesion through interfacial interactions of PLA carboxyl end groups and the hydroxyl entities of the nanoclay contributes to efficient stress transfer from the polymer matrix to the filler giving rise to high tensile modulus of the PLA/OMMT nanocomposite.

As documented in Figure 7, for all the blending sequences the modulus dropped steadily as the rubber quantity is increased owing to the soft nature of the rubber with low modulus.[1–8,10,11,13–16,18,19,21–26] When the elastomer was added at 5 wt %, the modulus decreased from 2373.4 MPa to approximately 2100.0 MPa for all the nanocomposites, but at 10 wt % rubber content, the Young's modulus was more or less retained, especially for PC-I and PI-C mixing orders. Above this rubber content, PC-I and PI-C still displayed the highest modulus that might be due to the fine dispersion of the OMMT in the PC-I mixing order that contributed to chain immobilization, responsible of increased chain stiffening. For the PI-C mixing order, the increase might be ascribable not only to the fine clay dispersion, but also to promoted chain extension associated with significant reaction extent between the functional groups of PLA and those of the impact modifier that increased the molecular weight, and resulted in more stabilized and strengthened interface.

For the CI-P and ALL-S mixing orders, the OMMT was mostly present in the elastomer phase as discussed in TEM section. This indicates that encapsulation of the clay layers by the rubber phase has an adverse effect on their stiffening effectiveness.

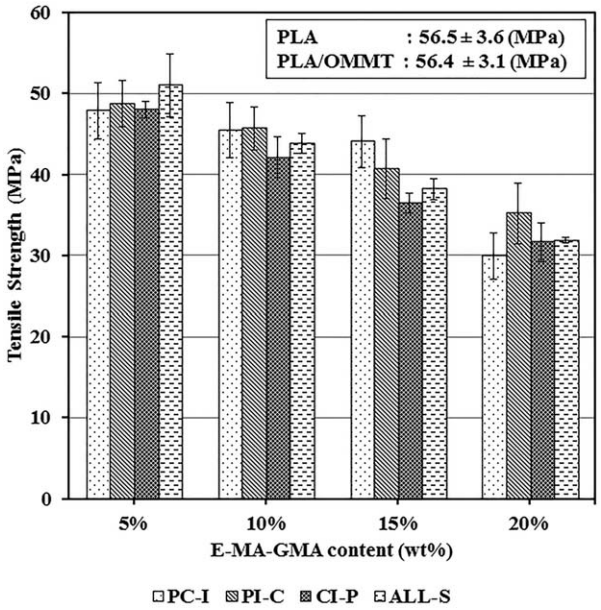

Figure 8. Tensile strength of the ternary nanocomposites as a function of the the rubber content at 2 wt % clay.

Tensile Strength

PLA showed a high tensile strength of 56.5 MPa [Figure 8]. No significant change of this property was distinguished after addition of 2 wt % OMMT to PLA. The nanocomposite exhibited intercalated/partially exfoliated nanostructure which should facilitate the stress transfer between the phases. However, the tensile strength of the material is strongly dependent on the orientation of the clay layers, and if the clay layers in the tensile bar are not preferentially oriented in the testing direction the increase in the tensile strength would be minimal.

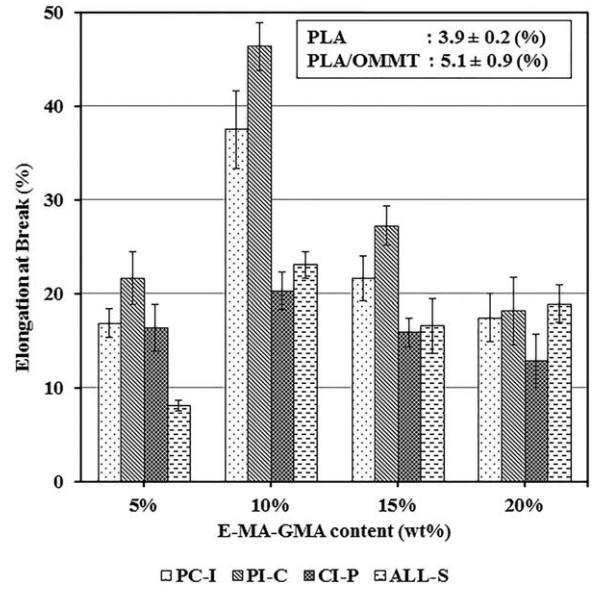

Figure 9. Elongation at break of the ternary nanocomposites as a function of the rubber content at 2 wt % clay.

The tensile strength as a function of the rubber ratio followed the same trend as that of the tensile modulus [Figure 8]. It decreased as the elastomer fraction was increased, regardless of the compounding protocol which is again attributed to the elastomeric nature of the rubber. This reduction in the tensile strength is consistent with previous research that reported reduced tensile strength in rubber-toughened PLA blends[1–4,6,10,11,13,15–17] and in other toughened polymer blends.[18–20,23]

At 5 wt % rubber content, the tensile strength was almost retained at 49.0 MPa independent of the compounding order, as a result of the somewhat similar OMMT dispersion level developed at this rubber ratio in all the compounding sequences. At this low rubber content, the location of the clay in the nanocomposites did not significantly affect the tensile strength, and the presence of clay agglomerates in the CI-P nanocomposite was not so detrimental. At 10 wt % rubber concentration, the tensile strength of all the nanocomposites underwent approximately the same decrease.

At 15 wt % elastomer content, the high tensile strengths of PC-I and PI-C compared with those for CI-P and All-S can be attributed to the presence of most of the clay in the PLA matrix in PC-I,[25,26] and to extensive reaction between the functional groups of the PLA and those of the rubber in PI-C, and to the enhanced clay dispersion in both of these nanocomposites as evaluated by XRD and TEM. However, the low tensile strengths of CI-P and ALL-S are due to the encapsulation of most of the clay inside the rubber. Moreover, the agglomerates in CI-P, especially at 15 wt % rubber content, might have acted as stress concentrators facilitating easy initiation and propagation of microcracks and leading to premature failure.[11,12,17,22]

When the rubber content reached 20 wt %, the tensile strength underwent a drastic drop in all the mixing protocols that could be due to the considerable softening effect induced by the rubber that hindered the benefits of the OMMT.[6,8]

Elongation at Break

Figure 9 illustrates the effect of rubber and clay addition on the elongation at break (ε_b) of the prepared nanocomposites. PLA is a stiff and brittle material, therefore as expected, it displayed low extensibility of 3.9% with slight stress whitening around the broken surfaces indicating that PLA deformed primarily by crazing mechanism,[6,9,10] and because of the absence of craze stoppers and/or craze diverting processes, the crazes that formed during extension grew and coalesced rapidly to form catastrophic cracks that resulted in premature breakup with low energy consumption and limited deformation.

Upon inclusion of 2 wt % OMMT into PLA, the tensile strain at break increased to 5.1% with substantial stress whitening on the specimen surfaces exhibiting higher degree of crazing and toughness enhancement. This result is in line with nanofiller reinforced impact modified PLA.[11,15] This slight increase in PLA drawability is attributed to intercalated/partially exfoliated dispersion of clay that promotes effective crack deflection that lengthens crack propagation paths and retards crack growth to fatal cracks.[6,29] Furthermore, the strong interfacial adhesion that

results from interactions between the functional groups of PLA and those of the OMMT enables efficient load transfer between the phases. However, this improvement was low due to the presence of tactoids as detected by XRD and TEM, and likely to the low OMMT content (2 wt %).

For all the mixing methods, when the rubber was incorporated to PLA/OMMT, all of the formulations displayed higher ε_b than pristine PLA with extensive stress whitening throughout the specimens induced by large amount of crazes giving rise to ductile deformation. The increase in tensile strain at break can be attributed to the high flexibility of the elastomer and to the effective stress transfer between the PLA and the rubber owing to the strengthened interface by the *in situ* formed PLA-g-rubber copolymer at the interface via the chemical reaction between the PLA and the rubber functional groups. The energy dissipation and high extension stemmed from a combination of massive crazes observed on the specimens and debonding/cavitation of the rubber particles as observed by SEM. Cavitation occurs during debonding and results in plastic deformation of the matrix and energy dissipation that improves tensile toughness.[2,7–11,15,30] This increase in elongation at break due to rubber addition is consistent with results published on rubber-toughened PLA.[1–8,10,11,13,15]

The ε_b attained a maximum at 10 wt % rubber fraction for all the preparation protocols without significant sacrifice of strength and toughness, but beyond this rubber content it declined steadily. The highest ε_b observed for PI-C and PC-I at this rubber loading is attributed to enhanced clay dispersion and to small rubber phase size in these mixing orders as observed by SEM. PI-C showed higher ε_b than PC-I did, due to the higher intermolecular reaction between the end groups of PLA and rubber in this mixing order compared with PC-I. The low ε_b for ALL-S and CI-P mixing orders might be due to the location of the clay in the dispersed phase in these nanocomposites that reduced rubber toughening efficiency by hindering its cavitation ability, and to the large rubber particle size as determined by SEM.

Beyond 10 wt % rubber content, the ε_b decreased considerably in all the preparation sequences owing to the presence of clay tactoids for PI-C and ALL-S and even agglomerates for CI-P that might have acted as flaws and defects, and to increased rubber domain size as observed by SEM. Because of the high difference in modulus between the rubber and the matrix, these large rubber domains might have acted as stress concentration points causing microdamages to develop readily to fatal cracks that lead to low ε_b.[3,4,8,11,15] When the rubber quantity reached 20 wt %, the ε_b dropped below 20% for all the nanocomposites.

Impact Strength

Figure 10 exhibits the effect of mixing sequences on unnotched Charpy impact strength (IS) as a function of rubber loading. As expected, neat PLA failed in a brittle manner with a recorded IS of only 18.4 J/m^2. Addition of 2 wt % OMMT to PLA reduced its IS to 17.0 J/m^2. This is a well-known fact, that is, the stiffness and strength improvement in nanocomposites is generally accompanied with a reduction in fracture-toughness. This slight reduction in impact toughness is due to the constraining effect

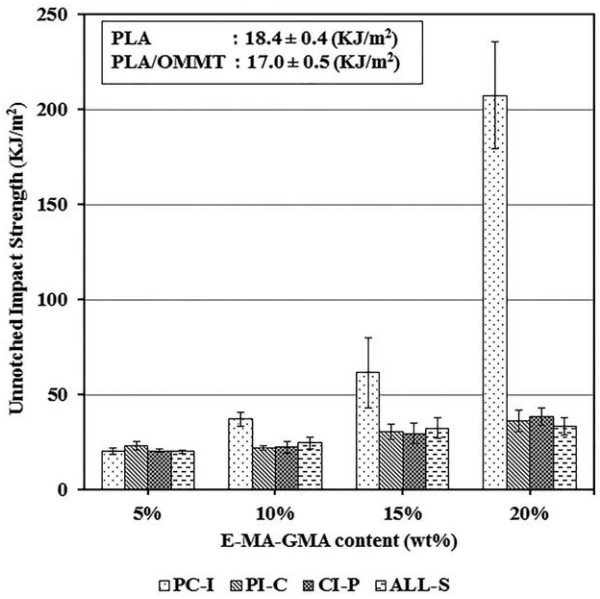

Figure 10. Unnotched Charpy impact strength of the ternary nanocomposites as a function of rubber content at 2 wt % clay.

of the OMMT on molecular mobility, and to the absence of efficient toughening mechanisms such as crack-tip blunting and crack bridging encountered in fracture processes of traditional polymer micro-composites, because the intercalated/partially exfoliated nanosheets are unable of producing such energy dissipating mechanisms.[30] Another reason for the decline in IS can also be assigned to the presence of tactoids in the PLA/OMMT nanocomposite as revealed by XRD and TEM analyses. These tactoids act as stress raisers and lead to early failure.[22,23] However, the decrease in IS was not high, because the effects of the negative factors are counteracted by the effective interactions between the clay nanoplatelets and PLA contributing to enhanced load transfer between the matrix and the nanoreinforcement.

For all the preparation procedures, the IS was gradually improved as the rubber fraction increased from 5 to 20 wt % [Figure 10]. This correlates with the elastomeric nature of the rubber and with the *in situ* formation of graft copolymer (PLA-g-rubber) at the interface. This copolymer situated at the interface promotes load transfer, consequently improving the IS. In addition, the homogeneous dispersion of the rubber domains initiates multiple crazes (as observed by the intense stress whitening on fractured specimens) and stops and/or deflects the crazes and cracks giving rise to efficient strain energy dissipation responsible of enhanced IS. This improvement of IS owing to addition of the low stiffness-low strength E-MA-GMA rubber to PLA corroborates with the results of different research studies.[1,2,4–8,11,15,17,18,20,22–26]

At 5 wt % rubber concentration, all of the nanocomposites displayed similar IS of nearly 20.0 J/m^2. However, at 10 wt % and higher rubber content, the PC-I nanocomposites exhibited the highest IS owing to their small rubber domain size and to superior clay dispersion, as detected by XRD and TEM techniques. Especially, above 10 wt % rubber content high degree of clay

Table I. Calorimetric Characteristics of PLA and its Nanocomposites

	T_g (°C)	T_c (°C)	T_m (°C)	χ_c (%)
PLA	56.13	115.79	147.07	5.94
PLA/OMMT, Clay (2 wt %)	57.20	109.40	150.74	3.70
PC-I, Rubber (wt %)				
5	58.55	102.76	149.30	4.42
10	57.44	102.93	148.25	5.78
15	58.28	104.52	147.51	7.20
20	57.58	108.58	148.11	7.82
PI-C, Rubber (wt %)				
5	58.89	104.12	149.08	4.39
10	58.96	103.38	148.09	4.88
15	57.45	103.78	147.58	5.08
20	57.70	103.90	145.07	6.26
CI-P, Rubber (wt %)				
5	57.39	105.79	146.44	3.92
10	57.08	105.38	145.92	6.10
15	55.98	107.48	146.20	7.05
20	57.55	110.51	150.58	7.62
ALL-S, Rubber (wt %)				
5	58.70	104.26	146.13	4.07
10	59.16	105.28	145.91	5.51
15	58.91	105.01	146.34	5.99
20	58.71	105.78	146.66	7.62

dispersion was achieved resulting in favorable impact resistance enhancement. Furthermore, the likely presence of most of the clay in the PLA continuous phase, as discussed earlier, should be another important factor for the high IS recorded for PC-I nanocomposites.[25,26]

A super tough PC-I nanocomposite was obtained at 20 wt % rubber content with an IS above 207.3 J/m^2 representing 11-fold increase compared with that of neat PLA. The PC-I specimens with 10 and 15 wt % rubber content were partially broken, whereas some of the specimens with 20 wt % rubber did not break, but only bended indicating that the actual IS would be greater than 207.3 J/m^2.

PI-C, CI-P, and ALL-S nanocomposites displayed almost similar IS at all rubber contents, and this value was lower than that of the IS of PC-I owing to their larger rubber particle size compared with PC-I. Large rubbery domain size increase stress concentration effects, thus reducing the beneficial effect of the rubber. The results on IS demonstrate that, especially for PI-C and PC-I, at 10 wt % stiffness-toughness balance was accomplished.

Thermal Analyses

DSC was performed to investigate the thermal behavior of PLA and its nanocomposites. The DSC data were determined from only one heating scan (0–200°C), because the crystallinity of PLA in the as molded specimens would affect the mechanical performance of the nanocomposites, and the goal was to find the crystallinity of the tensile samples. PLA and the nanocomposites exhibited similar thermograms (not shown here) characterized by three prominent transitions namely: a glass transition temperature (T_g), a crystallization exotherm (T_c and ΔH_c), and a melting endotherm (T_m and ΔH_m). Values of these relevant thermal properties derived from the thermograms are shown in Table I including the estimates of the degree of crystallinity (χ_c) of PLA computed using eq. (3) and a value of 93 J/g for the heat of fusion of 100% crystalline PLA.[3,8]

The T_g of PLA was clearly observed on all the DSC traces and that of the rubber which is below room temperature was not detected by this DSC analysis, consequently it was not studied here. The pure rubber shows only a melting temperature (T_m) recorded at 53.10°C. Neat PLA had a T_g centered at 56.13°C, a crystallization peak T_c at 115.79°C and a subsequent melting peak T_m at 147.07°C. The areas of the crystallization and melting peaks on its thermogram were almost the same indicating that PLA was primarily in the amorphous state after the injection process. This was also confirmed through its computed degree of crystallization using eq. (3) ($\chi_c \approx 5.94\%$).

As can be noticed from Table I, neither clay and rubber addition nor the blending protocols and rubber fraction significantly affected the T_g of PLA in the nanocomposites suggesting that after blending the macromolecular chains conserved their mobility and that the PLA and the rubber were immiscible.[8,16] Interestingly, T_m of all the nanocomposites also remained relatively unchanged with variations of about only 1–3°C implying that the rubber and the clay did not significantly modify the PLA crystal structure and did not affect the integrity of its crystals.[1] Unaltered T_g after OMMT and rubber addition to PLA was observed in various studies[6,11,14] and similar results were also found by Chow et al.[15] for PLA/SEBS-g-MA/nanoprecipitated $CaCO_3$ (NPCC), and by Alyamac and Yilmazer[21] for PET/E-MA-GMA/OMMT nanocomposites.

There was a substantial shift to lower temperature of the PLA crystallization transition peaks (Table I). The T_c of PLA decreased from 115.79 to 109.40°C after addition of 2 wt % OMMT showing that clay served as a heterogeneous nucleating agent.[6,11–14,16,17] The nucleating effect of OMMT was more significant in the case of PC-I, PI-C and ALL-S nanocomposites owing to their high clay dispersion level (high aspect ratio) and high contact area that are favorable for crystal nucleation. In a previous work on PET/E-MA-GMA/OMMT, a decrease of T_c from 138 to 128°C was detected at 1 wt % OMMT. The decrease in T_c was more significant at higher clay contents, and this decrease in T_c was found to be independent of the compounding sequence of the nanocomposites and it was attributed to the nucleating effect of OMMT.[21]

Regardless of the mixing order, addition of the rubber in all the nanocomposites induced a further decrease in T_c (Table I) pointing out to the nucleating activity of the rubber.[6,16] The T_c of PLA decreased after being toughened by an ethylene copolymer (Biostrong from DuPont), and then underwent a progressive decrease as the clay content increased. This effect was attributed to the nucleating behavior of both clay and

Biostrong.[17] Dasari et al.[25] also reported the nucleating effect of SEBS-g-MA in binary PA66/SEBS-g-MA blend, before incorporation of OMMT. The thermal results reported here (T_g, T_m, T_c) are also in line with those obtained by Balakrishnan et al.[17] It was reported that T_g and T_m were unchanged after Biostrong and clay addition; whereas both of these additives were found to exert strong nucleating effect on PLA and reduced its T_c.

According to Table I, significant decrease in T_c is observed for PC-I, because it was in this compounding order that the clay was best dispersed and the clay mostly resided in PLA phase permitting the clay to serve as effective heterogeneous nucleating agent for PLA. The lowest drop in T_c was recorded for CI-P probably due to confinement of most of the clay particles inside the rubber phase which therefore blocked its ability to act as nucleating species.[11,14] In the study of PLA/SEBS-g-MA/NPCC, Chow et al.[15] found that the nucleating effect of the NPCC was inhibited owing to its embedment in the rubber.

The degree of crystallinity (χ_c) of PLA decreased slightly from 5.94 to 3.70% after incorporation of OMMT to PLA, because the clay imposed restrictions to chain motion necessary for crystallization.[6,11,13,18,23] For all the mixing sequences there was a slight increase in χ_c as the rubber loading increased, but the level of crystallinity was less than 8%.

Finally, it can be stated that the interfacial strength associated with the effective physical and chemical interactions between the phases were the key factors for tensile and impact properties that were highly affected by the compounding protocol, clay dispersion and size of the rubber domains. However, in the present study, all of the nanocomposites had nearly comparable low crystallinity levels in the range of 4–8% irrespective of the preparation sequence. Thus, the crystallinity did not significantly affect the mechanical properties in this study.

CONCLUSIONS

PLA was reactively melt blended with an E-MA-GMA rubber in the presence of 2 wt % of an OMMT. The rubber content was varied from 5 to 20 wt % and four components addition protocols were used to prepare the nanocomposites in a co-rotating twin screw extruder.

XRD results, which were confirmed by TEM, revealed that PC-I resulted in the best clay dispersion and CI-P resulted in the worst one. Complete exfoliation of OMMT was not achieved, and all of the nanocomposites exhibited intercalated/partially exfoliated structures.

SEM observations revealed that PLA and the rubber were immiscible, but compatible attributed to the effective chemical reaction between the functional groups of the polymers. The rubber formed sub-micron dispersed phase, the size of which was influenced by the preparation procedure. PC-I and PI-C nanocomposites exhibited the smallest rubber particle size associated with their superior clay dispersion and with the active role of clay that acted as a barrier for coalescence, whereas ALL-S and CI-P nanocomposites showed larger phase size as a result of the encapsulation of most of the clay in the rubber, which hindered the barrier effect of clay for coalescence and reduced droplet breakup by stiffening the rubber. Incorporation of the rubber into the nanocomposites resulted in debonding/cavitation, crazing and shear yielding energy dissipating mechanisms in all of the nanocomposites and changed PLA deformation behavior from brittle to ductile.

Mechanical performance of the nanocomposites was influenced by the mixing sequence. The rubber and OMMT addition improved ductility and toughness of PLA without significantly sacrificing the strength, and optimum stiffness-fracture toughness was achieved at 10 wt % rubber content. PC-I nanocomposites showed the highest impact toughness and PI-C nanocomposites exhibited the highest elongation at break in tensile tests, owing to their better clay dispersion and their small rubber particle size. ALL-S and CI-P displayed lower mechanical performance than the PC-I and PI-C, because of their large particle size and reduced rubber cavitation ability due to the encapsulation of most of the clay in the rubber in these nanocomposites.

DSC analyses confirmed the immiscibility of the blended polymers. After addition of rubber and OMMT to PLA, T_g and T_m of the matrix remained relatively unaltered, but T_c underwent a substantial decrease demonstrating the heterogeneous nucleating role of the elastomer and the clay. These thermal characteristics and the degree of crystallinity were found to be independent of the preparation procedure.

REFERENCES

1. Zeng, J.; Li, Y.; He, Y.; Li, S.; Wang, Y. *Ind. Eng. Chem. Res.* **2011**, *50*, 6124.
2. Zhao, Q.; Ding, Y.; Yang, B.; Ning, N.; Fu, Q. *Polym. Test.* **2013**, *32*, 299.
3. Yeh, J.; Tsou, C.; Li, Y.; Xiao, H.; Wu, C.; Chai, W.; Lai, Y.; Wang, C. *J. Polym. Res.* **2012**, *19*, 9766.
4. Juntuek, P.; Ruksakulpiwat, C.; Chumsamrong, P.; Ruksakulpiwat, Y. *J. Appl. Polym. Sci.* **2012**, *125*, 745.
5. Sun, S.; Zhang, M.; Zhang, H.; Zhang, X. *J. Appl. Polym. Sci.* **2011**, *122*, 2992.
6. Baouz, T.; Rezgui, F.; Yilmazer, U. *J. Appl. Polym. Sci.* **2013**, *128*, 3193.
7. Zhang, N.; Wang, Q.; Ren, J.; Wang, L. *J. Mater. Sci.* **2009**, *44*, 250.
8. Taib, R. M.; Ghaleb, Z. A.; Mohd Ishak, Z. A. *J. Appl. Polym. Sci.* **2012**, *123*, 2715.
9. Bhardwaj, R.; Mohanty, A. K. *Biomacromolecules* **2007**, *8*, 2476.
10. Meng, B.; Deng, J.; Liu, Q.; Wu, Z.; Yang, W. *Eur. Polym. J.* **2012**, *48*, 127.
11. Leu, Y. Y.; Mohd Ishak, Z. A.; Chow, W. S. *J. Appl. Polym. Sci.* **2012**, *124*, 1200.
12. Balakrishnan, H.; Hassan, A.; Wahit, M. U.; Yussuf, A. A.; Abdul Razak, S. B. *Mater. Des.* **2010**, *31*, 3289.
13. Yu, Z.; Yin, J.; Yan, S.; Xie, Y.; Ma, J.; Chen, X. *Polymer* **2007**, *48*, 6439.

14. Chow, W. S.; Lok, S. K. *J. Therm. Anal. Calorim.* **2009**, *95*, 627.
15. Chow, W. S.; Leu, Y. Y.; Mohd Ishak, Z. A. *Express Polym. Lett.* **2012**, *6*, 503.
16. Lewitus, D.; McCarthy, S.; Ophir, A.; Kenig, S. *J. Polym. Environ.* **2006**, *14*, 171.
17. Balakrishnan, H.; Masoumi, I.; Yussuf, A. A.; Imran, M.; Hassan, A.; Wahit, M. U. *Polym-Plast. Technol.* **2012**, *51*, 19.
18. Ahn, Y.; Paul, D. R. *Polymer* **2006**, *47*, 2830.
19. Coskunses, F. I.; Yilmazer, U. *J. Appl. Polym. Sci.* **2011**, *120*, 3087.
20. Yeniova, C. E.; Yilmazer, U. *Polym. Comp.* **2010**, *31*, 1853.
21. Alyamac, E.; Yilmazer, U. *Polym. Comp.* **2007**, *28*, 251.
22. Martins, C. G.; Larocca, N. M.; Paul, D. R.; Pessan, L. A. *Polymer* **2009**, *50*, 1743.
23. Borah, J. S.; Karak, N.; Chaki, T. K. *Mat. Sci. Eng. A* **2011**, *528*, 2820.
24. Oliveira, A. D.; Larocca, N. M.; Paul, D. R.; Pessan, L. A. *Polym. Eng. Sci.* **2012**, *52*, 1909.
25. Dasari, A.; Yu, Z.; Yang, M.; Zhang, Q.; Xie, X.; Mai, Y. *Comp. Sci. Tech.* **2006**, *66*, 3097.
26. Dasari, A.; Yu, Z.; Mai, Y. *Polymer* **2005**, *46*, 5986.
27. Hong, J. S.; Namkung, H.; Ahn, K. H.; Lee, S. J.; Kim, C. *Polymer* **2006**, *47*, 3967.
28. Oyama, H. T.; Kitagawa, T.; Ougizawa, T.; Inoue, T.; Weber, M. *Polymer* **2004**, *45*, 1033.
29. Balakrishnan, S.; Start, P. R.; Raghavan, D.; Hudson, S. D. *Polymer* **2005**, *46*, 11255.
30. Lim, S.; Dasari, A.; Yu, Z.; Mai, Y.; Liu, S.; Yong, M. S. *Comp. Sci. Tech.* **2007**, *67*, 2914.
31. Pillin, I.; Montrelay, N.; Bourmaud, A.; Grohens, Y. *Polym. Degrad. Stab.* **2008**, *93*, 321.
32. Zenkiewicz, M.; Richert, J.; Rytlewski, P.; Moraczewski, K.; Stepczynska, M.; Karasiewicz, T. *Polym. Test.* **2009**, *28*, 412.

Résumé: Ce travail de recherche a pour objectif la modification du PLA pour l'amélioration essentiellement de son endurance et son extensibilité afin de développer un nouveau matériau pour une utilisation en emballage. A cette fin, le caoutchouc EMAGMA et une charge argileuse (montmorillonite organiquement modifiée «Cloisite®30B» on été choisi comme additifs modificateurs. Les mélanges ont été préparés sur une extrudeuse bi-vis co-rotatives à un taux de charge constant à 2% et en variant le taux de caoutchouc de 0 à 30% avec un pas de 5%. Le travail de recherche est scindé en deux parties, dont la première a été consacré à l'étude des mélanges binaires (PLA/EMAGMA) et ternaires (PLA/EMAGMA/Cloisite®30B). Les différentes techniques de caractérisations (DRX, MET, MEB, DSC, indice de fluidité, test au choc et de traction) ont permis de constater une importante amélioration des propriétés ciblées à un taux de 10% en caoutchoucs. Dans la deuxième partie, les effets de quatre modes d'addition des composés des mélanges ternaires sur la performance des nanocomposites a été étudié. Il a été trouvé que la séquence d'addition des composants avait une grande influence sur la structure et la performance des nanocomposites. Un équilibre rigidité-endurance a été trouvé pour un taux de 10% en caoutchouc dans les mélanges sans une grande perte en robustesse. Une importante endurance en choc a été atteinte lorsque le PLA est mélangé en premier lieu avec la charge avant que le caoutchouc soit ajouté, et la plus haute endurance en tension a été obtenue lorsque le PLA est d'abord ajouté au caoutchouc et la charge ajouté par la suite au mélange.

Mots-clés: acid polylactique, nanocomposite, argile organique, modification par caoutchouc, méthacrylate de glycidyle.

Abstract:

This research work aims to modify PLA to essentially enhance its toughness and its extensibility to develop a new material for packaging application. For this aim, an EMAGMA rubber and a clay filler (an organo-modified montmorillonite «Cloisite®30B») have been chosen as modifying additives. The compounds were prepared on a co-rotative twin screw-extruder at constant filler content of 2wt% and varying the rubber content from 0 to 30wt% with an increment of 5wt%. The research work is divided into two parts, the first of which focuses on the study of the binary (PLA/EMAGMA) and ternary nanocomposites (PLA/EMAGMA/Cloisite®30B). The various characterization techniques (XRD, TEM, SEM, DSC, MFI, impact and tensile tests) evidenced a significant improvement of the targeted properties at 10wt% rubber ratio. In the second part, the effects of four addition modes of the components of the ternary compounds on the performance of the nanocomposites were investigated. It was found that components addition sequence had significant influence on the structure and performance of the nanocomposites. Balanced stiffness-toughness was observed at 10 wt % rubber content in the compounds without significant sacrifice of the strength. High impact toughness was attained when PLA was first mixed with the clay before the rubber was added, and the highest tensile toughness was obtained when PLA was first compounded with the rubber, and then clay was incorporated into the mixture.

Keywords: Poly(lactic acid); nanocomposite, organoclay, rubber toughening, glycidyl methacrylate.

ملخص:

يهدف هذا البحث إلى تعديل بوليمر حمض اللبنيك لتحسين صلابته و مدوديته من أجل تطوير مادة جديدة للإستعمال في ميدان التغليف. لهذه الغاية، تم اختيار المطاط EMAGMA و حشوة طينية (المونتموريللونيت المعدلة عضويا«Cloisite®30B») كمضافات معدلة. تم تحضير المخاليط في آلة باثقة مزدوجة البراغي ذات نفس اتجاه الدوران بمعدل ثابت ب2% من الحشوة الطينية، وتغيير معدل المطاط من 0 إلى 30% بخطوات متزايدة قدرها 5%. ينقسم العمل إلى قسمين، كرس الأول لدراسة المخاليط الثنائية (PLA/EMAGMA) و الثلاثية (PLA/EMAGMA/Cloisite®30B). أظهرت مختلف تقنيات التوصيف (XRD, TEM, SEM, DSC, MFI, impact and tensile tests) تحسنا كبيرا للخصائص المستهدفة عند معدل 10% من المطاط. في القسم الثاني تمت دراسة الأثار المترتبة على إستعمال أربعة أنماط لإضافة مكونات المخاليط الثلاثية على أداءالـnanocomposite. وجد أن نمط إضافة المكونات كان له تأثيرا كبيرا على هيكل و أداء الـnanocomposite. تم الحصول على توازن صلابة-قوة عند 10% من المطاط في المخاليط دون خسارة في قوة التحمل، كما تم الحصول على صلابة معتبرة على تحمل الصدمة عند خلط الـPLA أولا مع الحشوة الطينية قبل إضافة المطاط، و على أكبر صلابة للشد عند خلط الـPLA أولا مع المطاط و إضافة الحشوة الطينية فيما بعد إلى الخليط.

كلمات البحث: بوليمر حمض اللبنيك، مركبات النانو، الطين العضوية، التشديد المطاطي،قلسديل الميتاكريليت.